Time-Resolved Spectroscopic Investigation of Structure and Dynamics of Deep Eutectic Solvents

A Thesis Submitted

in Partial Fulfilment of the Requirements

for the Degree of

DOCTOR OF PHILOSOPHY

By

Navin Subba

to the

DEPARTMENT OF CHEMISTRY

INDIAN INSTITUTE OF TECHNOLOGY KANPUR

KANPUR, INDIA

April, 2021

This Page Intentionally Left Blank

Declaration

This is to certify that the thesis entitled "Time-Resolved Spectroscopic Investigation of Structure and Dynamics of Deep Eutectic Solvents" is authored by me. It presents the research conducted by me under the supervision of Prof. Pratik Sen.

To the best of my knowledge, it is an original work, both in terms of research content and narrative, and has not been submitted elsewhere, in part or in full, for a degree. Further, due credit has been given to the relevant past work, facilities and collaborators with appropriate citations and acknowledgements, in line with established norms and practices.

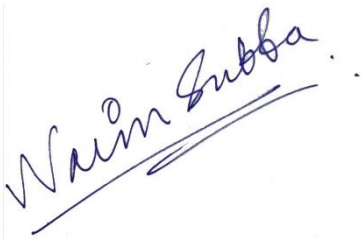

Navin Subba
(Roll Number 14107285)
Programme: Ph.D.
Department of Chemistry
Indian Institute of Technology Kanpur
Kanpur – 208 016, India

This Page Intentionally Left Blank

Certificate

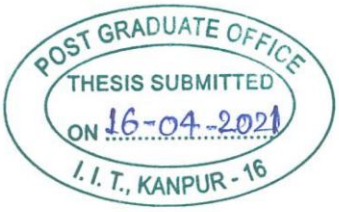

It is certified that the work contained in the thesis entitled "**Time-Resolved Spectroscopic Investigation of Structure and Dynamics of Deep Eutectic Solvents**" by **Mr. Navin Subba (Roll Number 14107285)** has been carried out under my supervision and that this work has not been submitted elsewhere for a degree.

Pratik Sen.

Prof. Dr. Pratik Sen
Thesis Supervisor
Department of Chemistry
Indian Institute of Technology Kanpur
Kanpur – 208 016, India

This Page Intentionally Left Blank

Department of Chemistry
Indian Institute of Technology Kanpur

Certificate of Course Work

This is to certify that **Mr. Navin Subba (Roll No. 14107285)** has satisfactorily completed all the courses required for the Ph.D. degree. The courses include:

CHM621A	Chemical Binding
CHM629A	Principles of Physical Chemistry
CHM664A	Modern Physical Methods in Chemistry
CHM683A	Surfaces, Interfaces, Thin Films & Related Analytical Techniques
CHM799A	Research
CHM800A	General Seminar
CHM801A	Graduate Seminar

Mr. Navin Subba was admitted to the candidacy of the Ph.D. degree in **August 2015** after he successfully completed the written and oral qualifying examinations.

Head
Department of Chemistry
Indian Institute of Technology Kanpur
Kanpur – 208 016, UP, India

Convener, DPGC
Department of Chemistry
Indian Institute of Technology Kanpur
Kanpur – 208 016, UP, India

This Page Intentionally Left Blank

Dedicated to the

Research Scholars

This Page Intentionally Left Blank

Acknowledgements

Research for many is very exciting as well as somewhat intimidating at the beginning and I am no exception to the same feeling. My decision to join the research was completely a blind one and somewhat a leap of faith. While I still question my decision to do research, over the years, I have realized that a guide plays a pivotal role in shaping the scientific thinking and motivation of a student. In this regard, I feel lucky enough to have *Professor Pratik Sen* as my thesis advisor and I am immensely grateful and indebted to him for guiding me through Ph.D. until the very end. The atmosphere and the freedom in terms of research he has provided in our laboratory are commendable. When it comes to communication, he is an approachable person who is open for discussions, frank conversations and also open to listen to the ideas the students would like to share. At times, when I felt that things were stuck, he showed me the way. I really believe that he gives his best to impart the knowledge and experience he has to the students. As I am quite a slow learner, I would like to thank him for showing patience with my inability to grasp physical chemistry. I have had asked him even silly and very basic questions to which he has never denied to answer. His constant encouragement is something I am going to miss after the graduation.

Extending gratitude to our/my collaborators, first, I would also like to thank *Prof. Ranjit Biswas* (S. N. Bose National Centre for Basic Sciences, Kolkata), who has been an excellent collaborator as well as an important ~~big~~ contributor to my thesis. His pioneering work in the area of the systems I have studied has helped me a lot. I am also thankful to his student *Ejaj* (now a member of our group). I would also like to extend my gratitude to the research group of *Prof. Wojciech Gadomski* (InFemto Lab, University of Warsaw, Poland). They have been an important part of the present thesis. I would specially like to thank *Dr. Kamil* and *Dr. Piotr* with whom I did part of the experiments of this thesis during my visit to Warsaw, Poland. They were wonderful hosts and took care of everything to ensure my comfortable stay in Poland. It was a memorable trip the three of us took to Kraków. Finally, I would like to thank *Abhineet* (Department of Chemistry, Banaras Hindu University) and his supervisor *Dr. Satyen Saha* for letting me access their viscometer. I cannot thank *Abhineet* enough as he measured the viscosity of my samples as and when needed.

I am thankful to all the faculties for their wonderful teaching during the course work of PhD.

I am grateful to IIT Kanpur and the Department of Chemistry for all the facilities provided. I would also like to extend my gratitude to IIT Kanpur and MHRD, Government of India, for

providing me research fellowship. Finally, I would like to thank IIT Kanpur for making me a part of it and I am very much proud and cherish to be a part of an IIT.

I would also like to thank all the staff and service providers of the Department of Chemistry and other bodies of IIT Kanpur for helping and facilitating smooth official or unofficial services. I would also like to thank all the mess and sanitation workers of Hall-7 which has been my home for the past few years. Mess workers deserve an applause as Hall-7 food is the best in the entire campus. Period.

I would like to thank all the lab members, former (*Rajeev, Shradhey, Bhaswati, Pushpal, Vaishakh, Vipin* and *Faizi*) and present (*Nilimesh, Aritra, Shovon, Sandeep, Tanmay, Kuldeep, Arghya, Abhijit* and *Sonu*) with whom I learned to grow academically and socially. I would like to ask all of you to forget what I have said or done that made you feel bitter. I am very grateful and deeply indebted to *Bhaswati* for guiding me through the initial stage of my Ph.D. I would like to thank *Nilimesh* who is always up for scientific and non-scientific discussion cum argument. He has been more of a friend than a colleague and main intra-lab collaborator. All the lab members have great sense of humour, which is an important part of this lab. Perhaps this is one of the liveliest labs. I would also like to thank *Puspkant* (Pandit Ravi Shankar Shukla University, Raipur), who worked with me for his M.Sc. project. I would also like to thank former lab member *Vijaykant* and his wife. Frequent dinner invitations for Rajasthani food at their residence gave me much needed break from hostel and canteen foods. I will certainly miss the conversations, tête-à-tête and giggles I had with the members of the lab.

I would like to thank all the teachers who taught me in my college and university days. I would like to particularly thank *Dr. Bhaskar Chakraborty* (Nar Bahadur Bhandari Degree College, Tadong) and *Dr. Biswajit G. Roy* (Sikkim University) who were excellent organic chemistry teachers. I would also like to thank my school (Enchey Sr. Sec. School) and tuition teachers who taught me and gave me the thrill of education.

I really appreciate the company of my friends (*Zafar, Bapan* and *Kishore* and many others) here at IIT Kanpur. I would also like to take this opportunity to thank my friends (*Nima, Purna, Ashoke, Sujal, Deepak* and *Sonam*) back in my home town. They have been an integral part of my growth since the school days and I have had great and adventurous days with them.

I cannot thank enough my family members whose support has been incredible throughout. Obviously, I cannot describe the support and contribution of my *Aama*. I am very grateful to my *Dada* who has relentlessly supported me and took care of my education since a very early

age. I would also like to thank my *Bhauju* who has become an important part of our family. *Baba* has also extended to me much needed support. I would also like to thank all the relatives for their love and support.

I really appreciate the company of my *Guitar* with which I sort of conversate. Playing guitar takes me away from everything and brings peace and calmness to me. I forget everything in that moment of joy.

Lastly, I would like to thank my partner *Kinchok Choden* for standing by me no matter what. It has only been a decade since the two of us together and I already see you with me for decades to come.

- Navin Subba

This Page Intentionally Left Blank

SYNOPSIS

Name of Student:	Navin Subba
Roll No.	14107285
Degree for which submitted:	Ph.D.
Department:	Chemistry
Thesis Title:	Time-Resolved Spectroscopic Investigation of Structure and Dynamics of Deep Eutectic Solvents
Name of Thesis Supervisor:	Professor Pratik Sen
Month and year of thesis submission:	March 2021

The goal of this thesis is to understand the structure and dynamics of deep eutectic solvents (DESs), which is relatively a new class of solvent. It is the mixture of two or more compounds that are usually solid and interact with each other, primarily via hydrogen bonding. DESs are liquid at operating temperature (usually room temperature) as a result of massive depression of freezing point through intermolecular interaction, apart from the concentration effect (i.e. colligative property). Here, I explored the heterogeneity aspect of various DESs using time resolved spectroscopic techniques. Specifically, rotational, translational and solvation dynamics and their temperature dependence has been explored in different classes of DESs (ionic, non-ionic and hydrophobic). To assess the hydrodynamic theory in DESs, the time constants associated with each of these dynamics have been analysed to determine the nature of coupling with the medium viscosity. Finally, activity of an enzyme was investigated in hydrated non-ionic DESs.

Summary of the work done

(a) Temperature-Dependent Ultrafast Solvation Response and Solute Diffusion in Acetamide–Urea Deep Eutectic Solvent

Temperature dependent ultrafast solvent response of a non-ionic DES based on acetamide and urea [0.6 CH_3CONH_2 + 0.4 $CO(NH_2)_2$] was investigated using femtosecond transient absorption (TA) and optical Kerr effect (OKE) spectroscopy. Translational diffusion of a fluorescent probe in the same DES was also studied at various temperatures using fluorescence correlation spectroscopy (FCS). These were used to study the viscosity coupling of the measured relaxation times and thus to verify

the dynamical heterogeneity aspect of this medium. From FCS study the translational diffusion time of a solute in the DES found to show a fractional viscosity dependence, with exponent 0.758, which, when compared with the viscosity–diffusion relationship for the same solute in common molecular solvents, suggests moderate deviation from the Stokes–Einstein relation. The solvent response have been found to be triexponential in nature, dominated by a ∼100 fs component. The other two components are characterized by time constants in ∼5 and ∼50 ps regimes. Subsequent comparison with the femtosecond OKE measurements suggests that the relatively slower picosecond solvation components originate from the reorientation of the solvent molecules, while the subpicosecond solvation response arises from the participation of the collective low-frequency solvent modes (such as intermolecular vibrations and librations). We find that the rotational diffusion lifetimes also exhibit fractional power dependence on medium viscosity and thus deviate from the Stokes–Einstein–Debye prediction. All of these results therefore suggest that the non-ionic acetamide–urea DES is a moderately heterogeneous medium.

(b) Partial Viscosity Decoupling of Solute Solvation, Rotation, and Translation in Lauric Acid/Menthol Deep Eutectic Solvent: Modulation of Dynamic Heterogeneity with Length Scale

My next choice of DE was a less studied hydrophobic DES prepared from lauric acid and menthol (LA/Men DES). Here, I have examined the structure and dynamics of LA/Men DES through steady-state emission, solvation dynamics, time-resolved fluorescence anisotropy, and translational diffusion dynamics. The zero shift in the emission spectra of coumarin 153 (a solvatochromic dye) as a function of the excitation wavelength suggests that LA/Men DES is spatially homogenous. Decoupling (p = 0.63) of the average solvation time $\langle \tau_s \rangle$ from medium viscosity suggests the presence of dynamic heterogeneity in the system. Rotational time $\langle \tau_r \rangle$, which reflects the nature of the first solvation shell, shows little decoupling (p = 0.81), suggesting it to be fairly dynamically homogeneous at a shorter length scale. An Arrhenius-type analysis also proves that rotation is mainly controlled by medium viscosity. Translational diffusion time $\langle \tau_D \rangle$ which provides information at a larger length scale, is found to be strongly decoupled from medium viscosity (p = 0.29). This indicates that at a larger length scale, the DES is quite dynamically heterogeneous. The slow component of solvation time, which is believed to originate at a larger length scale, correlates well with the

translational diffusion timescale having similar activation energies. This suggests that their origin is same. Expectedly, for the long component of solvation time, the decoupling is quite strong (p = 0.30). Overall, the study demonstrates the structure and dynamics of the LA/Men DES, and the existence of length scale-dependent heterogeneity has been proposed. The finding of this study should definitely invite the study of this DES with scattering experiments and simulations to complete the picture.

(c) Sub-picosecond Solvation Response and Partial Viscosity Decoupling of Solute Diffusion in Ionic Deep Eutectic Solvents

Previous solvation dynamics study (with 70 ps instrument response) of DESs based on acetamide and LiBr/NO_3 missed about 50 % of the Stokes shift dynamics despite considerable bulk viscosity. Here, fluorescence up-conversion (~250 fs instrumental response) coupled with time correlated single photon counting measurements was used to explore the complete Stokes shift dynamics of a dipolar solute probe, coumarin 153 (C153), in several ionic acetamide deep eutectic solvents (DESs) that contained lithium nitrate/bromide/perchlorate as electrolyte. Combined measurements near room temperature reflected a total dynamic Stokes shift of approximately 800–1100 cm^{-1} and triexponential solvation response functions. Interestingly, the average rate of solvation became faster upon successive replacement of bromide by nitrate in these deep eutectics, and a sub-picosecond time scale emerged in the measured solvation response when bromide was fully replaced by nitrate. Temperature dependent solute diffusion in these deep eutectics at the single molecule level using FCS, revealed pronounced fractional viscosity dependence of the solute's translational motion. Subsequently, this partial decoupling of solute translation was attributed to the micro-heterogeneous nature of these ionic DESs after examining the diffusion–viscosity relationship of molecular solvents at room temperature and in a liquid amide solvent at different temperatures.

(d) Rational design, preparation and characterization of a ternary non-ionic room-temperature deep eutectic solvent derived from urea, acetamide, and sorbitol

Although DESs have emerged as an excellent alternative solvents, most of the DESs reported are ionic, and to the best of our knowledge, only a handful of non-ionic DESs are available, which are liquid at room temperature. Non-ionic DESs may be desirable in applications such as organic synthesis because many reactants might not dissolve in ionic media. Here, we rationally design and report a new ternary non-ionic DES comprising of acetamide, urea, and sorbitol, which is liquid at the room temperature. I

reported temperature dependent refractive index (n_D), sound velocity (u), density (ρ), and dynamic viscosity (η) in this DES. This study shows that the third component in the DES has a strong impact on its physico-chemical properties.

(e) Correlating Bromelain's Activity with its Structure, Active-site Dynamics and Media's Physical Properties in a Hydrated Deep Eutectic Solvent

DESs have been shown to be biocompatible and therefore, emerging as a new media for bio-catalysis. Biomolecules like proteins haven been shown to be stable in DESs while retaining its activity. However, only few studies have been devoted to understand the structure and activity of proteins in DESs. This work represents a systematic study deciphering the behaviour of bromelain in a ternary DES with a composition of acetamide:urea:sorbitol = 0.5:0.3:0.2 (0.5Ac/0.3Ur/0.2Sor) along with various degree of hydration. The purposefully chosen DES here is non-ionic and liquid at room temperature. It provides us a unique opportunity to contemplate protein behaviour in a non-ionic DES for the very first time. I chose bromelain as the model enzyme for this study. The result infers that at low DES concentration (up to 30% V/V DES), bromelain takes up a more compact structural conformation; whereas at higher DES concentration; it becomes somewhat elongated. Microsecond conformational fluctuation time around the active-site of bromelain gradually increases with increasing DES concentration, especially beyond 30% V/V. Interestingly, bromelain retains most of its enzymatic activity inside DES, and at some hydration level it is even higher as compared to that in buffer. Furthermore, we correlate bromelain's activity with its structure, active-site dynamics and media's physical property. Our results demonstrate that compact structural conformation and flexibility of active-site of bromelain favours its proteolytic activity. Similarly, an increased polarity and decreased viscosity of the medium is favourable for its activity.

THESIS OUTLINE

This thesis is divided into following chapters.

Chapter 1. In this chapter, DESs has been introduce.

Chapter 2. This chapter briefly describes the experimental techniques that have been employed to study DESs. Data analysis and sample preparation methods have also been discussed in brief.

Chapter 3. This chapter describes the first ever study of ultrafast solvation dynamics in DES using femtosecond transient absorption spectroscopy and Optical-Kerr effect spectroscopy. Diffusion nature of a fluorescent dye has also been investigated.

Chapter 4. In this chapter, various dynamics such as rotation and translation of solute in hydrophobic DES have been studied along with the solvent dynamics. Micelle-like structure has been proposed from the results of these dynamics.

Chapter 5. In this chapter, solvation dynamics of acetamide based ionic DESs using fluorescence up-conversion and TCSPC has been investigated. Also, nature of translational diffusion of a fluorescent probe in these DESs has been compared with common solvents.

Chapter 6. (a) This chapter reports synthesis of new ternary non-ionic DESs. Temperature dependent physical properties of this DESs have been reported at several mole fractions.

(b) This chapter describes the correlation of activity of an enzyme with its structure and dynamics and with various solvent properties to understand why it remains active inside a hydrated DESs.

Chapter 7 Concluding Remarks and Future Prospects

This Page Intentionally Left Blank

Table of Contents

Chapter 1

Deep Eutectic Solvents – A Survey

1.1 Brief Introduction – Solvents

Chemistry without solvents is unimaginable and therefore, a discussion on the importance of solvents should precede the discussion of deep eutectic solvents (DESs). Solvents are important part of numerous processes in laboratory and beyond.[1-4] In the world of living organisms, water acts as solvent and facilitate vital processes.[5] In laboratories, solvents are primarily used as media for chemical reaction and extraction. Solvents are not just there but they interact with the solute (i.e. solvation) and control the chemistry. There are wide variety of solvents and they are classified on the basis of various parameters and properties.[4] For example, molecular solvents and ionic liquids are differed on the basis of the intermolecular interaction. On the other hand, polar and non-polar solvents are classified based on the dielectric constant and refractive index.

Water is "*The Best*" of all the solvents from the viewpoint of toxicity and its solvating and dissolving power which makes it the most important solvent in green chemistry. It is known as "*Universal Solvent*" as it can dissolve a wide spectrum of solute molecules. Even the reaction of hydrophobic solutes can be accelerated in water which is the result of hydrophobic effect.[6-9] This was specifically shown for the first time when famous Diels-Alder reaction was carried out in water.[10] Since then, use of water even in organic chemistry is widespread.[11,12] Nevertheless, use of water also comes with limitations and drawbacks.[13] There are many catalysts, reagents and reactants that are not stable in tolerate water. *Tert*-butyl lithium, a common strong base used in organic synthesis reacts violently with water. Apart from this, many organic reactants cannot be solubilized in water.

Apart from water, most of the conventionally used are organic solvents and their ease and extent of usability is wide. Obviously they are preferred because of their specific physic-chemical properties and easy availability. However, many of them have serious disadvantages like negative environmental impact, bio-incompatibility and toxicity. Many of the organic solvents are volatile (results in atmospheric pollution) and flammable. Among the organic solvents, chlorinated solvents are quite popular in use in the laboratories and a recent review by Jordan et al. has highlighted their advantages, disadvantages.[14] They also highlighted alternatives of chlorinated solvents. All the disadvantages set the foundation for the development of green chemistry[15-17] and a need for green solvents. Of course, the best alternative to these solvents is not to use solvents at all or to minimise its use or use innocuous solvent according *principle 5* of green chemistry.[18] However, the development of solvent-free

chemistry or solvent-free synthesis (mechanochemistry) is still in infancy or limited to some synthetic procedures.[19-22] Worst still, many reaction do not proceed at all in the absence of the solvents. The use of microwave reactor and ball mill enhances the rate of chemical reactions but they are not in widespread use.[15,23-26] This makes the future of solvent-free synthetic era uncertain. Keeping in mind the drawbacks of conventional solvents, many alternatives have been developed. However, these alternative solvents too have challenges and drawbacks, which will be briefly discussed below.

Supercritical fluids (e.g. supercritical water and supercritical CO_2) are a class of alternative solvents that is widely used in synthetic chemistry.[27] In fact, *Chemical Reviews* has dedicated its second issue of volume 99 (1999) to supercritical fluids. Supercritical fluids are formed at temperature and pressure above its critical point where gaseous and liquid phases do not co-exist.[28] Intermolecular space in supercritical fluids is greater than that in normal liquids. Therefore, diffusion coefficient of solute is much higher in such systems. Also, the viscosity of supercritical fluids is lower than normal solvents. This makes it an ideal solvent for many applications. However, the handling of supercritical fluids require sophisticated instruments that makes its use "impractical" in day to day usage in laboratory and other applications.

Ionic liquids (ILs) are another class of alternative solvents which has gained tremendous attention and popularity in the last 3/4 decades. Earlier, ILs were expected to be go-to solvent for any application.[29] ILs indeed found many applications such as in chemical industry.[30] However, there are concerns regarding toxicity, biocompatibility and biodegradability of ILs. Besides this, ILs are quite costly. Therefore, ILs may not be answer to the call for green and sustainable alternative solvents. Kunz et al. has asserted that ILs are not as promising as hyped by huge number of publications.[31] Nevertheless, ILs are finding applications in some specific area such as in lubrication etc.[32]

In recent years, DES has emerged as another alternative media. DESs have been touted as "*Green Solvents*" and presents several advantages over conventional and other alternative solvents. A quick search in "Scopus" with the term/phrase "deep eutectic solvent" gives an idea about the rapid progress in DESs based research activity. Figure 1.1 shows the number of publications/documents over the years which shows almost an exponential growth most of which have been published in the last 5-6 years. With the current rate of intense research on related to DESs, this class of alternative solvent will certainly find wider application than any other alternative solvents. DESs have been shown to resolve ~~to~~ the problem associated with

water sensitive reactions.[33] First phrase of the abstract of a paper by Mamajanov et al. reads "Hold the water!" highlighting that DESs as the most non-aqueous solvent where the "*structural integrity*" of the nucleic acids is preserved.[34]

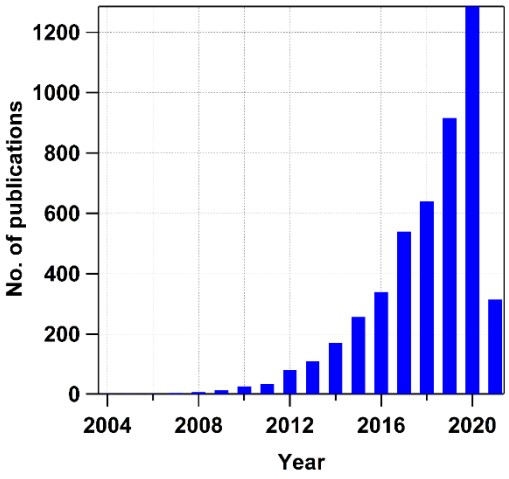

Figure 1.1 Number of publications/documents returned in scopus search which totals to 4743, with the key word "Deep Eutectic Solvent" as on 24th February 2021 (1440 hours IST).

Apart from exploring the applications and the physical science of DESs, DESs are now being linked to biological activity of the cell.[35] Verpoorte and co-workers have attempted to find the link between living cells and natural deep eutectic solvents (NADES).[35,36] Verpoorte argues that DES is the third phase in a living cells apart from lipid and water phase. This suggestion comes from the solubility experiment of variety of biomolecules and biopolymers in various DESs.[36]

Personally I believe that the formation of NADES in the cells and body of some animals (especially cold blooded) could explain how they survive extremely cold environment. For example, mountain stone wētā (*Hemideina maori*), an insect endemic to New Zealand can survive in sub-zero temperatures during winter months.[37] It can survive even though a large proportion of the water molecules in its body freezes.[38] Study by Sinclair et al. has confirmed that in this insect, intracellular freezing is avoided.[38] Perhaps formation of NADES by various molecules present in their cytoplasm prevents complete freezing of the fluid in the body of this insect to facilitate minimum metabolism for survival. A perspective by Gertrudes et al. has summarized the studies on how animals survive huge temperature variation[39] and relation with NADES which also somewhat backs up what I believe in the case of wētā. Certainly further studies are required to confirm angle of NADES formation that contributes to the survival of species.

1.2 Deep Eutectic Solvents (DESs)

The term "Deep Eutectic Solvents" was first used by Abbott et al. in 2003 to describe the eutectic mixtures of quaternary ammonium salts and amides which were liquid at ambient condition/temperature.[40] The most widely known eutectic mixture is that of choline chloride and urea at 1:2 mole ratio. The freezing point of this eutectic mixture is 12 °C which is very low (or deep) compared to the freezing points of the corresponding constituents, choline chloride (m.p 302 °C) and urea (m.p. 133 °C). And hence the term "Deep" is used instead of simply "Eutectic mixtures" or "Eutectic solvents". However, there is no demarcation on the extent of freezing point depression below which a eutectic mixture can be termed as a "DES". Figure 1.2 shows simple solid-liquid phase diagram for binary mixture and can be used to represent the phase diagram for DESs. Frequently ionic liquids (ILs) are compared with DESs (in terms of physical properties) and sometimes DESs itself is considered as a class of ionic liquids. However, they are different with ILs being pure compounds while DESs are mixtures. DESs has been defined as the eutectic mixture of Brønsted and Lewis acids and bases containing various anionic and/or cationic species.[41] DESs are characterized by huge depression of freezing point and are usually liquid around room temperature. Since the depression of freezing point is inherent nature/characteristic of any mixture system, it is difficult but important to assign whether a mixture is DES or simply eutectic mixture. For this, Coutinho and co-workers have defined DES as the mixture of two or more pure compounds having melting/freezing temperature of eutectic point below that of an ideal mixture.[42] It is also required that the depression of freezing point should render the mixture liquid state at operating temperature for a range of compositions. Although pure components of most of the DESs reported are solids, there are several DESs where one of the components is liquid.

DESs or not? The development of DESs is strongly linked to synthesis of certain ILs. While ILs are salts which are liquid at temperatures below 100 °C and represents pure compounds, the practice of preparing room temperature ILs using the mixture of salts is not new. For example, Hurley et. al. in 1951 reported one of the first ILs which was the mixture of ethyl pyridinium bromide and aluminium chloride.[43] ILs prepared by mixing 1-butyl-3-methylimidazolium chloride and Fe(II) and Fe(III) salts is another example.[44] Abbott's own work in 2001[45] reported the synthesis of 'moisture-stable' ILs comprising the mixture of quaternary ammonium salts and metal salts and this ILs have now been classified as a type of

DESs. Of course these mixtures, previously presented as ILs are different from ILs we know that comprises large organic cation (imidazolium, pyridinium etc.) and inorganic anions (halides, BF_3, PF_6 etc). So there is a grey area in classifying or defining these mixtures as illustrated by an argument in the literature.[46,47] The term "Deep Eutectic Solvents" was Christened with the introduction of a non-ionic molecule which acts as a hydrogen bond donor (HBD). Therefore, the presence of at least one non-ionic compound (preferably organic) in DESs makes it different from ILs prepared from mixing salts which solely consists of ionic species. Examples are mixtures of choline chloride with various organic molecules likes amides,[40] carboxylic acids and alcohols.[41] Most of the earlier generation of the DESs are mostly based on quaternary ammonium salts.[41] Recently, Coutinho and co-workers has disputed/suggested that choline chloride is actually unable to form DESs with fatty acids or alcohols[48] contrasting the report by Abbott el al. in which mixture of carboxylic acids and choline chloride was reported as DESs.[49] Coutinho suggests that a complete phase diagram is necessary to assign whether a mixture is DES or simple eutectic mixture. I shall not delve into judging whether the mixed systems that I have studied or studied by others is DESs or not. This is beyond the scope of this thesis.

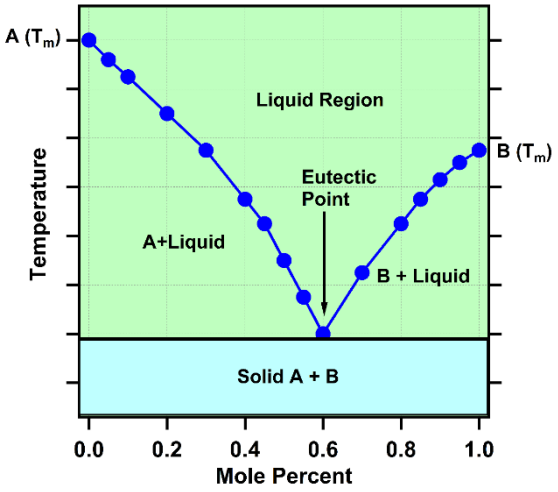

Figure 1.2 Solid-liquid phase diagram of binary component mixture.

1.2.1 Classification of DESs

Over the years many DESs have been reported and with growth in the number, it becomes necessary to organise and classify these solvents. Smith et al. has classified DESs into four types (I, II, III and IV) according to the constituents.[41] The general formula of DESs is given by

$$Cat^{+}X^{-}zY$$

In the above formula, Cat^{+} is usually an organic cations like ammonium, phosphonium etc. and X^{-} is a Lewis base (e.g. halide ions). Y is either Lewis or Brønsted acid and z is the number of Y interacting with X^{-} to form the complex.

Type I DESs are formed when Y is a metal chloride (MCl_x). Examples include mixtures of dialkylimidazolium chloride with aluminium chloride, iron chloride [Fe(II) and Fe(III)] and gold chloride.[44,45,50-52]

Type II DESs are formed if Y is hydrated metal chloride or metal chloride having water of crystallization. Anhydrous metal salts generally have high melting point and therefore the use of hydrated metal salts, which have relatively lower melting temperature, can be used to prepare DESs. Therefore *Type II* DES is just an extension of *Type I* DESs. Example include eutectic mixture of choline chloride and chromium (III) chloride.[53]

Type III DESs are the most popular among all as it is metal free, easy to prepare, stable to moisture and some are biodegradable. This type of DESs could be highly desirable for metal-free chemical synthesis and processes. Also, metal free DESs are important for few other reasons well described the Perspective by Gurkan et al.[54] *Type III* DESs are cost effective as most of the components are cheaply available. In *Type III* DESs, Y is a hydrogen bond donor (HBD). Common HBDs are amides, carboxylic acids, alcohols etc.[41] Carbohydrates like glucose, fructose have also been known to form DESs.[55-57] Given the huge availability of HBDs (some are naturally available), DESs with wide range of properties can be prepared. Interestingly, some of the choline chloride based *Type III* DESs are able dissolve variety of molecules like amino acids, metal salts and metal oxides.[40,58]

Type IV DESs are mixture of metal chlorides (MCl_x) and amides/alcohols. Unlike *Type I, II* and *III*, the cation in this DES type is a metal ion. There are only limited metal ions available for this type of DESs. Examples are eutectic mixtures of $ZnCl_2$ with amides (urea and acetamide) and alcohols (ethylene glycol and hexanediol).[59] Recently, Hammond et al. have reported DESs synthesized from lanthanide nitrate hydrates and urea.[60] Since heavy atoms are involved in these DESs, the density is quite high (>1.7 gcm^{-3}).

Type V DESs have been introduced recently by Coutinho and co-workers.[61,62] These are phenol or phenolic compound based DESs and are non-ionic and hydrophobic in nature. *Type V* DESs are formed because of resonance effect and subsequent hydrogen bond formation by phenolic

OH with other component. Examples in this category includes mixture of thymol and menthol. Eutectic mixture of salol and lidocaine[63] was known before *type V* was established as a class of DESs.

1.2.2 Hydrophobic and non-ionic DESs

Type I, II, III and *IV* DESs are ionic and therefore, most of them are water soluble and hygroscopic. Because of this, the use of these DESs becomes limited only to certain applications. Of course, *Type V* DESs are hydrophobic and non-ionic but only a handful of them are known. Few hydrophobic DESs were reported before *Type V* DESs was introduced formally. There has been an impressive progress in field of hydrophobic DESs in last few years.[64,65] One may ask why are they important? The importance of hydrophobic DESs can be understood from the viewpoint of green chemistry. For example, many of the organic compounds are soluble only in organic solvents, which are mostly not environment friendly. Same is true for the extraction and separation of important hydrophobic molecules from the mixture. Under such circumstances, water, which is the greenest solvent, is rendered useless. Hence, green hydrophobic solvents are highly desirable. Applications of hydrophobic DESs in the upcoming section highlights its importance. Kroon and co-workers in 2015 reported the first ever hydrophobic DESs based on quaternary ammonium salts (and therefore ionic) with long alkyl chains and decanoic acid (it is *Type III* DESs).[66] In the same year, Marrucho and co-workers reported hydrophobic eutectic solvents based on menthol and carboxylic acids with low viscosity.[67] Both the works highlighted the excellent extraction ability of these solvents from aqueous solutions containing dissolved solutes. In the subsequent years, many hydrophobic DESs have been reported.[64,65] In general, viscosities of hydrophobic DESs have been found to be relatively less compared to other DESs.

1.3 General Properties of DESs

1.3.1 Non-Toxicity

One of the properties of an ideal green solvent is that it should be non-toxic. DESs have been touted as a green and biocompatible solvents probably because the constituents are usually benign. There are exception like ethylene glycol which is inherently toxic.[68,69] However, very few studies have been dedicated to this topic. Although incorporation of bacteria into the DESs was achieved in 2010 by freeze drying method.[70] Hayyan et al. in 2013 first reported the study of toxicity and cytotoxicity of choline chloride based DESs on bacteria and found that DESs have no toxic effect on them, but the cytotoxicity was higher than the aqueous solution of the

individual components.[71] However, study by the same group found that phosphonium based DESs have significant toxic effect on bacteria.[72] These studies have concluded that the charge delocalization through hydrogen bonding might contribute to the toxicity of the resulting DESs. Juneidi et al. extended the toxicity study to other living organisms (fungi and fish) and found that toxicity depends on the constituents of DESs.[73] They also found *Type III* DESs are least toxic while *Type I* DESs are most toxic. Most of the DESs showed biodegradability in water. Macário et al. further extended the study of cytotoxicity of quaternary ammonium based DESs on human skin cells and got mixed results.[74] Some of the DESs were compatible to human skin cells opening the possibility of DESs being used in cosmetic products. From these results, it cannot be concluded that DESs in general is non-toxic. Halder et al. suggested that least toxicity is offered by sugar alcohols and straight chain alcohols as hydrogen bond donors.[75] Yang has nicely summarised the toxicity and biodegradability of DESs in his book chapter.[76]

1.3.2 Stoichiometry

The mole fraction of the constituents certainly plays a crucial role in the formation of DESs. In the case of binary mixtures, 1:2, 1:1, 1:1.5 or 1:3 are common. So definitely a question arises whether a complex of specific stoichiometry is formed in DESs, especially if one of the constituents is a non-ionic hydrogen bond donor. Earlier, it was assumed that a complex of specific stoichiometry is formed as a result of which DESs are formed.[77] This is intuitive as eutectic point of many reported DESs are at above mentioned mole ratio. Alizadeh et al. studied the effect of composition on the structure of DESs of choline chloride and ethylene glycol using *Ab Initio* molecular dynamics (MD) simulation.[78] They found that changing the mole fraction results in the change in the rigidity of the hydrogen bond network. At some mole fraction, hydrogen bond network is flexible and the authors have speculated that this could be the reason for lower melting point at a particular mole fraction.

1.3.3 Viscosity

Viscosity is very important property of a solvent and it dictates the possibility of finding the application. In general, the viscosity of DESs are relatively higher compared to conventional solvents and are comparable to that of ILs. Of course it depends on the constituents. There are many non-ionic hydrophobic DESs (mainly terpene and carboxylic acid based) for which viscosity is very low compared to ionic DESs.[41,64,67,77,79] Viscosity could be a reflection of the magnitude of interactions between the constituents and best explained if one of the constituents is liquid. For example, DESs comprising of choline chloride and liquid alcohols such as

ethylene glycol and glycerol which act as hydrogen bond donor. The viscosity of DES of choline chloride and ethylene glycol is more than that of pure ethylene glycol itself whereas the viscosity of DES of choline chloride and glycerol is less than that of pure glycerol. These opposite results tells us that in some cases, the interspecies/intermolecular interaction may become weaker or stronger compared to that in pure components.[80-85] It is thought that in the case of ethylene glycol, new hydrogen bonds are formed which are stronger than intra and inter molecular hydrogen bonds in ethylene glycol molecules.

Abbott et al. has presented the application of hole theory for designing ionic liquids and DESs.[86-88] According to hole theory, holes (which are voids or empty spaces) are present in a molten ionic compounds or molecular liquids. The holes are of various sizes and are in constant flux. For the liquid to have good fluidity, the size of the diffusing ions or molecules must be relatively small or comparable to that hole. Since hole size is related to the surface tension of the liquid, holes with large size can be obtained by preparing liquid with low surface tension. This can be achieved by using long chain alky moieties.

1.3.4 Polarity

Polarity is probably the most important property of a solvent after viscosity. Polarity of the DESs have been (qualitatively) assessed with electronic spectroscopies (absorption and fluorescence spectroscopy). Absorption spectra of Reichardt's dye (betaine dye 30) has been extensively used to qualitatively assess the polarity of solvents.[89,90] Betaine dye shows negative solvatochromism resulting in large red shift of the absorption spectra with decreasing polarity. Using absorption maximum of this dye, $E_T(30)$ polarity scale is constructed and more often normalized ($E_T^N(30)$) scale is used taking water as the most polar (E_T^N=1) and tetramethylsilane as the least polar (E_T^N=0) medium. A comparison of polarities of some of the normal solvents, ILs and DESs can be found in reference 91. Abbott et al. found E_T^N to be >0.8 for choline chloride and glycerol mixtures.[92] Pandey et. al. also assessed the polarity of choline-chloride based DESs and found E_T^N to be about 0.8 which makes choline chloride based DESs quite polar.[93] They found the DESs containing alcohols as HBDs are slightly polar compared to HBDs of other functionalities (carboxylic and amide). Florinda et al. has also studied polarity of both hydrophilic and hydrophobic DESs.[94] Surprisingly, it was found that even for hydrophobic DESs based on menthol and quaternary ammonium salt, E_T^N values were quite high (~0.65-0.74) indicating polar nature. Overall, $E_T^N(30)$ scale shows DESs are polar compared to common solvents.[89]

1.3.5 Density

Density is another important property of any material and gives qualitative idea as to how good the packing is among the constituent molecules. Most of the DESs have densities (>1.1 gcm^{-3}) higher than water and most of the other common solvents.[77] As expected, densities of lanthanide based DESs are quite high as mentioned earlier.[60]

1.4 Mixture of DESs and Common Solvents

It is important to discuss the mixture of DES and common solvent although there is no study of the said system in the present thesis. ILs have also been studied in the presence of other conventional solvents.[95] There are at least two reasons to study and understand the mixture of a DES and a common conventional solvent. First, many of the DESs (particular one with the ionic components) are quite hygroscopic in nature and naturally water will almost be present in the system when exposed to the atmosphere. Second, barring few, the viscosity of DESs in general is very high compared to conventional solvents. This will pose major problem for DESs to be used as solvent in many applications. For example, in the application of DESs as extraction media, if the viscosity of the solvent is high, mass transfer to solvent becomes difficult. Also, solute dissolution might be challenging if the viscosity is high in certain applications. Problem associated with the dissolution might be solved to some extent by raising the temperature. This, however, might not be good solution for the samples sensitive to high temperatures. There are several reports where researchers have resorted to addition of certain quantity of other conventional solvents, thereby reducing the viscosity, and still reaping the benefits of DESs. Common conventional solvents like water, ethanol and DMSO can be added depending upon the requirement. Water is preferable when it comes to working with the biological molecules like proteins and DNA. Needless to say, water is "The Green Solvent" and therefore preferable over other solvents. Duan et al. added small amount of water to DES to reduce viscosity (and also probably to further lower the freezing temperature of the mixture) for the extraction of various bioactive natural products.[96] With the addition of conventional solvent a natural question arises that is, does DES remains as DES or becomes solution of the constituent components? And how does the structure and properties of DES change or affected? There are few reports that suggests that the structure (and therefore interaction) of DESs remain unaffected or retained in presence of additional solvents up to certain concentration. Hammond et al. studied the evolution of structure of urea and choline chloride DES at various degree of

hydration using neutron scattering and empirical potential structure refinement.[97] It was found that even very small amount of water does alter the structure of DES. However, the nanostructures of the DES is retained despite the presence of water up to certain concentration. They also studied malic acid and choline chloride DES in presence of water using neutron scattering and quasi elastic neutron scattering (QENS) and found that the DES structure is retained under hydrated condition.[98] Other experiments[99] and simulations[100,101] also points toward the presence of cluster formation or segregation of water molecules up to certain concentration at least for choline based DES. A review by Ma et al. has nicely summarized the effect of adding water in ILs as well as DESs.[102]

1.5 DESs vs Ionic Liquids: Which is better?

As DESs and ILs share many similar properties, they are often compared.[103] ILs have been known for a long time and the related studies are still active. DESs have been known only for less than two decades and only in the past 6-8 years, the research interest has increased significantly. These two classes of solvents share many similar physical properties.[103] Both of them have lower vapour pressure which makes them environment friendly. However, DESs are easy to prepare and cost effective.[40] ILs synthesis is much more complex involving multi-steps and requires purification.[31,103] On top of this, many of the starting materials are costly. Because of this, use of ILs becomes economically unviable on a large scale basis. For DESs, purification and separation are not required at the end. Also, many of the raw materials are relatively cheaper and are naturally available. Toxicity has already been addressed in earlier section, but one can choose environmentally and biologically benign starting materials to make DESs have less negative impact on the environment.

1.6 Preparation Methods of DESs

DESs were first prepared by heating method,[40] which is the most widely used method as of now. Heating method is not desirable as in some cases, it leads to unwanted side reactions. Florindo et al. found that heating method leads to side products when preparing DESs of choline chloride and carboxylic acids. To overcome this issue, grinding method has been developed.[104] Subsequently, several other unconventional methods have been developed in recent times to prepare DESs which are summarized below.

a. Heating[40]
b. Grinding[104]
c. Freeze-drying[105]

d. Vacuum evaporation method[106]
e. Twin screw extrusion method[107]
f. Microwave irradiation method[108]
g. Ultrasound-assisted method[108]

1.7 Applications of DESs

DESs find a wide range of applications including as a reaction media,[77,109] material synthesis,[77] battery recycling,[110] metal processing,[41] metal plating,[41] CO_2 capture,[41, 111] extraction media[112] and media for biotransformations.[77] Although DESs emerged as new type of solvent in early 2000,[40] however its potential as a versatile solvent has only been realized in the past decade (figure 1.1). There are number of reviews summarizing various aspects of DESs.[41,42,64,65,77,91,113,114] Few of the application of DESs will be discussed briefly in this section to highlight, realize and appreciate the importance of these solvents in the present and the future. Many other important applications related to CO_2 capture, metal plating and other miscellaneous will not be covered in the discussion.

1.7.1 Extraction Media

DESs have huge potential as extraction media of important molecules.[112] This is reflected in a number of reports with promising results for various applications. Some of the important extraction processes are briefly discussed below.

Extraction-Desulphurization. Organosulphurs present in the fuels are a major concern as it produces sulphur dioxide upon combustion, which is one of the main culprits of the pollution. Therefore huge emphasis is given to desulphurization of fuel. However, traditional methods are not efficient in terms of cost and energy.[115] Recently, the use of DESs as desuphurization medium has gained momentum and this class of solvent have been shown to be quite effective and efficient in extraction-desulphurization of model fuels.[116] For example, Li et al. showed that DES comprising of formic acid and tetrabutyl ammonium bromide is effective in removing sulphur compounds (thiophenes) from model fuel.[117] Several other works have also shown that DESs is effective and efficient in the extraction-desulphurization[118-121] compared to traditional methods.[115]

Metal Extraction/Removal. Heavy metal contamination of water could be health and environmental risks. On the other hand, some metals are valuable and economically important. Therefore, recovery or extraction of metals from water becomes important. In this context,

DESs have been shown to be efficient.[122-125] DESs have shown to efficiently remove cadmium from rice flour.[126] Recently, an enhancement in the lithium extraction method was reported by a "*synergistic*" DES (binary mixture) from a solution containing sodium and potassium ions.[127] In synergistic DESs, both the components of DES are involved in complex formation with the metal ion and thereby, enhances the extraction. Exploring DESs for metal extraction/removal application is still an ongoing field and DESs may play a major role in future.

Bioactive molecule extraction. Extraction of biologically active molecules from various sources is crucial to food, cosmetic and pharmaceutical industries.[128] Several methods of extraction exists including solvent extraction which uses organic solvents.[128] Depending upon the polarity of the bioactive molecule, either hydrophilic or hydrophobic DESs have been used for extraction.[96] Nam et al. in 2015 reported enhanced extraction of flavonoid from biomass using proline/glycerol DES.[129] They also observed that the efficiency of DES is better than methanol as extraction media. Similarly, Cao et al. employed hydrophobic DES to extract Artemisinin, a very important drug against malaria, from *Artemisia annua* leaves.[130] In this case too, extraction efficiency of DES was found to better than conventional petroleum ether. Recently, Cao et al. has developed two-phase solvent system using hydrophilic and hydrophobic DESs for simultaneous extraction of bioactive compounds.[131] This is helpful if biomass contains several bioactive molecules. Depending upon the polarities of bioactive molecules, they can be simultaneously extracted using two-phase solvent system.

Water Purification. The ability of DESs to extract/remove metals and bio-molecules from aqueous solution can be used to clean water. Water pollution is a major concern globally and pollution due to micropollutants are increasingly worrisome.[132] Micropollutants from various sources end up in the water bodies most of the time and if wastewater is not treated properly, level of micropollutants in water bodies will reach to a toxic level. Therefore, purification of water contaminated with micropollutants is necessary for health and environmental point of view.[133] In this context, Marrucho and co-workers have reported the extraction of selected micropollutants from water using hydrophobic DESs resulting in a cleaner water.[134-136] They also regenerated the DES by activated charcoal treatment for sustainable use.[134]

1.7.2 Reaction Media

Organic synthesis. The biggest success DESs can achieve will be its extensive use in organic chemistry and in chemistry in general as a solvent replacing conventional organic solvents. Use of DESs in organic synthesis is gradually growing.[91,137] Shankarling and co-workers in 2010

used DES for efficient bromination of 1-aminoanthra-9,10-quinone.[138] The same group also carried out Perkin reaction in DES in mild condition without using catalyst and yet, yield was better.[139] Marullo et al. investigated Diels-Alder reaction in various DESs in which ultrasound was used to promote the reaction. It was found that the yield of product was better than in conventional solvents.[140]

Nanoparticle and materials synthesis. DESs are proving to be important solvent in the synthesis of nanomaterials.[141,142] Liao et al. have reported shape controlled synthesis of star-shaped gold nanoparticles in DES.[143] Also, they were able to tune shape as well as size by changing the amount of water content in DES. Recently, Exposito et al. reported sustainable synthesis CeO_2 nanoparticle in choline chloride/urea DES.[144]

1.7.3 Bio-fuel Production

In the production of bio-fuels like ethanol, effective pretreatment is essential for economic viability and sustainability.[145] Pretreatment involves the conversion of biomass to a simpler form and therefore enables the hydrolysis of biopolymers like cellulose by enzymes. Sugars obtained from the hydrolysis is used to produce ethanol via fermentation. DESs have shown excellent capability in the pretreatment of biomass.[146-148] Biomass contains other polymers like lignin which hinders the efficiency of the bio-fuel production[145] needs to be removed to increase the efficiency. Once the pretreatment is complete, DESs is usually washed to avoid its impact on enzymes and microbes used for fermentation.[146,147] However, Xu et al. showed certain DESs are compatible with hydrolytic enzymes and microbe used for fermentation.[148] This further increases the sustainability of bio-fuel production.

1.8 Proteins and Enzymes in DES

Proteins are bio-macromolecules made up of amino acids that are primarily stable in water and buffer solutions.[149] Because of this, applications of many important enzymes are limited to water and buffer solutions. In the past decade, several reports have emerged indicating that proteins retain its structure and function in certain hydrated and non-hydrated DESs. In some cases, proteins were found to be more stable in hydrated DESs than the pure DESs. In some DESs, hydrogen bond donors like urea are present which beyond certain concentration denatures proteins. Despite this anticipation, Gorke et al. in 2008 showed hydrolase-catalyzed biotransformation of ethyl valerate to butyl valerate (transesterification) in choline chloride/glycerol DESs.[150] Since then, similar biotransformations in DESs have already been reported[151-153] and these enzyme catalysed reactions show that enzymes and proteins retain the

activity in a solvent other than water. However, there was a lack of understanding about the conditions in which these proteins retain its structure and function. Nardecchia et al. studied the phase behaviour of synthetic protein in DES composed of urea and choline chloride and found that DES stabilized the collapsed state of the protein.[154] Esquembre et al. studied thermal folding of lysozyme in DESs (choline chloride and urea/glycerol).[155] Secondary and tertiary structure of lysozyme remained intact in pure DESs at room temperature. However, protein's thermal stability as well as folding reversibility decreased in pure DESs. In hydrated DESs, reversibility of lysozyme activity is recovered. Zeng et al. showed that DES based aqueous two-phase system is a potential media for protein extraction using bovine serum albumin (BSA) although they could not 'back-extract' protein from DESs.[156] Sanchez-Fernandez et al. studied conformation of proteins (BSA and lysozyme) in DES and mixture of DES and water.[157] This study found that secondary structure of the proteins is minimally affected on solvent transition from buffer to DES. It was also found that although protein folding is similar in both buffer and DES/water mixture (up to 75 wt% of DES), in pure DESs, BSA denatured irreversibly when heated to 80 °C. Apart from proteins, other bio-macromolecules like DNA and RNA are also known to retain functional abilities in DESs[34,158] which will not be discussed here.

1.9 Heterogeneity

The concept of heterogeneity has long been associated with glass forming liquids (like ortho terphenyl and glycerol),[159,160] polymers,[161,162] ionic liquids,[163-166] and binary mixture[167,168]. DESs have also been shown to be heterogeneous as discussed in the next section and therefore warrants a brief discussion about heterogeneity in the present thesis. General meaning of the term "Heterogeneity" is the distribution or diversity or non-uniformity of some quantity or property. Common solvents as we understand are said to be homogeneous as the properties (such as viscosity, diffusion coefficient, density, polarity etc.) measured in any region (with length scale larger than the molecular dimension) in space are same. Intuitively, these properties should be invariant to the region where it is measured. Surprisingly, the same is not true for some liquid families and even few common solvents like water[169,170] at supercooled state, even though they appear to be homogeneous. In the context of some ILs, it is easier to understand what the heterogeneity is? In many ILs, because of the presence of ions as well as long alkyl chains, polar and non-polar domains are formed.[163,171] This is an example of heterogeneity due to environment. The study of dynamics in supercooled liquids and glasses led to the idea of heterogeneity due to dynamics and this has been excellently reviewed by Ediger[172] and Richert[173] (After these two reviews, there have been so many publications in

regards to heterogeneity, both experimental and non-experimental (theory and simulation). Therefore, I feel it is high time to review and revise the topic once again). Therefore, in the case of supercooled liquids, heterogeneity arises because of different dynamics. It has been recognized that the difference in dynamics is the outcome of structural or spatial heterogeneity. As a result, the terms "Spatial Heterogeneity", "Dynamic Heterogeneity", "Spatially Heterogeneous Dynamics", "Heterogeneous Dynamics" and "Temporal Heterogeneity" found are often used interchangeably. The term "Temporal Heterogeneity" was used by Kaufman and co-workers to account for the evolution or change in the dynamics of a specific spatial region over time.[174] The idea of heterogeneous dynamics arose from the observation of the non-exponential relaxation processes (following perturbation) in bulk experiments.[172,173] The correlation or relaxation functions associated with the molecular motions (such as translation, rotation or reorientation etc.) becomes non-exponential in nature as the glass transition temperature is approached. This non-exponential relaxation can often be described by stretched exponential or Kohlrausch–Williams–Watts (KWW) function

$$C(t) \approx \exp[-(t/\tau)^{\beta}], \ \beta < 1 \qquad 1.1$$

This implies that there is a distribution of relaxation times. The observation of non-exponential decay can be explained by taking two extreme scenarios of the relaxation processes. In the first scenario, one can think of system relaxing intrinsically non-exponentially with the same rate in all the different locations of space. This situation indicates dynamic homogeneity. The other scenario is where the system is relaxing exponentially at different rates at different regions in space. This situation is dynamic heterogeneity. Most of the experiments support latter explanation for observation of non-exponential relaxation i.e. dynamic heterogeneity.[159,160,172-178] In fact Weeks et al. made direct imaging of structural relaxation using confocal microscope colloids.[179] Single-molecule and ensemble average experiments by Zondervan et al. also points towards heterogeneity.[180] Theoretical/simulation studies predict that the dynamics of nearby domains could differ by orders of magnitude.[172,173] As mentioned earlier, the terms dynamic heterogeneity and spatial heterogeneity are often used interchangeably and they represent the same phenomenon. However, it has been observed that the rate of relaxation of a particular region evolves with time (Temporal Heterogenegity).[159,174,181] That means a region represented by A is relaxing with a rate *x* and after some time, the same region relax at the rate *y* or we can say continuous transition of mobile region to immobile or less mobile region and vice-versa (inter-domain fluctuation). Therefore the term dynamic heterogeneity (apart from temporal heterogeneity) is particularly used by some to encompass this fluctuation of rate of relaxation

apart from spatial distribution of relaxation times.[182] If the time required for a region to evolve is very long i.e. if the exchange rate is slow, then the heterogeneity is static (static heterogeneity). The fluctuation must occur because of ergodic nature of supercooled liquids.[181]

1.9.1 Spatial Heterogeneity with Excitation Wavelength Dependence.

Red edge excitation shift (REES) is the red shift of fluorescence emission band upon excitation of the fluorophore at red edge of its absorption spectra.[183] REES is generally observed for viscous solvent usually at very low temperatures and known among spectroscopy community for a long time.[184-186] REES can be understood by comparing the lifetime of the fluorophore(τ_f) and the solvent relaxation time (τ_s). In a viscous liquid where the solvent relaxation is relatively slow ($\tau_f < \tau_s$), fluorophores have different configurations of solvent molecules that leads to the distribution of solvated states and some of the fluorophores have solvent configuration similar to that of a relaxed state. Therefore, the excitation at the red edge of the absorption band excites only those fluorophores with lower transition energy. Since the solvent relaxation is slower compared to the fluorescence lifetime, the configuration of the solvent molecules persists during the fluorescence lifetime. Therefore, the emission is red shifted. This simple technique has been exploited regularly for assessing the heterogeneity in solvents. Samanta and co-workers first observed REES in ILs[165,187] which they attributed to spatial heterogeneity. MD simulation by Hu et al. has confirmed the origin of REES as dynamic heterogeneity.[166] REES has also been observed in some DESs which shall be discussed in later section.

1.9.2 Heterogeneity and Viscosity Decoupling

Stokes Einstein (SE) and Stokes Einstein Debye (SED) equations relates diffusion coefficient, which is a microscopic property, to the viscosity, which is the bulk macroscopic property.[188] SE and SED relations are for translational and rotational diffusions, respectively. In supercooled liquids the dynamics have been found to be fractional power dependent on the temperature reduced viscosity and original SE and SED relations are not applicable.[169,170,172,173,188,189,190] According to SE or SED relation, diffusion coefficient is related to viscosity and temperature by following relation,[188]

$$D \propto \frac{T}{\eta} \qquad 1.2$$

As mentioned above, in many cases, including supercooled liquids, the relationship is best described by[169,170,172,173,191]

$$D_{Trans} \propto \left(\frac{T}{\eta}\right)^{p} \quad 1.3$$

where p≠1. This means that the dynamics (translation, rotation etc.) are decoupled from the viscosity. This decoupling of dynamics is indicative of the presence of dynamics heterogeneity. Although the "decoupling" has been used in the literature for the departure of diffusion from SE prediction, it does not mean that the diffusion is completely independent of viscosity, rather it is differently coupled.

Most studies on dynamic heterogeneity began with supercooled liquids near glass transition where the viscosity is very high and characteristic relaxation times are in the range of ~10^{-3} to ~10^{3} s.[192] Using solvation dynamics, Richert and co-workers showed that the heterogeneous dynamics is present in a glass forming liquid at temperatures much higher than the glass transition temperature.[192,193] At high temperatures, the viscosity of the liquid is low and relaxation rate is faster. At some temperature, the time scale of the relaxation becomes comparable to the lifetime of the fluorophore and at this temperature, they observed broadening of the spectra which could only be explained in terms of heterogeneity. In DESs also, heterogeneity has been observed at high temperatures where the dynamics is a lot faster (discussed in the later section). The time scale associated with the dynamics like solvation, rotation and translation can be measured and compared with the bulk viscosity to assess the decoupling and subsequently, heterogeneity. In SE and SED relations, it is the diffusion coefficient that is related to the viscosity. But sometimes, diffusion coefficient is difficult to measure and rather, the time associated with a particular dynamics is easier to measure and these two are inversely proportional to each other.

$$\tau_x \propto \frac{1}{D} \quad 1.4$$

And therefore, the following relation is usually analysed to ascertain the heterogeneity in literatures.

$$\tau_x \propto \left(\frac{\eta}{T}\right)^{p} \quad 1.5$$

Above equation 1.5 is used to ascertain the extent of dynamic heterogeneity of a system.

1.9.3 Analytical Derivation of Fractional Viscosity Dependence

Experimental observation of fractional power dependence of solvation, rotational and translational dynamics in heterogeneous systems is believed to be the result of dynamic heterogeneity of the system as suggested by Tarjus et al.[189] However a molecular level

understanding and physical interpretation is difficult to find in the literature. Towards this goal, Das et al. tried to give the physical interpretation of this assumption and gave an analytical expression to estimate dynamic heterogeneity.[194] In this interpretation, it is assumed that the system is dynamically heterogeneous and the probe is preferentially distributed in some domains that are responsible for dynamic heterogeneity. That means each local domains has its own viscosity.

Also, it is assumed that SE and SED relations are not violated within these domains. A visualization of this situation is given in figure 1.3 with domains represented by different shapes to denote different relaxation rates. For simplicity, only two micro-domains are which are different than the bulk region and they also are different from one another. The dynamics sensed by the probe in this different regions are different as depicted in the figure.

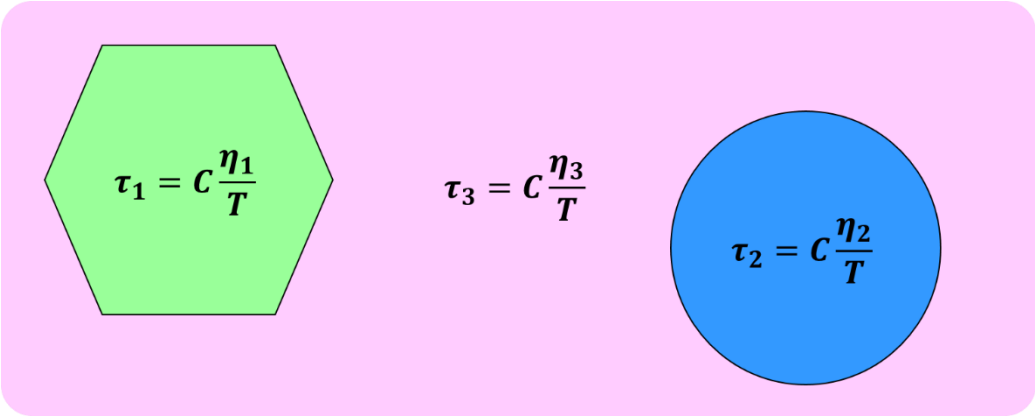

Figure 1.3 Depiction of dynamically heterogeneous system with domains of different viscosities.

If the probe is uniformly distributed in all the regions, the average relaxation time for any event is given by

$$\tau_{avg} = \frac{\sum_i x_i \tau_i}{x_i} \qquad 1.6$$

where τ_i is the relaxation rate in region 'i' and x_i is the amplitude of the contribution of region 'i'.

Similarly, the average viscosity is given by

$$\eta_{avg} = \frac{\sum_i x_i \eta_i}{x_i} \qquad 1.7$$

where η_i is the viscosity of region 'i'.

Combining the two preceding equations (1.6 and 1.7) with the assumption that SE or SED relation is valid in all the regions, we can rewrite the equation in terms of average quantities as

$$\log[\tau_{avg}] = \log\left[\frac{\eta_{avg}}{T}\right]+\mathrm{C} \qquad 1.8$$

Thus a plot of $\log[\tau_{avg}]$ vs. $\log\left[\frac{\eta_{avg}}{T}\right]$ will give a straight with slope of unity. In the present scenario η_{avg} is the same as η_{bulk} as the probe is present in all the locations, and η_{bulk} can be measured easily by a viscometer.

However, as assumed, if the probe is preferentially distributed in the micro-domains over the bulk regions (i.e. the probes are only in green and blue regions in figure 1.3), then the average viscosity is given by

$$\eta_{avg} = \frac{x_1\eta_1 + x_2\eta_2}{x_1 + x_2} = \eta_\mu \qquad 1.9$$

This average is not equal to the bulk (η_{bulk}) and has been termed as micro-viscosity (η_μ).

Using equations 1.9 in equation 1.8, we get,

$$\log[\tau_\mu] = \log\left(\frac{\eta_{bulk}}{T} + \frac{x_3}{(x_1 + x_2)T}(\eta_{bulk} - \eta_3)\right) + C \qquad 1.10$$

If the viscosity contribution from micro-domains in the above equation is negligible i.e. $\eta_{bulk} \approx \eta_3$, a plot of $\log[\tau_\mu]$ vs $\log\left(\frac{\eta_{bulk}}{T}\right)$ will be a straight line with the slope of unity. I believe this to be the case in normal molecular liquids and therefore it apparently looks homogeneous. Equation 1.10 can be simplified as

$$\log[\tau_\mu] = \log\left(\frac{\eta_{bulk}}{T}\right) + \log\left(\frac{\eta_\mu}{\eta_{bulk}}\right) + C \qquad 1.11$$

If the ratio $\frac{\eta_\mu}{\eta_{bulk}}$ has same temperature dependence, equation 1.11 becomes analogous to 1.8 i.e.

$$\log[\tau_\mu] = \log\left(\frac{\eta_{bulk}}{T}\right) + C \qquad 1.12$$

Here also, viscosity decoupling is not observed. On the other hand if $\frac{\eta_\mu}{\eta_{bulk}}$ has a different temperature dependence, a plot of $\log[\tau_\mu]$ vs $\log\left(\frac{\eta_{bulk}}{T}\right)$ will not yield a straight line with unity slope. Further Das et al. considered that temperature dependent viscosity follows Arrhenius relation.

$$\eta_{\mu,bulk} = \eta_\infty \exp\left(\frac{E_{\mu,bulk}}{RT}\right) \qquad 1.13$$

Using equation 1.13 in 1.11, we get

$$\log[\tau_\mu] = \log\left(\frac{\eta_{bulk}}{T}\right) + \left(\frac{\Delta E}{2.303RT}\right) + C \qquad 1.14$$

where $\Delta E = E_\mu - E_{bulk}$.

This equation predicts that as long as $\Delta E \neq 0$, the plot of $\log[\tau_\mu]$ vs $\log\left(\frac{\eta_{bulk}}{T}\right)$ will not give a straight line with unity slope. Note here that ΔE value can be calculated if one measure temperature dependent bulk and micro-viscosity.

Using equation 1.14, $\log[\tau_\mu]$ can also be numerically calculated for given value of ΔE and C over a range of temperatures. η_{bulk} can be calculated for each temperature assuming Arrhenius relation (equation 1.13) for a given E_{bulk}. Finally, plot of $Log[\tau_\mu]$ against $Log\left(\frac{\eta_{bulk}}{T}\right)$ can be fitted with equation 1.5 to estimate/predict p.

1.10 Structure and Dynamics of DESs – Literature survey

While structure and dynamics of molecular solvents, ILs and supercooled liquids have been studied extensively for a long time, DESs have not been studied to a similar extent in spite of the tremendous importance of DESs. Using pulsed field gradient NMR, Abbott et al. have studied the self-diffusion properties of different components of DESs.[195] It was found that choline cation in three DESs (choline chloride and urea/ethylene glycol/glycerol) diffuses slower that than the corresponding HBDs, which was found to be opposite in the DES with malonic acid as HBD. Also, the diffusion coefficient of the choline cation follow same correlation with the viscosity and temperature in the same three DESs except the one with malonic acid. This was attributed to the dimerization of malonic acid.

Many ionic DESs are known to be dynamically heterogeneous,[196-198] which has been recognized/established by observing the fractional power dependence of the diffusive molecular motions on solvent viscosity and temperature, that is, $1/D \propto (\eta/T)^p$ with $p < 1$ as mentioned in the earlier section.

Biswas and co-workers have been actively involved in the spectroscopic and simulation studies of DESs. The group first did fluorescence spectroscopic study of acetamide and sodium/potassium thiocyanates DES.[196] Solvation and fluorescence anisotropy results showed that solvation and probe rotation times were found to have fractional power dependence on bulk viscosity i.e. p=0.46 for solvation and p=0.65. Similar decoupling of dynamics was found in molten mixture of acetamide and lithium salts.[197] It is interesting to note that these

observations in DESs were found at temperatures much higher than their glass transition temperature. In these mixtures, excitation wavelength dependence of the fluorescence was observed. All these unusual results were attributed to solvent heterogeneity. Simulation study also indicates that heterogeneity is partly responsible for decoupling of the dynamics observed in these mixtures.[199] Strangely, Maroncelli and co-workers found $p \approx 1.2$ for solvation[200,201] and $p \approx 1$ for probe rotation[200,202] in ILs. Biswas group for the first time reported the spectroscopic and simulation study of non-ionic DESs comprising of acetamide and urea.[203,204] Probe rotation study using fluorescence anisotropy revealed that rotational diffusion of C153 adheres to SED relation.[203] Simulation results also showed that mean squared displacement of the particles followed normal distribution.[203] From these results it was concluded that non-ionic DESs might be dynamically homogeneous. However, Dielectric relaxation study of the same system found some degree of heterogeneity in this media.[204] Recently, partial decoupling of probe rotation from medium viscosity in ternary DESs of glucose, urea and water was observed.[205] This result indicates that the idea of non-ionic DESs being homogeneous cannot be generalized. Among non-ionic DESs, probably the difference lies in whether the system is associated (extensive H-bond network) or non-associated.

Samanta and co-workers also have studied DESs using various spectroscopic techniques. They studied translational diffusion of various fluorescent probes in various quaternary ammonium salt based DESs using fluorescence correlation spectroscopy (FCS).[206] The probes in all the DESs was found to undergo anomalous diffusion that was attributed to dynamic heterogeneity. Samanta group also studied probe rotation using fluorescence anisotropy in these media.[206] In these studies, different probe molecules were used which show different rotation behaviour, i.e. different extent of stick and slip boundary condition. This indicates that probe molecules reside in different environments where the interaction is different. The rotational diffusion time of the probe molecules in these media had fractional power dependence on the medium viscosity. The effect of alkyl chain length in the structure of DESs was also studied.[207] First they investigated the effect of chain length of HBD (diols) as well as the position of hydroxyl groups. Position of hydroxyl group in the diols was found to have insignificant effect on the heterogeneity aspect of the solvent. However, chain length of HBD had significant effect on the DESs, which is reflected in the excitation wavelength dependence of emission maxima of 2-amino-7-nitrofluorene (ANF), the magnitude of which increases with increasing chain length. This was attribution to spatial heterogeneity of the media that becomes pronounced with increase in the chain length of HBD. Similar result was obtained in the study of the effect

of alkyl chain length of cation (tetraalkylammonium bromide) i.e. heterogeneity becomes more pronounced with increasing alkyl chain length.[208] Samanta group has also studied nature of solvent dynamics of tetraalkylammonium bromide and ethylene glycol based DESs where two time constant were observed.[209] The fast time constant was found to be independent of medium viscosity and was attributed to ultrafast local dynamics. The slow time constant depended strongly on viscosity indicating diffusive motion as its origin. However, it is unclear how the slow time component arises from *heterogeneous dynamical processes* as mentioned in the conclusion.

Gautam et al. suggested that N, N-diethyl ethanol ammonium chloride and urea DES is more heterogeneous compared to choline chloride urea DES by measuring fluorescence quantum yield and fluorescence lifetime of thioflavin T.[210] A recent report by Cui et al. on a nonionic *N*-methyl acetamide/lauric acid DES suggests the presence of nanosegregation of polar and nonpolar domains.[211] This nanosegregation is similar to that of micelles. In this sense, a eutectic mixture of *N*-methyl acetamide and lauric acid is "spatially heterogeneous," which is a result of "environmental segregation" driven by hydrophobic and hydrophilic interactions.

Structural organization of the molecules in DESs has garnered a lot of attention. Kashyap and co-workers have studied DESs using MD simulation. MD simulation studied x-ray and neutron scattering structures of DESs of amides and lithium perchlorate shows nanoscale spatial heterogeneity driven by the segregated domains of lithium and perchlorate ions.[212] The group also studied ethaline (DES of choline chloride and ethylene glycol) with MD simulation and showed that there is competition between choline cation and ethylene glycol for hydrogen bonding with anion.[81] Also, intra and inter molecular hydrogen bonding between ethylene glycol molecules was observed. The simulation study on effect of hydration of ethaline showed that nanostructure of DESs is retained up to 40 % of water.[213] This finding is similar to that found for other DESs discussed earlier.[97-102] In excess of water, ethylene glycol molecules were found to be segregated. These simulation findings have been backed up by neutron scattering study. Percevault et al. has studied different classes of pure and hydrated DESs with small-angle neutron scattering (SANS).[214] First, SANS study of pure and hydrated ethaline has supported the findings of simulation by Kashyap group confirming the formation of segregated domains. The authors suggest that the ethylene glycol domain formation is driven by higher affinity of water molecules towards ionic species. SANS study of hydrated non-ionic DES of lactic acid and glycerol found no such segregation or domain formation. Finally SANS study

on hydrophobic DES of menthol and decanoic acid found micelle-like structures of small size of molecular scale.

Using MD simulation, Srinivasan et al. has tried to explain large viscosity in acetamide and lithium salt based DESs.[215] MD simulation shows that long range diffusion of acetamide is restricted as a result of formation of hydrogen bond complex of acetamide and ionic species. This complex formation leads to higher viscosity and forbids crystallization process which lowers the freezing point.

1.11 Consequences of Heterogeneity on Chemistry

A lot has been said and done about structure and dynamics solvent. However, it is often forgotten to ask "what is the importance of heterogeneity?" Solutions of surfactants forming micelles and reverse-micelles are heterogeneous although not like what has been discussed in this chapter. But these solutions containing molecular assemblies have been understood and have found numerous applications. As of now, little attention has been given to study the consequences of solvent heterogeneity on chemical and biological systems. There are no major studies on how does spatial and dynamic heterogeneity of the solvent impact a chemical reactions and processes. Perhaps the best way to understand the importance of heterogeneity is indirect approach with some examples for now.

Simulation study by Pronk et al. have shown that dynamic heterogeneity has profound effect at the biological interface.[216] At or near the interface, decoupling of viscosity and diffusion was observed although to the extent seen in supercooled liquids. Because of this, solutes like protein are expected to undergo relatively slow diffusion near the interface. Solvent heterogeneity has been shown to have effect on the interaction between nanoassembles.[217] Shape-controlled of synthesis of nanoparticles in DES by Liao et al. suggests that heterogeneity of solvent play strong role in some applications.[143] Also, solubilisation of certain moieties can be rendered by solvent heterogeneity. For Benay et al. has shown that metal ions are preferably solvated by methanol in a chloroform/methanol mixture although methanol is present only in small amount (10%), thus enabling the solubilisation in chloroform.[218] Mellmer et al. has shown that the rate of reactivity (i.e. acid catalysed dehydration of some compound) is enhanced in the mixture of organic solvent and water which they have attributed to solvation of acidic protons of the reactants by water.[219]

1.12 Motivation of the Thesis Work/Outline of the present thesis

Physical chemistry of DESs have been understood to some good extent as reflected in the literature survey in the earlier sections. However many properties, characteristics and applications are yet to be unravelled. Also, from the literature survey, it is not hard to realize that the future of DESs look bright and promising. Therefore, I ventured into area of DESs. In the present thesis, I have tried to understand structural and dynamical aspects of various DESs through fluorescence based spectroscopic techniques described in forthcoming chapters. For this, I have taken a non-ionic, a hydrophobic and an ionic DESs. To further the scope of DESs in the biological domain, I have also studied structure and conformational fluctuation of a protein in hydrated non-ionic DESs.

References

1. Handbook of Solvents, Wypych, G., Eds.; ChemTec publishing and William Andrew Inc., Toronto and New York, 2001.
2. Marcus, Y. The Properties of Solvents. Wiley Series in Solution Chemistry, Vol. 4, John Wiley & Sons Ltd., Great Britain, 1999.
3. Paints, Coatings and Solvents, Stoye, D., Freitag, W., Eds.; Wiley-VCH, Second edition, Federal Republic of Germany, 1998.
4. Reichardt, C. Solvents and solvent effects in organic chemistry, 3rd Ed.; Wiley-VCH, Federal Republic of Germany, 2004.
5. Ball, P. Water is an active matrix of life for cell and molecular biology. *Proc. Natl. Acad. Sci. U.S.A.* **2017**, *114*, 13327-13335.
6. Chandler, D. Interfaces and the driving force of hydrophobic assembly. *Nature* **2005**, *437*, 640–647.
7. Ben-Amotz, D. Water-Mediated Hydrophobic Interactions. *Annu. Rev. Phys. Chem.* **2016**, *67*, 617–638.
8. Xi, E.; Patel, A. J. The hydrophobic effect, and fluctuations: The long and the short of it. *Proc. Natl. Acad. Sci. U.S.A.* **2016**, *113*, 4549-4551.
9. Narayan, S.; Muldoon, J.; Finn, M. G.; Fokin, V. V.; Kolb, H. C.; Sharpless, K. B. "On Water": Unique Reactivity of Organic Compounds in Aqueous Suspension. *Angew. Chem. Int. Ed.* **2005**, *44*, 3275–3279.
10. Rideout, D. C.; Breslow, R. Hydrophobic acceleration of Diels-Alder reactions. *J. Am. Chem. Soc*. **1980**, *102*, 7816–7817.
11. Li, C.-J.; Chen, L. Organic chemistry in water. *Chem. Soc. Rev*. **2006**, *35*, 68-82.
12. Kitanosono, T.; Masuda, K.; Xu, P.; Kobayashi, S. Catalytic Organic Reactions in Water toward Sustainable Society. *Chem. Rev*. **2018**, *118*, 679−746.
13. Li, C.-J.; Trost, B. M. Green chemistry for chemical synthesis. *Proc. Natl. Acad. Sci. U.S.A.* **2008**, *105*, 13197–13202.
14. Jordan, A.; Stoy, P.; Sneddon, H. F. Chlorinated Solvents: Their Advantages, Disadvantages, and Alternatives in Organic and Medicinal Chemistry. *Chem. Rev*. **2021**, *121*, 1582−1622.
15. Kerton, F., Marriott, R. Alternative Solvents for Green Chemistry, 2nd ed.; Green Chemistry series; Royal Society of Chemistry (RSC), 2013

16. Sheldon, R. A. Green solvents for sustainable organic synthesis: state of the art. *Green Chem*. **2005**, *7*, 267– 278.
17. DeSimone, J. M. Practical approaches to green solvents. *Science* **2002**, *297*, 799– 803.
18. Principles of Green Chem https://www.acs.org/content/acs/en/greenchemistry/principles/12-principles-of-green-chemistry.html (accesed 12 February 2021).
19. Erythropel, H. C.; Zimmerman, J. B.; de Winter, T. M. et al. The Green ChemisTREE: 20 years after taking root with the 12 principles. *Green Chem*. **2018**, *20*, 1929-1961.
20. Tanaka, K. Solvent-free Organic Synthesis, 2nd ed.; Wiley-VCH, Federal Republic of Germany, 2009.
21. Do, J.-L.; Friščić, T. Mechanochemistry: A Force of Synthesis. *ACS Cent. Sci*. **2017**, *3*, 13−19.
22. James, S. L.; Adams, C. J.; Bolm, C. et al. Mechanochemistry: opportunities for new and cleaner synthesis. *Chem. Soc. Rev*. **2012**, *41*, 413–447.
23. Polshettiwar, V.; Varma, R. S. Microwave-Assisted Organic Synthesis and Transformations using Benign Reaction Media. *Acc. Chem. Res*. **2008**, *41*, 629–639.
24. Varma, R. S. Solvent-free organic syntheses using supported reagents and microwave irradiation. *Green Chem*. **1999**, *1*, 43-55.
25. Stolle, A.; Szuppa, T.; Leonhardt, S. E. S.; Ondruschka, B. Ball milling in organic synthesis: solutions and challenges. *Chem. Soc. Rev*. **2011**, *40*, 2317–2329.
26. Rodríguez, B.; Bruckmann, A.; Rantanen, T.; Bolm, C. Solvent-Free Carbon-Carbon Bond Formations in Ball Mills. *Adv. Synth. Catal*. **2007**, *349*, 2213 – 2233.
27. Chemical Synthesis Using Supercritical Fluids, Jessop, P. G., Leitner, W., Eds,; Wiley-VCH, Federal Republic of Germany, 1999.
28. Levine, I. N. Physical Chemistry, 6th edition; McGraw-Hill, New York, 2008.
29. Rogers, R. D.; Seddon, K. R. Ionic Liquids--Solvents of the Future? *Science* **2003**, *302*, 792-793.
30. Plechkova, N. V.; Seddon, K. R. Applications of ionic liquids in the chemical industry. *Chem. Soc. Rev*. **2008**, *37*, 123–150.
31. Kunz, W.; Häckl, K. The hype with ionic liquids as solvents. *Chem. Phys. Lett*. **2016**, *661*, 6–12.
32. Zhou, Y.; Qu, J. Ionic Liquids as Lubricant Additives: A Review. *ACS Appl. Mater. Interfaces* **2017**, *9*, 3209−3222.

33. Vidal, C.; García-Álvarez, J.; Hernán-Gómez, A.; Kennedy, A. R.; Hevia, E. Introducing Deep Eutectic Solvents to Polar Organometallic Chemistry: Chemoselective Addition of Organolithium and Grignard Reagents to Ketones in Air. *Angew. Chem. Int. Ed*. **2014**, *53*, 5969-5973.
34. Mamajanov, I.; Engelhart, A. E.; Bean, H. D.; Hud, N. V. DNA and RNA in Anhydrous Media: Duplex, Triplex, and G-Quadruplex Secondary Structures in a Deep Eutectic Solvent. *Angew. Chem. Int. Ed*. **2010**, *49*, 6310 –6314.
35. Eutectic Solvents and Stress in Plants, Verpoorte, R., Witkamp, G.-J., Choi, Y. H., Eds.; Advances in Botanical Research, Vol. 97, 2020.
36. Choi, Y. H.; van Spronsen, J.; Dai, Y.; Verberne, M.; Hollmann, F.; Arends, I. W. C. E.; Witkamp, G.-J.; Verpoorte, R. Are Natural Deep Eutectic Solvents the Missing Link in Understanding Cellular Metabolism and Physiology? *Plant Physiol*. **2011**, *156*, 1701-1705.
37. Ramløv, H. Microclimate and variations in haemolymph composition in the freezing-tolerant New Zealand alpine weta *Hemideina maori* Hutton (Orthoptera: Stenopelmatidae). *J. Comp. Physiol. B* **1999**, *169*, 224-235.
38. Sinclair, B. J.; Wharton, D. A. Avoidance of Intracellular Freezing by the Freezing-Tolerant New Zealand Alpine Weta *Hemideina maori* (Orthoptera: Stenopelmatidae). *J. Insect Physiol*. **1997**, *43*, 621–625.
39. Gertrudes, A.; Craveiro, R.; Eltayari, Z.; Reis, R. L.; Paiva, A.; Duarte, A. R. C. How Do Animals Survive Extreme Temperature Amplitudes? The Role of Natural Deep Eutectic Solvents. *ACS Sustainable Chem. Eng*. **2017**, *5*, 9542-9553.
40. Abbott, A. P.; Capper, G.; Davies, D. L.; Rasheed, R. K.; Tambyrajah, V. Novel solvent properties of choline chloride/urea mixtures. *Chem. Commun*. **2003**, 70-71.
41. Smith, E. L.; Abbott, A. P.; Ryder, K. S. Deep eutectic solvents (DESs) and their applications. *Chem. Rev*. **2014**, *114*, 11060–11082.
42. Martins, M. A. R.; Pinho, S. P.; Coutinho, J. A. P. Insights into the Nature of Eutectic and Deep Eutectic Mixtures. *J. Solution Chem*. **2019**, *48*, 962–982.
43. Hurley, F. H.; WIer Jr., T. P. Electrodeposition of Metals from Fused Quaternary Ammonium Salts. *J. Electrochem. Soc*. **1951**, *98*, 203-206.
44. Sitze, M. S.; Schreiter, E. R.; Patterson, E. V.; Freeman, R. G. Ionic Liquids Based on $FeCl_3$ and $FeCl_2$. Raman Scattering and *ab Initio* Calculations. *Inorg. Chem*. **2001**, *40*, 2298-2304.

45. Abbott, A. P.; Capper, G.; Davies, D. L.; Munro, H. L.; Rasheed, R. K.; Tambyrajah, V. Preparation of novel, moisture-stable, Lewis-acidic ionic liquidscontaining quaternary ammonium salts with functional side chains. *Chem. Commun*. **2001**, 2010–2011.
46. Rogers, R. D.; Gurau, G. Is"choline and geranate"an ionic liquid or deep eutectic solvent system? *Proc. Natl. Acad. Sci. U.S.A.* **2018**, *115*, E10999.
47. Banerjee, A.; Ibsen, K.; Brown, T.; Chen, R.; Agatemor, C.; Mitragotri, S. Definitions of ionic liquids and deep eutectic solvents. *Proc. Natl. Acad. Sci. U.S.A.* **2018**, *115*, E11000–E11001.
48. Abranches, D. O.; Martins, R. O.; Silva, L. P.; Martins, M. A. R.; Pinho, S. P.; Coutinho, J. A. P. Liquefying Compounds by Forming Deep Eutectic Solvents: A Case Study for Organic Acids and Alcohols. *J. Phys. Chem. B* **2020**, *124*, 4174–4184.
49. Abbott, A. P.; Boothby, D.; Capper, G.; Davies, D. L.; Rasheed, R. K. Deep Eutectic Solvents Formed between Choline Chloride and Carboxylic Acids: Versatile Alternatives to Ionic Liquids. *J. Am. Chem. Soc*. **2004**, *126*, 9142–9147.
50. Wilkes, J. S.; Levisky, J. A.; Wilson, R. A.; Hussey, C. L. Dialkylimidazolium chloroaluminate melts: a new class of room-temperature ionic liquids for electrochemistry, spectroscopy and synthesis. *Inorg. Chem*. **1982**, *21*, 1263–1264.
51. Abbott, A. P.; Capper, G.; Davies, D. L.; Rasheed, R. Ionic Liquids Based upon Metal Halide/Substituted Quaternary Ammonium Salt Mixtures. *Inorg. Chem*. **2004**, *43*, 3447–3452.
52. Schreiter, E. R.; Stevens, J. E.; Ortwerth, M. F.; Freeman, R. G. A Room-Temperature Molten Salt Prepared from $AuCl_3$ and 1-Ethyl-3-methylimidazolium Chloride. *Inorg. Chem*. **1999**, *38*, 3935–3937.
53. Abbott, A. P.; Capper, G.; Davies, D. L.; Rasheed, R. K. Ionic Liquid Analogues Formed from Hydrated Metal Salts. *Chem. Eur. J*. **2004**, *10*, 3769- 3774.
54. Gurkan, B.; Squire, H.; Pentzer, E. Metal-Free Deep Eutectic Solvents: Preparation, Physical Properties, and Significance. *J. Phys. Chem. Lett*. **2019**, *10*, 7956–7964.
55. Hayyan, A.; Mjalli, F. S.; AlNashef, I. M.; Al-Wahaibi, Y. M.; Al-Wahaibi, T.; Hashim, M. A. Glucose-based deep eutectic solvents: Physical properties. *J. Mol. Liq*. **2013**, *178*, 137–141.
56. Hayyan, A.; Mjalli, F. S.; AlNashef, I. M.; Al-Wahaibi, T.; Al-Wahaibi, Y. M.; Hashim, M. A. Fruit sugar-based deep eutectic solvents and their physical properties. *Thermochim. Acta* **2012**, *541*, 70– 75.

57. Silva, L. P.; Fernandez, L.; Conceição, J. H. F.; Martins, M. A. R.; Sosa, A.; Ortega, J.; Pinho, S. P.; Coutinho, J. A. P. Design and Characterization of Sugar-Based Deep Eutectic Solvents Using Conductor-like Screening Model for Real Solvents. *ACS Sustainable Chem. Eng*. **2018**, *6*, 10724−10734.
58. Abbott, A. P.; Capper, G.; Davies, D. L.; McKenzie, K. J.; Obi, S. U. Solubility of Metal Oxides in Deep Eutectic Solvents Based on Choline Chloride. *J. Chem. Eng. Data* **2006**, *51*, 1280–1282.
59. Abbott, A. P.; Barron, J. C.; Ryder, K. S.; Wilson, D. Eutectic-Based Ionic Liquids with Metal-Containing Anions and Cations. *Chem. Eur. J*. **2007**, *13*, 6495–6501.
60. Hammond, O. S.; Bowron, D. T.; Edler, K. J. Structure and Properties of "Type IV" Lanthanide Nitrate Hydrate:Urea Deep Eutectic Solvents. *ACS Sustainable Chem. Eng*. **2019**, *7*, 4932–4940.
61. Abranches, D. O.; Martins, M. A. R.; Silva, L. P.; Schaeffer, N.; Pinho, S. P.; Coutinho, J. A. P. Phenolic hydrogen bond donors in the formation of non-ionic deep eutectic solvents: the quest for type V DES. *Chem. Commun*. **2019**, *55*, 10253—10256.
62. Schaeffer, N.; Abranches, D. O.; Silva, L. P.; Martins, M. A. R.; Carvalho, P. J.; Russina, O.; Triolo, A.; Paccou, L.; Guinet, Y.; Hedoux, A.; Coutinho, J. A. P. Non-Ideality in Thymol + Menthol Type V Deep Eutectic Solvents. *ACS Sustainable Chem. Eng*. **2021**, *9*, 2203–2211.
63. Lazerges, M.; Rietveld, I. B.; Corvis, Y.; Céolin, R.; Espeau, P. Thermodynamic studies of mixtures for topical anesthesia: Lidocaine–salol binary phase diagram. *Thermochim. Acta* **2010**, *497*, 124–128.
64. van Osch, D. J. G. P.; Dietz, C. H. J. T.; Warrag, S. E. E.; Kroon, M. C. The Curious Case of Hydrophobic Deep Eutectic Solvents: A Story on the Discovery, Design, and Applications. *ACS Sustainable Chem. Eng*. **2020**, *8*, 10591–10612.
65. Florindo, C.; Branco, L. C.; Marrucho, I. M. Quest for Green-Solvent Design: From Hydrophilic to Hydrophobic (Deep) Eutectic Solvents. *ChemSusChem* **2019**, *12*, 1549-1559.
66. van Osch, D. J. G. P.; Zubeir, L. F.; van den Bruinhorst, A.; Rocha, M. A. A.; Kroon, M. C. Hydrophobic deep eutectic solvents as water-immiscible extractants. *Green Chem*. **2015**, *17*, 4518–4521.

67. Ribeiro, B. D.; Florindo, C.; Iff, L. C.; Coelho, M. A. Z.; Marrucho, I. M. Menthol-based Eutectic Mixtures: Hydrophobic Low Viscosity Solvents. *ACS Sustainable Chem. Eng*. **2015**, 3, 2469−2477.
68. Fowles, J.; Banton, M.; Klapacz, J.; Shen, H. A toxicological review of the ethylene glycol series: Commonalities and differences in toxicity and modes of action. *Toxicol. Lett*. **2017**, *278*, 66–83.
69. Kadiiska, M. B.; Mason, R. P. Ethylene Glycol Generates Free Radical Metabolites in Rats: An ESR in Vivo Spin Trapping Investigation. *Chem. Res. Toxicol*. **2000**, *13*, 1187–1191.
70. Gutiérrez, M. C.; Ferrer, M. L.; Yuste, L.; Rojo, F.; del Monte, F. Bacteria Incorporation in Deep-eutectic Solvents through Freeze-Drying. *Angew. Chem. Int. Ed*. **2010**, *49*, 2158 –2162.
71. Hayyan, M.; Hashim, M. A.; Hayyan, A.; Al-Saadi, M. A.; AlNashef, I. M.; Mirghani, M. E. S.; Saheed, O. K. Are deep eutectic solvents benign or toxic? *Chemosphere* **2013**, *90*, 2193–2195.
72. Hayyan, M.; Hashim, M. A.; Al-Saadi, M. A.; Hayyan, A.; AlNashef, I. M.; Mirghani, M. E. S. Assessment of cytotoxicity and toxicity for phosphonium-based deep eutectic solvents. *Chemosphere* **2013**, *93*, 455–459.
73. Juneidi, I.; Hayyan, M.; Hashim, M. A. Evaluation of toxicity and biodegradability for cholinium-based deep eutectic solvents. *RSC Adv*. **2015**, *5*, 83636–83647.
74. Macário, I. P. E.; Oliveira, H.; Menezes, A. C.; Ventura, S. P. M.; Pereira, J. L.; Gonçalves, A. M. M.; Coutinho, J. A. P.; Gonçalves, F. J. M. Cytotoxicity profiling of deep eutectic solvents to human skin cells. *Sci. Rep*. **2019**, *9*, 3932.
75. Halder, A. K.; Cordeiro, M. N. D. S. Probing the Environmental Toxicity of Deep Eutectic Solvents and Their Components: An In Silico Modeling Approach. *ACS Sustainable Chem. Eng*. **2019**, *7*, 10649−10660.
76. Yang, Z. Toxicity and Biodegradability of Deep Eutectic Solvents and Natural Deep Eutectic Solvents. In *Deep Eutectic Solvent: Synthesis, Properties and Applications*, Ramón, D. J., Guillena, G., Eds.; Wiley-VCH Weinheim, Germany 2020.
77. Zhang, Q.; Vigier, K. De O.; Royer, S.; Jérôme, F. Deep eutectic solvents: syntheses, properties and applications. *Chem. Soc. Rev*. **2012**, *41*, 7108–7146.
78. Alizadeh, V.; Malberg, F.; Pádua, A. A. H.; Kirchner, B. Are There Magic Compositions in Deep Eutectic Solvents? Effects of Composition and Water Content

in Choline Chloride/Ethylene Glycol from Ab Initio Molecular Dynamics. *J. Phys. Chem. B* **2020**, *124*, 7433–7443.

79. Martins, M. A. R.; Crespo, E. A.; Pontes, P. V. A.; Silva, L. P.; Bülow, M.; Maximo, G. J.; Batista, E. A. C.; Held, C.; Pinho, S. P.; Coutinho, J. A. P. Tunable Hydrophobic Eutectic Solvents Based on Terpenes and Monocarboxylic Acids. *ACS Sustainable Chem. Eng*. **2018**, *6*, 8836−8846.
80. Turner, A. H.; Holbrey, J. D. Investigation of glycerol hydrogen-bonding networks in choline chloride/glycerol eutectic-forming liquids using neutron diffraction. *Phys. Chem. Chem. Phys*. **2019**, *21*, 21782—21789.
81. Kaur, S.; Malik, A.; Kashyap, H. K. Anatomy of Microscopic Structure of Ethaline Deep Eutectic Solvent Decoded through Molecular Dynamics Simulations. *J. Phys. Chem. B* **2019**, *123*, 8291–8299.
82. Abbott, A. P.; Harris, R. C.; Ryder, K. S. Application of Hole Theory to Define Ionic Liquids by their Transport Properties. *J. Phys. Chem. B* **2007**, *111*, 4910–4913.
83. Wang, H.; Liu, S.; Zhao, Y.; Wang, J.; Yu, Z. Insights into the Hydrogen Bond Interactions in Deep Eutectic Solvents Composed of Choline Chloride and Polyols. *ACS Sustainable Chem. Eng*. **2019**, *7*, 7760–7767.
84. Stefanovic, R.; Ludwig, M.; Webber, G. B.; Atkin, R.; Page, A. J. Nanostructure, hydrogen bonding and rheology in choline chloride deep eutectic solvents as a function of the hydrogen bond donor. *Phys. Chem. Chem. Phys*. **2017**, *19*, 3297-3306.
85. Faraone, A.; Wagle, D. V.; Baker, G. A.; Novak, E. C.; Ohl, M.; Reuter, D.; Lunkenheimer, P.; Loidl, A.; Mamontov, E. Glycerol Hydrogen-Bonding Network Dominates Structure and Collective Dynamics in a Deep Eutectic Solvent. *J. Phys. Chem. B* **2018**, *122*, 1261−1267.
86. D'Agostino, C. Hole theory as a prediction tool for Brownian diffusive motion in binary mixtures of liquids. *RSC Adv*. **2017**, *7*, 51864-51869.
87. Abbott, A. P. Application of Hole Theory to the Viscosity of Ionic and Molecular Liquids. *ChemPhysChem* **2004**, *5*, 1242 -1246.
88. Abbott, A. P.; Capper, G.; Gray, S. Design of Improved Deep Eutectic Solvents Using Hole Theory. *ChemPhysChem* **2006**, *7*, 803 – 806.
89. Reichardt, C. Solvatochromic Dyes as Solvent Polarity Indicators. *Chem. Rev*. **1994**, *94*, 2319–2358.
90. Reichardt, C. Polarity of ionic liquids determined empirically by means of solvatochromic pyridinium N-phenolate betaine dyes. *Green Chem*. **2005**, *7*, 339–351.

91. Ruß, C.; König, B. Low melting mixtures in organic synthesis – an alternative to ionic liquids? *Green Chem*. **2012**, *14*, 2969–2982.
92. Abbott, A. P.; Harris, R. C.; Ryder, K. S.; D'Agostino, C.; Gladden, L. F.; Mantle, M. D. Glycerol eutectics as sustainable solvent systems. *Green Chem*. **2011**, *13*, 82–90.
93. Pandey, A.; Rai, R.; Pal, M.; Pandey, S. How polar are choline chloride-based deep eutectic solvents? *Phys. Chem. Chem. Phys*. **2014**, *16*, 1559—1568.
94. Florindo, C.; McIntosh, A. J. S.; Welton, T.; Branco, L. C.; Marrucho, I. M. A closer look into deep eutectic solvents: exploring intermolecular interactions using solvatochromic probes. *Phys. Chem. Chem. Phys*. **2018**, *20*, 206—213.
95. MacFarlane, D. R.; Chong, A. L.; Forsyth, M.; Kar, M.; Vijayaraghavan, R.; Somers, A.; Pringle, J. M. New dimensions in salt–solvent mixtures: a 4th evolution of ionic liquids. *Faraday Discuss.* **2018**, *206*, 9–28.
96. Duan, L.; Dou, L.-L.; Guo, L.; Li, P.; Liu, E.-H. Comprehensive Evaluation of Deep Eutectic Solvents in Extraction of Bioactive Natural Products. *ACS Sustainable Chem. Eng*. **2016**, *4*, 2405–2411.
97. Hammond, O. S.; Bowron, D. T.; Edler, K. J. The Effect of Water upon Deep Eutectic Solvent Nanostructure: An Unusual Transition from Ionic Mixture to Aqueous Solution. *Angew. Chem. Int. Ed*. **2017**, *56*, 9782 –9785.
98. Hammond, O. S.; Bowron, D. T.; Jackson, A. J.; Arnold, T.; Sanchez-Fernandez, A.; Tsapatsaris, N.; Sakai, V. G.; Edler, K. J. Resilience of Malic Acid Natural Deep Eutectic Solvent Nanostructure to Solidification and Hydration. *J. Phys. Chem. B* **2017**, *121*, 7473–7483.
99. Posada, E.; López-Salas, N.; Riobóo, R. J. J.; Ferrer, M. L.; Gutiérrez, M. C.; del Monte, F. Reline aqueous solutions behaving as liquid mixtures of H-bonded co-solvents: microphase segregation and formation of co-continuous structures as indicated by Brillouin and ^{1}H NMR spectroscopies. *Phys. Chem. Chem. Phys*. **2017**, *19*, 17103-17110.
100. Kumari, P.; Shobhna; Kaur, S.; Kashyap, H. K. Influence of Hydration on the Structure of Reline Deep Eutectic Solvent: A Molecular Dynamics Study. *ACS Omega* **2018**, *3*, 15246–15255.
101. Sapir, L.; Harries, D. Restructuring a Deep Eutectic Solvent by Water: The Nanostructure of Hydrated Choline Chloride/Urea. *J. Chem. Theory Comput*. **2020**, *16*, 3335–3342.

102. Ma, C.; Laaksonen, A.; Liu, C.; Lu, X.; Ji, X. The peculiar effect of water on ionic liquids and deep eutectic solvents. *Chem. Soc. Rev*. **2018**, *47*, 8685-8720.
103. Płotka-Wasylka, J.; de la Guardia, M.; Andruch, V.; Vilková, M. Deep eutectic solvents *vs* ionic liquids: Similarities and differences. *Microchem. J*. **2020**, *159*, 105539.
104. Florindo, C.; Oliveira, F. S.; Rebelo, L. P. N.; Fernandes, A. M.; Marrucho, I. M. Insights into the Synthesis and Properties of Deep Eutectic Solvents Based on Cholinium Chloride and Carboxylic Acids. *ACS Sustainable Chem. Eng.* **2014**, *2*, 2416–2425.
105. Gutiérrez, M. C.; Ferrer, M. L.; Mateo, C. R.; del Monte, F. Freeze-Drying of Aqueous Solutions of Deep Eutectic Solvents: A Suitable Approach to Deep Eutectic Suspensions of Self-Assembled Structures. *Langmuir* **2009**, *25*, 5509–5515.
106. Farooq, M. Q.; Abbasi, N. M.; Anderson, J. L. Deep eutectic solvents in separations: Methods of preparation, polarity, and applications in extractions and capillary electrochromatography. *J. Chromatogr. A*. **2020**, *1633*, 461613.
107. Crawford, D. E.; Wright, L. A.; James, S. L.; Abbott, A. P. Efficient continuous synthesis of high purity deep eutectic solvents by twin screw extrusion. *Chem. Commun.* **2016**, *52*, 4215—4218.
108. Santana, A. P. R.; Mora-Vargas, J. A.; Guimarães, T. G. S.; Amaral, C. D. B.; Oliveira, A.; Gonzalez, M. H. Sustainable synthesis of natural deep eutectic solvents (NADES) by different methods. *J. Mol. Liq*. **2019**, *293*, 111452.
109. Zhang, Z.-H.; Zhang, X.-N.; Mo, L.-P.; Li, Y.-X.; Ma, F.-P. Catalyst-free synthesis of quinazoline derivatives using low melting sugar–urea–salt mixture as a solvent. *Green Chem*. **2012**, *14*, 1502-1506.
110. Tran, M. K.; Rodrigues, M.-T. F.; Kato, K.; Babu, G.; Ajayan, P. M. Deep eutectic solvents for cathode recycling of Li-ion batteries. *Nat. Energy* **2019**, *4*, 339–345.
111. García, G.; Aparicio, S.; Ullah, R.; Atilhan, M. Deep Eutectic Solvents: Physicochemical Properties and Gas Separation Applications. *Energy Fuels* **2015**, *29*, 2616–2644.
112. Cunha, S. C.; Fernandes, J. O. Extraction techniques with deep eutectic solvents. *TrAC, Trends Anal. Chem*. **2018**, *105*, 225-239.
113. Hansen, B. B.; Spittle, S.; Chen, B.; Poe, D.; Zhang, Y.; Klein, J. M.; Horton, A.; Adhikari, L,; Zelovich, T.; Doherty, B. W.; Gurkan, B.; Maginn, E. J.; Ragauskas, A.; Dadmun, M.; Zawodzinski, T. A.; Baker, G. A.; Tuckerman, M. E.; Savinell, R. F.;

Sangoro, J. R. Deep Eutectic Solvents: A Review of Fundamentals and Applications. *Chem. Rev*. **2021**, *121*, 1232−1285.

114. Tomé, L. C.; Mecerreyes, D. Emerging Ionic Soft Materials Based on Deep Eutectic Solvents. *J. Phys. Chem. B* **2020**, *124*, 8465−8478.
115. Srivastava, V. C. An evaluation of desulfurization technologies for sulfur removal from liquid fuels. *RSC Adv*. **2012**, *2*, 759–783.
116. Chandran, D.; Khalid, M.; Walvekar, R.; Mubarak, N. M.; Dharaskar, S.; Wong, W. Y.; Gupta, T. C. S. M. Deep eutectic solvents for extraction-desulphurization: A review. *J. Mol. Liq.* **2019**, *275*, 312-322.
117. Li, J.-j.; Xiao, H.; Tang, X.-d.; Zhou, M. Green Carboxylic Acid-Based Deep Eutectic Solvents as Solvents for Extractive Desulfurization. *Energy Fuels* **2016**, *30*, 5411–5418.
118. Li, C.; Li, D.; Zou, S.; Li, Z.; Yin, J.; Wang, A.; Cui, Y.; Yao, Z.; Zhao, Q. Extraction desulfurization process of fuels with ammonium-based deep eutectic solvents. *Green Chem*., **2013**, *15*, 2793–2799.
119. Wang, X.; Jiang, W.; Zhu, W.; Li, H.; Yin, S.; Chang, Y.; Li, H. A simple and cost-effective extractive desulfurization process with novel deep eutectic solvents. *RSC Adv*. **2016**, *6*, 30345–30352.
120. Makoś, P.; Boczkaj, G. Deep eutectic solvents based highly efficient extractive desulfurization of fuels–Eco-friendly approach. *J. Mol. Liq*. **2019**, *296*, 111916.
121. Lima, F.; Dave, M.; Silvestre, A. J. D.; Branco, L. C.; Marrucho, I. M. Concurrent Desulfurization and Denitrogenation of Fuels Using Deep Eutectic Solvents. *ACS Sustainable Chem. Eng*. **2019**, *7*, 11341–11349.
122. van Osch, D. J. G. P.; Parmentier, D.; Dietz, C. H. J. T.; van den Bruinhorst, A.; Tuinier, R.; Kroon, M. C. Removal of alkali and transition metal ions from water with hydrophobic deep eutectic solvents. *Chem. Commun*. **2016**, *52*, 11987-11990.
123. Tereshatov, E. E.; Boltoeva, M. Y.; Folden, C. M. First evidence of metal transfer into hydrophobic deep eutectic and low-transition-temperature mixtures: indium extraction from hydrochloric and oxalic acids. *Green Chem*. **2016**, *18*, 4616–4622.
124. Söldner, A.; Zach, J.; König, B. Deep eutectic solvents as extraction media for metal salts and oxides exemplarily shown for phosphates from incinerated sewage sludge ash. *Green Chem*. **2019**, *21*, 321-328.

125. Damilano, G.; Laitinen, A.; Willberg-Keyriläinen, P.; Lavonen, T.; Häkkinen, R.; Dehaen, W.; Binnemans, K.; Kuutti, L. Effects of thiol substitution in deep-eutectic solvents (DESs) as solvents for metal oxides. *RSC Adv*. **2020**, *10*, 23484–23490.
126. Huang, Y.; Feng, F.; Chen, Z.-G.; Wu, T.; Wang, Z.-H. Green and efficient removal of cadmium from rice flour using natural deep eutectic solvents. *Food Chem*. **2018**, *244*, 260–265.
127. Hanada, T.; Goto, M. Synergistic Deep Eutectic Solvents for Lithium Extraction. *ACS Sustainable Chem. Eng*. **2021**, *9*, 2152–2160.
128. Gil-Chávez, G. J.; Villa, J. A.; Ayala-Zavala, J. F.; Heredia, J. B.; Sepulveda, D.; Yahia, E. M.; González-Aguilar, G. A. Technologies for Extraction and Production of Bioactive Compounds to be Used as Nutraceuticals and Food Ingredients: An Overview. *Compr. Rev. Food Sci. Food Saf*. **2013**, *12*, 5-23.
129. Nam, M. W.; Zhao, J.; Lee, M. S.; Jeong, J. H.; Lee, J. Enhanced extraction of bioactive natural products using tailor-made deep eutectic solvents: application to flavonoid extraction from *Flos sophorae*. *Green Chem*, **2015**, *17*, 1718–1727.
130. Cao, J.; Yang, M.; Cao, F.; Wang, J.; Su, E. Well-Designed Hydrophobic Deep Eutectic Solvents As Green and Efficient Media for the Extraction of Artemisinin from *Artemisia annua* Leaves. *ACS Sustainable Chem. Eng*. **2017**, *5*, 3270−3278.
131. Cao, J.; Chen, L.; Li, M.; Cao, F.; Zhao, L.; Su, E. Two-phase systems developed with hydrophilic and hydrophobic deep eutectic solvents for simultaneously extracting various bioactive compounds with different polarities. *Green Chem*. **2018**, *20*, 1879–1886.
132. Schwarzenbach, R. P.; Egli, T.; Hofstetter, T. B.; von Gunten, U.; Wehrli, B. Global Water Pollution and Human Health. *Annu. Rev. Environ. Resour*. **2010**. *35*, 109–36.
133. Eggen, R. I. L.; Hollender, J.; Joss, A.; Schärer, M.; Stamm, C. Reducing the Discharge of Micropollutants in the Aquatic Environment: The Benefits of Upgrading Wastewater Treatment Plants. *Environ. Sci. Technol*. **2014**, *48*, 7683–7689.
134. Florindo, C.; Lima, F.; Branco, L. C.; Marrucho, I. M. Hydrophobic Deep Eutectic Solvents: A Circular Approach to Purify Water Contaminated with Ciprofloxacin. *ACS Sustainable Chem. Eng*. **2019**, *7*, 14739−14746.
135. Florindo, C.; Branco, L. C.; Marrucho, I. M. Development of hydrophobic deep eutectic solvents for extraction of pesticides from aqueous environments. *Fluid Phase Equilib*. **2017**, *448*, 135-142.

136. Florindo, C.; Monteiro, N. V.; Ribeiro, B. D.; Branco, L. C.; Marrucho, I. M. Hydrophobic deep eutectic solvents for purification of water contaminated with Bisphenol-A. *J. Mol. Liq*. **2020**, *297*, 111841.
137. Guajardo, N.; Müller, C. R.; Schrebler, R.; Carlesi, C.; de María, P. D. Deep Eutectic Solvents for Organocatalysis, Biotransformations, and Multistep Organocatalyst/Enzyme Combinations. *ChemCatChem* **2016**, *8*, 1020 –1027.
138. Phadtare, S. B.; Shankarling, G. S. Halogenation reactions in biodegradable solvent: Efficient bromination of substituted 1-aminoanthra-9,10-quinone in deep eutectic solvent(choline chloride : urea). *Green Chem*. **2010**, *12*, 458–462.
139. Pawar, P. M.; Jarag, K. J.; Shankarling, G. S. Environmentally benign and energy efficient methodology for condensation; an interesting facet to the classical Perkin reaction. *Green Chem*. **2011**, *13*, 2130–2134.
140. Marullo, S.; Meli, A.; D'Anna, F. A Joint Action of Deep Eutectic Solvents and Ultrasound to Promote Diels−Alder Reaction in a Sustainable Way. *ACS Sustainable Chem. Eng*. **2020**, *8*, 4889−4899.
141. Wagle, D. V.; Zhao, H.; Baker, G. A. Deep Eutectic Solvents: Sustainable Media for Nanoscale and Functional Materials. *Acc. Chem. Res*. **2014**, *47*, 2299−2308.
142. Tomé, L. I. N.; Baião, V.; da Silva, W.; Brett, C. M. A. Deep eutectic solvents for the production and application of new materials. *Appl. Mater. Today* **2018**, *10*, 30–50.
143. Liao, H.-G.; Jiang, Y.-X.; Zhou, Z.-Y.; Chen, S.-P.; Sun, S.-G. Shape-Controlled Synthesis of Gold Nanoparticles in Deep Eutectic Solvents for Studies of Structure–Functionality Relationships in Electrocatalysis. *Angew. Chem. Int. Ed*. **2008**, *47*, 9100 –9103.
144. Exposito, A. J.; Barrie, P. J.; Torrente-Murciano, L. Fast Synthesis of CeO_2 Nanoparticles in a Continuous Microreactor Using Deep Eutectic Reline As Solvent. *ACS Sustainable Chem. Eng*. **2020**, *8*, 18297−18302.
145. Agbor, V. B.; Cicek, N.; Sparling, R.; Berlin, A.; Levin, D. B. Biomass pretreatment: Fundamentals toward application. *Biotechnol. Adv*. **2011**, *29*, 675–685.
146. Kim, K. H.; Dutta, T.; Sun, J.; Simmons, B.; Singh, S. Biomass pretreatment using deep eutectic solvents from lignin derived phenols. *Green Chem*. **2018**, *20*, 809–815.
147. Kim, K. H.; Eudes, A.; Jeong, K.; Yoo, C. G.; Kim, C. S.; Ragauskas, A. Integration of renewable deep eutectic solvents with engineered biomass to achieve a closed-loop biorefinery. *Proc. Natl. Acad. Sci. U.S.A.* **2019**, *116*, 13816–13824.

148. Xu, F.; Sun, J.; Wehrs, M.; Kim, K. H.; Rau, S. S.; Chan, A. M.; Simmons, B. A.; Mukhopadhyay, A.; Singh, S. Biocompatible Choline-Based Deep Eutectic Solvents Enable One-Pot Production of Cellulosic Ethanol. *ACS Sustainable Chem. Eng*. **2018**, *6*, 8914−8919.
149. Klibanov, A. M. Why are enzymes less active in organic solvents than in water? Trends Biotechnol. **1997**, *15*, 97-101.
150. Gorke, J. T.; Srienc, F.; Kazlauskas, R. J. Hydrolase-catalyzed biotransformations in deep eutectic solvents. *Chem. Commun*. **2008**, 1235–1237.
151. Lindberg, D.; de la Fuente Revenga, M.; Widersten, M. Deep eutectic solvents (DESs) are viable cosolvents for enzyme-catalyzed epoxide hydrolysis. J. Biotechnol. **2010**, *147*, 169–171.
152. de María, P. D.; Maugeri, Z. Ionic liquids in biotransformations: from proof-of-concept to emerging deep-eutectic-solvents. *Curr. Opin. Chem. Biol*. **2011**, *15*, 220–225.
153. Papadopoulou, A. A.; Efstathiadou, E.; Patila, M.; Polydera, A. C.; Stamatis, H. Deep Eutectic Solvents as Media for Peroxidation Reactions Catalyzed by Heme-Dependent Biocatalysts. *Ind. Eng. Chem. Res*. **2016**, *55*, 5145−5151.
154. Nardecchia, S.; Gutiérrez, M. C.; Ferrer, M. L.; Alonso, M.; López, I. M.; Rodríguez-Cabello, J. C.; del Monte, F. Phase Behavior of Elastin-Like Synthetic Recombinamers in Deep Eutectic Solvents. *Biomacromolecules* **2012**, *13*, 2029–2036
155. Esquembre, R.; Sanz, J. M.; Wall, J. G.; del Monte, F.; Mateo, C. R.; Ferrer, M. L. Thermal unfolding and refolding of lysozyme in deep eutectic solvents and their aqueous dilutions. *Phys. Chem. Chem. Phys*. **2013**, *15*, 11248-11256.
156. Zeng, Q.; Wang, Y.; Huang, Y.; Ding, X.; Chen, J.; Xu, K. Deep eutectic solvents as novel extraction media for protein partitioning. *Analyst* **2014**, *139*, 2565-2573.
157. Sanchez-Fernandez, A.; Edler, K. J.; Arnold, T.; Venero, D. A.; Jackson, A. J. Protein conformation in pure and hydrated deep eutectic solvents. *Phys. Chem. Chem. Phys*. **2017**, *19*, 8667—8670.
158. Mondal, D.; Sharma, M.; Mukesh, C.; Gupta, V.; Prasad, K. Improved solubility of DNA in recyclable and reusable bio-based deep eutectic solvents with long-term structural and chemical stability. *Chem. Commun*. **2013**, *49*, 9606-9608.
159. Cicerone, M. T.; Ediger, M. D. Relaxation of spatially heterogeneous dynamic domains in supercooled ortho-terphenyl. *J. Chem. Phys*. **1995**, *103*, 5684-5692.

160. Reinsberg, S. A.; Qiu, X. H.; Wilhelm, M.; Spiess, H. W.; Ediger, M. D. Length scale of dynamic heterogeneity in supercooled glycerol near T_g. *J. Chem. Phys*. **2001**, *114*, 7299-7302.
161. Tracht, U.; Wilhelm, M.; Heuer, A.; Feng, H.; Schmidt-Rohr, K.; Spiess, H. W. Length Scale of Dynamic Heterogeneities at the Glass Transition Determined by Multidimensional Nuclear Magnetic Resonance. *Phys. Rev. Lett*. **1998**, *81*, 2727-2730.
162. Di Lorenzo, F.; Seiffert, S. Nanostructural heterogeneity in polymer networks and gels. *Polym. Chem*. **2015**, *6*, 5515–5528.
163. Wang, Y.; Voth, G. A. Unique Spatial Heterogeneity in Ionic Liquids. *J. Am. Chem. Soc*. **2005**, *127*, 12192–12193.
164. Habasaki, J.; Ngai, K. L. Heterogeneous dynamics of ionic liquids from molecular dynamics simulations. *J. Chem. Phys*. **2008**, *129*, 194501.
165. Mandal, P. K.; Sarkar, M.; Samanta, A. Excitation-Wavelength-Dependent Fluorescence Behavior of Some Dipolar Molecules in Room-Temperature Ionic Liquids. *J. Phys. Chem. A* **2004**, *108*, 9048–9053.
166. Hu, Z.; Margulis, C. J. Heterogeneity in a room-temperature ionic liquid: Persistent local environments and the red-edge effect. *Proc. Natl. Acad. Sci. U.S.A.* **2006**, *103*, 831-836.
167. Chattoraj, S.; Chowdhury, R.; Ghosh, S.; Bhattacharyya, K. Heterogeneity in binary mixtures of dimethyl sulfoxide and glycerol: Fluorescence correlation spectroscopy. *J. Chem. Phys*. **2013**, *138*, 214507.
168. Gazi, H. A. R.; Biswas, R. Heterogeneity in Binary Mixtures of (Water + Tertiary Butanol): Temperature Dependence Across Mixture Composition. *J. Phys. Chem. A* **2011**, *115*, 2447–2455.
169. Mazza, M. G.; Giovambattista, N.; Stanley, H. E.; Starr, F. W. Connection of translational and rotational dynamical heterogeneities with the breakdown of the Stokes-Einstein and Stokes-Einstein-Debye relations in water. *Phys. Rev. E* **2007**, *76*, 031203.
170. Xu, L.; Mallamace, F.; Yan, Z.; Starr, F. W.; Buldyrev, S. V.; Stanley, H. E. Appearance of a fractional Stokes–Einstein relation in water and a structural interpretation of its onset. *Nat. Phys*. **2009**, *5*, 565–569.

171. Ivanov, M. Y.; Krumkacheva, O. A.; Dzuba, S. A.; Fedin, M. V. Microscopic rigidity and heterogeneity of ionic liquids probed by stochastic molecular librations of the dissolved nitroxides. *Phys. Chem. Chem. Phys.* **2017**, *19*, 26158—26163.
172. Ediger, M. D. Spatially Heterogeneous Dynamics in Supercooled Liquids. *Annu. Rev. Phys. Chem*. **2000**. *51*, 99–128.
173. Richert, R. Heterogeneous dynamics in liquids: fluctuations in space and time. *J. Phys.: Condens. Matter* **2002**, *14*, R703-R738.
174. Mackowiak, S. A.; Herman, T. K.; Kaufman, L. J. Spatial and temporal heterogeneity in supercooled glycerol: Evidence from wide field single molecule imaging. *J. Chem. Phys*. **2009**, *131*, 244513.
175. Blackburn, F. R.; Wang, C.-Y.; Ediger, M. D. Translational and Rotational Motion of Probes in Supercooled 1, 3, 5-Tris(naphthyl)benzene. *J. Phys. Chem*. **1996**, *100*, 18249-18257
176. Paeng, K.; Park, H.; Hoang, D. T.; Kaufman, L. J. Ideal probe single-molecule experiments reveal the intrinsic dynamic heterogeneity of a supercooled liquid. *Proc. Natl. Acad. Sci. U.S.A.* **2015**, *112*, 4952-4957.
177. Russell, E. V.; Israeloff, N. E. Direct observation of molecular cooperativity near the glass transition. *Nature* **2000**, *408*, 695-698.
178. Berthier, L.; Biroli, G.; Bouchaud, J.-P.; Cipelletti, L.; El Masri, D.; L'Hôte, D.; Ladieu, F.; Pierno, M. Direct Experimental Evidence of a Growing Length Scale Accompanying the Glass Transition. *Science* **2005**, *310*, 1797-1800.
179. Weeks, E. R.; Crocker, J. C.; Levitt, A. C.; Schofield, A.; Weitz, D. A. Three-Dimensional Direct Imaging of Structural Relaxation Near the Colloidal Glass Transition. *Science* **2000**, *287*, 627-631.
180. Zondervan, R.; Kulzer, F.; Berkhout, G. C. G.; Orrit, M. Local viscosity of supercooled glycerol near T_g probed by rotational diffusion of ensembles and single dye molecules. *Proc. Natl. Acad. Sci. U.S.A.* **2007**, *104*, 12628-12633.
181. Wang, C.-Y.; Ediger, M. D. How Long Do Regions of Different Dynamics Persist in Supercooled *o*-Terphenyl? *J. Phys. Chem. B* **1999**, *103*, 4177-4184.
182. Berthier, L. Dynamic Heterogeneity in Amorphous Materials. *Physics* **2011**, *4*, 42.
183. Lakowicz, J. R. Principles of Fluorescence Spectroscopy, 3rd edition; Springer, 2010.

184. Itoh, K.; Azumi, T. Shift of emission band upon excitation at the long wavelength absorption edge. 1. A preliminary survey for quinine and related compounds. *Chem. Phys. Lett*. **1973**, *22*, 395-399.
185. Itoh, K.; Azumi, T. Shift of the emission band upon excitation at the long wavelength absorption edge. II. Importance of the solute–solvent interaction and the solvent reorientation relaxation process. *J. Chem. Phys*. **1975**, *62*, 3431-3438.
186. Azumi, T.; Itoh, K; Shiraishi, H. Shift of emission band upon the excitation at the long wavelength absorption edge. III. Temperature dependence of the shift and correlation with the time dependent spectral shift. *J. Chem. Phys*. **1976**, *65*, 2550-2555.
187. Paul, A.; Mandal, P. K.; Samanta, A. On the Optical Properties of the Imidazolium Ionic Liquids. *J. Phys. Chem. B* **2005**, *109*, 9148–9153.
188. Stillinger, F. H.; Hodgdon, J. A. Translation-rotation paradox for diffusion in fragile glass-forming liquids. *Phys. Rev. E* **1994**, *50*, 2064-2068.
189. Tarjus, G.; Kivelson, D. Breakdown of the Stokes–Einstein relation in supercooled liquids. *J. Chem. Phys*. **1995**, *103*, 3071 -3073.
190. Cicerone, M. T.; Ediger, M. D. Enhanced translation of probe molecules in supercooled o-terphenyl: Signature of spatially heterogeneous dynamics? *J. Chem. Phys*. **1996**, *104*, 7210 -7218.
191. Swallen, S. F.; Bonvallet, P. A.; McMahon, R. J.; Ediger, M. D. Self-Diffusion of *tris*-Naphthylbenzene near the Glass Transition Temperature. *Phys. Rev. Lett*. **2003**, *90*, 015901.
192. Yang, M.; Richert, R. Observation of heterogeneity in the nanosecond dynamics of a liquid. *J. Chem. Phys*. **2001**, *115*, 2676 -2680.
193. Richert, R. Spectral diffusion in liquids with fluctuating solvent responses: Dynamical heterogeneity and rate exchange. *J. Chem. Phys*. **2001**, *115*, 1429 -1434.
194. N. Das and P. Sen (unpublished data)
195. D'Agostino, C.; Harris, R. C.; Abbott, A. P.; Gladden, L. F.; Mantle, M. D. Molecular motion and ion diffusion in choline chloride based deep eutectic solvents studied by ^{1}H pulsed field gradient NMR spectroscopy. *Phys. Chem. Chem. Phys*. **2011**, *13*, 21383–21391.
196. Guchhait, B.; Gazi, H. A. R.; Kashyap, H. K.; Biswas, R. Fluorescence Spectroscopic Studies of (Acetamide + Sodium/Potassium Thiocyanates) Molten Mixtures: Composition and Temperature Dependence. *J. Phys. Chem. B* **2010**, *114*, 5066–5081.

197. Guchhait, B.; Daschakraborty, S.; Biswas, R. Medium decoupling of dynamics at temperatures ∼100 K above glass-transition temperature: A case study with (acetamide + lithium bromide/nitrate) melts. *J. Chem. Phys*. **2012**, *136*, 174503.
198. Das, A.; Biswas, R. Dynamic Solvent Control of a Reaction in Ionic Deep Eutectic Solvents: Time-Resolved Fluorescence Measurements of Reactive and Nonreactive Dynamics in (Choline Chloride + Urea) Melts. *J. Phys. Chem. B* **2015**, *119*, 10102–10113.
199. Pal, T.; Biswas, R. Heterogeneity and viscosity decoupling in (acetamide + electrolyte) molten mixtures: A model simulation study. *Chem. Phys. Lett*. **2011**, *517*, 180–185.
200. Jin, H.; Baker, G. A.; Arzhantsev, S.; Dong, J.; Maroncelli, M. Solvation and Rotational Dynamics of Coumarin 153 in Ionic Liquids: Comparisons to Conventional Solvents. *J. Phys. Chem. B* **2007**, *111*, 7291–7302.
201. Zhang, X.-X.; Liang, M.; Ernsting, N. P.; Maroncelli, M. Conductivity and Solvation Dynamics in Ionic Liquids. *J. Phys. Chem. Lett*. **2013**, *4*, 1205–1210.
202. Rumble, C. A.; Uitvlugt, C.; Conway, B.; Maroncelli, M. Solute Rotation in Ionic Liquids: Size, Shape, and Electrostatic Effects. *J. Phys. Chem. B* **2017**, *121*, 5094–5109.
203. Das, A.; Das, S.; Biswas, R. Density relaxation and particle motion characteristics in a non-ionic deep eutectic solvent (acetamide + urea): Time-resolved fluorescence measurements and all-atom molecular dynamics simulations. *J. Chem. Phys*. **2015**, *142*, 034505.
204. Mukherjee, K.; Das, S.; Tarif, E.; Barman, A.; Biswas, R. Dielectric relaxation in acetamide + urea deep eutectics and neat molten urea: Origin of time scales via temperature dependent measurements and computer simulations. *J. Chem. Phys.* **2018**, *149*, 124501.
205. Tarif, E.; Mondal, J.; Biswas, R. Interaction and Dynamics in a Fully Biodegradable Glucose-Containing Naturally Abundant Deep Eutectic Solvent: Temperature-Dependent Time-Resolved Fluorescence Measurements. *J. Phys. Chem. B* **2019**, *123*, 9378–9387.
206. Hossain, S. S.; Samanta, A. Solute rotation and translation dynamics in an ionic deep eutectic solvent based on choline chloride. *J. Phys. Chem. B* **2017**, *121*, 10556– 10565.

207. Hossain, S. S.; Samanta, A. How do the hydrocarbon chain length and hydroxyl group position influence the solute dynamics in alcohol-based deep eutectic solvents? *Phys. Chem. Chem. Phys.* **2018**, *20*, 24613– 24622.
208. Hossain, S. S.; Paul, S.; Samanta, A. Liquid Structure and Dynamics of Tetraalkylammonium Bromide-Based Deep Eutectic Solvents: Effect of Cation Chain Length. *J. Phys. Chem. B* **2019**, *123*, 6842–6850.
209. Hossain, S. S.; Paul, S.; Samanta, A. Complete Solvation Dynamics of Coumarin 153 in Tetraalkylammonium Bromide-Based Deep Eutectic Solvents. *J. Phys. Chem. B* **2020**, *124*, 2473−2481.
210. Gautam, R. K.; Ahmed, S. A.; Seth, D. Photophysics of Thioflavin T in deep eutectic solvents. *J. Lumin.* **2018**, *198*, 508–516.
211. Cui, Y.; Rushing, J. C.; Seifert, S.; Bedford, N. M.; Kuroda, D. G. Molecularly Heterogeneous Structure of a Nonionic Deep Eutectic Solvent Composed of N-Methylacetamide and Lauric Acid. *J. Phys. Chem. B* **2019**, *123*, 3984– 3993.
212. Kaur, S.; Gupta, A.; Kashyap, H. K. Nanoscale Spatial Heterogeneity in Deep Eutectic Solvents. *J. Phys. Chem. B* **2016**, *120*, 6712–6720.
213. Kaur, S.; Gupta, A.; Kashyap, H. K. How Hydration Affects the Microscopic Structural Morphology in a Deep Eutectic Solvent. *J. Phys. Chem. B* **2020**, *124*, 2230–2237.
214. Percevault, L.; Jani, A.; Sohier, T.; Noirez, L.; Paquin, L.; Gauffre, F.; Morineau, D. Do Deep Eutectic Solvents Form Uniform Mixtures Beyond Molecular Microheterogeneities? *J. Phys. Chem. B* **2020**, *124*, 9126–9135.
215. Srinivasan, H.; Sharma, V. K.; Sakai, V. G.; Embs, J. P.; Mukhopadhyay R.; Mitra, S. Transport Mechanism of Acetamide in Deep Eutectic Solvents. *J. Phys. Chem. B* **2020**, *124*, 1509–1520.
216. Pronk, S.; Lindahl, E.; Kasson, P. M. Dynamic heterogeneity controls diffusion and viscosity near biological interfaces. *Nat. Commun.* **2014**, *5*, 3034.
217. Chun, J.; Mundy, C. J.; Schenter, G. K. The Role of Solvent Heterogeneity in Determining the Dispersion Interaction between Nanoassemblies. *J. Phys. Chem. B* **2015**, *119*, 5873–5881.
218. Benay, G.; Wipff, G. The effect of solvent heterogeneity on the solvation and complexation of alkali cations by 18-crown-6: a simulation study in the 90:10 chloroform/methanol mixture. *New J. Chem.* **2016**, *40*, 4662-4671.

219. Mellmer, M. A.; Sanpitakseree, C.; Demir, B.; Bai, P.; Ma, K.; Neurock, M.; Dumesic, J. A. Solvent-enabled control of reactivity for liquid-phase reactions of biomass-derived compounds. *Nat. Catal*. **2018**, *1*, 199-207.

This Page Intentionally Left Blank

Chapter 2

Experimental Techniques

In this chapter, experimental techniques used in the present thesis are briefly discussed. I used steady-state absorption and emission, time-correlated single photon counting (TCSPC), fluorescence correlation spectroscopy (FCS), fluorescence up-conversion and transient absorption spectroscopy. Basic principle, instrumentation and data analysis of these spectroscopic techniques are described. Materials and methods pertaining to samples preparation are also discussed.

2.1 Steady-State Absorption and Emission

Steady-state absorption spectra of the samples were measured in a commercial UV-Vis spectrophotometer (Shimadzu UV-2450, Japan) retrofitted with Peltier based temperature controller (TCC-100, Shimadzu, Japan). Steady-state fluorescence spectra were taken in a commercial spectrofluorimeter (Fluoromax-4, Horiba Jobin Yvon). Fluorescence emission spectra were corrected for wavelength dependent efficiency of the detector.

2.2 Time-Resolved Fluorescence Measurement

Time-resolved fluorescence measurement is an important technique in fluorescence spectroscopy and has several advantages over steady-state measurements. Fluorescence lifetime is the average amount time a fluorophore remains in the excited state.[1] For example, fluorophores present in two different environments may not be resolved in the steady-state measurement because of the spectral overlap. However, time-resolved measurement may give insight into the difference in the environments by simply measuring the fluorescence lifetime. Fluorescence quenching study with steady-state spectra cannot distinguish whether the quenching is dynamic or static. On the other hand, from the fluorescence lifetime measurement, one can easily resolve this ambiguity.[1] Time-resolved fluorescence measurements also provide invaluable information about the various dynamics of the system like solvent relaxation and solute rotation. While there are many time-resolved fluorescence techniques, most prominent techniques are Time-correlated Single Photon Counting (TCSPC) and Fluorescence Up-conversion, which will be discussed in this section. These two techniques are different in terms of time-resolution and accessible time window. TCSPC has time resolution of about 100 picoseconds while fluorescence up-conversion has a time resolution of about 100-300 fs.

2.2.1 Time-Correlated Single Photon Counting (TCSPC)

TCSPC is one of the most widely used techniques for time-resolved fluorescence measurements. There are dedicated books for this technique.[2,3] This technique involves the measurement of arrival time, *t*, of the first detected photon for every pulsed excitation. The probability of detecting this single photon at time *t* is proportional to the fluorescence intensity at that time. Fluorescence is a random process and the photons are emitted from the various stages of relaxation from the Franck-Condon state. This results in the distribution of emitted photons in terms of time (decay). Collecting a large number of single photons following the excitation, fluorescence intensity decay is reconstructed.

Figure 2.1 shows the schematic of the TCSPC setup. In this technique, a light pulse excites the sample and the arrival time of the emitted photons are measured. A signal is fed to a constant function discriminator (CFD) at the same time when the samples is excited to mark the start of fluorescence event. CFD is used to increase the accuracy of the time measurement. CFD triggers time-to-amplitude converter (TAC) to ramps up the voltage in the capacitor. It is very important for voltage to increase linearly with time. Meanwhile, signal from detected fluorescence photons reaches CFD which in turn triggers TAC to stop the voltage ramp. Multichannel plate photomultiplier tube (MCP PMT) is used for single photon detection which are fed through monochromator (MC). Measurement of accurate arrival time of the photons is a challenge in TCSPC. Due to amplitude jitter of the detector and unstable light source, there is a distribution in the heights of the pulses reaching CFD. Because of this, there is a timing jitter which affects the instrument response function (IRF). CFD solves this problem by splitting the signal into two parts, where one part is delayed and other part is inverted. The two signals are finally combined and *zero crossing point* becomes independent of pulse amplitude. It is important to remember that at most only one photon is detected per excitation. Voltage ramp in the TAC is proportional to the arrival time excitation and emission signals. This voltage is amplified and is converted to a numerical value in the analog-to-digital convertor (ADC). This numerical value is stored and taken as a single event. This cycle of excitation and detection is repeated numerous times until a histogram of number of counts/photons with time information is obtained for sufficient precision. This histogram represents the measured intensity decay. For lifetime measurement, the emission polarizer is set in magic angle (54.9°) with respect to the excitation polarizer. In this thesis, a commercial TCSPC setup (LifeSpec II, Edinburgh Instruments, U.K.) has been used.[4]

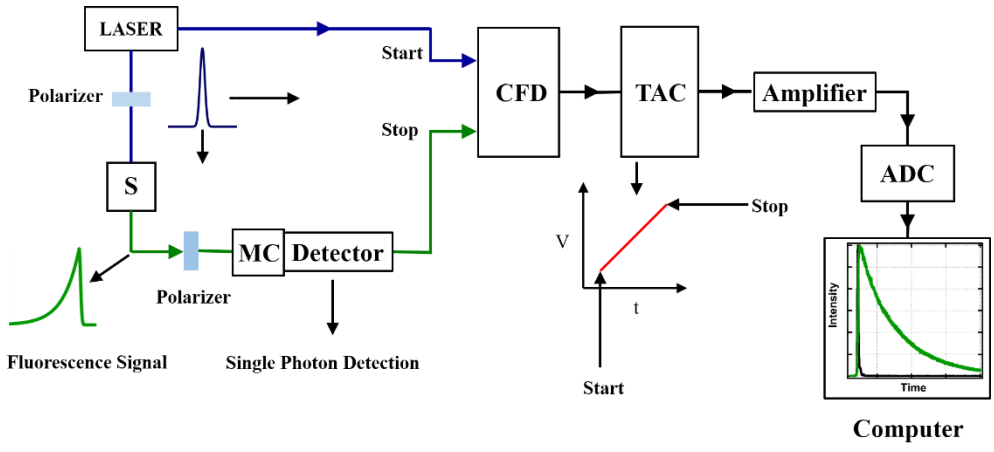

Figure 2.1 Schematic for Time-Correlated Single Photon Counting (TCSPC) setup.

2.2.2 Data Analysis

In TCSPC, it is not possible to observe the true intensity decay law or impulse response function, I(t), which would have been the result of δ-function excitation or δ-function like instrument response function, IRF (i.e. infinitely short pulse width). In reality, instrument response function has a finite temporal width and as a result, the observed data (decay) is the convolution with the IRF. Convolution is a mathematical operation on two functions that results in a new function. This new function captures the effect of the shape of one function on other, which is similar to cross-correlation. Mathematically, convolution is the integral of the product of the two functions.[1,3,5]

$$f \otimes g = \int_{-\infty}^{\infty} f(\tau)g(t-\tau)d\tau = \int_{-\infty}^{\infty} f(t-\tau)g(\tau)d\tau \qquad 2.1$$

In the analysis of TCSPC data, IRF and actual decay represents these functions and the observed decay is the convolution of IRF and actual decay as mentioned earlier. Concept of convolution is used in TCSPC to analyse the data to get the actual decay. Excitation pulse can be thought of as a series or sum of δ-pulses $P(t)$ each resulting in an actual or true decay $I(t)$. The amplitude of the decay is proportional to the intensity of δ-pulse and the excitation at time $t_i$is given by

$$I(t_i) = P(t_i)I(t-t_i) \qquad 2.2$$

The measured decay $I'(t_i)$ is the sum over all the δ-pulse excitation responses for all times preceding t_i given by

$$I'(t) = \int_{0}^{t} P(t_i)I(t-t_i)dt_i \qquad 2.3$$

Deconvolution of the TCSPC data was achieved by iterative non-linear least square.[1,3,5] In this method, a parameter that relates the experiment and calculated data point is minimized by iteration method to give the best possible value. Goodness of fit parameter χ^2 which is used to judge end result is given by[1,3]

$$\chi^2 = \sum_{i=1}^{n} \left[\frac{N(t_i) - N_C(t_i)}{\sigma_i} \right]^2 \qquad 2.4$$

where n is the number of data points (channels), σ_i is the standard deviation of the ith point, $N(t_i)$ and $N_C(t_i)$ are measured and calculated decays, respectively. Above equation is

dependent on the number of data points taken and the number of fitting parameters. To overcome this dependence, reduced χ^2 is used, and is given by

$$\chi_R^2 = \frac{\chi^2}{n-p} = \frac{1}{v}\sum_{i=1}^{n}\left[\frac{N(t_i) - N_C(t_i)}{\sigma_i}\right]^2 \qquad 2.5$$

where v is the number of degrees of freedom, n is the number of data points and p is number of floating parameters. For two exponentials fitting equation, p=3, i.e. two time constants and one amplitude. Since number of data points taken is usually high, $n \approx v$. Therefore χ_R^2 has a value near unity as average χ^2 for each data point is nearly 1. Since the TCSPC measurement follows Poisson distribution, $\sigma_i \sim \sqrt{N(t_i)}$, the above equation becomes

$$\chi_R^2 = \frac{\chi^2}{n-p} = \frac{1}{v}\sum_{i=1}^{n}\frac{[N(t_i) - N_C(t_i)]^2}{N(t_i)} \qquad 2.6$$

Deconvolution starts with the initial guess values of the time-constants and the corresponding amplitudes. For the given values, the expected decay is reconvoluted with IRF and is compared to the observed decay. Then the mathematical algorithm is used for the iteration, which continues until the values of the parameters are found for best fit. Fortunately, above analysis can easily be performed with commercial analysis software FAST provided with the instrument.

2.2.3 Fluorescence Up-Conversion

Fluorescence Up-Conversion is an ultrafast spectroscopic technique widely used to study ultrafast dynamics.[1,4,6] As the name suggests, this technique is based on the sum frequency generated signal (upconverted signal) wtih emission and the gate pulse. This technique provides the resolution of ~100 fs and 1-2 ns. Unlike TCSPC, time resolution in up-conversion method is not limited by the electronics. In this technique, a laser beam of fundamental frequency (ω_1) with ultrashort pulse (~100 fs) is divided into two parts with a beam splitter. One of these beams is focused on a non-linear crystal to generate second harmonic signal ($\omega_2 = 2\omega_1$). The second harmonic is separated from the fundamental light using dichroic mirror and acts as the excitation pulse (pump pulse). Third harmonic is used for the samples with absorption in the UV region. The other part of the beam passes through an optical delay line and acts as the probe or gate pulse. The pump pulse is focussed on the sample and the resulting fluorescence from the sample with frequency ω_{FL} is focused on second non-linear crystal. Gate pulse is also focused on the same non-linear crystal in the same region where the fluorescence

is focused under magic angle condition. As a result, an up-converted signal is generated with frequency equal to the sum of the frequencies of fluorescence and gate pulse ($\omega_3 = \omega_{FL} + \omega_1$). Spatial and temporal overlap of the two signals is necessary for efficient up-conversion. Fluorescence decay can be obtained from the intensity of the up-converted signal as the delay time is varied for gate pulse if the intensity of the gate pulse remain unaltered during the measurement. The intensity of the up-converted signal (I_{SF}) at any delay time (τ) is proportional to the correlation function of the fluorescence intensity with the gate pulse intensity (I_{Pr}),

$$I_{SF}(\tau) = \int_{-\infty}^{\infty} I_{FL}(t)\, I_{Pr}(t-\tau)dt \qquad 2.7$$

The fluorescence decay, which is the plot of $I_{SF}(\tau)$ against delay time (τ), is deconvoluted from the IRF using following function

$$F(t) = \frac{1}{2}\sum_i a_i exp\left(\frac{\tau_G^2}{2\tau_i} - \frac{(t-t_0)}{\tau_i}\right)\text{erf}\left(\frac{\tau_G^2 - \tau_i(t-t_0)}{\sqrt{2}\tau_i\tau_G}\right) \qquad 2.8$$

where $\tau_G$is the width of the IRF, a_i and τ_i are the amplitude and the time constants and t_0 is the time shift between the IRF and the fluorescence decay. Using the time constants and the corresponding amplitudes obtained from the fitting, time-resolved emission spectra is constructed as described in the next section. For this a commercial femtosecond up-conversion setup (FOG 100, CDP Corp., Moscow, Russia) was used. The samples were excited with the second harmonics generated from the mode-locked Ti:Sapphire laser (Mai-Tai-HP, Spectra Physics, USA).[4] The instrument response function (IRF) of the up-conversion setup is ~250 fs.

2.3 Time-Resolved Emission Spectra (TRES)

TRES is an important method to study various dynamics in the excited state of the fluorophore. TRES is the emission spectra at some instant of time following pulsed excitation. The electronic excitation of the fluorophores to the Franck-Condon state (0 to 1) is instantaneous and there is a significant increase in the dipole moment of the fluorophore for positive solvatochromic molecules. The emission spectra, if captured at this stage, will be blue shifted. The solvent molecules reorient around the excited fluorophores to reduce its energy and gradually attains the relaxed state.[1,3] It takes finite time to reach this solvent relaxed state where the emission spectra is red shifted.

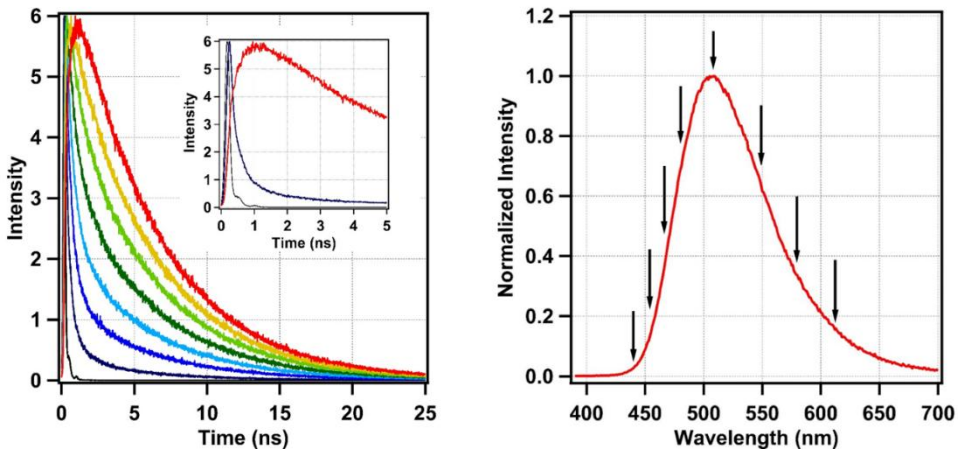

Figure 2.2 Time-resolved fluorescence decay (right) is measured at wavelengths (shown by the black arrows) across the steady-state emission spectra (left). Rise component is observed for decays measured at long wavelengths (right inset).

TRES is indirectly measured (reconstructed) using wavelength dependent fluorescence decay method.[1,3,7] A series of time-resolved fluorescence decay is measured at wavelengths across the emission spectra as shown in figure 2.2. These fluorescence transients are analysed as described above. The intensity of the TRES is the function of the wavelength (λ) at which it is measured and the time (*t*) which can be mathematically represented by the product of the functions of independent variables λ and t as

$$I(\lambda, t) = A(\lambda)B(t) \qquad 2.9$$

Mathematically, steady-state emission spectra (I_{SS}) is represented as,

$$I_{SS} = \int_0^\infty I(\lambda, t)dt \qquad 2.10$$

Replacing equation 2.9 in 2.10, we get

$$I_{SS} = \int_0^\infty A(\lambda)B(t)dt \qquad 2.11$$

$$I_{SS} = A(\lambda)\int_0^\infty B(t)dt \qquad 2.12$$

where *B(t)* can be represented by sum of exponentials, which is obtained from time-resolved fluorescence decay. Therefore using

$$B(t) = \sum_i \alpha_i \exp(-t/\tau_i) \qquad 2.13$$

(using the relation $\int_0^\infty ae^{-\frac{t}{\tau}}dt = \alpha\tau$)

we get,

$$I_{SS} = A(\lambda)\sum_i \alpha_i\tau_i \qquad 2.14$$

$$A(\lambda) = \frac{I_{SS}}{\sum_i \alpha_i\tau_i} \qquad 2.15$$

therefore,

$$I(\lambda, t) = \frac{I_{SS}}{\sum_i \alpha_i\tau_i}\sum_i \alpha_i \exp\left(-\frac{t}{\tau_i}\right) \qquad 2.16$$

The above equation represents the intensity of different wavelengths at a given time. A common way to quantify the temporal change of the TRES, that is to measure time-dependent Stokes shift, is to monitor the shift in the peak position or peak frequency $\nu(t)$. This can be achieved by fitting the lognormal function[7]

$$g(\nu) = g_0 exp\left[-\ln(2)\left(\frac{\ln\left[1 + 2b\left(\nu - \nu_p\right)/\Delta\right]}{b}\right)^2\right] \qquad 2.17$$

for $\alpha > 1$, and

$$g(\nu) = 0$$

for $\alpha < 1$, where $\alpha = 2b\left(\nu - \nu_p\right)/\Delta$

For comparisons, peak frequency $\nu(t)$ is converted to solvent response function $C(t)$ which is the normalized form as,

$$C(t) = \frac{\nu(t) - \nu(\infty)}{\nu(0) - \nu(\infty)} \qquad 2.18$$

$C(t)$ can be fitted with exponential or sum of exponentials to obtain average solvation time ($\langle\tau_s\rangle$).

2.4 Time-Resolved Fluorescence Anisotropy

When fluorophores are excited with a linearly polarized light, polarized emission is observed.[1,3,7] The extent of polarization of the emission is expressed by anisotropy (*r*). When the sample is illuminated with linearly polarized light, only those fluorophores are preferably excited that have their absorption transition moment oriented along the electric field vector of the incident light. This is known as photoselection. The create/induced polarization is not

permanent. The loss of polarization of the emission spectra (fluorescence depolarization) results from many processes and rotational diffusion is one of the main reasons.

Rotational diffusion changes the orientation of the transition moment and eventually the emission becomes de-polarized. The time dependent fluorescence anisotropy, thus, can be written as

$$r(t) = \frac{I_{\parallel}(t) - GI_{\perp}(t)}{I_{\parallel}(t) + 2GI_{\perp}(t)} \qquad 2.19$$

where $I_{\parallel}(t)$ and $I_{\perp}(t)$ are the fluorescence decay at parallel and perpendicular polarization with respect to the polarization of excitation light, respectively, constant G is called G-factor which is the ratio of sensitivity of monochromator and detector towards parallel and perpendicular emission intensities. G-factor is estimated by tail-matching of $I_{\parallel}(t)$ and $I_{\perp}(t)$ decays at sufficiently long time.

Time-resolved fluorescence anisotropy, $r(t)$, is fitted with exponential or sum of exponentials function to estimate the average rotation time ($\langle\tau_r\rangle$). Anisotropy measurement was done in the same TCSPC setup (LifeSpec II, Edinburgh Instruments, U.K.).

2.5 Fluorescence Correlation Spectroscopy (FCS)

Fluorescence correlation spectroscopy (FCS) is one of the widely used single molecular level techniques based on confocal microscopy setup.[1,5,8,9] In this technique, light beam is focused into a small region (called observation volume or focal volume) of the sample using an objective as shown in figure 2.3. The volume of this region is about ~1 fL and the concentration of the fluorophore in the sample is in the order of nM such that there is only about 1 fluorophore in the observation volume on an average. The reason for focussing on the tiny region is to circumvent interference of the Raman scattering from the solvent molecules to the fluorescence signal. The fluorescence is collected only from the observation volume using a pinhole. Thus, fluorescence signal persists as long as the fluorophore remains inside this observation volume and the signal is lost when there is no fluorophore inside. Thus it gives fluorescence fluctuation as a function of time arising from the concentration fluctuation of the fluorophore within the observation volume, resulted due to the translational diffusion of the fluorophore.

The autocorrelation function of the intensity fluctuation due to random diffusion can be expressed as.[1]

$$G(\tau) = \frac{\langle \delta F(t) \delta F(t+\tau) \rangle}{\langle F(t) \rangle^2} \qquad 2.20$$

where $<F(t)>$ is the average fluorescence intensity, $\delta F(t)$ and $\delta F(t+\tau)$ are the magnitudes of fluorescence intensity fluctuation from the average value at time t and $t+\tau$, respectively.

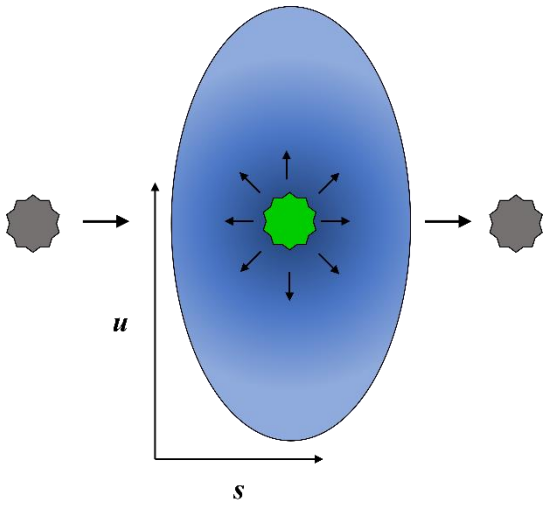

Figure 2.3 Observation volume in the FCS measurement from the fluorescence is recorded.

For a particle (one kind of particles to be precise) diffusing in 3D Gaussian volume, this autocorrelation function can be expressed as[1]

$$G(\tau) = G(0)\left(1+\frac{\tau}{\tau_D}\right)^{-1}\left(1+\frac{1}{w^2}\frac{\tau}{\tau_D}\right)^{-\frac{1}{2}} \qquad 2.21$$

where $G(0)=1/N$ ($G(\tau)$ at $\tau=0$), N is the number of particles present in the observation volume. $w=u/s$ is the ratio of radius and the half-length of the depth of the observation volume and τ_D is the average translational diffusion time constant of the particle through the observation volume. Equation 2.21 is used to fit the raw data and determine τ_D and $G(0)$. The quantity w can be obtained by calibrating the instrument with aqueous solutions of R6G with different concentrations and globally fitting the resulting autocorrelation curves. If desired, the dimensions (u and s) of the focal volume can easily be determined by using known diffusion coefficient of R6G in water ($D_t = 4.14 \times 10^{-6}$ cm^2 s^{-1}) at 298 K[10] by using the relation $\tau_D = s^2/4D$.[1] In many instances, the particle does not undergo normal diffusion but show anomalous diffusion[11] which can represented by following autocorrelation function[12, 13]

$$G(\tau) = G(0)\left[1+\left(\frac{\tau}{\tau_D}\right)^{\alpha}\right]^{-1}\left[1+\frac{1}{w^2}\left(\frac{\tau}{\tau_D}\right)^{\alpha}\right]^{-\frac{1}{2}} \qquad 2.22$$

where α is the exponent showing deviation from normal diffusion. Three types of diffusions have been classified on the basis of exponent α[11]

1. Sub-diffusion ($0< \alpha <1$). Frequently observed in crowded environments.
2. Normal diffusion ($\alpha=1$).

3. Super diffusion (α>1).

If there are multiple diffusing species or if the same fluorophore is diffusing with two diffusion constants as a result of environmental heterogeneity, the autocorrelation function is given by[1]

$$G(\tau) = \frac{1}{[N_1 + N_2]^2}[N_1 D_1 + N_2 D_2] \qquad 2.23$$

where

$$D_i(\tau) = G(0)\left(1 + \frac{\tau}{\tau_{D_i}}\right)^{-1}\left(1 + \frac{1}{w^2}\frac{\tau}{\tau_{D_i}}\right)^{-\frac{1}{2}} \qquad 2.24$$

If the fluorescence fluctuation has contribution from processes other than diffusion, equation 2.21 can be rewritten as follows,

$$G(\tau) = G(0)\left[1 + \left(\frac{\tau}{\tau_D}\right)\right]^{-1}\left[1 + \frac{1}{w^2}\left(\frac{\tau}{\tau_D}\right)\right]^{-\frac{1}{2}}\left(1 + A.exp\left(-\frac{\tau}{\tau_R}\right)\right) \qquad 2.25$$

where A is the amplitude of the process apart from diffusion and τ_R is the time scale of such process. One of the processes that cause this additional fluctuation is triplet state blinking.[1] In proteins, it is important to determine its hydrodynamic radius which can be obtained by following SE relation

$$r_H = \frac{k_B T}{6\pi\eta D_t} \qquad 2.26$$

where D_t is the translational diffusion coefficient of protein calculated using relation $\tau_D = s^2/4D$. τ_D is obtained by fitting the FCS data.

In the presence of external additives, the solution's refractive index and viscosity may change significantly in addition to the diffusion. In the study protein in the present thesis (chapter 6B), the effect of the viscosity change was rectified by performing a control experiment at every experimental point by taking R6G as the fluorophore. R6G is a rigid molecule and will not undergo any structural change when exposed to DES at various degree of hydration. In this way, any change in its diffusion time through the detection volume will be because of the difference in the medium viscosity solely. Using this information and the reported value of the hydrodynamic radius of R6G (7.7 Å) in pH 7.4 buffer, the hydrodynamic radius of protein can be calculated at every experimental point according to the following equation.

$$r_H = r_H^{R6G} \times \frac{\tau_D}{\tau_D^{R6G}} \qquad 2.27$$

Above equation gives the hydrodynamic radius of the protein without having to determine the viscosity of the medium. The refractive index change is compensated by changing the objective

collar position and setting it to have the highest G(0) value for each of the samples. In this way, the lowest detection volume attainable is maintained for each sample.

In the work presented here, FCS measurements were performed in a home built setup based on confocal microscope.[14] Schematic of FCS setup is shown in figure 2.4. It consists of an inverted microscope (Olympus IX-71) and a water immersion objective (60x, 1.2 NA, Olympus, Japan). CW laser source (MDL-III-405-5mW, China, for excitation at 405 nm and MGL-III-532-5mW, China, for excitation at 532 nm depending on the fluorophore employed) is used to excite the samples. The excitation light is focused on to the samples using the objective and the same objective is used to collect the fluorescence from the samples (epifluorescence setup). A dichroic mirror is used to direct the fluorescence beam towards the pinhole and is focused using a lens. An optical fibre guides the fluorescence signal to the photon counting module (SPCM-AQRH-13-FC, Excelitas Tech. In., Canada). Finally, a correlator card is used to generate autocorrelation function and recorded in a computer under LabVIEW® platform.

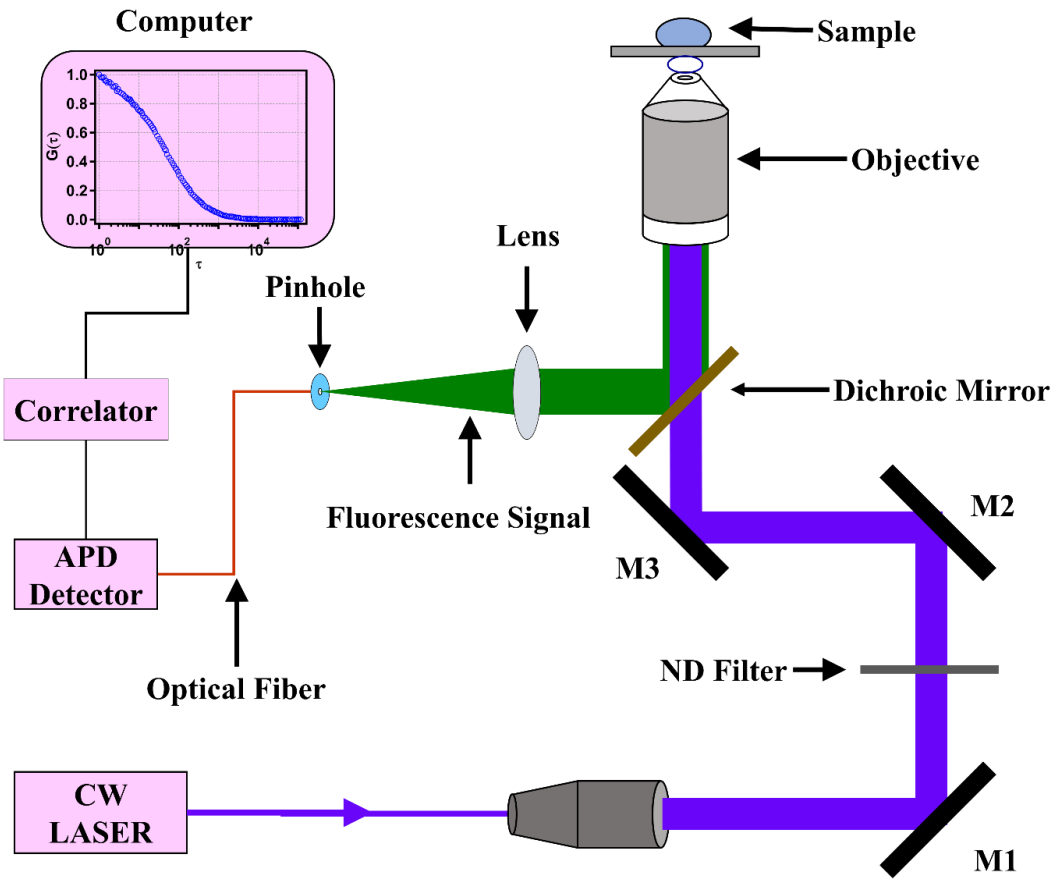

Figure 2.4 Home built FCS setup

2.6 Femtosecond Transient Absorption (TA) Spectroscopy

Transient absorption spectroscopy is another ultrafast technique.[15] In this technique, pump pulse with a particular frequency excites the molecule from S_0 to S_1 state and then the probe pulse, which is a white light, probes the molecule while still in the excited state at different time delays between the pump and the probe pulse. The probe pulse may further excite the molecule to higher excited state resulting the excited state absorption or de-excite the molecule to S_0 resulting the stimulated emission. In the transient absorption spectroscopy, the difference in absorption spectra is measured i.e. the difference of the absorption spectra (OA) of the sample when it is excited (pumped) and non-excited (unpumped) states by measuring the probe pulse intensity. According to Lambert-Beer's Law, intensity of the probe pulse after passing the pumped sample is

$$I_{Pumped}(\lambda) = I_0(\lambda)10^{-A_{Pumped}(\lambda)} \qquad 2.28$$

where I_0 is the intensity of the incident probe pulse and A_{Pumped} is the absorbance of the pumped sample. Similarly for unpumped sample,

$$I_{Unpumped}(\lambda) = I_0(\lambda)10^{-A_{Unpumped}(\lambda)} \qquad 2.29$$

Dividing equation 2.28 by equation 2.29 and taking the log, we get

$$\Delta A = A_{Pumped}(\lambda) - A_{Unpumbed}(\lambda) = -Log\left[\frac{I_{Pumped}(\lambda)}{I_{Unpumped}(\lambda)}\right] \qquad 2.30$$

Above equation is the difference absorption ΔA at fixed time delay "t" of probe pulse with respect to the pump pulse. Temporal evolution of ΔA can be obtained as the delay time is varied. ΔA is positive for process like excited state absorption and negative for processes like ground state bleaching and stimulated emission. In the present thesis, I used transient absorption spectroscopy for the solvation dynamics study for which temporal shift of stimulated emission was monitored.

The femtosecond transient absorption spectrometer used in this study comprises of a Ti:sapphire oscillator (Micra 10, Coherent) amplified by a 1 kHz regenerative amplifier (Legend Elite, Coherent). The wavelength of the amplified output pulse is centred at 800 nm. The temporal width of the pulse is ~45 fs with an energy of 3.5 mJ. This 800 nm beam is split into two parts. One part of the beam generates the pump pulse in an optical parametric amplifier (OPERA SOLO, Coherent) and the other part is directed to the sapphire crystal generating white light continuum that covers the spectral range between 400 and 1100 nm. The detection system is composed of a monochromator (Acton SP2300, Princeton Instruments) and a pair of

diode array detectors working in spectral range between 400 and 1000 nm. The samples were excited at 450 nm with pump intensity of 85 μW. To detect the isotropic response of the medium, the magic angle configuration of pump and probe beams was applied. The instrument response function of the setup is 70 fs.

2.7 Optical Kerr Effect Spectroscopy

The optical Kerr effect (OKE) experiment was used to study the bulk solvent dynamics, where the time evolution of birefringence induced by a pump laser pulse is investigated with a delayed probe pulse. The measurements were made with ~20 fs pulses using the home built setup, described in details in elsewhere.[16] The OKE signal consists of ultrafast electronic (hyperpolarizability) response, centered around zero delay, and a slower nuclear response, which includes components due to the intermolecular dynamics and intramolecular vibrations. As in the present study, only the intermolecular nuclear dynamics is important, we get rid of the contributions due to the electronic response around zero delay and due to the intramolecular vibrations by a modified version of the McMorrow and Lotshaw deconvolution procedure.[17] The modification is to set the spectra to zero at wavenumbers above 350 cm^{-1}, where the chosen cut off frequency corresponds to a minimum between the intermolecular and intramolecular parts of the spectra. The IRF used in the deconvolution procedure is obtained from the Kerr signal of a properly cut and oriented CaF_2 single crystal, where only the electronic response is present.[16,18]

2.8 CD Spectroscopy: Circular dichroism (CD) spectra was recorded on a commercial CD spectrometer (J-815, Jasco, Japan) using 2 mm pathlength cuvette. CD data was analyzed using CDNN software (http://gerald-boehm.de).[19]

2.9 Measurement of Thermophysical properties

Density. Densities of the samples were measured in a home-built glass apparatus (see figure 2.5), which is temperature-controlled by an external water bath (LLCB-202, Labocon, UK). In this setup, the glass material's thermal expansion/compression was neglected, which might result in a small error. The known value of the density of the water was used to calculate the volume. To verify its accuracy, we measured the density of glycerol at various temperatures and compared with reported values as shown in table 2.1. We also measured the density of non-volatile solvents (data not shown) at lower temperatures to check the accuracy of the pycnometer.

Figure 2.5 Picture showing home built temperature controlled pycnometer.

Table 2.1 Experimental densities (gL^{-1}) of glycerol at different temperature and comparison with reported values.

T (°C)	T(K)	Experiment	Literature
20	293	1.261	1.26099[a]
25	298	1.257	1.25791[a], 1.2589[b]
30	303	1.255	1.2556[b]
35	308	1.252	1.25166[a], 1.2527[b]
40	313	1.249	1.2495[b]
45	318	1.247	1.2462[b]
50	323	1.244	1.24211[a], 1.2429[b]
55	328	1.242	1.2396[b]
60	333	1.238	1.23571[a], 1.2360[b]
65	338	1.235	1.2348[c]
70	343	1.233	-
75	348	1.230	1.22579[a], 1.2287[c]
80	353	1.222	~1.220[d]

a) Egorov, G. I.; Makarov, D. M.; Kolker, A. M. Volume properties of liquid mixture of water + glycerol over thetemperature range from 278.15 to 348.15 K at atmospheric pressure. *Thermochim. Acta* **2013**, *570*, 16-26
b) Li, Q.-S.; Su, M.-G.; Wang, S. Densities and Excess Molar Volumes for Binary Glycerol + 1-Propanol, +2-Propanol, + 1,2-Propanediol, and + 1,3-Propanediol Mixtures at Different Temperatures. *J. Chem. Eng. Data* **2007**, *52*, 1141-1145.
c) Prieto, N. M. C. T.; Souza, T. A.; Egas, A. P.; Ferreira, A. G. M.; Lobo, L. Q.; Portugal, A. T. A. Liquid glycerol: Experimental densities at pressures of up to 25 MPa, and some derived thermodynamic properties. *J. Chem. Thermodyn*. **2016**, *101*, 64-77.
d) McDuffie, G. E.; Forbes, J. W.; Madigosky, W. M.; von Bretzel, J. J. Density and compressibility of four higher alcohols for pressures to 2800 kg./sq. cm. *J. Chem. Eng. Data* **1969**, *14*, 176-180.

Refractive index. The Refractive index was measured in a commercial Abbe refractometer (DR-A1, Atago, Japan). The refractive index can be measured with a precision of 0.0001, and the uncertainty involved in the measurement of the refractive index is better than ±0.0004. Temperature was controlled by external water bath (LLCB-202, Labocon, UK).

Sound velocity. Sound velocity was measured using an ultrasonic interferometer (F-05, Mittal Enterprises, India). Here also, the temperature was controlled by external water bath (LLCB-202, Labocon, UK).

Viscosity. Dynamic viscosity was measured by a rolling ball viscometer (Lovis 2000 M, Anton Paar, Austria) with an in built temperature controller.

2.10 Materials and Methods

Materials. Fluorescent probes 4-(Dicyanomethylene)-2-methyl-6-(4-dimethylaminostyryl)-4*H*-pyran (DCM), coumarin 153 (C153) and rhodamine 6G (R6G) were purchased from Sigma Aldrich and used without further purification. Bromelain and Casein purchased from Sigma Aldrich were used without further purification. Tetramethylrhodamine-5-maleimide (TMR) and 7-diethylamino-3-(4-maleimidophenyl)-4-methylcoumarin (CPM) were used to tag bromelain for spectroscopic studies were also purchased from Sigma Aldrich. Lithium nitrate, lithium bromide, urea, D-menthol and lauric acid were all purchased from Sigma Aldrich and used without further purification. D-sorbitol was purchased from SD Fine Chemicals and used without further purification. Lithium nitrate, lithium bromide, sorbitol and urea were dried under vacuum for several hours before use. Acetamide was purchased from Fisher Scientific

and was recrystallized in methanol and dried before use. Unfortunately we could not report the water in the samples because of the lack of Karl-Fisher setup. Therefore enough care was taken while handling these chemicals as many of them are hygroscopic. Analytical grade di-sodium hydrogen phosphate and sodium dihydrogen phosphate were purchased from Merck, India, and was used to prepare buffer (pH 7.4). Dialysis membrane tubing (12 kDa cut-off) was purchased from Sigma-Aldrich and was washed according to the procedure given by Sigma-Aldrich. Centrifugal filtration unit (Amicon Ultra, 10 kDa cut-off) have been purchased from Merck Millipore, Germany. HPLC grade dimethyl sulfoxide (DMSO) was purchased from S. D. Fine Chemicals Limited, India, and used after distillation. Scheme 1 shows structure of some of the molecules involved in the present thesis.

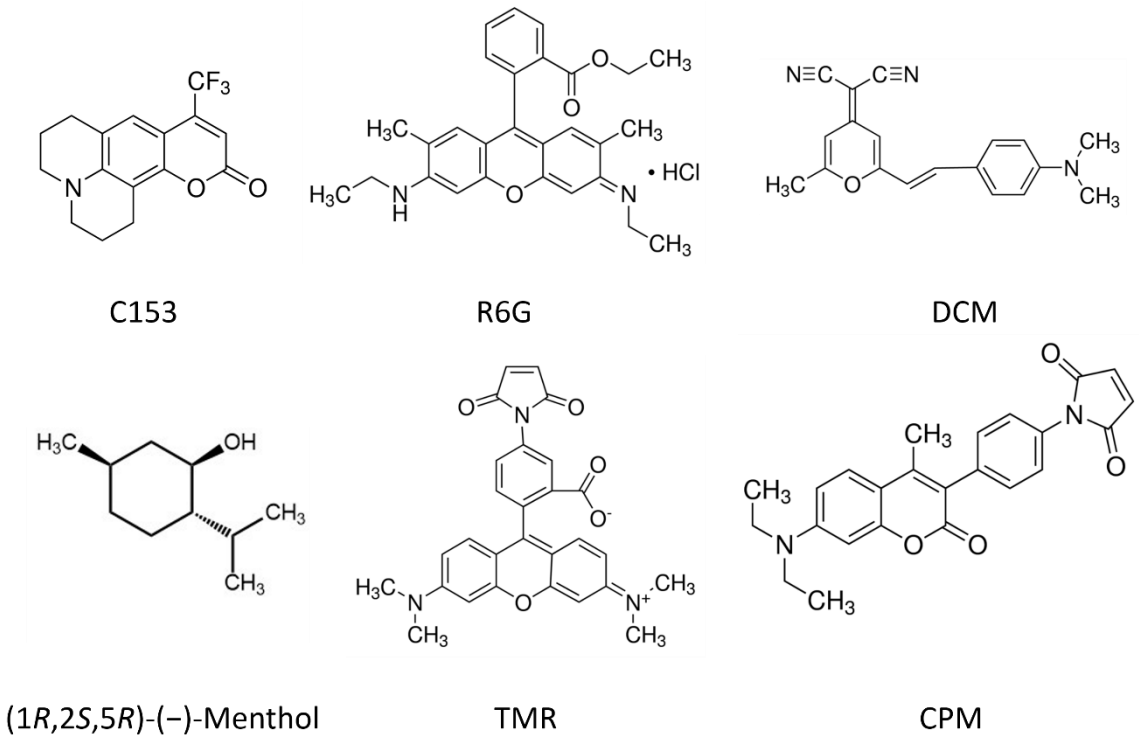

Scheme 2.1 Molecular structures of some of the chemicals used in the present thesis.

Sample/DES preparation. All the DESs were prepared by taking required proportions of the components heating the mixtures to a suitable temperature while continuously stirring. In the preparation of non-ionic ternary DES the mixture containing 0.4 mole fraction of sorbitol requires prolonged heating. However, prolonged heating should be avoided for two reasons; (a) sublimation of acetamide, which results in the change of mole fraction of the mixture, and (b) sorbitol turns brownish although sugar polyols are not known to caramelize. Although the exact freezing point cannot be measured, the resulting DES is liquid even at 280 K. The density of our DES system is 1.2521 g mL^{-1} at 303 K.

Protein Labelling. Standard procedure of thiol chemistry was followed for protein labeling. Both CPM and TMR have previously been tagged site specifically to free thiol group of bromelains, and we follow a similar technique (chapter 6B).[20-22] Briefly, 192 mg of bromelain was dissolved in 19 ml of phosphate buffer (50 mM, pH 7.4). 3.2/3.8 mg CPM/TMR dissolved in 1 ml of DMSO was added dropwise to the protein solution with continuous stirring. The reaction mixture was then kept at 20°C in stirring condition for 12 hrs followed by dialysis at 5 °C using 1000 ml of 15:1 (V/V) phosphate buffer (50 mM, pH 7.4) and DMSO. The dialysis medium was changed for every 12 hrs for 4 days and after that dialysis was done with buffer until the dialyzed solution shows no appreciable fluorescence. The CPM/TMR tagged bromelain was then concentrated by using 10 kDa cut-off centrifugal filtration unit. Tagging efficiency is calculated from the ratio of the concentration of bromelain and the dye in the CPM/TMR tagged bromelain using $\varepsilon_{bromelain}^{280}$, ε_{CPM}^{390} and ε_{TMR}^{555} as 63500 $M^{-1}cm^{-1}$, 33000 $M^{-1}cm^{-1}$, and 75000 $M^{-1}cm^{-1}$, respectively.[21-23]

Protein sample preparation. For all the experiments related to proteins, 50 mM pH 7.4 phosphate buffer was used. The samples are equilibrated overnight. The concentration of bromelain is measured using its molar absorption coefficient of 63,500 $M^{-1}cm^{-1}$ at 280 nm.[23] Untagged bromelain was used for activity measurement, CPM tagged bromelain for steady-state emission, and TMR tagged bromelain for FCS study. Bromelain concentration is kept ~10 µM for CD measurements, ~ 4 µM for steady-state emission experiment, and ~5 nM for FCS measurement. Due to high absorbance of DES, CD data of bromelian with DES could not be recorded. We back-extracted bromelain from DES, dissolved it in buffer and recorded the CD spectra. For back extraction, the overnight-equilibrated samples are taken in a centrifugal filtration unit (Amicon Ultra, 10 kDa cut-off) and washed with buffer several times.

Protein Activity Measurement. Bromelain activity is assayed by spectrophotometric method using casein as the substrate.[24-26] For activity measurement, untagged bromelain is used. Casein (0.3 mL, 1.5% w/v) was denatured at 70 °C for 15 min and was treated with bromelain (0.3 mL, 0.12 mg mL^{-1}) in 50 mM pH 7.4 phosphate buffer at 37 °C for 10 min. The reaction was then stopped by the addition of 0.3 mL 200 mM trichloroacetic acid. The precipitate was removed through centrifugation, and the absorbance of the supernatant was measured at 280 nm. The value of the absorbance at 280 nm is proportional to the degree of the proteolysis of bromelain. Thus, bromelain's activity is represented as the absorbance value obtained for 10 min digestion. Appropriate blank (consists of all the constituent except bromelain) is subtracted from every measurements.

References

1. Lakowicz, J. R. Principles of Fluorescence Spectroscopy. 3rd ed.; Springer, 2010.
2. Advanced Time-Correlated Single Photon Counting Applications, Becker, W., Ed.; Springer Series in Chemical Physics, Vol. 111, Switzerland, 2015.
3. O'Connor, D. V., Phillips, D. Time-correlated Single Photon Counting, Academic Press, London, U.S.A 1984.
4. Rafiq, S.; Sen, P. Spectroscopic Evidence of the Presence of an Activation Barrier in the Otherwise Barrierless Excited State Potential Energy Surface of Auramine-O: A Femtosecond Fluorescence Up-Conversion study. *J. Chem. Phys*. **2013**, *139*, 124302.
5. Valeur, B., Berberan-Santos, M. N. Molecular Fluorescence Principles and Applications 2nd Ed.; Wiley-VHC, Weinheim, Germany, 2012.
6. Chosrowjan, H.; Taniguchi, S.; Tanaka, F. Ultrafast fluorescence upconversion technique and its applications to proteins. *FEBS J*. **2015**, *282*, 3003–3015.
7. Maroncelli, M.; Fleming, G. R. Picosecond solvation dynamics of coumarin 153: The importance of molecular aspects of solvation. *J. Chem. Phys*. **1987**, *86*, 6221-6239.
8. Magde, D.; Elson, E.; Webb, W. W. Thermodynamic fluctuations in a reacting system- measurement by fluorescence correlation spectroscopy. *Phys. Rev. Lett*. **1972**, *29*, 705– 708.
9. Elson, E.; Magde, D. Fluorescence correlation spectroscopy: Conceptual basis and theory. *Biopolymers* **1974**, *13*, 1– 27.
10. Müller, C. B.; Loman, A.; Pacheco, V.; Koberling, F.; Willbold, D.; Richtering, W.; Enderlein, J. Precise measurement of diffusion by multi-color dual-focus fluorescence correlation spectroscopy. *Europhys. Lett*. **2008**, 83, 46001.
11. Metzler, R.; Jeon, J.-H.; Cherstvy, A. G.; Barkai, E. Anomalous diffusion models and their properties: Non-stationarity, nonergodicity, and ageing at the centenary of single particle tracking. *Phys. Chem. Chem. Phys*. **2014**, *16*, 24128– 24164.
12. Schwille, P.; Korlach, J.; Webb, W. W. Fluorescence correlation spectroscopy with single-molecule sensitivity on cell and model membranes. *Cytometry* **1999**, *36*, 176–182.
13. Banks, D. S.; Fradin, C. Anomalous diffusion of proteins due to molecular crowding. *Biophys. J*. **2005**, *89*, 2960– 2971.

14. Das, N.; Sen, P. Shape Dependent Macromolecular Crowding on the Thermodynamics and Microsecond Conformational Dynamics of Protein Unfolding Revealed at the Single Molecular Level. *J. Phys. Chem. B* **2020**, *124*, 5858– 5871.
15. Berera, R.; van Grondelle, R.; Kennis, J. T. M. Ultrafast transient absorption spectroscopy: principles and application to photosynthetic systems. *Photosynth. Res.* **2009**, *101*, 105–118.
16. Polok, K.; Gadomski, W.; Ratajska-Gadomska, B. Femtosecond optical Kerr effect setup with signal "live view" for measurements in the solid, liquid, and gas phases. *Rev. Sci. Instrum.* **2015**, *86*, 103109.
17. McMorrow, D.; Lotshaw, W. T. Intermolecular dynamics in acetonitrile probed with femtosecond Fourier-transform Raman spectroscopy. *J. Phys. Chem.* **1991**, *95*, 10395–10406.
18. Taschin, A.; Bartolini, P.; Eramo, R.; Righini, R.; Torre, R. Evidence of two distinct local structures of water from ambient to supercooled conditions. *Nat. Commun.* **2013**, *4*, 2401.
19. Böhm, G.; Muhr, R.; Jaenicke, R. Quantitative analysis of protein far UV circular dichroism spectra by neural networks. *Protein Eng. Des. Sel.* **1992**, *5*, 191–195.
20. Sasmal, D. K.; Mondal, T.; Mojumdar, S. S.; Choudhury, A.; Banerjee, R.; Bhattacharyya, K. An FCS Study of Unfolding and Refolding of CPM-Labeled Human Serum Albumin: Role of Ionic Liquid. *J. Phys. Chem. B* **2011**, *115*, 13075–13083.
21. Yadav, R.; Sengupta, B.; Sen, P. Conformational Fluctuation Dynamics of Domain I of Human Serum Albumin in the Course of Chemically and Thermally Induced Unfolding Using Fluorescence Correlation Spectroscopy. *J. Phys. Chem. B* **2014**, *118*, 5428– 5438.
22. Sengupta, B.; Das, N.; Sen, P. Monomerization and aggregation of β-lactoglobulin under adverse condition: A fluorescence correlation spectroscopic investigation. Biochim. Biophys. Acta, Proteins Proteomics **2018**, *1866*, 316–326.
23. Murachi, T.; Yasui, M.; Yasuda, Y. Purification and Physical Characterization of Stem Bromelain. *Biochemistry* **1964**, *3*, 48–55.
24. Rani, A.; Venkatesu, P. Insights into the interactions between enzyme and co-solvents: Stability and activity of stem bromelain. *Int. J. Biol. Macromol.* **2015**, *73*, 189–201.

25. Rani, A.; Venkatesu, P. A Distinct Proof on Interplay between Trehalose and Guanidinium Chloride for the Stability of Stem Bromelain. *J. Phys. Chem. B* **2016**, *120*, 8863– 8872.
26. Bhakuni, K.; Venkatesu, P. Does macromolecular crowding compatible with enzyme stem bromelain structure and stability? *Int. J. Biol. Macromol.* **2019**, *131*, 527–535.

Chapter 3

Temperature-Dependent Ultrafast Solvation Response and Solute Diffusion in Acetamide-Urea Deep Eutectic Solvent

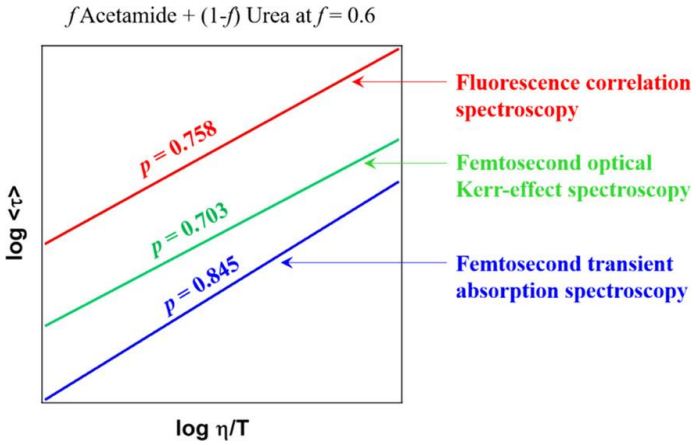

N. Subba, K.Polok, P. Piatkowski, B. Ratajska-Gadomska, R. Biswas, W. Gadomski and P. Sen. *J. Phys. Chem. B* **2019**, *123*, 9212-9221

Temperature dependent ultrafast solvent response of a non-ionic DES based on acetamide and urea [0.6 CH_3CONH_2 + 0.4 $CO(NH_2)_2$] was investigated using femtosecond transient absorption (TA) and optical Kerr effect (OKE) spectroscopy. Translational diffusion of a fluorescent probe in the same DES was also studied at various temperatures using fluorescence correlation spectroscopy (FCS). These were used to study the viscosity coupling of the measured relaxation times and thus to verify the dynamical heterogeneity aspect of this medium. From FCS study the translational diffusion time of a solute in the DES found to show a fractional viscosity dependence, with exponent 0.758, which, when compared with the viscosity–diffusion relationship for the same solute in common molecular solvents, suggests moderate deviation from the Stokes–Einstein relation. The solvent response have been found to be triexponential in nature, dominated by a ~100 fs component. The other two components are characterized by time constants in ~5 and ~50 ps regimes. Subsequent comparison with the femtosecond OKE measurements suggests that the relatively slower picosecond solvation components originate from the reorientation of the solvent molecules, while the subpicosecond solvation response arises from the participation of the collective low-frequency solvent modes (such as intermolecular vibrations and librations). We find that the rotational diffusion lifetimes also exhibit fractional power dependence on medium viscosity and thus deviate from the Stokes–Einstein–Debye prediction. All of these results therefore suggest that the non-ionic acetamide–urea DES is a moderately heterogeneous medium.

3.1 Introduction

Most of the extensively studied DESs are ionic as discussed in chapter 1, little attention has been given to non-ionic DESs. There is a lack of structural and dynamical studies on non-ionic DESs. A possible reason could be that only few non-ionic DESs were reported until recently. This is understandable as the interaction between non-ionic components is much weaker compared to ionic ones which makes the formation of non-ionic DESs difficult. In the case of non-ionic hydrophobic DESs, hydrophobic interaction leads to relatively easier formation of DESs. In many fronts, a non-ionic solvent may be desirable for applications involving dissolution of solutes which otherwise are not soluble in ionic DESs. In this context, acetamide based DESs could be an excellent choice as acetamide is considered to be a very good solvent[1,2] that can dissolve a variety of solutes. This is attributed to the unique molecular structure and large dielectric constant of acetamide.[1,3]

Few acetamide based ionic DESs are known and have been explored. For example, time-resolved fluorescence studies of these DESs has revealed their heterogeneous (spatially and dynamically) nature from the breakdown of SE and SED as mentioned earlier.[4-7] One of the known non-ionic DESs based on acetamide is that with urea.[8] In contrast to ionic DESs, Biswas and co-workers found non-ionic acetamide–urea DES to be quite dynamically homogeneous (with exponent *p* close to unity) when studied by fluorescence anisotropy of a probe molecule and simulation.[9] However, dielectric relaxation (DR) study, with a $0.2 \leq \nu\ (\text{GHz}) \leq 50$ frequency coverage, shows that there is a fractional power dependency of the average DR time on the viscosity and a substantial decoupling exists between re-orientational dynamics of the component molecules and solution viscosity, indicating dynamic heterogeneity.[10] However, this experiment covers only a narrow window and hence it is hard to observe any relaxation on a time scale shorter than tens of picosecond and longer than nanosecond. This is to note that typical time dependent fluorescence Stokes shift method with an instrument response function (IRF) of ~80 ps could not reveal any solvation dynamics component[9] and thus the possibility of having a component larger than nanosecond might be ruled out. On the other hand, the presence of a faster (order of a few picoseconds or less) relaxation component is anticipated, which has been verified in the present chapter. Herein, transient absorption (TA) was used to measure the ultrafast solvation response of acetamide–urea DES having a eutectic temperature of ~319 K at approximately 0.6 mole fraction of acetamide[8] (i.e. [*f* CH_3CONH_2 + (1-*f*) $CO(NH_2)_2$] at $f = 0.6$) within the temperature range of $328 \leq T\ (K) \leq 358$ to verify if the system is truly dynamically homogeneous. In order to understand the origin of the solvation time

components, bulk solvent intermolecular dynamics was measured using femtosecond optical Kerr effect (OKE) in the temperature range of 322.5 ≤ T (K) ≤ 373.

Apart from solvation dynamics, the nature of the dynamic heterogeneity of the acetamide–urea DES from the translational diffusion of a probe molecule also explored. For this, fluorescence correlation spectroscopy (FCS) was employed, which is a highly sensitive technique to study the molecular diffusion through a media.[11] While FCS has been extensively used to establish the existence of heterogeneity in ionic liquids, there are only few reports on the FCS study of DESs.[12-14] The translational diffusion of various probe molecules in these DES was found to be anomalous instead of simple single component diffusion and it has been attributed to the presence of dynamic heterogeneity. However, the observation of anomalous diffusion may originate from other source (see discussion section) and a temperature dependent FCS study is necessary to ascertain the presence of dynamics heterogeneity in the DES, which have done in the present chapter. The viscosity values for the acetamide–urea DES [f CH_3CONH_2 + (1-f) $CO(NH_2)_2$, f = 0.6] at various temperatures were obtained by inter/extrapolation of the data from ref. 9 with Reynolds exponential model fit.

3.2 Result and Discussion

3.2.1 Solvation dynamics studied by the time dependent Stokes shift method

In order to study the solvation dynamics of acetamide–urea DES, 4-(dicyanomethylene)-2-methyl-6-(4-dimethylaminostyryl)-4*H*-pyran (DCM) is used as the solvatochromic dye molecule.[15,16] Upon excitation, the dipole moment of DCM changes from 6 D to 26 D and the time scale of the solvation induced stabilization of the excited state is measured by monitoring time dependent shift of the stimulated emission band using transient absorption (TA) spectroscopy.[16] Figure 3.1a shows the representative transient absorption spectra of DCM in acetamide–urea DES [f CH_3CONH_2 + (1-f) $CO(NH_2)_2$, f = 0.6] at 333 K. The TA spectra is dominated by emission band with its maximum shifting towards longer wavelengths with increasing pump-probe delay time. In order to quantify the dynamic Stokes shift, the stimulated emission band was fitted with log-normal function to determine the peak position for each delay time. A representative plot of the shift in the peak frequency as a function of the pump-probe delay time is shown in figure 3.1b.

Figure 3.2a shows $C(t)$ obtained for f CH_3CONH_2 + (1-f) $CO(NH_2)_2$ DES with f = 0.6 at seven different temperatures ranging from 328 K to 358 K. Each $C(t)$ is best fitted with a three exponential function $\left[C(t) = a_1 e^{\frac{-t}{\tau_1}} + a_2 e^{\frac{-t}{\tau_2}} + a_3 e^{\frac{-t}{\tau_3}}\right]$ and the fitted parameters are tabulated in

table 3.1. It is worth to note that the ultrafast sub-picosecond component (τ_3) does not show dependence on the temperature, whereas, the slower components exhibit a strong temperature dependence. Solvation is a complex relaxation process, which involves different types of molecular motions, e.g. libration, rotation and translation.[17,18] This type of motions for the bulk solvent can be observed using the femtosecond optical Kerr effect (OKE) technique (*vide infra*). Librations and translations in a local cage formed by neighbouring molecules are considered to be the fastest events in a hydrogen-bonded solvent and involve small amplitude motion of the solvent molecule[19-21] For the slower time constants (τ_1 and τ_2) a strong temperature dependence is expected as they originate from the reorientation of the solvent molecules. The average of the two slower components is plotted against η/T in figure 3.2b as a log-log plot where the fractional SED exponent is found to be 0.845, which is more close to unity than for the ionic DES. This suggests that the effect of viscosity on the solvation dynamics of acetamide-urea DES more closely follows the Stokes-Einstein-Debye relation and the mixture is dynamically more homogeneous.

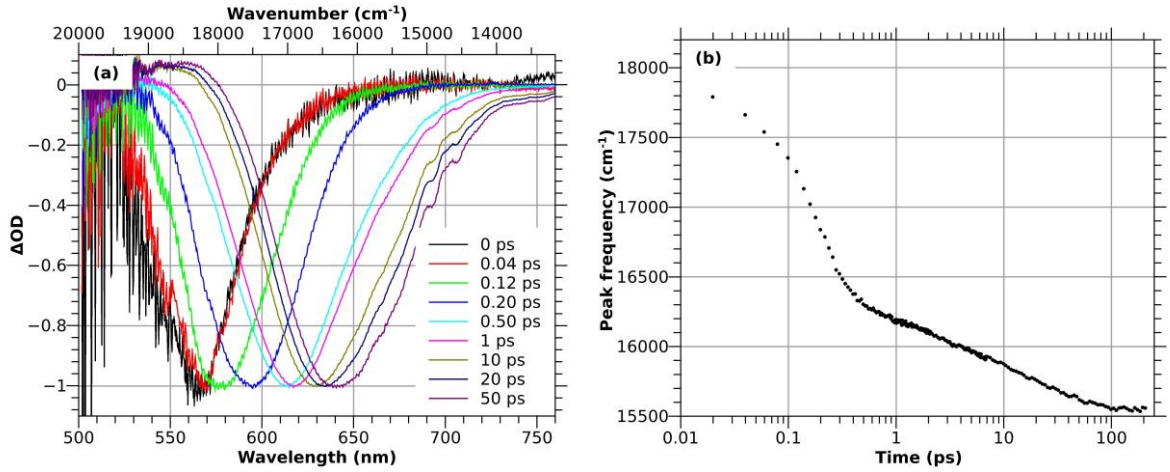

Figure 3.1 (a) Normalized transient absorption spectra and (b) variation of peak frequency of the stimulated emission band of DCM dye in acetamide–urea DES [f CH_3CONH_2 + (1-f) $CO(NH_2)_2$, f = 0.6] at 333 K.

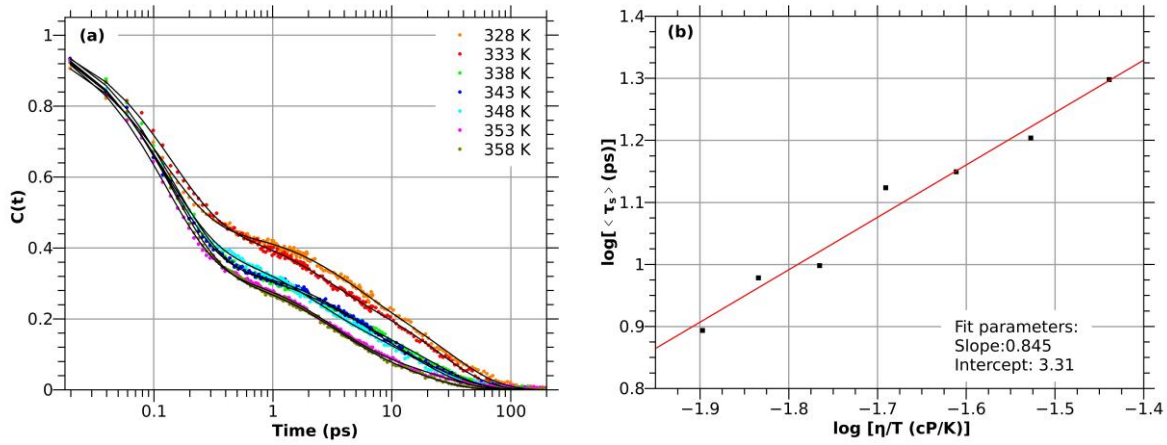

Figure 3.2 (a) Solvent response function, C(t), of DCM dye in acetamide–urea DES [*f* CH_3CONH_2 + (1-*f*) $CO(NH_2)_2$, *f* = 0.6] at various temperatures and the corresponding solid line represents the fitted line with a three exponential function. (b) Plot of $log(\tau_S)$ vs $log(\eta/T)$ in acetamide–urea DES [*f* CH_3CONH_2 + (1-*f*) $CO(NH_2)_2$, *f* = 0.6].

Table 3.1 Viscosity, observed dynamic Stokes shift and the fitted parameters of the solvent response functions of DCM dye in acetamide–urea DES [*f* CH_3CONH_2 + (1-*f*) $CO(NH_2)_2$, *f* = 0.6] at various temperatures. The viscosity data were taken from ref. 9 after inter/extrapolation of the data with Reynolds exponential model.

Temp (K)	**η (cP)**	**Observed dynamic Stokes shift (cm^{-1})**	**a_1**	**a_2**	**a_3**	**τ_1 (ps)**	**τ_2 (ps)**	**τ_3 (ps)**	**$\tau_s = \frac{a_1\tau_1 + a_2\tau_2}{a_1 + a_2}$ (ps)**
328	11.93	2340	0.28	0.18	0.53	30.2	3.8	0.12	19.9
333	9.89	2200	0.29	0.18	0.54	24.5	2.3	0.14	16.0
338	8.27	2420	0.22	0.14	0.67	21.3	2.8	0.14	14.1
343	6.99	2520	0.18	0.17	0.66	21.9	4.2	0.13	13.3
348	5.97	2510	0.22	0.19	0.60	17.0	1.8	0.12	10.0
353	5.17	2740	0.13	0.22	0.68	20.9	2.8	0.12	9.5
358	4.54	2620	0.14	0.19	0.69	14.8	2.7	0.14	7.8

3.2.2 Solvent dynamics in the bulk studied through femtosecond OKE

We have applied the OKE technique to investigate the timescales of the bulk solvent dynamics, where for the analysis we have used only the intermolecular part of the response. Intermolecular part of the OKE response for the acetamide–urea DES [*f* CH_3CONH_2 + (1-*f*) $CO(NH_2)_2$, *f* = 0.6] at various temperatures ranging from 322 K to 373 K is shown in figure 3.3a in log-log scale. In the case of molecules with anisotropic polarizability, the slowest

picosecond components are due to the diffusive reorientation, whereas the faster components correspond to the librations and translations of a molecule in the transient cage formed by its neighbours.[21,22] Usually for hydrogen-bonded systems the translational motion involving hydrogen bond stretching can be distinguished,[23,24] and it was shown to decay within few hundreds of femtoseconds. Herewith we fit only the time domain OKE response starting at 1 ps, corresponding to diffusive molecular motions. The best fit was obtained with a sum of 4 exponential functions, where τ_{ri} and τ_i correspond to the rise and decay times, respectively.

$$R(t) = \sum_{i=1}^{4} a_i\left(1 - e^{-t/\tau_{ri}}\right) e^{-t/\tau_i} \qquad 3.1$$

The rise times were fixed at 200 fs. A representative fit for 333 K is given in figure 3.3b. The two slowest components are assigned to the reorientation of molecules (*vide infra*), whereas the faster two are considered as a tail of the response due to faster relaxation processes. The fit parameters for the two reorientational components at all the temperatures are gathered in table 3.2.

The analysis of the OKE response in urea-water mixture gives two highest decay times of 2.3 ps and 6.5 ps at 333 K, where the value of η/T ratio is 0.00445 cP/K.[23] A study with the same technique for the acetamide-water system reports decay times of 1.81 ps and 6.84 ps at 296 K (η/T ratio is 0.0045 cP/K).[25] The η/T ratios in both cases are almost equal and at the same time the decay times for urea and acetamide are close. In our case the lowest value of η/T = 0.0089 cP/K is obtained at 373 K, which is double that mentioned for urea/acetamide-water systems. According to the SED equation the decay times should also double (assuming small contribution of the free rotation part), which almost takes place in our case and the obtained times are τ_2=3.6 ps and τ_1=11.8 ps (see table 3.2). We conclude that both of the investigated molecules contribute to each of the two slowest components of our fit. The slower one is clearly due to the reorientation of the molecules with anisotropic polarizability, which is the slowest process captured by OKE.[19,21] In the case of the other one, Idrissi et al.[25] suggested that it may originates from the reorientation of molecules about a different molecular axis. The fast dynamics obtained after subtracting the reorientation (figure 3.3b) is due to librations and translations of the molecules in the transient cage formed by their neighbours. The detailed analysis of this part is out of the scope of this paper. Here we would like to state that the vibration observed in the signal may be due to the stretching of hydrogen bonds, just like for water[24] and we also expect a considerable contribution of the librations due to the high anisotropy of the investigated molecules.

At this point it is fair to make a comparison between the solvation dynamics studied by time dependent fluorescence Stokes shift of a dye molecule and the bulk solvent dynamics. We find that the longest reorientation time obtained from OKE is very close to the longest solvation time – 15.1 ps vs 14.8 ps at 358 K and 33.9 ps vs 30.2 ps at 328 K. On the other hand, the second longest component in solvation is faster by 30-45% than the second longest component in OKE. In the case of the fastest solvation component, we expect it to originate from librations or translations of solvent molecule in its local cage.

Just like in the case of solvation dynamics we have plotted the $log(\tau_i)$ vs $log(\eta/T)$ for the picosecond reorientation times in figure 3.4. For consistency with previously published solvation data, we have fitted the logarithmed data with a linear function.

$$\log \tau_i = \log B + p \log\left(\frac{\eta}{T}\right) \qquad 3.2$$

In order to test the importance of free rotor component and the use of logarithm of noisy data in the fit, we have additionally fitted the non-logarithmed data with the following function.

$$\tau_i = \frac{A}{\sqrt{T}} + B\left(\frac{\eta}{T}\right)^p \qquad 3.3$$

where the first component is due to the free rotor contribution. A free fit of such equation resulted in unphysical parameters, and thus we have fixed the value of A for nonzero free rotor part. We estimated the free rotor time using the following equation:[26,27]

$$\tau_{FR} = \frac{2\pi}{9}\sqrt{\left(\frac{I}{k_B T}\right)} \qquad 3.4$$

where I and k_B are the moment of inertia about the selected rotation axis and Boltzmann constant, respectively. We used the average of the times obtained for the two molecules for rotations about the axes in molecular plane, which resulted in $A = 5300 fs\sqrt{K}$. The obtained fit parameters are given in table 3.3. What we observed is that the p exponent significantly depends on the quality of the data and that for noisy data the fits for logarithmed and non-logarithmed data show difference. In the table we have put the results for both components and their average value (calculated like in the case of solvation, see table 3.1). We show also the data for solvation for comparison (individual times are not included due to very high scatter of the data points). The values of p exponent in the fractional SED equation were not significantly influenced by the use of free rotor component, showing that the free rotor part can be neglected. In figure 3.4 one can see that the curves obtained with and without free rotor component overlap very well (non-logarithmed data).

When comparing the slope and exponent for the average reorientation time in OKE and solvation responses, we see some difference. The lower value of the exponent in the case of OKE can indicate somewhat higher dynamic inhomogeneity in the bulk, which correlates well with higher inhomogeneous broadening for librations, discussed above. The disagreement is attributed to the difference in solvent-solvent and solvent-solute interactions. In general, the values of the p exponents ranging from 0.703 to 0.845 indicates some degree of dynamic inhomogeneity of the investigated system both in the bulk and around the solute. We note that the reorientation times obtained from the OKE experiment are in a very good agreement with the dielectric relaxation and molecular dynamics simulations data.[10] It was theoretically shown that the ratio of the decay times for first and second order orientational correlation functions is 3 for Debye diffusion and 1 if the relaxation is dominated by large jumps.[26,27] This ratio was calculated by us by taking from ref. 10 the slowest component of multiexponential fit to those correlations and averaging it for both molecules. The value obtained at 335 K is 1.68, which indicates that the reorientation deviates from the Debye model. The reorientation observed in dielectric relaxation follows the first order correlation function, whereas in OKE the second order relaxation is valid, thus the relaxation times should be related by the calculated ratio. For the slowest component of the OKE response, measured at 336 K, we obtain after rescaling 25.7 ps × 1.68 = 43.2 ps, which is in a very good agreement with the value of 39 ps obtained from the DR measurement. Moreover, the exponent obtained from the fit to the fractional SED equation to the average relaxation time matches very well between the dielectric relaxation and OKE data (0.68 vs 0.703).

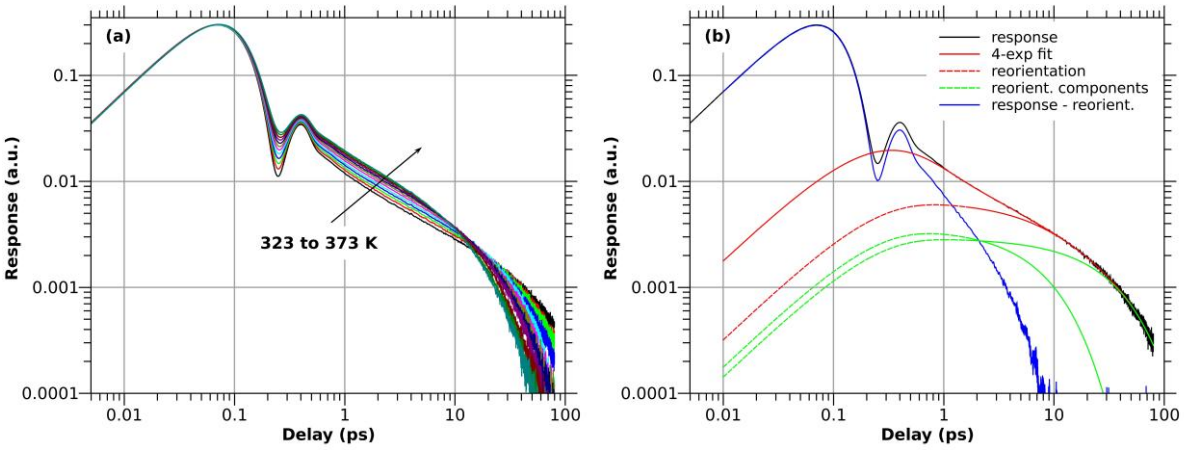

Figure 3.3 Intermolecular part of the OKE response obtained from OKE signal with normalized hyperpolarizability acetamide–urea DES [*f* CH_3CONH_2 + (1-*f*) $CO(NH_2)_2$, *f* = 0.6] in log-log scale (a) at temperatures from 323 to 373 K (b) at 332 K with its fit.

Table 3.2 Fit parameters for the reorientation in the OKE response

	η [cP]	τ_i [ps]		a_i [10^{-3}]	
T [K]\i		1	2	1	2
322.2	14.96	42.5	9.23	2.56	2.10
326.8	12.48	33.9	7.14	3.14	2.68
331.4	10.48	31.0	6.80	3.37	3.11
336.0	8.87	25.7	5.84	4.01	3.15
340.6	7.57	24.2	4.95	4.20	5.02
345.2	6.52	19.9	4.15	5.11	5.06
349.8	5.67	18.7	4.57	5.27	4.72
354.3	4.99	16.7	3.94	5.89	5.69
358.9	4.43	15.1	3.83	6.40	5.63
363.5	3.99	13.5	3.69	6.77	5.88
368.1	3.63	12.3	4.02	7.13	4.68
372.7	3.34	11.8	3.63	7.08	7.43

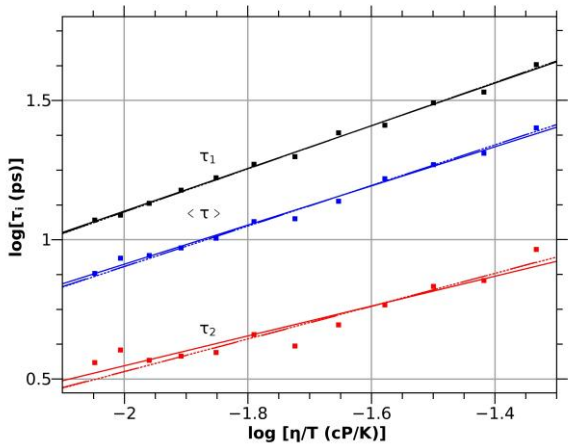

Figure 3.4 Plot of the $log(\tau_i)$ from OKE experiment vs $log(\eta/T)$ in acetamide–urea DES [f CH_3CONH_2 + (1-f) $CO(NH_2)_2$, f = 0.6]. Solid lines are the fits of the plotted data (see equation 3.2), whereas dashed and dotted lines are for the fits of of τ_i vs η/T using equation 3.3 with and without free rotor component, respectively.

Table 3.3 Fit parameters for fractional SED equation (B is given in engineering notation). The log fit scale refers to linear fit of $log(\tau_i)$ vs $log(\eta/T)$ (see equation 3.2), whereas linear fit scale refers to fit of τ_i vs η/T using equation 3.3. Equation 3.2 corresponds to the equation 3.3 with A fixed at 0. One of the fits in linear scale was made with A fixed at 0 for comparison with the fit in log scale, whereas the other had A fixed at value obtained from equation 3.4, as described in text.

						OKE				Solvation
		τ_1			τ_2			$\langle\tau\rangle$		$\langle\tau\rangle$
Fit scale	***log***	***lin***	***lin***	***log***	***lin***	***lin***	***log***	***lin***	***lin***	***log***
A $(fs\sqrt{K})$	0	0	5300	0	0	5300	0	0	5300	0
B $(K/cP)^p$	430e3	444e3	455e3	416e2	504e2	540e2	208e3	229e3	237e3	326e3
p	0.765	0.774	0.784	0.536	0.588	0.621	0.703	0.728	0.743	0.845

3.2.3 Translational diffusion of a solute studied by fluorescence correlation spectroscopy

Figure 3.5a shows the normalized fluorescence autocorrelation curves of R6G in acetamide–urea DES [*f* CH_3CONH_2 + (1-*f*) $CO(NH_2)_2$, *f* = 0.6] at various temperatures ranging from 328 K to 353 K. As expected, the translational diffusion time (τ_D) of R6G in this DES decreases with increasing temperature. Figure 3.5b shows the fits of the fluorescence autocorrelation curve for [*f* CH_3CONH_2 + (1-*f*) $CO(NH_2)_2$, *f* = 0.6] at 333 K using single (equation 2.21) and anomalous (equation 2.22) diffusion components and we observed that anomalous diffusion fits the data best. The fitting parameters for all the temperatures are tabulated in table 3.4. The value of α obtained from the fitting ranged from 0.88 to 0.90 in our study. Earlier, it has been reported that the apparent anomalous diffusion could be the result of the mismatch between refractive indices of the sample and immersion liquid (which in our case is water).[28] The refractive index of acetamide–urea DES [*f* CH_3CONH_2 + (1-*f*) $CO(NH_2)_2$, *f* = 0.6] is reported to be around 1.38-1.39.[10] Clearly, there is a mismatch of the refractive indices, and thus the observation of the anomalous diffusion may be apparent. The true nature of the diffusion could only be confirmed with a two-focus FCS.[28] However, due to the lack of availability of dual-focus FCS setup, we could not further confirm whether the apparent anomalous diffusion is the result of the mismatch between refractive indices or it is actually the case. Nonetheless, we used both the values of obtained τ_D for further discussion.

As mentioned earlier, here we would like to study the nature of Stokes-Einstein behaviour in acetamide–urea DES using translational diffusion of a probe to see if this is a unique solvent. Figure 3.6a shows the plot of $log[\tau_D]$ vs. $log[\eta/T]$ for R6G in acetamide–urea DES [*f*

CH_3CONH_2 + (1-*f*) $CO(NH_2)_2$, *f* = 0.6]. The slopes (*p*) obtained for both normal and anomalous diffusion times are similar (~0.75) and are less than unity, which may indicate that this DES is to some extent dynamically heterogeneous and there is a decoupling of translational diffusion time from the solvent viscosity. This result prompted us to study the validity of Stokes-Einstein relationship for diffusion of a solute in normal molecular solvents. For this, we made FCS measurement of R6G in various solvents of varying viscosities (see table 3.5 for the details). Figure 3.6b shows the plot of $log[\tau_D]$ vs. $log[\eta/T]$ for R6G in various solvents and the slope is found to be 0.82. It was a surprise to find that even in normal solvents, translational diffusion time of R6G has a fractional power dependence on viscosity. It is important to recall that Stokes-Einstein relation is based on spherical solute particle diffusing through a solvent continuum. Here, we speculate that the deviation observed in normal solvents is because of the non-spherical nature of the probe molecule and/or charge of the probe. Further scrutiny is required to ascertain these speculations. Compared to normal solvents, the translational diffusion time of R6G in acetamide–urea DES shows only a marginal deviation in the fractional power dependence. This indicates that the DES under study is mildly heterogeneous only.

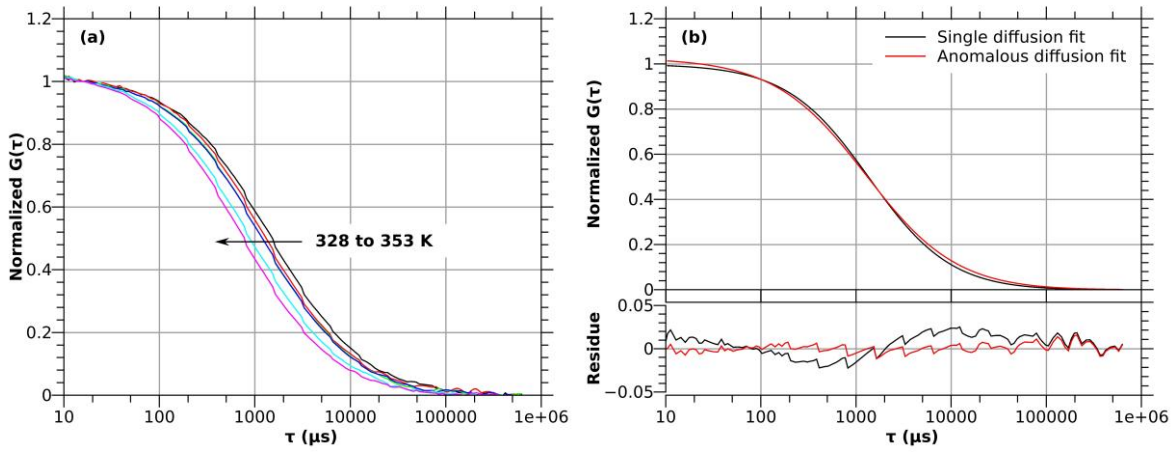

Figure 3.5 (a) Normalised fluorescence autocorrelation curve for R6G in acetamide–urea DES [*f* CH_3CONH_2 + (1-*f*) $CO(NH_2)_2$, *f* = 0.6] at various temperatures. (b) Comparison of fitting and the corresponding residuals are shown by solid red line (single diffusion) and solid blue line (anomalous diffusion) for [*f* CH_3CONH_2 + (1-*f*) $CO(NH_2)_2$, *f* = 0.6] at 333 K.

Table 3.4 Viscosities and fitting parameters of the fluorescence autocorrelation function with single and anomalous diffusion model for R6G in acetamide–urea DES [*f* CH_3CONH_2 + (1-*f*) $CO(NH_2)_2$, *f* = 0.6] at various temperatures. The viscosity data were taken from ref. 9 after inter/extrapolation of the data with Reynolds exponential model.

T (K)	η (cP)	Anomalous diffusion		Single diffusion
		τ_D (μs)	α (anomalous exponent)	τ_D (μs)
328	11.93	1470±30	0.88	1610±30
333	9.89	1270±25	0.90	1380±20
338	8.27	1180±30	0.90	1280±30
343	6.99	935±20	0.89	1030±25
348	5.97	865±15	0.89	960±20
353	5.17	735±20	0.90	805±15

Table 3.5 Viscosities and fitting parameters of the fluorescence autocorrelation function with single diffusion model for R6G in various molecular solvents. The viscosity data were taken from refs. 29-33.

Solvents	T (K)	η (cP)	τ_D (μs)
Acetone	293	0.32	45±2
Acetonitrile	293	0.37	50
Ethanol	298	1.09	115
Acetic acid	298	1.12	125
Propanol	298	1.95	190
Butanol	298	2.53	215
Pentanol	298	3.47	295±13
Octanol	298	7.59	515±35
Decanol	298	11.51	1140
Ethylene glycol	298	16.63	1025±40

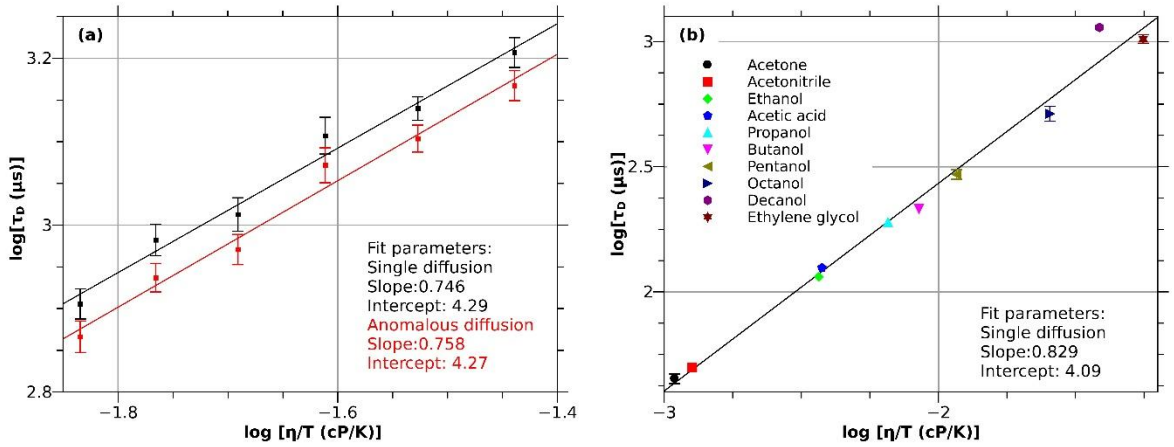

Figure 3.6 Plot of $log[\tau_D]$ vs $log[\eta/T]$ for (a) acetamide–urea DES [f CH_3CONH_2 + (1-f) $CO(NH_2)_2$, f = 0.6] and (b) normal molecular solvents.

3.3 Conclusion

In summary, the present work employs three different spectroscopic techniques, namely, FCS, TA and OKE, to explore and characterize the dynamic heterogeneity aspect of a non-ionic DES made of acetamide and urea via temperature dependent measurements in the range $322 \leq T/K \leq 373$. Reference FCS measurements with the same dipolar solute in several common solvents at room temperatures have been carried out for interpreting the observed fractional viscosity dependence of average solute diffusion in terms of dynamic heterogeneity of the medium under study. A comparison of the FCS data between the DES and common solvents does reflect a dynamic heterogeneity, albeit moderate, for the DES studied. Solvent rotational times also show deviation from the SED prediction for homogeneous media, and reflect a relatively stronger dynamic heterogeneity than that by dynamic Stokes shift and FCS measurements. In addition, the OKE data indicate that the picosecond components in the total solvation response, arise from the rotational diffusion of the solvating particles, whereas the sub-picosecond response originates from the low frequency collective solvent modes, such as, inter-molecular vibrations and librations. The detection of a strong ultrafast solvation response in the ~100 fs domain, an observation hitherto un-explored for this DES, and finding the origin of the picosecond solvation components, are new and novel aspects of this study. Reference measurements for solute's centre-of-mass diffusion in common room temperature solvents have also been done here for the first time to generate a better interpretation of the observed fractional viscosity dependence of average relaxation times in terms of dynamic heterogeneity.

References

1. Stafford, O. F. Acetamide as a Solvent. *J. Am. Chem. Soc.* **1933**, *55*, 3987–3988.
2. Davis Jr., J. C. Acetamide as a solvent for freezing point depression and solubility experiments. *J. Chem. Educ*. **1966**, *43*, 611.
3. Harder, E.; Anisimov, V. M.; Whitfield, T.; MacKerell, A. D.; Roux, B. Understanding the Dielectric Properties of Liquid Amides from a Polarizable Force Field. *J. Phys. Chem. B* **2008**, *112*, 3509–3521.
4. Guchhait, B.; Gazi, H. A. R.; Kashyap, H. K.; Biswas, R. Fluorescence Spectroscopic Studies of (Acetamide + Sodium/Potassium Thiocyanates) Molten Mixtures: Composition and Temperature Dependence. *J. Phys. Chem. B* **2010**, *114*, 5066–5081.
5. Guchhait, B.; Daschakraborty, S.; Biswas, R. Medium decoupling of dynamics at temperatures ∼100 K above glass-transition temperature: A case study with (acetamide + lithium bromide/nitrate) melts. *J. Chem. Phys*. **2012**, *136*, 174503.
6. Das, A.; Biswas, R. Dynamic Solvent Control of a Reaction in Ionic Deep Eutectic Solvents: Time-Resolved Fluorescence Measurements of Reactive and Nonreactive Dynamics in (Choline Chloride + Urea) Melts. *J. Phys. Chem. B* **2015**, *119*, 10102–10113.
7. Pal, T.; Biswas, R. Heterogeneity and viscosity decoupling in (acetamide + electrolyte) molten mixtures: A model simulation study. *Chem. Phys. Lett*. **2011**, *517*, 180–185.
8. Walbrugh, L. “Amitraj solid dosage form,”, M.S. thesis, University of Pretoria, Pretoria, South Africa, 2006.
9. Das, A.; Das, S.; Biswas, R. Density relaxation and particle motion characteristics in a non-ionic deep eutectic solvent (acetamide + urea): Time-resolved fluorescence measurements and all-atom molecular dynamics simulations. *J. Chem. Phys*. **2015**, *142*, 034505.
10. Mukherjee, K.; Das, S.; Tarif, E.; Barman, A.; Biswas, R. Dielectric relaxation in acetamide + urea deep eutectics and neat molten urea: Origin of time scales via temperature dependent measurements and computer simulations. *J. Chem. Phys*. **2018**, *149*, 124501.
11. Magde, D; Elson, E; Webb, W. W. Thermodynamic fluctuations in a reacting system-measurement by fluorescence correlation spectroscopy. *Phys. Rev. Lett.* **1972**, *29*, 705–708.

12. Hossain, Sk. S.; Samanta, A. Solute rotation and translation dynamics in an ionic deep eutectic solvent based on choline chloride. *J. Phys. Chem. B* **2017**, *121*, 10556–10565.
13. Hossain, Sk. S.; Samanta, A. How do the hydrocarbon chain length and hydroxyl group position influence the solute dynamics in alcohol-based deep eutectic solvents? *Phys. Chem. Chem. Phys.* **2018**, *20*, 24613–24622.
14. Hossain, S. S.; Paul, S.; Samanta, A. Liquid Structure and Dynamics of Tetraalkylammonium Bromide-Based Deep Eutectic Solvents: Effect of Cation Chain Length. *J. Phys. Chem. B* **2019**, *123*, 6842–6850.
15. Gupta, S.; Rafiq, S.; Sen, P. Dynamics of solvent response in methanol–chloroform binary solvent mixture: A case of synergistic solvation. *J. Phys. Chem. B* **2015**, *119*, 3135–3141.
16. Maciejewski, A.; Naskrecki, R.; Lorenc, M.; Ziolek, M.; Karolczak, J.; Kubicki, J.; Matysiak, M.; Szymanski, M. Transient absorption experimental set-up with femtosecond time resolution. Femto- and picosecond study of DCM molecule in cyclohexane and methanol solution. *J. Mol. Struct.* **2000**, *555*, 1–13.
17. Stratt, R. M.; Maroncelli, M Nonreactive dynamics in solution: The emerging molecular view of solvation dynamics and vibrational relaxation. *J. Phys. Chem.* **1996**, *100*, 12981–12996.
18. Ladanyi, B. M.; Stratt, R. M. Short-time dynamics of solvation: Relationship between polar and nonpolar solvation. *J. Phys. Chem.* **1996**, *100*, 1266–1282.
19. Shirota, H.; Fujisawa, T.; Fukazawa, H.; Nishikawa, K. Ultrafast dynamics in aprotic molecular liquids: A femtosecond Raman-induced Kerr effect spectroscopic study. *Bull. Chem. Soc. Jpn.* **2009**, *82*, 1347–1366.
20. Jimenez, R.; Fleming, G. R.; Kumar, P. V.; Maroncelli, M. Femtosecond solvation dynamics of water. *Nature* **1984**, *369*, 471-473.
21. Smith, N. A.; Meech, S. R. Optically-heterodyne-detected optical Kerr effect (OHD-OKE): Applications in condensed phase dynamics. *Int. Rev. Phys. Chem.* **2002**, *21*, 75–100.
22. Ratajska-Gadomska, B. Temperature evolution of the low-frequency optical Kerr effect spectra of liquid benzene in quasi crystalline approach. *J. Chem. Phys.* **2002**, 116, 4563–4576.
23. Shirota, H.; Ushiyama, H. Hydrogen-bonding dynamics in aqueous solutions of amides and acids: Monomer, dimer, trimer, and polymer. *J. Phys. Chem. B* **2008**, *112*, 13542–13551.

24. Ratajska-Gadomska, B.; Białkowski, B.; Gadomski, W.; Radzewicz, C. Ultrashort memory of the quasicrystalline order in water by optical Kerr effect spectroscopy. *Chem. Phys. Lett.* **2006**, *429*, 575–580.
25. Idrissi, A.; Bartolini, P.; Ricci, M.; Righini, R. Temperature dependence of the re-orientational dynamics and low-frequency response of aqueous urea solutions investigated by femtosecond optical Kerr-effect spectroscopy and molecular-dynamics simulation. *Phys. Chem. Chem. Phys.* **2003**, *5*, 4666–4671.
26. Berne, B. J.; Pecora, R. Dynamic light scattering: John Wiley, New York, 1976.
27. Bauer, D. R.; Brauman, J. I.; Pecora, R. Molecular reorientation in liquids. Experimental test of hydrodynamic models. *J. Am. Chem. Soc.* **1974**, *96*, 6840–6843.
28. Lehmann, S.; Seiffert, S.; Richtering, W. Refractive index mismatch can misindicate anomalous diffusion in single-focus fluorescence correlation spectroscopy. *Macromol. Chem. Phys.* **2015**, *216*, 156−163.
29. Howard, K. S.; McAllister, R. A. The viscosity of acetone-water solutions up to their normal boiling points. *AIChE J.* **1958**, *4*, 362–366.
30. Sadeghi, R.; Azizpour, S. Volumetric, compressibility, and viscometric measurements of binary mixtures of poly(vinylpyrrolidone)+water, +methanol, +ethanol, +acetonitrile, +1-propanol, +2-propanol, and +1-butanol. *J. Chem. Eng. Data* **2011**, *56*, 240–250.
31. García, B.; Alcalde, R.; Aparicio, S.; Leal, J. M. The N-methylpyrrolidone–(C_1–C_{10}) alkan-1-ols solvent systems. *Phys. Chem. Chem. Phys.* **2002**, *4*, 1170–1177.
32. González, B.; Domínguez, A.; Tojo, J. Dynamic viscosities, densities, and speed of sound and derived properties of the binary systems: Acetic acid with water, methanol, ethanol, ethyl acetate and methyl acetate at 293.15, 298.15 and 303.15 K at atmospheric pressure. *J. Chem. Eng. Data* **2004**, *49*, 1590–1596.
33. Bohne, D.; Fischer, S.; Obermeier, E. Thermal conductivity, density, viscosity, and prandtl-numbers of ethylene glycol-water mixtures. *Ber. Bunsenges. Phys. Chem.* **1984**, *88*, 739–742.

This Page Intentionally Left Blank

Chapter 4

Partial Viscosity Decoupling of Solute Solvation, Rotation and Translation in Lauric Acid/Menthol Deep Eutectic Solvent: Modulation of Dynamic Heterogeneity with Length Scale

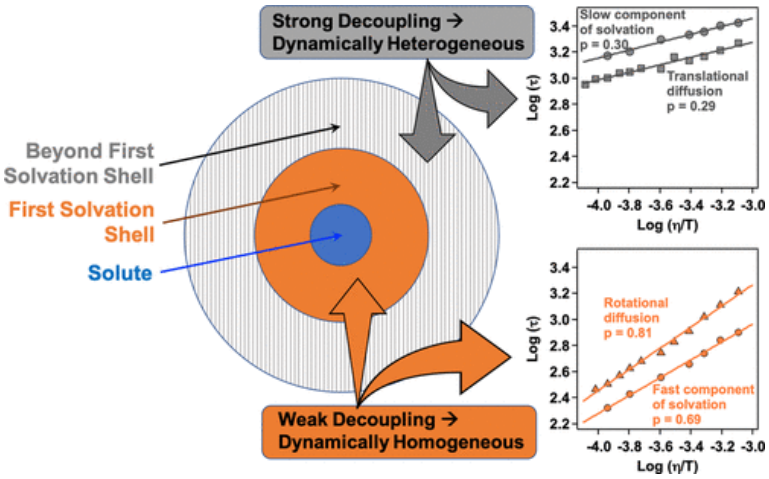

N. Subba, N. Das and P. Sen. *J. Phys. Chem. B* **2020**, *124*, 6875-6884

In this chapter, I have studied a hydrophobic DES comprising of lauric acid and menthol (LA/Men DES). Here, I have examined the structure and dynamics of LA/Men DES through steady-state emission, solvation dynamics, time-resolved fluorescence anisotropy, and translational diffusion dynamics. The emission spectra of coumarin 153 (a solvatochromic dye) was found to be independent of excitation wavelength suggests that LA/Men DES is spatially homogenous. Decoupling (p = 0.63) of the average solvation time $\langle \tau_s \rangle$ from medium viscosity suggests the presence of dynamic heterogeneity in the system. Rotational time $\langle \tau_r \rangle$, which reflects the nature of the first solvation shell, shows little decoupling (p = 0.81), suggesting it to be fairly dynamically homogeneous at a shorter length scale (within first solvation shell). An Arrhenius-type analysis also proves that rotation is mainly controlled by medium viscosity. Translational diffusion time $\langle \tau_D \rangle$ which provides information over a larger length scale, is found to be strongly decoupled from medium viscosity (p = 0.29). This indicates that at a larger length scale, the DES is quite dynamically heterogeneous. The slow component of solvation time, which is believed to originate at a larger length scale, correlates well with the translational diffusion timescale having similar activation energies. This suggests that their origin is same. Expectedly, for the long component of solvation time, the decoupling is quite strong (p = 0.30). Overall, the study demonstrates the structure and dynamics of the LA/Men DES, and the existence of length scale-dependent heterogeneity has been proposed. In simple, this study has found that, although the viscosity of LA/Men DES is low, some molecular motions are highly hindered. Further study of this system with scattering experiments and simulations could give a complete picture and confirm the finding of this study.

4.1 Introduction

Most of the available DESs are ionic and hydrophilic in nature.[1-3] This limits its use in organic chemistry as a 'solvent' as hydrophobic molecules may not be soluble or have low solubility in ionic DES. As described in chapter 1, hydrophilic DESs are not promising when it comes application such as liquid-liquid extraction from aqueous solution. Moreover, DESs, barring few,[4] are quite viscous, which is not desirable in many applications. In this regard, hydrophobic DESs are getting wide attention recently and are finding a lot of applications.[5,6] There are ionic hydrophobic DESs[7,8] based on quaternary ammonium salts, however, those based on terpenes (such as menthol and thymol) and fatty carboxylic acids which are non-ionic are gaining a lot of popularity.[9,10] Terpenes and carboxylic acids are naturally available and many of these hydrophobic DESs have considerably low viscosity which is certainly appealing. This has led to an increase in scope of DESs as green solvent. A notable example of this class of DES is the lauric acid/menthol (LA/Men) DES.[9-11] The components of this eutectic mixture are biodegradable and naturally available. The freezing point of LA:Men = 1:2 mol ratio eutectic composition is ~290 K, which is not far from the freezing points of the pure components.[10] This hydrophobic DES along with several others have found important applications, such as, extraction of metal,[11,12] micropollutants,[13,14] etc.

The depression of freezing points of these mixtures are not very large, which could be due to the presence of weak non-ionic interaction. Also, in many cases, long chain carboxylic acid is used as one of the components. As a result, the structure and dynamics of these DESs are expected to be different from ionic DESs. A recent report by Cui et al. on non-ionic N-methyl acetamide/lauric acid DES suggests the presence of nano-segregation of polar and non-polar domains.[15] This nano-segregation is similar to that of micelles. In this sense, eutectic mixture of N-methyl acetamide and lauric acid is 'spatially heterogeneous', which is a result of 'environmental segregation' driven by hydrophobic and hydrophilic interactions.[15]

Structure and dynamics of mainly ionic and hydrophilic DESs have been explored to a good extent.[16-23] But, despite the tremendous importance of hydrophobic DESs, its structural and dynamical characterization has not been explored extensively. It has now been established that ionic DESs are dynamically heterogeneous.[16,17,19,20,22,23] While, non-ionic DESs of acetamide and urea are mildly heterogeneous[18], more such systems should be identified and explored to some degree of generalisation. Recently, we showed that in non-ionic acetamide-urea DES (which is hydrophilic) the solvation time has a relatively weak fractional power dependence on η/T (p ~ 0.845) indicating a feeble dynamically heterogeneous character of the DES.[21] Probe rotation also shows a similar value of p (~0.96) in this DES.[18] These results lead us to believe

that non-ionic DESs are nearly dynamically homogeneous. However, a recent report on non-ionic DES of glucose, urea and water says otherwise.[24] This non-ionic DES showed pronounced signature of dynamic heterogeneity (p ~ 0.3-0.5) from the view of probe rotation. Further study is required to conclude the behaviour of associated and non-associated non-ionic DESs. However, for non-ionic DESs such studies are rare and one can ask a simple question: Are non-ionic *hydrophobic* DESs dynamically heterogeneous like the ionic ones?

Along a similar line of studies, I have presented here the nature of viscosity decoupling of solvation, rotational and translational diffusion in non-ionic hydrophobic LA/Men DES.

4.2 Results

4.2.1 Viscosity measurement

The measured values of viscosities of LA/Men (1:2 mol ratio) DES at different temperatures are given in table 4.1.

Table 4.1 Measured values of viscosities of LA/Men (1:2 mol ratio) DES at different temperatures.

Temperature (K)	Viscosity (cP)
298	23.95
303	18.69
308	14.90
313	12.17
318	9.85
323	8.22
328	6.21
333	5.30
338	4.64
343	3.92
348	3.33
353	2.92

4.2.2 Steady-state measurements

Figure 4.1a shows normalized steady-state absorption and emission spectra of C153 in LA/Men DES at room temperature. The absorption and emission maxima are found to be 24,040 cm^{-1} (416 nm) and 19,685 cm^{-1} (508 nm), respectively. We have used first moment frequencies[25] of the absorption and emission (according to equation 4.1) to calculate the Stokes shift of C153 in LA/Men DES, which turns out to be 5440 cm^{-1}. Typically for non-polar solvents like cyclohexane and 2-methylbutane, the observed first moment Stokes shift for C153 is ~4,350

cm^{-1} and for polar solvents like methanol and acetonitrile its value is ~6,000 cm^{-1}.[26] We compared the observed Stokes shift of C153 in LA/Men DES with standard solvents as shown in figure 4.1b. The result clearly indicates that LA/Men DES is non-polar and is like tetrahydrofuran, benzyl alcohol and cyclohexanone. The absorption and emission spectrum of C153 in this DES is found to be temperature insensitive in the measured temperature range of 298 K to 353 K (see figures 4.2). C153 emission spectrum in LA/Men DES does not depends on the excitation wavelength (see figure 4.1c).

$$\bar{\nu}_{FM} = \frac{\int_0^\infty \bar{\nu} I(\bar{\nu}) d\bar{\nu}}{\int_0^\infty I(\bar{\nu}) d\bar{\nu}} \qquad 4.1$$

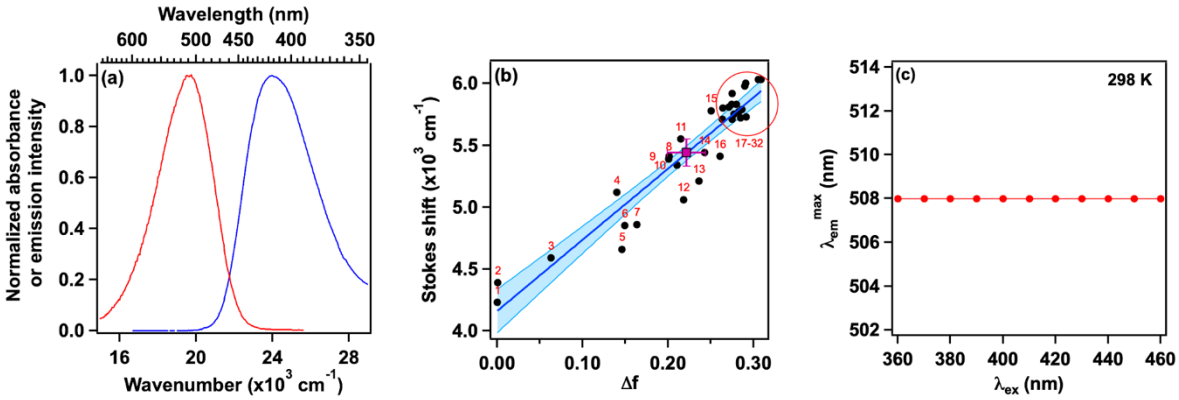

Figure 4.1 Steady-state measurements of solvatochromic dye, coumarin 153 (C153) in LA/Men DES. (a) Typical steady-state absorption (blue) and emission (red) spectra of C153 at 298 K. (b) Plot of Stokes shift of C153 as a function orientation polarizability (Δf) for benchmarking the polarity of DES. Black filled circles are reference solvents and the red filled square is LA/Men DES. The data for the reference samples are taken from *J. Phys. Chem.* **1995**, *99*, 17311−17337 (ref. 26). Black line is the best linear fit of the data reference data points. The shaded region represents the 95% confidence band of the fit coefficient. (c) Excitation wavelength dependence of emission spectra of C153 in LA/Men DES. The concentration of C153 is kept around 10 μM for steady-state measurements.

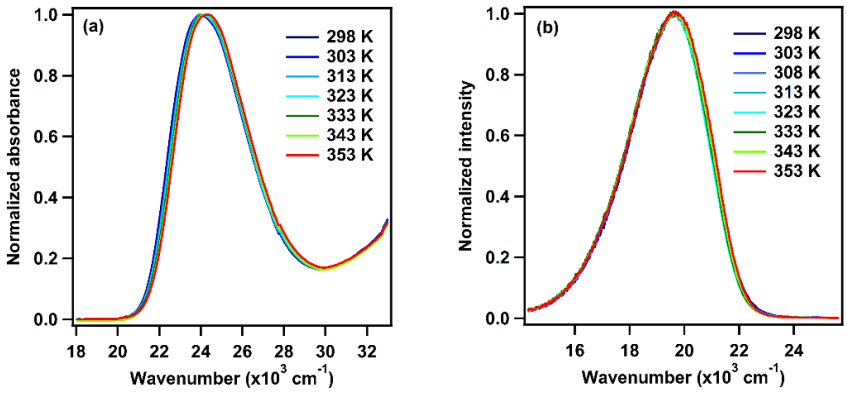

Figure 4.2 Temperature dependent (a) absorption and (b) emission spectra of C153 in LA/Men DES.

4.2.3 Time-resolved measurements

4.2.3.1 Solvation dynamics studied by time dependent fluorescence Stokes shift

Time-resolved emission spectra (TRES) were constructed employing traditional method by measuring wavelength dependent fluorescence transients across the steady-state emission spectrum(section 2.5).[27] Figures 4.3a and 4.3b shows typical fluorescence transients of C153 in LA/Men DES at 440 nm and 590 nm at two different temperatures (298 K and 343 K). A slow rise component and an ultrafast decay component is observed at the longer and shorter wavelengths, respectively. Such observation indicates a slow solvent relaxation dynamics of the media. As mentioned earlier, these transients were fitted with sum of exponential function to obtain fit parameters (α_i and τ_i). Using these fit parameters along with steady-state emission spectra, TRES was constructed as elaborated in chapter 2 (see figures 4.3c, 4.3d). Following, the solvent correlation function was constructed (using equation 2.18) for the system at different temperatures, which are shown in figure 4.3e. TRES constructed for other temperatures are shown in figure 4.4. All the $C(t)$s were fitted with bi-exponential function that gave two time constants. The amplitude of the shorter time component increases with increasing temperature. The fit parameters along with average solvation time $\langle\tau_s\rangle$ are tabulated in table 4.2.

The average solvation time at 298 K is found to be 1670 ps with a total dynamic Stokes shift of 1550 cm^{-1}. On increasing the temperature, the average solvation time becomes faster and the observed dynamic Stokes shift also decreases. At 343 K, the values become 470 ps and 1400 cm^{-1}, respectively. This shows a strong temperature dependence of solvation dynamics in

LA/Men DES. Usually, the observed dynamic Stokes shift is found to be less than the total ideal Stokes shift because usual experiment cannot capture the ultrafast regime (sub 100 fs or sub 100 ps, depending on the experimental method).[28]

We estimate the time-zero spectra of C153 in DES following the method proposed by Fee and Maroncelli.[29] The time-zero spectra can be estimated from the steady-state absorption and fluorescence spectra as[30]

$$\overline{\nu}^{p}_{em,md}(true\ 0) = \overline{\nu}^{p}_{ab,md} - \{\overline{\nu}^{np}_{ab,md} - \overline{\nu}^{np}_{em,md}\} \qquad 4.2$$

where the superscripts "*p*" and "*np*" refer to the polar (i.e. LA/Men DES in the present case) and nonpolar medium, respectively, and the wavenumbers here are not the values at maxima but correspond to the midpoint. The midpoint wavenumber is given by $\overline{\nu}_{md} = \frac{(\overline{\nu}_{-}+\overline{\nu}_{+})}{2}$ where $\overline{\nu}_{-}$ and $\overline{\nu}_{+}$ are the low and high wavenumbers on the half-height points of the spectrum. Cyclohexane is used as the nonpolar solvent in the present work. The maximum wavenumber at time zero, $\overline{\nu}^{p}_{em}(true\ 0)$, is estimated as the sum of $\overline{\nu}^{p}_{em,md}(true\ 0)$ and the difference between the midpoint and maximum wavenumber in the steady-state fluorescence spectrum of the same system. Using the value of $\overline{\nu}^{p}_{em}(true\ 0)$ the total ideal Stokes shift is found to be ~1730 cm^{-1}, which is independent on the temperature. The observed Stokes shift in the present study is about 10-20 % less than the ideal value, which implies that we have not missed any significant portion of the solvation dynamics in our experiment.

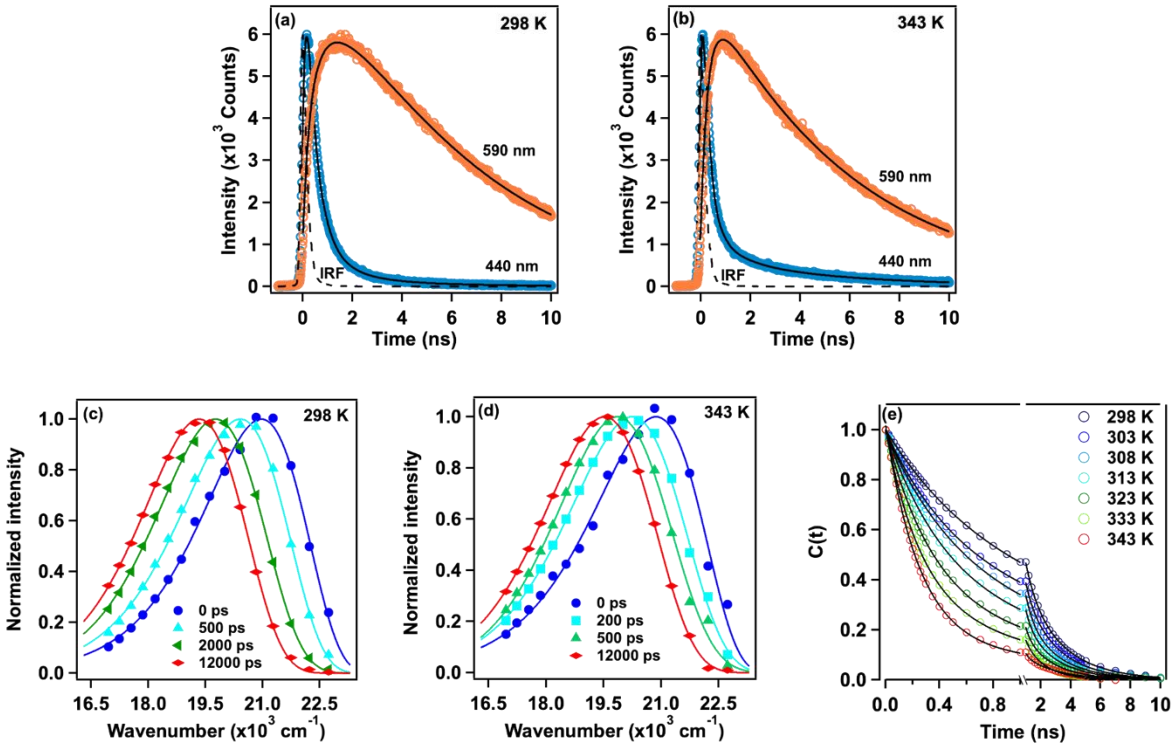

Figure 4.3 Representative fluorescence transients of C153 in LA/Men DES at 440 nm (blue circles) and 590 nm (red circles) at (a) 298 K and (b) 343 K. Dashed line is the instrument response function (IRF) and black solid lines represent the multi-exponential fit to the transients. Representative reconstructed normalized time resolved emission spectra (TRES) of C153 in LA/Men DES using the fitting parameters of the transients at (c) 298 K and (d) 343 K. The solid lines are the log-normal fit to the data points. (e) Solvent response function, $C(t)$, of C153 in LA/Men DES at different temperatures. Black solid lines represents the bi-exponential fit.

Table 4.2 Bi-exponential fitting parameters of solvent response function, $C(t)$, of C153 in LA/Men DES at different temperatures.

Temp (K)	$\bar{\nu}_{em}(0)$ (cm^{-1})	$\bar{\nu}_{em}(\infty)$ (cm^{-1})	Observed Stokes shift (cm^{-1})	% miss	a_1	τ_1 (ps)	a_2	τ_2 (ps)	$\langle\tau_s\rangle$ (ps)
298	21000	19450	1550	10%	0.53	800	0.47	2660	1670[a]
303	21000	19450	1550	10%	0.59	700	0.41	2529	1450
308	21000	19450	1550	10%	0.63	555	0.37	2290	1200[a]
313	21000	19450	1550	10%	0.67	455	0.33	2160	1020
323	20950	19450	1500	13%	0.72	360	0.28	1980	810
333	20900	19450	1450	16%	0.72	270	0.28	1600	640
343	20850	19450	1400	19%	0.80	210	0.20	1500	470[a]

[a] ± 50 ps

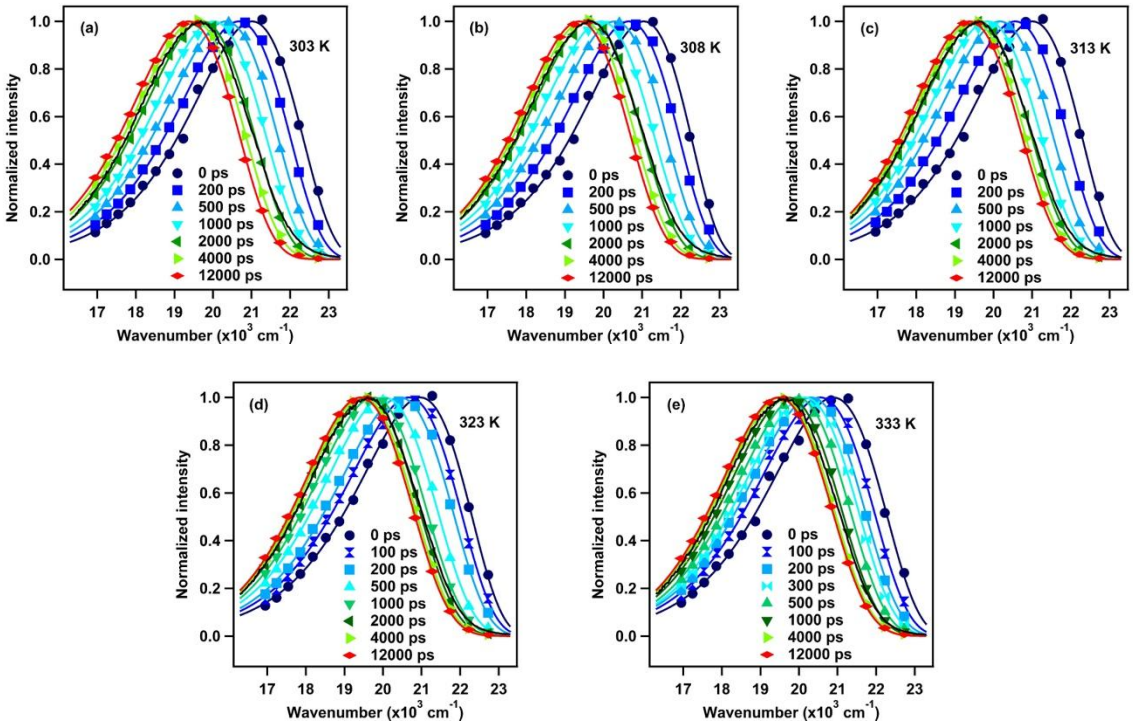

Figure 4.4 Reconstructed TRES of C153 in LA/Men DES at different temperatures indicated in each panel in Kelvin.

Solvent relaxation or solvation dynamics is a complex process involving various molecular motions including libration, rotation and translation. Here we are focussing on average solvation dynamics to begin with. The extent of decoupling of the average solvation time $\langle \tau_s \rangle$ on the η/T ratio of the medium is examined through the log-log plot of $\langle \tau_s \rangle$ vs η/T as shown in figure 4.5 and the extent of fractional power dependence (p) is found to be 0.63. This decoupling points towards the presence of dynamic heterogeneity in LA/Men DES.

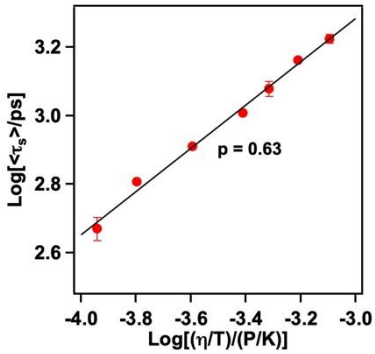

Figure 4.5 Log-log plot of average solvation time, $\langle \tau_s \rangle$, against η/T with linear fit (black solid line). Error bar indicates standard deviation from three independent measurements.

4.2.3.2 Solute rotation studied by time-resolved fluorescence anisotropy

In order to assess nature of the viscosity decoupling of solute rotation, time-resolved fluorescence anisotropy experiment was performed using C153 as the solute. Representative fluorescence anisotropy decay, $r(t)$, of C153 in LA/Men DES at two temperatures are shown in figure 4.6a (see figure 4.7 for complete data set). As expected, C153 undergoes a faster rotation as temperature increases.

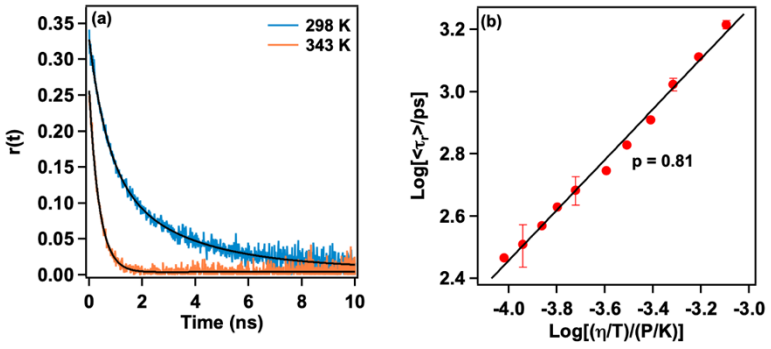

Figure 4.6 (a) Fluorescence anisotropy decay, $r(t)$, of C153 in LA/Men DES at different temperatures along with the bi-exponential fits (solid black lines). (b) Log-log plot of average reorientational time, $\langle\tau_s\rangle$, against η/T with linear fit (black solid line). Error bar indicates standard deviation from three independent measurements.

Table 4.3 Bi-exponential fitting parameters of fluorescence anisotropy decay, $r(t)$, of C153 in LA/Men DES at different temperatures.

Temperature (K)	a_1	τ_1 (ps)	a_2	τ_2 (ps)	$\langle\tau_r\rangle$ ps
298	0.18	550	0.15	2950	1641[a]
303	0.15	440	0.15	2150	1295
308	0.17	410	0.13	1900	1056[a]
313	0.18	390	0.13	1400	814
318	0.17	310	0.13	1150	674
323	0.16	280	0.13	900	558
328	0.18	320	0.11	750	483[a]
333	0.17	280	0.11	650	425
338	0.20	280	0.08	600	371
343	0.17	240	0.08	500	323[a]
348	0.20	240	0.05	500	292

[a] ± 50 ps

The decays were fitted with bi-exponential function and fitting parameters along with the average reorientational time constants at different temperatures are given in table 4.3. Ideally the value of r_0 (= a_1 + a_2) should be 0.4 for isotropic ground state distribution of C153 under the approximation of excitation photo selection when the absorption and emission dipoles are co-linear. However, in this case the value of r_0 found to be 0.33 for 298 K, which gradually decreased to 0.25 at 348 K. The lower value of r_0 may be because of the large IRF (150 ps) of our TCSPC setup. Log-log plot of $\langle \tau_r \rangle$ vs η/T is shown in figure 4.6b. Linear fit of this plot shows that the average rotational time of C153 has a fractional power dependence on the medium viscosity with p = 0.81, which is a slight deviation from hydrodynamic Stokes-Einstein-Debye (SED) prediction.

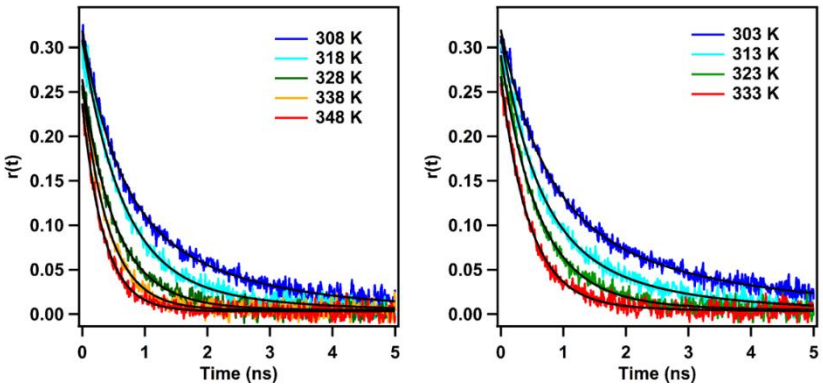

Figure 4.7 Fluorescence anisotropy decay of C153 in LA/Men DES at different temperatures along with fitting.

4.2.3.3 Solute translational diffusion studied by fluorescence intensity autocorrelation

Translational diffusion characteristics of a fluorescent molecule (R6G) in LA/Men DES is studied at the single molecular level through FCS measurement.[27,30,31] The normalized fluorescence intensity autocorrelation function ($G(\tau)$) at some representative temperatures are shown in figure 4.8a. Anomalous diffusion model (equation 2.22) with anomalous coefficient α = 0.85-0.91 fits the $G(\tau)$ slightly better as compared to normal diffusion (equation 2.21). A representative fitting comparison for 298 K is shown in figure 4.8b (see figure 4.9 for data at all the temperatures). Here to note that the value of τ_D obtained from the two models differs only by 10 %. Since anomalous model gives better fit, diffusion time obtained from this model is taken for further analysis. The value of translational diffusion time τ_D at 298 K is found to be 1870 μs, which decrease to 900 μs on increasing the temperature to 353 K (see table 4.4 for

complete data). Figure 4.8c shows Log-Log plot of τ_D against η/T with a linear fit showing a large fractional power dependence of translational diffusion time on the medium viscosity (p ~ 0.29).

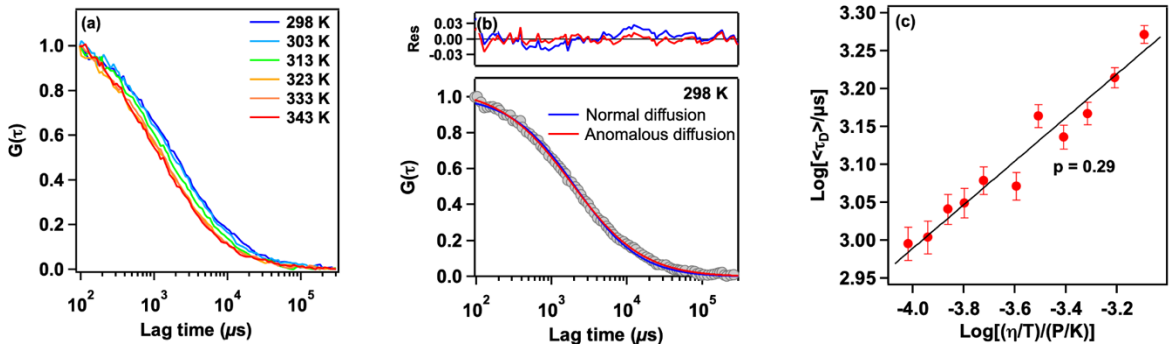

Figure 4.8 (a) Some representative autocorrelation function delineating the translational diffusion of R6G in LA/Men DES at some chosen temperatures. (b) Fitting comparison with normal (equation 6) and anomalous (equation 7) diffusion models of the fluorescence autocorrelation data at 298 K. The corresponding fitting residuals are also shown. (c) Log-log plot of translational diffusion time, τ_D, against η/T with linear fit (black solid line). Error bar indicates standard deviation from three independent measurements.

Table 4.4. Fitting parameters of fluorescence autocorrelation function of R6G in LA/Men DES along with the viscosities at different temperatures.

Temperature (K)	$\tau_D{}^a$ **(μs)**
298	1870
303	1640
308	1470
313	1370
318	1460
323	1180
328	1200
333	1120
338	1100
343	1010
348	990
353	900

[a] $\pm$ 50 μs

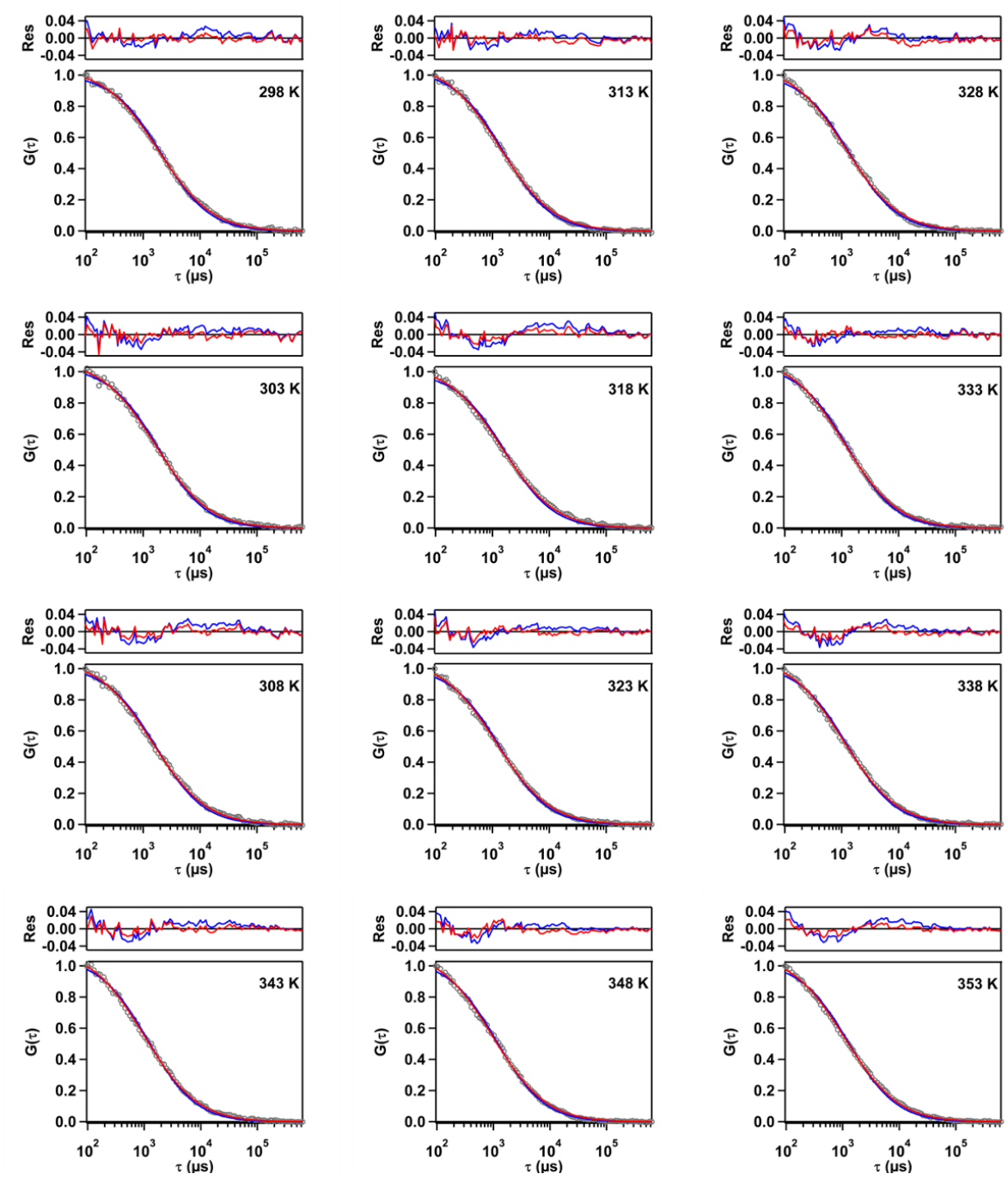

Figure 4.9. Fluorescence autocorrelation function of R6G at different temperatures in LA/Men DES along with their fitting.

4.3 Discussion

LA/Men DES turns out to be highly non-polar (see figure 4.1b), yet we do not see any vibrational fine structures. The absence of vibrational fine structure indicate the presence of solute-solvent interaction.[33] This interaction is probably through hydrogen bonding considering the constituents of the DES. The absence of excitation wavelength dependence on the emission

spectra of C153 in this DES (see figure 4.1c) suggests that either all the fluorophores are in similar environment or the solvent relaxation is fairly fast compared to the lifetime of the fluorophore. Thus we presume that LA/Men DES is spatially homogeneous or at least, the presence of heterogeneity could not be captured during the time of the measuring event (in this case during the excited state life-time of C153, i.e. ~ 5.3 ns). If latter is the case (i.e. if DES is heterogeneous), we should observe an appreciable viscosity decoupling of the solvation time, which is the manifestation of the presence of spatially heterogeneous dynamics, usually referred to as dynamic heterogeneity.

The solvation time of LA/Men DES is found to be considerably long (at 298 K $\langle\tau_s\rangle$ = 1670 ps, see table 4.2). Note that we have missed about 10% of total solvation in our study and we propose the presence of sub 100 ps solvation component in the system, though its magnitude is only 10%. Thus the origin of the solvation dynamics in this case is presumed to be due to the diffusive rotation and translation[34] with a small contribution of inter-molecular vibration and damped rotation.[35] Nevertheless, a detailed computer simulation and dielectric relaxation experiment is required to confirm this. Interestingly, we observed a viscosity/temperature decoupling of solvation time in LA/Men DES with p = 0.63, which suggests the decoupling of molecular motions from the viscosity. The observed dynamic heterogeneity is not large but is more than acetamide/urea DES where solvation was found to decouple from the viscosity to a lesser extent (p ~ 0.84).[21] Plausible reason could be the size of the constituent molecules and the nature of the interaction involved. In the case of acetamide/urea DES, the constituent molecules are of similar shape, size, and functionality and are much smaller than probe molecule. Therefore it might behaves like a solvent of single component (like normal solvent). While in the case of DES under investigation, the constituent molecules (LA and Men) are vastly different from each other in terms of their size, shape and functional group. As a result, one can expect the resulting mixture to be different from non-ionic acetamide/urea DES. LA being a surfactant like long chain fatty acid has a possibility to form micelle like structure, which results in the deviation from the Stokes-Einstein (SE) and/or Stokes-Einstein-Debye (SED) predicted molecular motion ($D \propto T/\eta$). One such similar DES based on lauric acid and N-methyl acetamide was found to have micelle like structure with hydrophobic and hydrophilic regions.[15] If such structures exist, the solvent molecules in this restricted environment will have difficulty to undergo diffusive motion, especially reorientation. This prediction is supported by the large solvation time in LA/Men DES. Note that in glycerol/choline chloride DES, which has relatively high viscosity (259 cP at 298 K), the average solvation time ($\langle\tau_s\rangle$) is ~338 ps[36] with the same probe and in acetamide/urea DES (~12 cP at 328 K) the solvation time is ~20 ps

with DCM as a probe.[21] In the present study, the solvation time $\langle\tau_s\rangle$ is 1670 ps while the viscosity is only ~24 cP at 298 K.

The absence of spatial heterogeneity and mild viscosity decoupling of average solvation time basically indicate that the environment of the solvation spheres of C153 in LA/Men DES is somewhat uniform. Next, we intend to check the viscosity decoupling of two solvation time components separately. We observed a similar viscosity decoupling of the fast component (p = 0.69) that of the average solvation time, however, for long component, the decoupling is quite strong (p = 0.30) as depicted in figure 4.10. Here to note that the origin of the short component is believed to be the immediate solvation shell, whereas, contribution from extended solvation shell is likely to be contributed in the long component of solvation dynamics. In the latter case, diffusive rotation and translation are important. Thus we propose that LA/Men DES is both spatially and dynamically homogeneous upto a certain length scale (probably within the first solvation shell), but, dynamically heterogeneous beyond that.

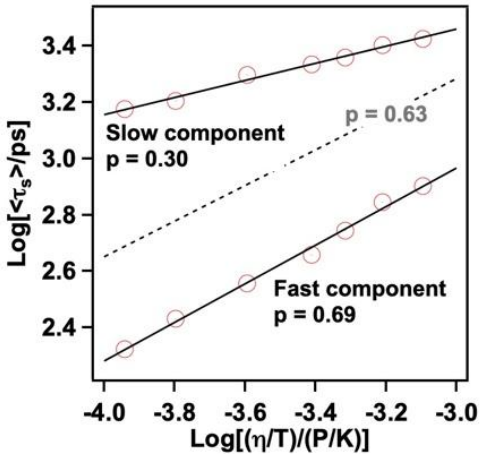

Figure 4.10. Log-log plot of different components of solvation dynamics of C153 in LA/Men DES against η/T with linear fit (solid black like). For comparison, viscosity decoupling of average solvation time, $\langle\tau_s\rangle$, is also shown (dotted line).

To test this, we studied the fluorescence anisotropy of C153 in LA/Men DES, which should reflect the nature of the first solvation shell. Here, we observed two time components of the re-orientation dynamics (table 4.3). Without a detail analysis on the origin of the biphasic anisotropy decay, we focus on the average re-orientational time ($\langle\tau_r\rangle$) of C153. The rotational dynamics of C153 is found to be slightly decoupled from viscosity/temperature (p = 0.81). The observed small deviation of molecular rotation from hydrodynamic SED relationship could be due to the distribution of the probe molecules in environments of different mobility. Here also a micelle like structure could be pictured wherein solutes could be present at different locations. Viscosity decoupling of molecular rotation has been observed in many DESs.[16,17,19,20,24] The

fractional dependence in acetamide-urea DES is $p \sim 0.96$[18] and in acetamide-$LiNO_3$/Br DES is $p \sim 0.55$.[17] Here to note that the rotational dynamics measured through fluorescence de-polarization experiment (as in the present case) basically reflects the hindrance of its local environment and a value of p = 0.81 indicates that the deviation of C153 rotation from the predicted SED is not large. The rotation is dictated mostly by the viscosity. Thus we conclude that the immediate solvation spheres of C153 in LA/Men DES is quite uniform among them, leading to a fairly spatially homogeneous environment, as evidenced from the excitation wavelength dependent emission measurement and mild viscosity decoupling of the fast component of solvation dynamics.

To ensure the proposed length scale of persistent homogeneity (i.e. solvation sphere), we studied the viscosity/temperature dependence of the translational diffusion of a probe molecule (R6G), where the probe diffuse through a longer distance and capture the picture beyond the solvation shell. R6G is found to undergo anomalous sub-diffusion in LA/Men DES (see figure 4.8b), which means that the mean square displacement (MSD) is proportional to t^{α} ($\alpha < 1$) where α is the anomalous coefficient.[37] Similar diffusion was observed in FCS study of choline chloride/ethylene glycol and acetamide/urea DES.[19,21] The α value is found to be 0.85-0.91 for the present case, which is not very far from the unity. The observed anomalous diffusion could be a result of refractive index mismatch of immersion liquid (water in this case) and DES ($n_D = 1.44$) and therefore, could be misleading.[38] Dual-focus FCS can resolve this problem, which is currently not available with us. From the temperature dependent FCS measurement a strong viscosity/temperature decoupling of the translational diffusion is observed (p = 0.29, see figure 4.8c). Thus LA/Men DES turns out to be quite dynamically heterogeneous at a larger length scale. As mentioned, the long component of solvation also shows a similar value of p (= 0.30) as the origin of the long component is probably outside of the solvation shell. Note, the mild extent of decoupling for rotational dynamics and short component of solvation dynamics indicate that the system is fairly dynamically homogeneous at a short length scale.

Considering our proposition we anticipated that the activation energies of these molecular processes (i.e. solvation, rotation and translation) should be uncorrelated and will be different than the activation energy of the viscous flow. Assuming these processes are nearly linear function of inverse temperature in the studied temperature range, we estimated the associated activation energies as shown in figure 4.11. The activation energies are found to be $E_a(\tau_s)$ = 23.2 kJmol^{-1}, $E_a(\tau_r)$ = 29.9 kJmol^{-1}, $E_a(\tau_D)$ = 10.5 kJmol^{-1} and $E_a(\eta)$ = 33.7 kJmol^{-1}, respectively for average solvation, average rotational, translational diffusion and viscosity.

This again show only a partially decoupled solvent relaxation from viscosity. Interestingly, the activation energy for rotation (29.9 kJmol^{-1}) is nearly similar to that of viscous flow and it seems that rotation is governed solely by viscosity. In a same line of analysis of dynamic heterogeneity of solvation, we then checked the activation energies for the fast and slow components of solvation. As proposed, the fast component of solvation probably originates within the first solvation shell and for slow solvation component, the involvement of solvent molecule outside the solvation shell is envisaged. Thus we expected that the activation energy for the fast component of solvation will be different compared to the slow component, and the latter should match well with the activation energy of translational diffusion. This is exactly what we observed. The activation energies for the fast and slow component of solvation are found to be 25.5 and 11.2 kJmol^{-1}, respectively. The activation energy for translational diffusion is also found to be 10.5 kJmol^{-1}, which is almost same as the long component of the solvation. The observed correlation of activation energies between (i) slow solvation component and translational diffusion, (ii) rotation and viscosity and (iii) average solvation and viscosity enforces our proposition of length dependent dynamic heterogeneity in LA/Men DES. The system is closely dynamically homogeneous at short length scale, while it is dynamically heterogeneous at larger length scale.

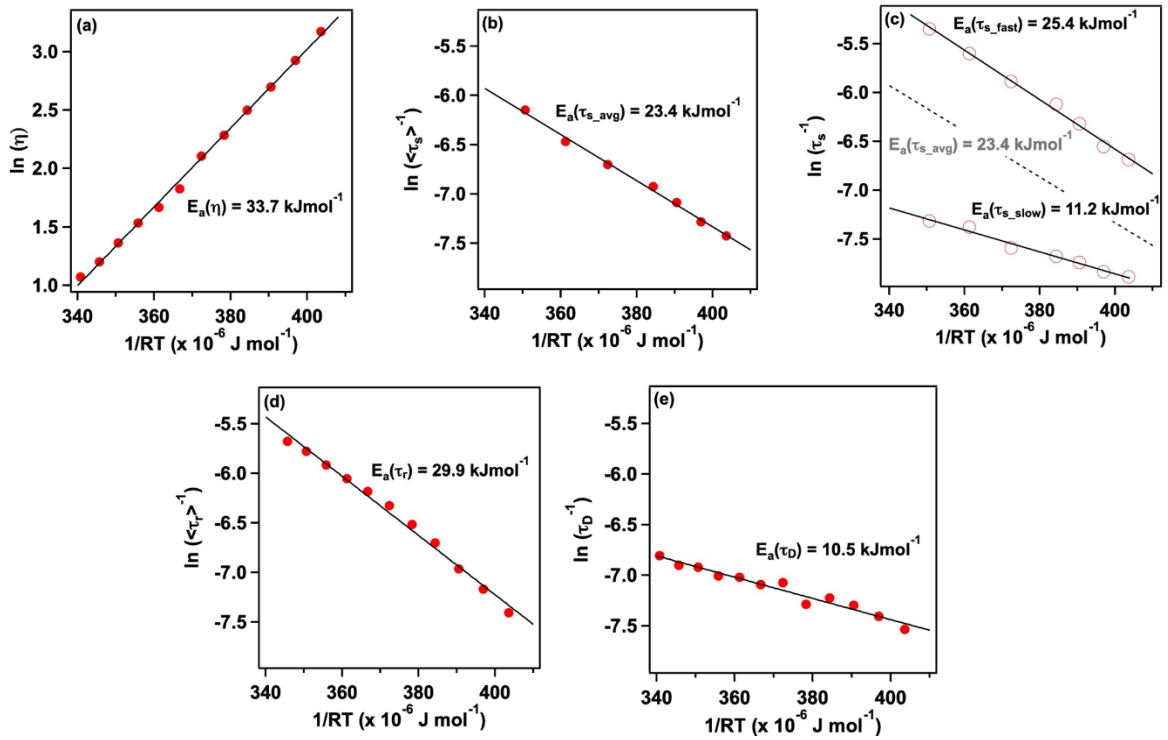

Figure 4.11 Arrhenius plot of (a) viscosity, (b) average solvation time, $\langle\tau_s\rangle$, (c) fast and slow component of solvation dynamics, (d) average probe reorientation time, $\langle\tau_r\rangle$, and (e) probe

translational diffusion time, τ_D, in LA/Men DES. Activation energies in each panel was obtained from slope of the linear fits (black solid line).

4.4 Conclusions

The main findings of this study are (i) Emission spectra of solvatochromic dye in lauric acid – menthol (LA/Men) DES does not depend on the excitation wavelength suggesting it to be spatially homogenous. (ii) The possibility of micelle like domains in LA/Men DES has been anticipated from the observed long solvation time compared to the DES having similar viscosities. LA being a surfactant like long chain fatty acid, such a possibility is logical. (iii) A little but definite decoupling (p = 0.63) of average solvation time, $\langle\tau_s\rangle$, from the medium viscosity suggests the presence of a mild dynamic heterogeneity in the system. To have the idea about the relative heterogeneity along length scale, the individual solvation parameters are subjected to further analysis. The short component, which is believed to be originated from the immediate solvation shell is not that much viscosity decoupled (p = 0.69). However, the long component, that probably originated from the extended solvation shell, is highly viscosity decoupled (p = 0.29). It appears that the first solvation shell is fairly homogenous, but beyond that there is heterogeneity. (iv) Rotational time, $\langle\tau_r\rangle$, which should reflect the nature of the first solvation shell shows a little decoupling (p = 0.81) suggesting at shorter length scale the solvent is fairly homogenous. (v) Translational diffusion, τ_D, that provides information at the large length scale, is strongly decoupled from medium viscosity (p = 0.29). This suggests that at a larger length scale the solvent is quite dynamically heterogenous. (vi) Using Arrhenius equation, we observed correlation of activation energies between (a) slow solvation component and translational diffusion and (b) fast solvation component, rotation and viscosity. This enforces our proposition of length dependent dynamic heterogeneity in LA/Men DES. The main finding of this report is summarised in scheme 4.1. Overall, our result demonstrates the structure and dynamics of the non-ionic LA/Men DES and the extent of heterogeneity as a function of the length scale has been contemplated. Probably, for the first time, we have tried to set a correlation between various dynamics in a DES using Arrhenius equation. We believe such an approach will help to understand the origin of unique structural features of DESs in future.

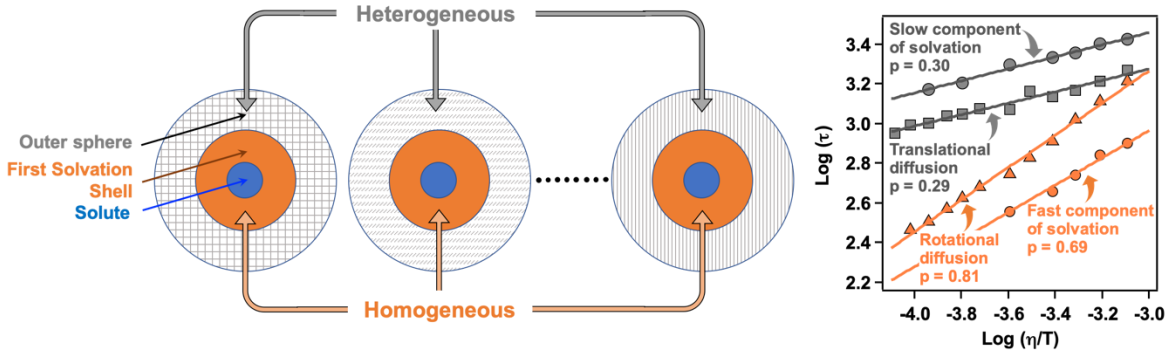

Scheme 4.1 Schematic representation of heterogeneity at different length scale in LA/Men DES.

References

1. Smith, E. L.; Abbott, A. P.; Ryder, K. S. Deep eutectic solvents (DESs) and their applications. *Chem. Rev*. **2014**, *114*, 11060–11082.

2. Zhang, Q.; Vigier, K. De O.; Royer, S.; Jérôme, F. Deep eutectic solvents: syntheses, properties and applications. *Chem. Soc. Rev*. **2012**, *41*, 7108–7146.

3. Hansen, B. B.; Spittle, S.; Chen, B.; Poe, D.; Zhang, Y.; Klein, J. M.; Horton, A.; Adhikari, L,; Zelovich, T.; Doherty, B. W.; Gurkan, B.; Maginn, E. J.; Ragauskas, A.; Dadmun, M.; Zawodzinski, T. A.; Baker, G. A.; Tuckerman, M. E.; Savinell, R. F.; Sangoro, J. R. Deep Eutectic Solvents: A Review of Fundamentals and Applications. *Chem. Rev*. **2021**, *121*, 1232−1285.

4. Lapeña, D.; Lomba, L.; Artal, M.; Lafuente, C.; Giner, B. Thermophysical characterization of the deep eutectic solvent choline chloride:ethylene glycol and one of its mixtures with water. *Fluid Phase Equilib*. **2019**, *492*, 1-9.

5. van Osch, D. J. G. P.; Dietz, C. H. J. T.; Warrag, S. E. E.; Kroon, M. C. The Curious Case of Hydrophobic Deep Eutectic Solvents: A Story on the Discovery, Design, and Applications. *ACS Sustainable Chem. Eng*. **2020**, *8*, 10591–10612.

6. Florindo, C.; Branco, L. C.; Marrucho, I. M. Quest for Green-Solvent Design: From Hydrophilic to Hydrophobic (Deep) Eutectic Solvents. *ChemSusChem* **2019**, *12*, 1549-1559.

7. van Osch, D. J. G. P.; Zubeir, L. F.; van den Bruinhorst, A.; Rocha, M. A. A.; Kroon, M. C. Hydrophobic deep eutectic solvents as water-immiscible extractants. *Green Chem*. **2015**, *17*, 4518–4521.

8. Li, T.; Song, Y.; Li, J.; Zhang, M.; Shi, Y.; Fan, J. New low viscous hydrophobic deep eutectic solvents in vortex-assisted liquid-liquid microextraction for the determination of phthalate esters from food-contacted plastics. *Food Chem*. 2020, *309*, 125752.

9. Ribeiro, B. D.; Florindo, C.; Iff, L. C.; Coelho, M. A. Z.; Marrucho, I. M. Menthol-based Eutectic Mixtures: Hydrophobic Low Viscosity Solvents. *ACS Sustainable Chem. Eng*. **2015**, 3, 2469−2477.

10. Martins, M. A. R.; Crespo, E. A.; Pontes, P. V. A.; Silva, L. P.; Bülow, M.; Maximo, G. J.; Batista, E. A. C.; Held, C.; Pinho, S. P.; Coutinho, J. A. P. Tunable Hydrophobic

Eutectic Solvents Based on Terpenes and Monocarboxylic Acids. *ACS Sustainable Chem. Eng*. **2018**, *6*, 8836−8846.

11. van Osch, D. J. G. P.; Parmentier, D.; Dietz, C. H. J. T.; van den Bruinhorst, A.; Tuinier, R.; Kroon, M. C. Removal of alkali and transition metal ions from water with hydrophobic deep eutectic solvents. *Chem. Commun*. **2016**, *52*, 11987-11990.
12. Tereshatov, E. E.; Boltoeva, M. Y.; Folden, C. M. First evidence of metal transfer into hydrophobic deep eutectic and low-transition-temperature mixtures: indium extraction from hydrochloric and oxalic acids. *Green Chem*. **2016**, *18*, 4616–4622.
13. Florindo, C.; Lima, F.; Branco, L. C.; Marrucho, I. M. Hydrophobic Deep Eutectic Solvents: A Circular Approach to Purify Water Contaminated with Ciprofloxacin. *ACS Sustainable Chem. Eng*. **2019**, *7*, 14739−14746.
14. Florindo, C.; Romero, L.; Rintoul, I.; Branco, L. C.; Marrucho, I. M. From Phase Change Materials to Green Solvents: Hydrophobic Low Viscous Fatty Acid–Based Deep Eutectic Solvents. *ACS Sustainable Chem. Eng*. **2018**, *6*, 3888-3895.
15. Cui, Y.; Rushing, J. C.; Seifert, S.; Bedford, N. M.; Kuroda, D. G. Molecularly Heterogeneous Structure of a Nonionic Deep Eutectic Solvent Composed of N-Methylacetamide and Lauric Acid. *J. Phys. Chem. B* **2019**, *123*, 18, 3984-3993.
16. Guchhait, B.; Gazi, H. A. R.; Kashyap, H. K.; Biswas, R. Fluorescence Spectroscopic Studies of (Acetamide + Sodium/Potassium Thiocyanates) Molten Mixtures: Composition and Temperature Dependence. *J. Phys. Chem. B* **2010**, *114*, 5066–5081.
17. Guchhait, B.; Daschakraborty, S.; Biswas, R. Medium decoupling of dynamics at temperatures ∼100 K above glass-transition temperature: A case study with (acetamide + lithium bromide/nitrate) melts. *J. Chem. Phys*. **2012**, *136*, 174503.
18. Das, A.; Das, S.; Biswas, R. Density relaxation and particle motion characteristics in a non-ionic deep eutectic solvent (acetamide + urea): Time-resolved fluorescence measurements and all-atom molecular dynamics simulations. *J. Chem. Phys*. **2015**, *142*, 034505.
19. Hossain, S. S.; Samanta, A. Solute rotation and translation dynamics in an ionic deep eutectic solvent based on choline chloride. *J. Phys. Chem. B* **2017**, *121*, 10556– 10565.

20. Hossain, S. S.; Samanta, A. How do the hydrocarbon chain length and hydroxyl group position influence the solute dynamics in alcohol-based deep eutectic solvents? *Phys. Chem. Chem. Phys.* **2018**, *20*, 24613– 24622.

21. Subba, N.; Polok, K.; Piatkowski, P.; Ratajska-Gadomska, B.; Biswas, R.; Gadomski, W.; Sen, P. Temperature-Dependent Ultrafast Solvation Response and Solute Diffusion in Acetamide–Urea Deep Eutectic Solvent. *J. Phys. Chem. B* **2019**, *123*, 9212–9221.

22. Kaur, S.; Gupta, A.; Kashyap, H. K. Nanoscale Spatial Heterogeneity in Deep Eutectic Solvents. *J. Phys. Chem. B* **2016**, *120*, 6712–6720.

23. Percevault, L.; Jani, A.; Sohier, T.; Noirez, L.; Paquin, L.; Gauffre, F.; Morineau, D. Do Deep Eutectic Solvents Form Uniform Mixtures Beyond Molecular Microheterogeneities? *J. Phys. Chem. B* **2020**, *124*, 9126–9135.

24. Tarif, E.; Mondal, J.; Biswas, R. Interaction and Dynamics in a Fully Biodegradable Glucose-Containing Naturally Abundant Deep Eutectic Solvent: Temperature-Dependent Time-Resolved Fluorescence Measurements. *J. Phys. Chem. B* **2019**, *123*, 9378–9387.

25. Pal, N.; Verma, S. D.; Sen, S. Probe Position Dependence of DNA Dynamics: Comparison of the Time-Resolved Stokes Shift of Groove-Bound to Base-Stacked Probes. *J. Am. Chem. Soc*. **2010**, *132*, 9277–9279.

26. Horng, M. L.; Gardecki, J. A.; Papazyan, A.; Maroncelli, M. Subpicosecond Measurements of Polar Solvation Dynamics: Coumarin 153 Revisited. *J. Phys. Chem*. **1995**, *99*, 17311−17337.

27. Lakowicz, J. R. Principles of Fluorescence Spectroscopy, 3rd ed.; Springer, New York, 2006.

28. Jimenez, R.; Fleming, G. R.; Kumar, P. V.; Maroncelli, M. Femtosecond solvation dynamics of water. *Nature* **1994**, *369*, 471−473.

29. Fee, R. S.; Maroncelli, M. Estimating the time-zero spectrum in time-resolved emission measurements of solvation dynamics. *Chem. Phys*. **1994**, *183*, 235-247.

30. Shirota, H.; Horie, K. Solvation Dynamics in Nonaqueous Reverse Micelles. *J. Phys. Chem. B* **1999**, *103*, 1437 – 1443.

31. Schwille, P.; Korlach, J.; Webb, W. W. Fluorescence correlation spectroscopy with single-molecule sensitivity on cell and model membranes. *Cytometry* **1999**, 36, 176−182.

32. Banks, D. S.; Fradin, C. Anomalous diffusion of proteins due to molecular crowding. *Biophys. J*. **2005**, *89*, 2960−2971.
33. Mühlpfordt, A.; Schanz, R.; Ernsting, N. P.; Farztdinov, V.; Grimme, S. Coumarin 153 in the gas phase: optical spectra and quantum chemical calculations. *Phys. Chem. Chem. Phys*. **1999**, *1*, 3209-3218.
34. Bagchi, B. Molecular Relaxation in Liquids, Oxford University Press; New York, 2012.
35. Bagchi, B. Water solvation dynamics in the bulk and in the hydration layer of proteins and self-assemblies. *Annu. Rep. Prog. Chem., Sect. C* **2003**, *99*, 127–175.
36. Turner, A. H.; Kim, D. Rotation and translation dynamics of coumarin 153 in choline chloride-based deep eutectic solvents. *J. Chem. Phys*. **2018**, *149*, 174503.
37. Metzler, R.; Jeon, J.-H.; Cherstvy, A. G.; Barkai, E. Anomalous diffusion models and their properties: Non-stationarity, nonergodicity, and ageing at the centenary of single particle tracking. *Phys. Chem. Chem. Phys*. **2014**, *16*, 24128−24164.
38. Lehmann, S.; Seiffert, S.; Richtering, W. Refractive index mismatch can misindicate anomalous diffusion in single-focus fluorescence correlation spectroscopy. *Macromol. Chem. Phys*. **2015**, *216*, 156−163.

This Page Intentionally Left Blank

Chapter 5

Sub-picosecond Solvation Response and Partial Viscosity Decoupling of Solute Diffusion in Ionic Deep Eutectic Solvents

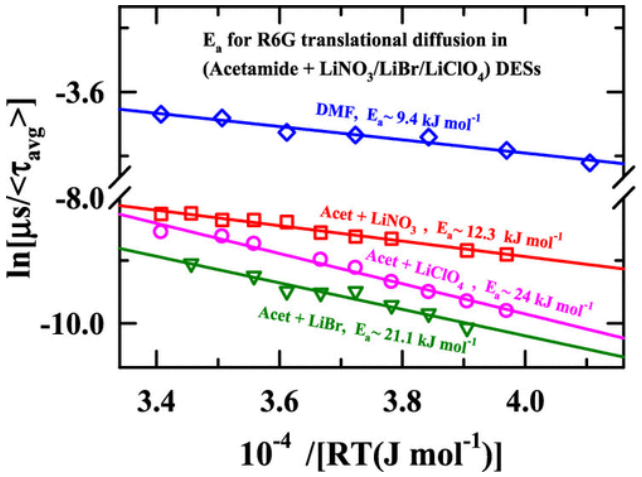

N. Subba, E. Tarif, R. Biswas and P. Sen. *J. Phys. Chem. B* **2020**, *124*, 6875-6884

Solvation dynamics study (with 70 ps instrument response) of DESs based on acetamide and LiBr/NO_3 missed about 50 % of the Stokes shift dynamics despite considerable its bulk viscosity. In this chapter, fluorescence up-conversion (~250 fs instrumental response) coupled with time correlated single photon counting measurements was used to explore the complete Stokes shift dynamics of a dipolar solute probe, coumarin 153 (C153), in several ionic acetamide deep eutectic solvents (DESs) that contained lithium nitrate/bromide/perchlorate as electrolyte. Combined measurements near room temperature reflected a total dynamic Stokes shift of approximately 800–1100 cm^{-1} and triexponential solvation response functions. Interestingly, the average rate of solvation became faster upon successive replacement of bromide by nitrate in these deep eutectics, and a sub-picosecond time scale emerged in the measured solvation response when bromide was fully replaced by nitrate. Temperature dependent solute diffusion in these deep eutectics at the single molecule level using FCS, revealed pronounced fractional viscosity dependence of the solute's translational motion. Subsequently, this partial decoupling of solute translation was attributed to the micro-heterogeneous nature of these ionic DESs after examining the diffusion–viscosity relationship of molecular solvents at room temperature and in a liquid amide solvent at different temperatures.

5.1 Introduction

Deep eutectic solvents (DESs) have recently received considerable attention because of their potential as host media for large scale and diverse applications in both industrial and technological sectors.[1-3] . This interest stems from the fact that several DESs offer stable liquid phase at or near room temperature although these are prepared via melting of multi-component mixtures where individual components are often room-temperature solids.[4-12] This introduces some sort of 'metastability' in the system, which may induce features that are reminiscent of deeply super-cooled systems near glass transition.[13-16] For example, pronounced fractional viscosity dependence of solute and solvent diffusion have been reported for several ionic acetamide DESs and subsequently interpreted in terms of heterogeneous molecular relaxations.[9, 17-19] The unique point here is, however, that such a strong viscosity decoupling has been found at temperatures ~100-150 K above the measured thermodynamic glass transition temperatures (T_g ~200-220K), and at a timescale much beyond the H-bond lifetime or molecular diffusion timescale of the dominant neat molten component of a given DES. Signature of mild heterogeneity in relaxation dynamics has been found for several other deep eutectics as well.[20-24] This fuels further research on DESs because medium heterogeneity may influence reactions in ways more diverse than conceivable via the static and the dynamic solvent effects[25-27] in otherwise homogeneous media.

Solvent static effects arise mainly from the medium static dielectric constant (ε_0), and recent megahertz-gigahertz (MHz-GHz) dielectric relaxation (DR) measurements[21,28] have provided semi-accurate estimates of ε_0 for several acetamide containing DESs. Available dynamic fluorescence Stokes shift studies, in contrast, report missing of a significant portion of the full solvation dynamics, and this missing was attributed to the broad temporal resolution (~85 ps) employed in those measurements.[17-19] These deep eutectics (made of acetamide and electrolyte) are H-bonded systems and such H-bonded systems are expected to generate sub-picosecond solvation response via collective intermolecular vibrations and librations.[29] Therefore, missing of this sub-picosecond response in those measurements is understandable. The missing amplitude was calculated via the Fee-Maroncelli method,[30] which allows one to estimate the time-zero emission frequency ($\nu_{em}(t = 0)$), that is, solute emission frequency immediately after laser excitation) from the steady state absorption spectrum of the solute in a polar medium under investigation, and the absorption and emission spectra of the same solute in a reference non-polar solvent. However, this method is expected to be semi-accurate if the densities of the polar medium and the non-polar reference system (usually a room temperature liquid alkane)

are not too different. This density difference is substantial for these deep eutectics (and for many ionic liquids) and, as a result, the estimated $\nu_{em}(t = 0)$ (and hence the missing amplitudes) in those studies might be associated with large errors. Experimental technique providing sub-picosecond temporal resolution, for example, fluorescence up-conversion measurements, is suitable in such scenarios to locate the $\nu_{em}(t = 0)$ and detect the complete fluorescence Stokes shift dynamics. Once the solvation response is fully characterized in this way, analyses of dynamic solvent effects on reactions occurring in these media become more meaningful. Moreover, these complete measurements will act as a positive feedback for qualitatively understanding the available DR data for several (acetamide+electrolyte) deep eutectics because of the inter-relationship between DR and dynamic fluorescence Stokes shift measurements.

Another important aspect that demands a rigorous investigation is the pronounced fractional viscosity (η) dependence of solute solvation and rotation times in several ionic acetamide DESs, represented by $\langle \tau_x \rangle \propto (\eta/T)^p$(equation 1.5), with p ~ 0.4-0.7 and T being the temperature.[17-19] This deviation from the hydrodynamic viscosity dependence (that is, deviation from p = 1) has been observed with an aspherical solute (coumarin 153, C153), and for a solute-solvent size ratio, R ~ 2 (assuming both acetamide and C153 as spheres with diameters ~4 Å and ~8Å, respectively).[21,31] In these studies solute rotation was followed by the dynamic fluorescence anisotropy measurements, while information on solvent translation was accessed indirectly (and through interpretation) from the dynamic fluorescence Stokes shift experiments. However, the coupling between the solute's centre-of-mass diffusion (translational diffusion) and the medium viscosity was not directly tracked in any of these measurements. A direct information along the line of 'translation-rotation decoupling' reported for deeply super-cooled systems is therefore still lacking. In addition, an answer to the question "how dynamically heterogeneous are these deep eutectics compared to otherwise homogeneous media?" is not known yet. This is because the extent of temporal heterogeneity interpreted from the deviation of p from unity for these DESs has not been referenced against systematic measurements employing the same solute in either a series of conventional molecular solvents at ambient condition or in a single solvent at different temperatures. One of the foci of the present work is to explore plausible answers to these queries by performing fluorescence correlation spectroscopic measurements, and comparing the diffusion-viscosity coupling observed for DESs against that obtained for conventional molecular solvents.

5.2 RESULTS AND DISCUSSION

5.2.1 FCS measurement: FCS study was performed in DESs at varying temperatures using R6G as a probe molecule. We mostly relied on R6G owing to its good fluorescence quantum yield. Figure 5.1a shows the normalized fluorescence autocorrelation curve for R6G in $0.78CH_3CONH_2+0.22LiNO_3$ DES at different temperatures. A representative fit to the FCS data (collected at 353 K) along with the residuals are shown in figure 5.1b.

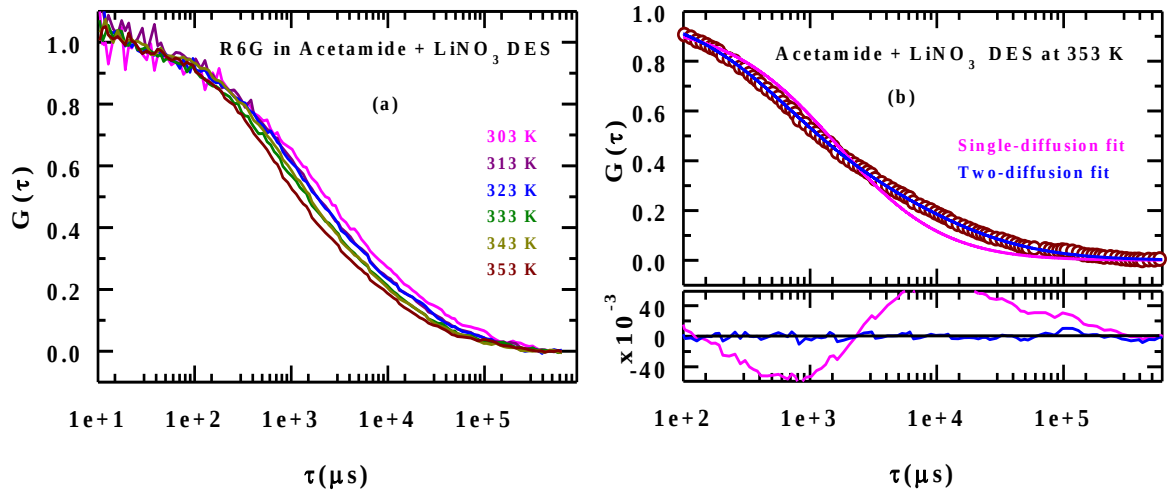

Figure 5.1 (a) Normalized FCS data for rhodamine 6G (R6G) in $[0.78CH_3CONH_2+0.22LiNO_3]$ DES at different temperatures. (b) FCS data for $[0.78CH_3CONH_2+0.22LiNO_3]$ DES at 353 K for R6G along with fits (single and two-diffusion components using equation 2.21 and equation 2.23, respectively), and the corresponding residuals (lower panel) for a comparison.

Table 5.1 Fit parameters obtained by using two-diffusion components (equation 2.23) for R6G in $[0.78CH_3CONH_2+0.22LiNO_3]$ DES at different temperatures.

Temperature (K)	Viscosity (cP)	N_1	τ_{D_1} (μs)	N_2	τ_{D_2} (μs)	$\langle\tau_D\rangle$ (μs)
303	210.57	0.64	997	0.38	18137	7359
308	152.37 (a)	0.62	904	0.34	17661	6896
318	82.24	0.63	825	0.36	14313	5720
323	62.32 (a)	0.66	852	0.34	14400	5529
328	47.57 (a)	0.67	850	0.32	14311	5198
333	39.35	0.65	657	0.34	11447	4387
338	29.49 (a)	0.68	732	0.30	12134	4253
343	24.11 (a)	0.69	797	0.29	12329	4248
348	21.59	0.66	643	0.29	11103	3820
353	17.52 (a)	0.70	623	0.27	12159	3861

a=These viscosity coefficients were extra/interpolated from the known viscosity data.[17]

Because the diffusion times are relatively longer in all the DESs,[17,18] the triplet-state decay appears distinctly at the shorter time region in the autocorrelation curve. Therefore, the data before 100 μs containing the triplet contribution was omitted during the data analysis. Here, a single diffusion component is anticipated, as only one kind of species is present in the sample. However, the single diffusion model (equation 2.21) did not fit the data well and a second diffusion component (equation 2.23 and 2.24) was incorporated in order to achieve a better description of the data (see figure 5.1b). Note that the need for the second diffusion component might have arisen from the inherent heterogeneity of the system, which was reflected in the excitation wavelength dependence of the fluorescence emission in these mixtures.[17] Clearly, a bimodal diffusion model describes the autocorrelation curve better than the single diffusion model and therefore, two diffusion model had been used throughout. Comparison of the fits for the remaining $0.78CH_3CONH_2+0.22\{fLiBr+(1-f)LiNO_3\}$ DESs are shown in figure 5.2. These data, upon fit to bimodal diffusion model, provided two time scales differing by almost two orders of magnitude. For $0.78CH_3CONH_2+0.22LiNO_3$ DES at 353 K, the longer time constant is ~ 12,000 μs while the shorter one is ~600 μs (see table 5.1 for the data at 353 K and for other temperatures as well). The diffusion time of R6G in water (in the same instrumental settings) is in the order of 50 μs, indicating a pronounced impact of viscosity for R6G diffusion in these DESs. We would like to mention here that a similar bimodal diffusion model was required to adequately describe the FCS data for ionic liquids (ILs).[32-34] This necessity of the bimodal diffusion model was interpreted in terms of the spatial heterogeneity. Moreover, the FCS study also could reveal a bimodal diffusion behaviour of a solute in less viscous DES (ethaline, 36 cP at 298 K) although no excitation wavelength dependence of steady state fluorescence emission was observed.[1,22] This indicates that bimodality in diffusion is not always completely dictated by the solution spatial heterogeneity (commonly expected for high viscous media[35,36]) and may originate from the temporally heterogeneous dynamics, inherent to the medium.[21,37] Earlier FCS measurements of neat ionic liquids have reported a distribution of local diffusion coefficients of a single dissolved solute and interpreted in terms of spatial heterogeneity.[38] Such a reflection of spatial heterogeneity has also been registered on subnanosecond relaxation dynamics in spatially heterogeneous media.[39,40] Nonexponential relaxation dynamics have been witnessed even for solute rotational dynamics in otherwise homogeneous media.[41] All these indicate that the time-profile of the underlying microscopic friction regulates the nature of the long-time diffusive dynamics, and as a result, the idea of multiple solutes diffusing in different microscopic domains possessing disparate relaxation times may not be necessary to explain the anomalous or multiexponential relaxation kinetics at long times. For such

inherently nonhomogeneous relaxation processes, therefore, the average relaxation rate is a better descriptor than the separate individual rates for exploring the coupling between the relaxation rate and the macroscopic medium friction.

Subsequently, the amplitude-weighted diffusion time $\langle \tau_{avg} \rangle$, were obtained from the bimodal fits as follows

$$\langle \tau_{avg} \rangle = \frac{N_1 \tau_{D_1} + N_2 \tau_{D_2}}{N_1 + N_2} \qquad 5.1$$

where τ_{D_i}(i=1,2) denotes the diffusion time constant associated with the amplitude N_i. This average diffusion time at different temperatures (see table 5.1) are now used to explore the nature of viscosity coupling of the solute translational diffusion in the DESs considered here. Figure 5.3 shows $\langle \tau_D \rangle$ for R6G as a function of temperature-reduced viscosity (η/T) in double-logarithmic fashion for $0.78CH_3CONH_2$+0.22{fLiBr+(1-f)$LiNO_3$} DESs with various fractions (f) of Br^- ion. Lines through the data points represent the following general viscosity dependence, $\langle \tau_D \rangle \propto (\eta/T)^p$ with $0 < p \leq 1$, where $p = 1$ denotes the predicted hydrodynamic behaviour[42] for a large spherical solute diffusing through a solvent continuum. Significant deviation of p from unity is evident for all Br^- fractions observed here. This suggests a break-down of the hydrodynamic description of solute diffusion in these highly viscous DESs.

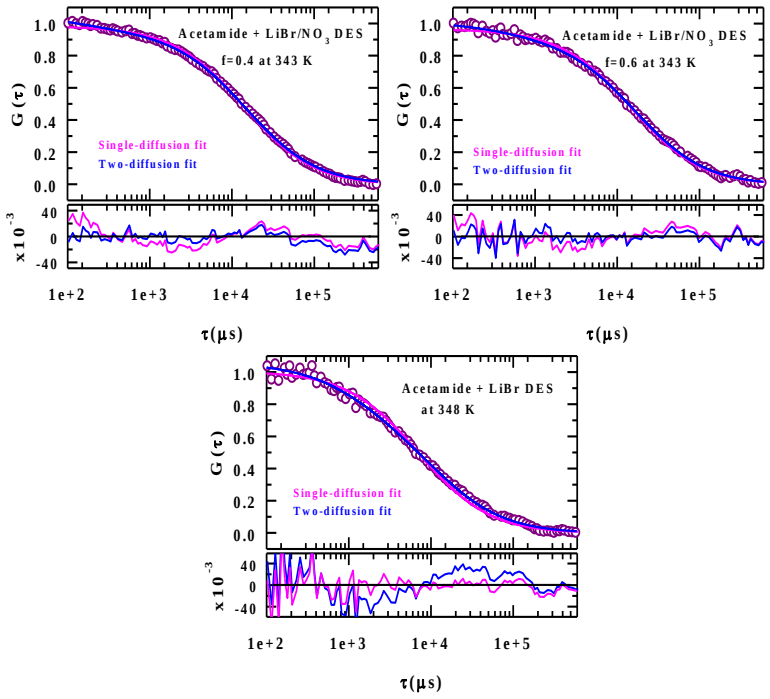

Figure 5.2 FCS data for various DESs using R6G as the probe molecule.

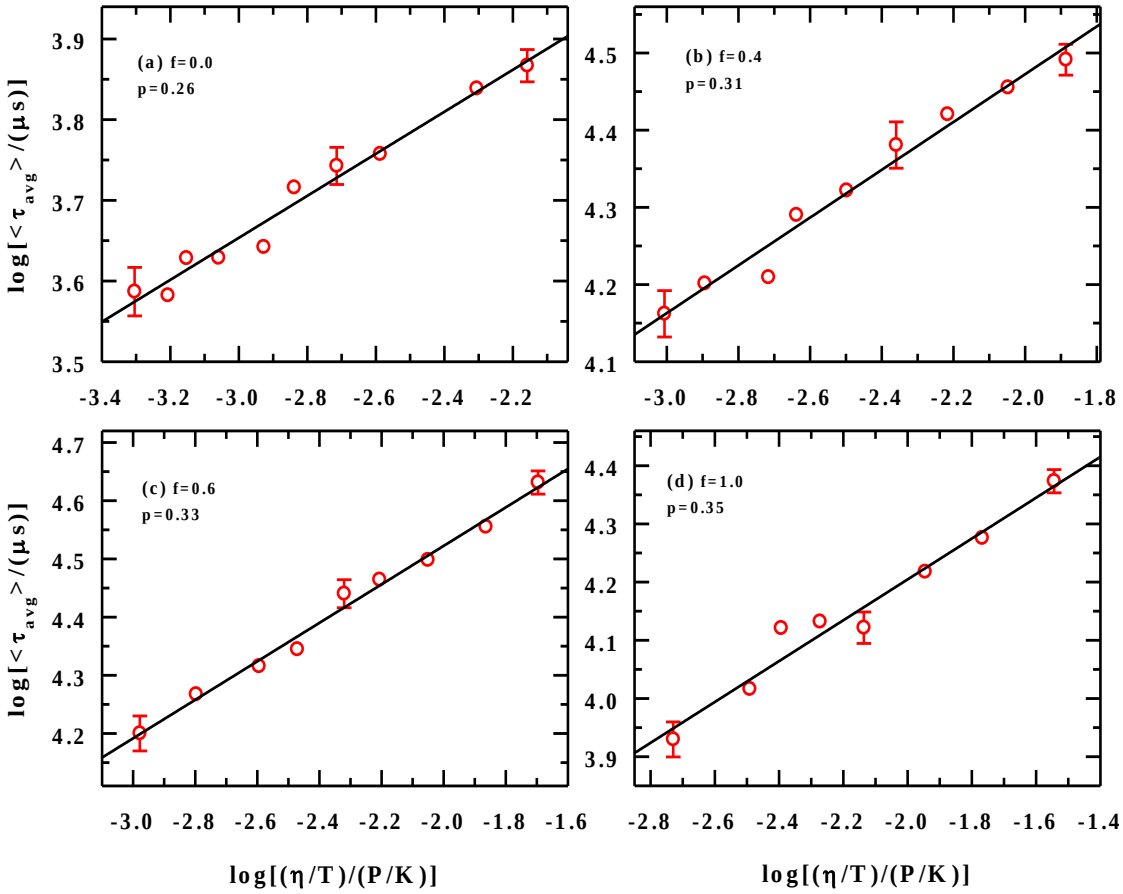

Figure 5.3. Log-log plot of R6G average diffusion time, $\langle\tau_{avg}\rangle$, as a function of temperature-reduced viscosity, η/T, in [0.78CH_3CONH_2+0.22{fLiBr+(1-f)$LiNO_3$}] DESs (at f=0.0 (a), 0.4 (b), 0.6 (c) and 1.0 (d)) using R6G as the probe molecule. The straight lines going through the data describe fits to the following expression:$log\left[\langle\tau_{avg}\rangle/(\mu s)\right] = A + p \times log[\langle\eta/T\rangle/(P/K)]$. Values of p signify the extent of viscosity decoupling for R6G translational diffusion in these ionic DESs. Error bars are representative and obtained from a limited set of 3-4 repeat measurements.

Subsequently, FCS measurements were performed for R6G in 0.81CH_3CONH_2+0.19$LiClO_4$ DES, and the autocorrelation function was best fitted to a two-diffusion models as before (see figure 5.4a). Figure 5.4b shows the viscosity dependence of $\langle\tau_{avg}\rangle$ and, the value of p in this case is found to be 0.58, which also suggests a considerable deviation from the hydrodynamic description.

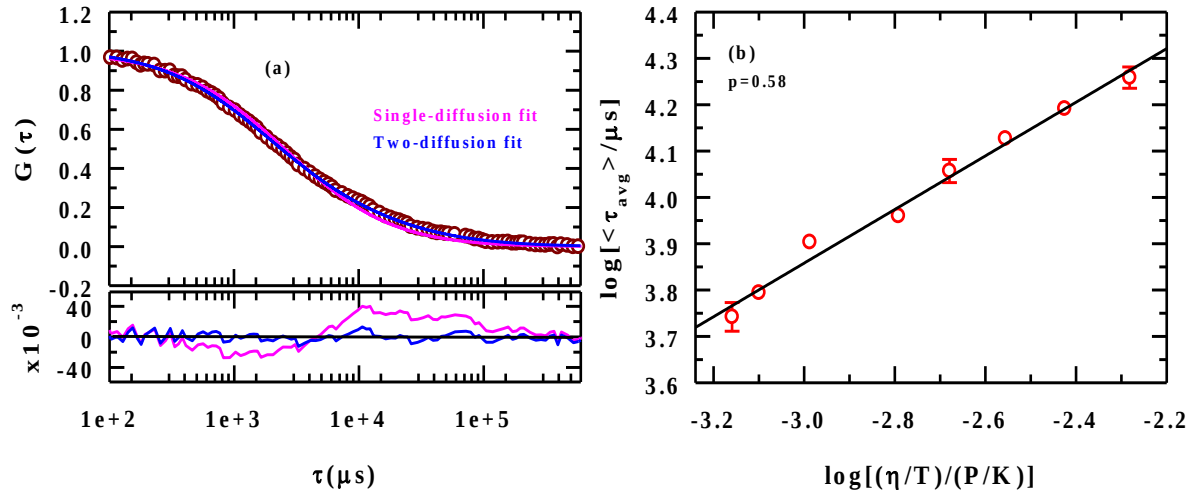

Figure 5.4 Autocorrelation curve measured for R6G in [0.81CH_3CONH_2+0.19$LiClO_4$] DES at 353 K along-with fits and residuals (a), and the viscosity dependence for the corresponding average diffusion times (b). Viscosity coefficients used here are from Ref. 18.

According to Stokes-Einstein relationship, diffusion constant (D) is proportional to $T/\eta(T)$ and $\tau_D \propto 1/D$ (equations 1.2 and 1.4, respectively). This leads to the prediction that $\tau_D \propto \eta(T)/T$ from Stokes-Einstein relation and it is expected to have a slope of unity in the log-log plot of τ_D and $\eta(T)/T$. In the studied temperature range the slope of log-log plots (figures 5.3 and 5.4b) for various DESs is found to be significantly less than unity and thus indicates a break-down of hydrodynamic viscosity dependence of solute diffusion in these highly viscous DESs ($0.25<p<0.6$). This deviation may be an indication of dynamic heterogeneity resulting either from spatially varying diffusive relaxation rates due to inhomogeneous solution structure or from accessing the non-hydrodynamic modes, such as, translational jumps by the particles in motion.[43,44] Such jumps can be facilitated by increasing the medium viscosity through lowering solution temperature.[45] Whatever be the origin for this fractional viscosity dependence, one needs to ascertain whether this partial viscosity dependence is a characteristic feature of the relaxation dynamics in these DESs or the diffusion of R6G is inherently anomalous regardless of the solvent condition.

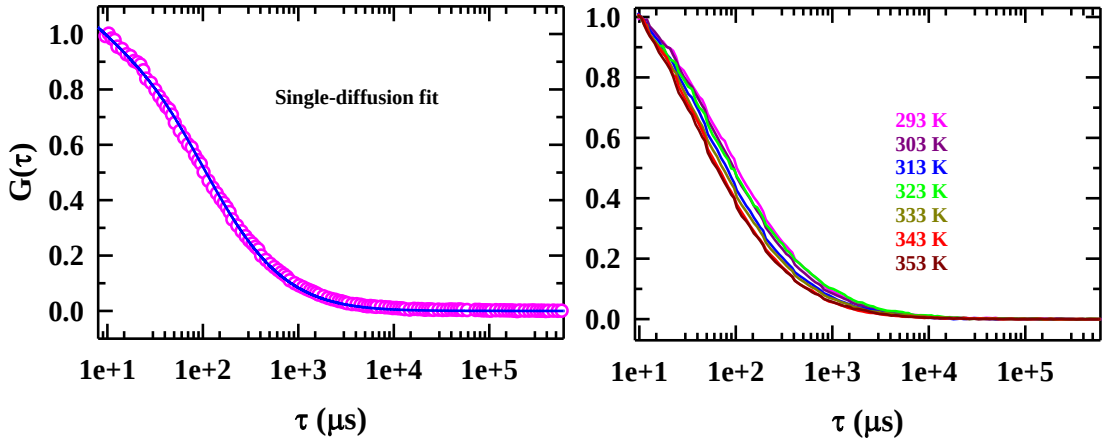

Figure 5.5 Representative normalized autocorrelation function for R6G in N, N-dimethyl formamide (DMF) at 293 K fitted with single diffusion component. Normalized autocorrelation curves for R6G in N, N-dimethyl formamide (DMF) at various temperatures showing faster decay with increasing temperature.

For a cross-examination, we investigated the temperature dependent translational motion of R6G in a normal solvent, N,N-dimethyl formamide (DMF). DMF was chosen because this is closely chemically related to acetamide and non-associative. Autocorrelation function for R6G in DMF at various temperatures is given in figure 5.5. Log-log plot of $\langle \tau_D \rangle$ vs $\eta(T)/T$ is shown in figure 5.6. A linear fit to this log-log plot yields a slope (p) ~0.82, suggesting a fractional viscosity dependence of R6G translational diffusion even in a normal low viscous neat solvent like DMF (η ~0.8 cP at 298 K).[46] However, this deviation from the Stokes-Einstein behaviour (that is, p=1) could be attributed to R6G being aspherical, positively charged, and the solvent (DMF) not being a structureless continuum. The temperature dependence in DMF therefore act as a reference for correctly realizing the break-down of the hydrodynamics for R6G diffusion in these high viscous ionic DES, and for appropriately interpreting the observation in terms of medium temporal heterogeneity. The fractional viscosity dependence of the R6G translational diffusion time, $\langle \tau_{avg} \rangle \propto (\eta(T)/T)^p$ with p ~ 0.25-0.6, can now be ascribed to the pronounced temporal heterogeneity of these ionic DESs. In addition, the p values indicate that the acetamide+$LiClO_4$ DES is relatively less temporally heterogeneous than the corresponding NO_3^-/Br^- containing DESs. Strikingly, these fractional values for the exponent p is quite similar to those obtained earlier (p~0.35 for NO_3^-/Br^- and ~0.57 for ClO_4^- containing DESs)[17,18] from the viscosity dependence of average solvation times measured via dynamic fluorescence Stokes shift experiments employing TCSPC technique with a temporal resolution of ~85 ps. The origin of such a similarity arises from the viscosity-controlled solvation response at longer

times, and the subsequent dominance of this slow diffusive timescale in determining the average solvation times.

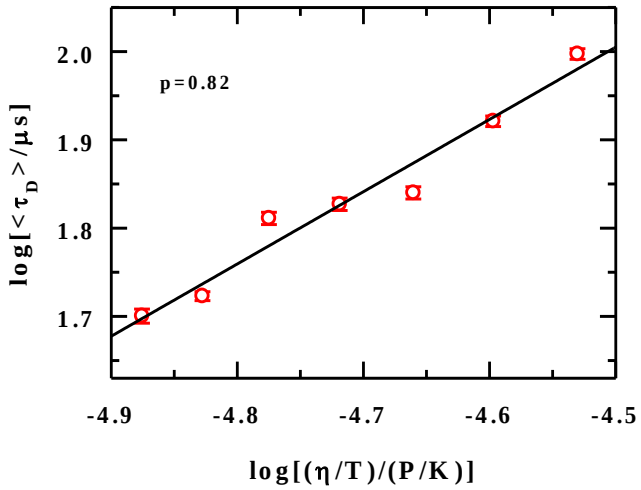

Figure 5.6 Log-log plot of R6G in N, N-dimethyl formamide (DMF) with a slope of 0.82 sets a reference point for the comparison of a normal solvent and DES. The DMF viscosities at different temperatures are given in references 46 and 47.

The observation of a strong fractional viscosity dependence of the centre-of-mass diffusion time for R6G, $\langle \tau_{avg} \rangle$, leads one to examine whether the measured diffusion times follow the Arrhenius-type temperature dependence. This is natural given that the viscosities of these ionic DESs exhibit a temperature dependence similar to those by several ionic liquids and glycerol[18] in the temperature range, $300 < T/K < 350$. These DESs therefore may reflect fragile-liquid like behaviour through the non-Arrhenius dependence of diffusion times. Figure 5.7 shows the temperature dependence of $\langle \tau_{avg} \rangle$ in these DESs, and in dimethyl formamide (DMF). The DMF data are representative for temperature dependence of R6G centre-of-mass diffusion in a non-hydrogen bonded small molecular solvent, which may act as a reference for the analysis of the DESs data. Clearly, $\langle \tau_{avg} \rangle$ in these DESs show Arrhenius-type dependence in the temperature range, $303 \leq T/K \leq 353$. Quite interestingly, the Arrhenius-type temperature dependence is also found for R6G diffusion in DMF, which is a low viscous and homogeneous solvent in this temperature regime. The Br^-composition dependent activation energy, E_a^{FCS}, ranges between ~12-21 kJmol^{-1} in these DESs, and increases with the increase in Br^- concentration in the system. For the ClO_4^-containing DES, the activation energy is ~24 kJmol^{-1}. For DMF, in contrast, E_a^{FCS} is ~9 kJmol^{-1} which is ~1.5-2.5 times less than those estimated for DESs under consideration.

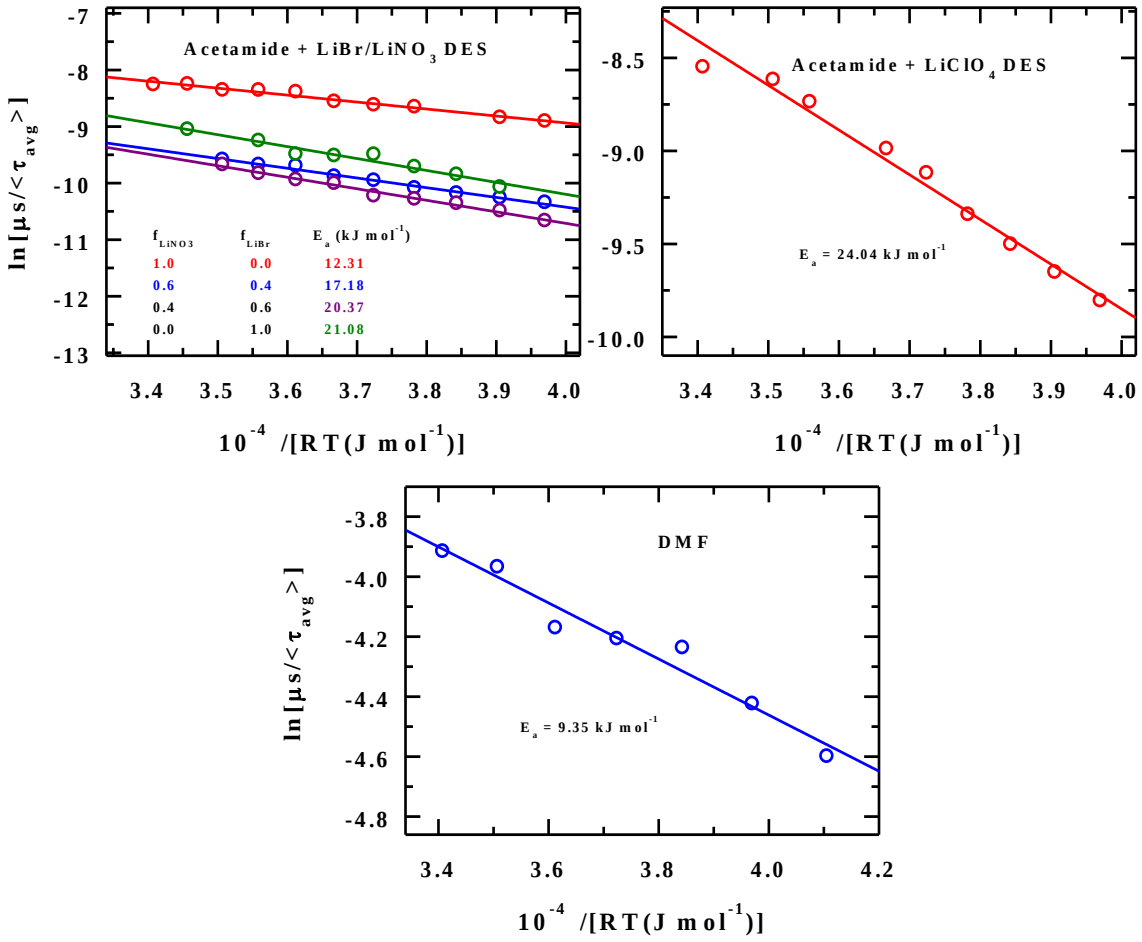

Figure 5.7 Estimation of activation energy (E_a) associated with R6G translational diffusion in [0.78CH_3CONH_2+0.22{fLiBr+(1-f)$LiNO_3$}] DES, [0.81CH_3CONH_2+0.19$LiClO_4$] DES and DMF.

The anion dependence of the E_a^{FCS} is analysed in table 5.2 where a comparison is made among activation energies estimated from the previous temperature dependent measurements of time-resolved fluorescence anisotropies and Stokes shifts (both employing C153), and temperature dependent viscosities. In addition, the values of the fraction power (p) determined from the viscosity dependence of the average solute solvation and rotation times are summarized in this table to correlate observation from different measurements. Note in this table that the viscosity activation energy (E_a^{η}) is the highest for acetamide + LiBr DES (~58 kJmol^{-1}) among the three single electrolyte containing DESs studied here, and E_a^{η} for the other two DESs are very similar (~44 kJmol^{-1}). This can be understood in terms of the viscosity ranges that these three DESs cover within the temperature window employed (see Table 5.3 a, b, c and d). However, E_a^{FCS}

is the highest for acetamide + $LiClO_4$ DES, and the lowest for acetamide + $LiNO_3$ DES. This indicates that the friction from the macroscopic viscosity does not fully control the centre-of-mass diffusion of R6G in these DESs, and the extent of coupling to the viscosity depends on the identity of the anion present in the system. This is to be contrasted to the findings for DMF where $E_a^{FCS} \approx E_a^{\eta}$, reflecting the fact that the centre-of-mass diffusion for R6G in this amide solvent is completely regulated by the medium viscosity. It is worth noting that the highest activation energy suggest the strongest coupling of the solute translation/rotation to the viscosity, and as a result, p values obtained from different measurements are the largest for acetamide + $LiClO_4$ DES among the three DESs studied here. Moreover, p values from FCS measurements are smaller than those from the time-resolved fluorescence anisotropy measurements, suggesting a stronger viscosity decoupling for solute translation than solute rotation. The latter observation, however, associates with measurements employing two different solutes and thus warrants further investigation. Difference in p values among experiments also explains the difference in activation energies estimated from different experiments and demonstrate that different measurements probe different motions.

Table 5.2 A comparison of activation energy (E_a) and fractional power (p) calculated from different experiments like FCS, time-resolved fluorescence anisotropy (DA) and solvation dynamics (SD) in acetamide + LiBr/NO_3/ClO_4 DESs and DMF.

Systems	**E_a (FCS/ R6G) kJ/mol**	**p (FCS/ R6G)**	**E_a (DA/C153) kJ/mol**	**p (DA/ C153)**	**E_a (SD/C153) kJ/mol**	**p (SD/ C153)**	**$E_a(\eta)$ kJ/mol**
Br^-	21.1	0.35	31.48	0.50	26.72	0.37	58.27
NO_3^-	12.3	0.26	30.06	0.66	23.13	0.43	44.07
ClO_4^-	24.0	0.58	35.40	0.75	30.05	0.57	44.34
DMF	9.4	0.82	-	-	-	-	8.79

Table 5.3 Temperature dependent viscosity coefficients for DESs and DMF.

(a)*Acetamide+LiBr		**(b)*Acetamide+$LiNO_3$**	
T (K)	**η (cP)**	**T (K)**	**η (cP)**
303	1311.90	**303**	210.57
313	534.025	**313**	109.25
318	360.49	**318**	82.24
333	134.53	**333**	39.35
348	64.88	**348**	21.59
363	22.13	**363**	12.73

Table 5.3 (continued) Temperature dependent viscosity coefficients for DESs and DMF.

(c)*Acetamide+$LiClO_4$	
T (K)	**η (cP)**
303	158.36
308	115.64
313	86.98
318	66.54
323	52.10
328	33.74
333	29.11
338	26.84
343	23.77
348	19.62

(d)*DMF	
T (K)	**η (cP)**
293	0.864
303	0.766
313	0.684
323	0.617
333	0.559
343	0.510
353	0.470

*These data taken from references 17(a,b), 18(c) and 46 and 47 (d).

Subsequently, we analyse in table 5.4 the dependence of the activation energy and fraction power for the R6G centre-of-mass diffusion on Br^- concentration in the acetamide + LiBr/NO_3 DESs. Data in this table clearly indicate that the activation energy, E_a^{FCS}, increases $as\ Br^-$ concentration increases in the system. Interestingly, the fraction power, p, decreases with the Br^- concentration. Similar trend for the fraction power has also been observed earlier from the dynamic anisotropy measurements employing C153 in these DESs.[17] Note here that η increases with Br^- concentration in these DESs, and this trend is reflected in the E_a^{FCS}. This increased solution viscosity then leads to stronger decoupling of the solute translation from the medium viscosity.

Table 5.4 Anion dependence of activation energy (from FCS) and fractional power (p) for R6G translational diffusion in acetamide + LiBr/NO3 DESs. Fractional power (p) from time-resolved fluorescence anisotropy of C153 is also given for comparison.

$f_{NO_3^-}$	f_{Br^-}	E_a (FCS/R6G) kJ/mol	p (FCS/R6G)	p* (DA/C153)
1	0	12.3	0.35	0.66
0.6	0.4	17.2	0.33	0.55
0.4	0.6	20.4	0.31	0.54
0	1	21.1	0.26	0.50

*Value taken from reference 17.

5.2.2 Femtosecond fluorescence up-conversion experiments: Fluorescence transients of C153 in DESs of acetamide and various electrolytes (LiBr, $LiClO_4$ and $LiNO_3$) were measured at various wavelengths from 470 nm to 590 nm by exciting at 375 nm and 390 for picosecond and femtosecond studies, respectively. Fluorescence transients from the femtosecond up-conversion were fitted with equation 2.8. The fitted parameters of fluorescence transients at various wavelengths combined with steady state emission spectra were used to reconstruct time resolved emission spectra (TRES) as described in chapter 2, which are shown in figure 5.8. The plots of the time evolution of peak frequency were obtained by merging peak frequencies obtained from femtosecond and picosecond experiments. It is thus possible to detect nearly full Stokes shift dynamics in these DESs by combining these two techniques. Following this, the solvent correlation function was constructed (using equation 2.18), which are shown in figure 5.9. Triple-exponential function was required to adequately fit the data and the fit parameters are summarized in table 5.5.

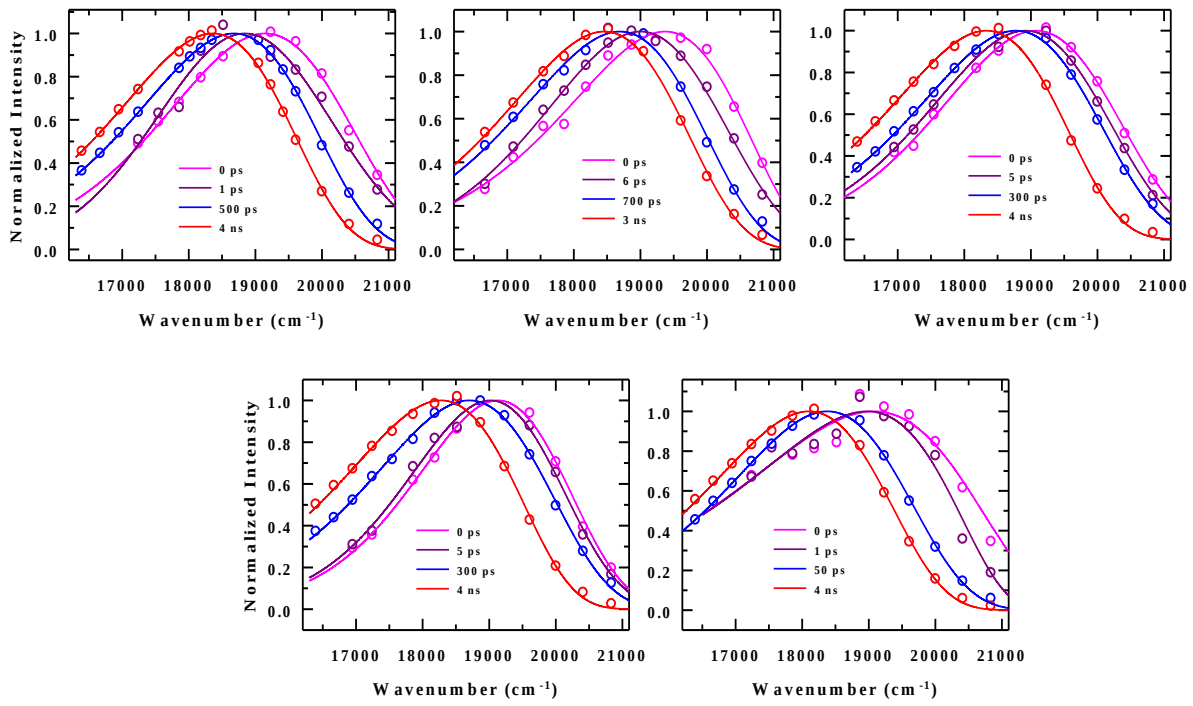

Figure 5.8 Reconstructed time resolved emission spectra (TRES) for C153 in $[0.78CH_3CONH_2+0.22\{fLiBr+(1-f)LiNO_3\}]$ DESs at f=0.0 (top left panel), 0.4 (top middle panel), 0.6 (top right panel) and 1.0 (bottom left panel) and in $[0.81H_3CONH_2+0.19LiClO_4]$ DES (bottom right panel) from fluorescence up-conversion and picosecond TCSPC experiments.

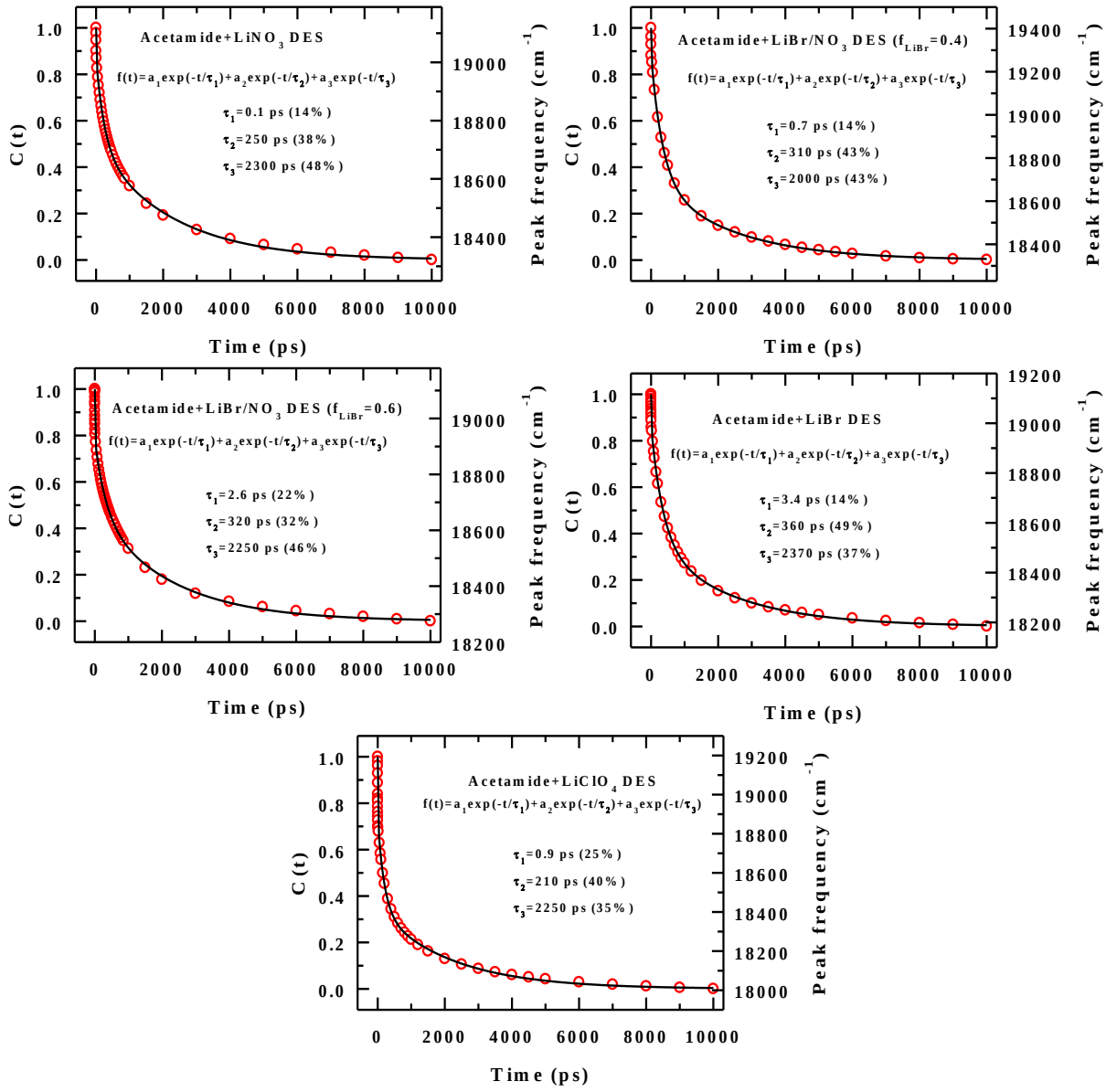

Figure 5.9 C(t) curves and corresponding peak frequency shifts obtained from the combined TCSPC and fluorescence up-conversion measurements for [0.78CH_3CONH_2+0.22{fLiBr+(1-f)$LiNO_3$}] DESs (at f=0.0, 0.4, 0.6 and 1.0) and [0.81H_3CONH_2+0.19$LiClO_4$] DES at 298 K. Tri-exponential fit was used for each C(t).

Table 5.5 Stokes shift and fitted parameter of C(t) curve obtained by merging fluorescence up-conversion and TCSPC data for [0.78CH_3CONH_2+0.22{fLiBr+(1-f)$LiNO_3$}] DESs using C153 as the probe molecule at 298 K. Last row in the table shows fitting parameters obtained for [0.81 CH_3CONH_2+0.19LiClO4] DES using C153 as the probe molecule.

DES	Stokes shift (cm^{-1})	a_1	τ_1 (ps)	a_2	τ_2 (ps)	a_3	τ_3 (ps)	$\langle\tau_S\rangle$ (ps)
$f_{NO_3^-}$ **= 1**	860	0.14	0.1	0.38	250	0.48	2300	1199
$f_{NO_3^-}$ **= 0.6**	1000	0.14	0.7	0.43	310	0.43	2000	993
$f_{NO_3^-}$ **= 0.4**	810	0.22	2.6	0.32	320	0.46	2250	1137
f_{Br^-} **= 1**	950	0.14	3.4	0.49	360	0.37	2370	1053
ClO_4^-	1100	0.25	0.9	0.40	210	0.35	2250	871

Dynamic Stokes shift magnitudes obtained from combined femtosecond fluorescence up-conversion and picosecond TCSPC measurements, as summarized in table 5.5, suggest that the shifts for C153 in these ionic DESs are rather low, and nearly half of what have been reported via complete measurements for moderate-to-strongly polar common solvents,[31] ionic liquids,[48,49] and its aqueous binary mixtures.[50,51] What is even more striking is that the shift magnitudes (~800–1100 cm^{-1}) from the present combined measurements are quite close to those from TCSPC measurements reported earlier.[17,18] This is intriguing because this close similarity suggests a substantial break-down of the inter-molecular H-bond network of liquid acetamide[21,43,52] in these molten (acetamide+LiX) systems, resulting negligible contributions to the early part of the Stokes shift dynamics. This switching off of the contributions from the collective low frequency modes derives some support from IR observations[53] of 'no spectral evidence of any residual inter-amide H-bonds' in mixtures of N-methylpropionamide and $LiClO_4$. Interestingly, femtosecond Raman-induced Kerr effect spectroscopic (fs-RIKES) measurements[54] indicated substantial weakening of the inter-acetamide H-bond dynamics, supporting the view that the collective low frequency intermolecular amide modes cannot contribute to the Stokes shift dynamics in these ionic acetamide deep eutectics, as much as found in neat liquid formamide and its derivatives.[31] Also notable here is that the present combined measurements, if considered to have detected the full dynamics in these systems, do not agree with the estimated missing percentages (~30-40%) reported earlier based on TCSPC measurements.[17,18] This is because the density difference between the current systems under

study (ρ~ 1.22 g/cc),[54] and a reference solvent, usually a liquid alkane, which in our case is cyclohexane with ρ~0.77 g/cc)[55] used for estimating the time-zero emission spectrum via the Fee-Maroncelli method.[30]

Solvation response functions shown in figure 5.9 and the corresponding tri-exponential fit parameters summarized in table 5.5 demonstrate that the shortest initial fast solvation response timescale of ~100 fs in acetamide+$LiNO_3$ DES gradually lengthens upon successive replacement of NO_3^- by Br^- and finally converts to a timescale of a few picoseconds in acetamide+LiBr DES, although the amplitude of this fast component remains within ~15–22 %. This presence of sub-picosecond component in acetamide containing DESs was expected based on observations for neat liquid amides,[31] but was totally missed in the previous measurements because of broader temporal resolution.[17,18] In fact, the detection of this fast component renders the measured solvation response functions in these ionic DESs a tri-exponential character that also features sub-nanosecond and nanosecond components of nearly equal amplitudes (~30–50 %). Interestingly, the sub-picosecond solvation response slows down and finally become a picosecond dynamics in the exclusive presence of Br^-. In acetamide+$LiClO_4$ DES also, the fast initial time constant is about a picosecond, supporting the view of a possible softening of the inter-amide H-bond network in these ionic DESs. In fact, this ion-specific disappearance of the sub-picosecond solvation response in a H-bonded system is a new observation, and warrants further study for establishing the generality of this observation. Note also that the present combined measurements not only uncover the fast initial solvation response but also place the slowest solvation component firmly in the nanosecond domain, up-scaling the earlier reported average solvation times from sub-nanosecond to nanosecond. What is even more interesting here (as was before) is that this slowest nanosecond timescale does not show much system dependence although viscosity varies by nearly an order of magnitude.[17,18] This indicates substantial decoupling of diffusive solvent motions from medium viscosity, which is proposed to have originated via non-hydrodynamic moves, such as, jumps punctuated by waiting times by recent simulation studies.[43,44]

Next we address briefly the origin of the three distinct time scales that characterize the measured solvation response functions for these DESs. Our previous theoretical analyses and model calculations[9,17] predicted that the inclusion of an underdamped collective solvent mode centered around 100 cm^{-1} (arising from intermolecular H-bonds among acetamide molecules) could lead to an ultrafast solvation response with a time scale in the subpicosecond regime. We believe that these low frequency collective modes involving the intermolecular acetamide H-

bond network generate the initial solvation response with time scale in the subpicosecond regime which, upon substantial softening through interaction with anions, lead to a slowing down to the picosecond regime. Such a proposition of anion-induced softening of intermolecular H-bond network in amide solvents should be re-examined in tera-Hertz measurements and appropriate simulations. Calculations of orientational and translational dynamic structure factors in those previous works[9,17] also suggested that the subnanosecond solvation time scales (0.2–0.4 ns in the present measurements) in these DESs originate from the nearest-neighbor ion density fluctuations and the collective orientational density fluctuations of the acetamide molecules. The nanosecond time scale (here ~2–2.5 ns), in contrast, might have arisen from the orientational solvent density fluctuations at the nearest neighbour length scales. However, these predicted origins are based on model calculations and in the absence of reliable experimental DR data over a broad frequency range. Once such DR data are made available, better understanding of contributions of ion and solvent density fluctuations at these length scales in carrying out solvation energy relaxations in these media can be generated and the origin of solvation time scales ascertained.

5.3 Conclusions

To conclude, the present work demonstrates, via FCS measurements of ionic deep eutectics and normal solvents, that these acetamide+LiX DESs are strongly temporally heterogeneous even at a temperature ~100-150 K above their respective glass transition temperatures. Pronounced fractional viscosity dependence has been found for solute translational diffusion while tracking the centre-of-mass motion through the FCS measurements. FCS data for the same solute in normal solvents have been collected to construct a reference for interpreting the corresponding data for these ionic DESs in terms of temporal heterogeneity. Combined fluorescence up-conversion and TCSPC measurements have revealed presence of ultrafast sub-picosecond solvation response which got slowed down to picosecond dynamics upon complete replacement of nitrate ion by bromide ion. Such an ion-induced slowing down of initial fast dynamics is ascribed to substantial softening of inter-amide H-bond network in these deep eutectics. Further measurements with a variety of electrolytes and protic solvents are required to generalize this new and novel observation. Computer simulations with realistic potentials capable of representing inter-molecular H-bonding may complement such experimental endeavours by revealing the microscopic details of the solution structure for understanding the relaxation dynamics in terms of ion-induced modification of the H-bond network. X-ray or neutron scattering measurements along the line of what has been done for alkylammonium

bromide + glycerol DESs[56] coupled with relevant simulations[57] as well as that for acetamide + + urea DES[58] can shed further light on the static structures of the ionic deep eutectics studied here.

References

1. Smith, E. L.; Abbott, A. P.; Ryder, K. S. Deep eutectic solvents (DESs) and their applications. *Chem. Rev*. **2014**, *114*, 11060–11082.
2. Zhang, Q.; Vigier, K. De O.; Royer, S.; Jérôme, F. Deep eutectic solvents: syntheses, properties and applications. *Chem. Soc. Rev*. **2012**, *41*, 7108–7146.
3. Hansen, B. B.; Spittle, S.; Chen, B.; Poe, D.; Zhang, Y.; Klein, J. M.; Horton, A.; Adhikari, L,; Zelovich, T.; Doherty, B. W.; Gurkan, B.; Maginn, E. J.; Ragauskas, A.; Dadmun, M.; Zawodzinski, T. A.; Baker, G. A.; Tuckerman, M. E.; Savinell, R. F.; Sangoro, J. R. Deep Eutectic Solvents: A Review of Fundamentals and Applications. *Chem. Rev*. **2021**, *121*, 1232−1285.
4. Abbott, A. P.; Capper, G.; Davies, D. L.; Rasheed, R. K.; Tambyrajah, V. Novel solvent properties of choline chloride/urea mixtures. *Chem. Commun*. **2003**, 70-71.
5. Abbott, A. P.; Boothby, D.; Capper, G.; Davies, D. L.; Rasheed, R. K. Deep Eutectic Solvents Formed between Choline Chloride and Carboxylic Acids: Versatile Alternatives to Ionic Liquids. *J. Am. Chem. Soc*. **2004**, *126*, 9142–9147.
6. Hayyan, A.; Mjalli, F. S.; AlNashef, I. M.; Al-Wahaibi, Y. M.; Al-Wahaibi, T.; Hashim, M. A. Glucose-based deep eutectic solvents: Physical properties. *J. Mol. Liq*. **2013**, *178*, 137–141.
7. Hammond, O. S.; Bowron, D. T.; Edler, K. J. Structure and Properties of "Type IV" Lanthanide Nitrate Hydrate:Urea Deep Eutectic Solvents. *ACS Sustainable Chem. Eng*. **2019**, *7*, 4932–4940.
8. Abranches, D. O.; Martins, M. A. R.; Silva, L. P.; Schaeffer, N.; Pinho, S. P.; Coutinho, J. A. P. Phenolic hydrogen bond donors in the formation of non-ionic deep eutectic solvents: the quest for type V DES. *Chem. Commun*. **2019**, *55*, 10253—10256.
9. Guchhait, B.; Gazi, H. A. R.; Kashyap, H. K.; Biswas, R. Fluorescence Spectroscopic Studies of (Acetamide+Sodium/Potassium Thiocyanates) Molten Mixtures: Composition and Temperature Dependence *J. Phys. Chem. B* **2010**, *114*, 5066-5081.
10. Gazi, H. A. R.; Guchhait, B.; Daschakraborty, S.; Biswas, R. Fluorescence dynamics in supercooled (acetamide + calcium nitrate) molten mixtures. *Chem. Phys. Lett.* **2011**, *501*, 358-3630.
11. Abbott, A. P.; Capper, G.; Davies, D. L.; Munro, H. L.; Rasheed, R. K.; Tambyrajah, V. Preparation of novel, moisture-stable, Lewis-acidic ionic liquids containing

quaternary ammonium salts with functional side chains. *Chem. Commun*. **2001**, 2010-2011.

12. Abbott, A. P.; Capper, G.; Davies, D. L.; Raymond, R. Ionic Liquids Based upon Metal Halide/Substituted Quaternary Ammonium Salt Mixtures. *Inorg. Chem*. **2004**, *43*, 3447-3452.
13. Ediger, M. D. Spatially Heterogeneous Dynamics in Supercooled Liquids. *Annu. Rev. Phys. Chem.* **2000**, *51*, 99-128.
14. Ediger, M. D.; Angell, C. A.; Nagel, S. R. Supercooled Liquids and Glasses. *J. Phys. Chem.* **1996**, *100*, 13200-13212.
15. Chang, I.; Fujara, F.; Geil, B.; Heuberger, G.; Mangel, T.; Sillescu H. Translational and rotational molecular motion in supercooled liquids studied by NMR and forced Rayleigh scattering. *J. Non-Cryst. Solids* **1994**, *172-174*, 248-255.
16. Chakrabarti, D.; Bagchi, B. Decoupling Phenomena in Supercooled Liquids: Signatures in the Energy Landscape. *Phys. Rev. Lett.* **2006**, *96*, 187801.
17. Guchhait, B.; Daschakraborty, S.; Biswas, R. Medium decoupling of dynamics at temperatures ∼100 K above glass-transition temperature: A case study with (acetamide + lithium bromide/nitrate) melts. *J. Chem. Phys.* **2012**, *136*, 174503.
18. Guchhait, B.; Das, S.; Daschakraborty, S.; Biswas, R. Interaction and dynamics of (alkylamide + electrolyte) deep eutectics: Dependence on alkyl chain-length, temperature, and anion identity. *J. Chem. Phys.* **2014**, *140*, 104514.
19. Das, A.; Das, S.; Biswas, R. Fast fluctuations in deep eutectic melts: Multi-probe fluorescence measurements and all-atom molecular dynamics simulation study. *Chem. Phys. Lett.* **2013**, *581*, 47-51.
20. Das, A.; Das, S.; Biswas, R. Density relaxation and particle motion characteristics in a non-ionic deep eutectic solvent (acetamide + urea): Time-resolved fluorescence measurements and all-atom molecular dynamics simulations. *J. Chem. Phys.* **2015**, *142*, 034505.
21. Mukherjee, K.; Das, S.; Tarif, E.; Barman, A.; Biswas, R. Dielectric relaxation in acetamide + urea deep eutectics and neat molten urea: Origin of time scales via temperature dependent measurements and computer simulations. *J. Chem. Phys.* **2018**, *149*, 124501.
22. Hossain, S. S.; Samanta, A. Solute Rotation and Translation Dynamics in an Ionic Deep Eutectic Solvent Based on Choline Chloride. *J. Phys. Chem. B* **2017**, *121*, 10556-10565.

23. Hossain, S. S.; Samanta, A. How do the hydrocarbon chain length and hydroxyl group position influence the solute dynamics in alcohol-based deep eutectic solvents? *Phys. Chem. Chem. Phys*. **2018**, *20*, 24613-24622.
24. Cui, Y.; Kuroda, D. G. Evidence of Molecular Heterogeneities in Amide-Based Deep Eutectic Solvents. *J. Phys. Chem. A* **2018**, *122*, 1185-1193.
25. van der Zwan, G.; Hynes, J. T. Chemical reaction rates and solvation dynamics in electrolyte solutions: ion atmosphere friction. *Chem. Phys.* **1991**, *152*, 169-183.
26. van der Zwan, G.; Hynes, J. T. Nonequilibrium solvation dynamics in solution reactions. *J. Chem. Phys.* **1983**, *78*, 4174.
27. Pradhan, T.; Biswas, R. Electrolyte-Concentration and Ion-Size Dependence of Excited-State Intramolecular Charge-Transfer Reaction in (Alkylamino)benzonitriles: Time-Resolved Fluorescence Emission Studies. *J. Phys. Chem. A* **2007**, *111*, 11524-11530.
28. Mukherjee, K.; Das, A.; Choudhury, S.; Barman, A.; Biswas, R. Dielectric Relaxations of (Acetamide + Electrolyte) Deep Eutectic Solvents in the Frequency Window, $0.2 \leq \nu/\mathrm{GHz} \leq 50$: Anion and Cation Dependence. *J. Phys. Chem. B* **2015**, *119*, 8063-8071.
29. Bagchi, B.; Biswas, R. Polar and Nonpolar Solvation Dynamics, Ion Diffusion, and Vibrational Relaxation: Role of Biphasic Solvent Response in Chemical Dynamics. *Adv. Chem. Phys.* **1999**, *109*, 207-433.
30. Fee, R. S.; Maroncelli, M. Estimating the time-zero spectrum in time-resolved emission measurements of solvation dynamics. *Chem. Phys*. **1994**, *183*, 235-247.
31. Horng, M. L.; Gardecki, J. A.; Papazyan, A.; Maroncelli, M. Sub picosecond Measurements of Polar Solvation Dynamics: Coumarin 153 Revisited. *J. Phys. Chem*. **1995**, *99*, 17311-17337.
32. Patra, S.; Samanta, A. Microheterogeneity of Some Imidazolium Ionic Liquids As Revealed by Fluorescence Correlation Spectroscopy and Lifetime Studies. *J. Phys. Chem. B* **2012**, *116*, 12275−12283.
33. Wu, E. C.; Kim, H. J.; Peteanu, L. A. Spectroscopic and MD Study of Dynamic and Structural Heterogeneities in Ionic Liquids. *J. Phys. Chem. B* **2017**, *121*, 1100–1107.
34. Guo, J.; Baker, G. A.; Hillesheim, P. C.; Dai, S.; Shaw, R. W.; Mahurin, S. M. Fluorescence correlation spectroscopy evidence for structural heterogeneity in ionic liquids. *Phys. Chem. Chem. Phys*. **2011**, *13*, 12395–12398.

35. Itoh, K.; Azumi, T. Shift of the emission band upon excitation at the long wavelength absorption edge. II. Importance of the solute–solvent interaction and the solvent reorientation relaxation process. *J. Chem. Phys*. **1975**, *62*, 3431.
36. Lakowicz, J. R.; Keating-Nakamoto, S. Red-Edge Excitation of Fluorescence and Dynamic Properties of Proteins and Membranes. *Biochemistry* **1984**, *23*, 3013– 3021.
37. Richert, R. Homogeneous dispersion of dielectric responses in a simple glass. *J. Non-Cryst. Solids*. **1994**. *172-174*, 209-213.
38. Sasmal, D. K.; Mandal, A. K.; Mondal, T.; Bhattacharyya, K. Diffusion of Organic Dyes in Ionic Liquid and Giant Micron Sized Ionic Liquid Mixed Micelle: Fluorescence Correlation Spectroscopy. *J. Phys. Chem. B* **2011**, *115*, 7781– 7787.
39. Adhikari, A.; Sahu, K.; Dey, S.; Ghosh, S.; Mandal, U.; Bhattacharyya, K. Femtosecond Solvation Dynamics in a Neat IL and Ionic Liquid Microemulsion: Excitation Wavelength Dependence. *J. Phys. Chem. B* **2007**, *111*, 12809– 12816.
40. Jin, H.; Li, X.; Maroncelli, M. Heterogeneous Solute Dynamics in Room Temperature Ionic Liquids. *J. Phys. Chem. B* **2007**, *111*, 13473– 13478.
41. Horng, M.-L.; Gardecki, J. A.; Maroncelli, M. Rotational Dynamics of Coumarin 153: Time-Dependent Friction, Dielectric Friction, and Other Nonhydrodynamic Effects. *J. Phys. Chem. A* **1997**, *101*, 1030– 1047.
42. Hansen, J. P.; McDonald, I. R. *Theory of Simple Liquids: with Applications to Soft Matter* 3rd edn., New York: Academic, 2013.
43. Das, S.; Biswas, R.; Mukherjee, B. Reorientational Jump Dynamics and Its Connections to Hydrogen Bond Relaxation in Molten Acetamide: An All-Atom Molecular Dynamics Simulation Study. *J. Phys. Chem. B* **2015**, *119*, 274−283.
44. Das, S.; Biswas,R.; Mukherjee, B. Orientational Jumps in (Acetamide + Electrolyte) Deep Eutectics: Anion Dependence. *J.Phys.Chem.B* **2015**, *119*, 11157−11168.
45. Dueby, S.; Dubey, V.; Daschakraborty, S. Decoupling of Translational Diffusion from the Viscosity of Supercooled Water: Role of Translational Jump Diffusion. *J. Phys. Chem. B* **2019**, *123*, 7178−7189.
46. Nikam, P. S.; Kharat, S. J. Density and Viscosity Studies of Binary Mixtures of N, N-Dimethylformamide with Toluene and Methyl Benzoate at (298.15, 303.15, 308.15, and 313.15) K. *J. Chem. Eng. Data* **2005**, *50*, 455-459.
47. Bernal-García, J. M.; Guzmán-López, A.; Cabrales-Torres, A.; Estrada-Baltazar, A.; Iglesias-Silva, G. A. Densities and Viscosities of (N,N-Dimethylformamide +

Water)at Atmospheric Pressure from (283.15 to 353.15) K. *J. Chem. Eng. Data* **2008**, *53*, 1024–1027.

48. Ito, N.; Arzhantsev, S.; Heitz, M.; Maroncelli, M. Solvation Dynamics and Rotation of Coumarin 153 in Alkylphosphonium Ionic Liquids. *J. Phys. Chem. B* **2004**, *108*, 5771-5777.
49. Ito, N.; Arzhantsev, S.; Maroncelli, M. The probe dependence of solvation dynamics and rotation in theionic liquid 1-butyl-3-methyl-imidazolium hexafluorophosphate. *Chem. Phys. Lett*. **2004**, *396*, 83–91.
50. Zhang, X.-X.; Liang, M.; Hunger, J.; Buchner, R.; Maroncelli, M. Dielectric Relaxation and Solvation Dynamics in a Prototypical Ionic Liquid + Dipolar Protic Liquid Mixture:1‑Butyl-3-MethylimidazoliumTetrafluoroborate + Water. *J. Phys. Chem. B* **2013**, *117*, 15356−15368.
51. Liang, M.; Zhang, X.-X.; Kaintz, A.; Ernsting,N. P.; Maroncelli, M. Solvation Dynamics in a Prototypical Ionic Liquid + Dipolar Aprotic Liquid Mixture: 1‑Butyl-3-methylimidazolium Tetrafluoroborate +Acetonitrile. *J. Phys. Chem. B* **2014**, *118*, 1340−1352.
52. Nasr, S.; Ghédira, M.; Cortès, R. H-bonding in liquid acetamide as studied byx-ray scattering. *J. Chem. Phys*. **1999**, *110*, 10487.
53. Diorio, A. F.; Lippincott, E.; Mandelkern, L. Complex Formation of Monomeric Amides with Lithium Perchlorate. *Nature* **1962**, *195*, 1296-1297.
54. Biswas, R.; Das, A.; Shirota, H. Low-frequency collective dynamics in deep eutectic solvents of acetamide and electrolytes: A femtosecond Raman-induced Kerr effect spectroscopic study *J. Chem. Phys*. **2014**, *141*, 134506.
55. Beg, S. A.; Tukur, N. M.; Al-Harbi, D. K., Hamad, E. Z. Saturated Liquid Densities of Benzene, Cyclohexane, and Hexane from 298.15 to 473.15 K. *J. Chem. Eng. Data* **1993**, 38, 461-464.
56. McDonald, S.; Murphy, T.; Imberti, S.; Warr, G. G.; Atkin, R. Amphiphilically Nanostructured Deep Eutectic Solvents. *J. Phys. Chem. Lett*. **2018**, *9*, 3922−3927.
57. Kaur, S.; Gupta, A.; Kashyap, H. K. Nanoscale Spatial Heterogeneity in Deep Eutectic Solvents. *J. Phys. Chem. B* **2016**, *120*, 6712−6720.
58. Subba, N.; Polok, K.; Piatkowski, P.; Ratajska-Gadomska, B.; Biswas, R.; Gadomski, W.; Sen, P. Temperature Dependent Ultrafast Solvation Response and Solute Diffusion in Acetamide–Urea DES. *J. Phys. Chem. B* **2019**, *123*, 9212-9221.

This Page Intentionally Left Blank

Chapter 6A

Rational design, preparation and characterization of a ternary non-ionic room-temperature deep eutectic solvent derived from urea, acetamide, and sorbitol

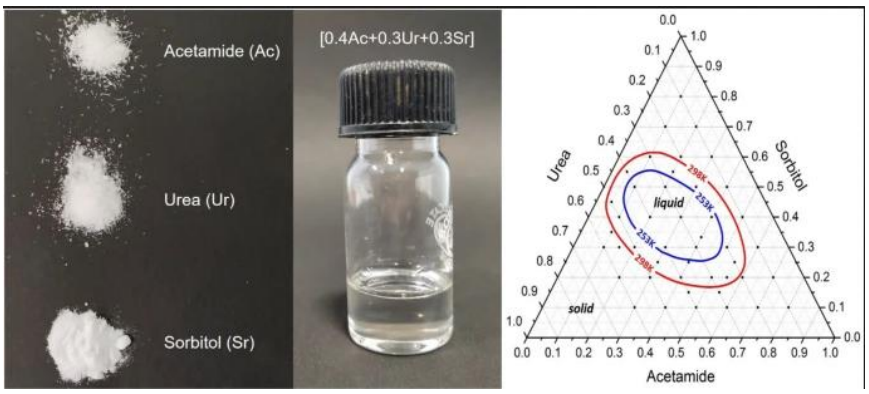

N. Subba, P. Sahu, N. Das and P. Sen. *J. Chem. Sci.* **2021**, *133*, 25.

Although DESs have emerged as an excellent alternative solvents, most of the DESs reported are ionic, and to the best of our knowledge, only a handful of non-ionic DESs are available, which are liquid at room temperature. Non-ionic DESs may be desirable in applications such as organic synthesis because many reactants might not dissolve in ionic media. Here, we rationally design and report a new ternary non-ionic DES comprising of acetamide, urea, and sorbitol, which is liquid at the room temperature. I reported temperature dependent refractive index (n_D), sound velocity (u), density (ρ), and dynamic viscosity (η) in this DES. This study shows that the third component in the DES has a strong impact on its physico-chemical properties.

6A.1 Introduction

The search for a better solvent with desired property without compromising the safety, cost, and availability is a never-ending pursuit.[1-3] Among all, deep eutectic solvents (DESs) have emerged as one of the most important alternative solvents owing their several advantages (chapter).[4-6] A large number of commercially available and natural compounds can be used to prepare DESs with desired properties.[4-8] There have been considerable interests in the development of natural deep eutectic solvents (NADESs) derived from naturally available materials.[9,10]

Most of the DESs are ionic by virtue of at least one of the constituents being ionic.[4-7] Naturally, organic solutes might be only sparingly soluble in ionic DES, and therefore, limit the use of DESs in various applications. Non-ionic DESs can overcome this issue. However, only a few non-ionic DESs are known till date[11-19], and there is a huge need to develop new ones.Among various applications and interests, understanding the behavior of proteins in DES is very important, which has gained considerable attention in recent times.[20-28] Few studies have shown that proteins are stable in some DESs (chapter 1), which otherwise is nearly impossible/difficult to stabilize in solvents other than water (or buffer).[20,23,24,26,27] However, most of these DESs are heterogeneous. Given that a protein is a very complex entity, understanding its behaviour in heterogeneous media comes with additional difficulty. To eliminate this extra complexity, we searched for homogeneous DES and found that urea/acetamide non-ionic DES is probably the only choice. However, the problem with urea/acetamide DES is that it is not liquid at room temperature. There are many other example in ref. 19 where non-ionic eutectic mixtures have high melting point. Therefore, we felt a need to develop new non-ionic and room temperature DESs. In addition to this, since hydrophobic DESs are already known, development of non-ionic hydrophilic DESs completes the spectrum of DESs in terms of polarity.

The rest of our paper describes the rational design, preparation, and characterization of a non-ionic ternary DES derived from urea, acetamide, and sorbitol. We determined the ternary phase diagram and found that the DES is liquid at room temperature at a wide range. We also measured some important physical properties, e.g., refractive index (n_D), sound velocity (v), density (ρ), and dynamic viscosity (η) of this new non-ionic DES denoted by [xAc+yUr+zSr], where x, y, and z represent the mole fractions of acetamide, urea, and sorbitol, respectively.

Rational Design of a non-ionic room temperature DES

We decided to start with urea acetamide DES as it is known to be nearly homogenous (follow Stokes-Einstein-Debye relation) and a non-ionic DES. We can lower the melting point of this further by adding an additional compound. Firstly, the compound must be non-ionic for our purpose, and secondly, it should interact strongly with the other two constituents. Note that the interspecies interaction is mainly hydrogen bonding in the case of non-ionic DES. As a result, we decided to use a non-ionic compound that has a potential to form hydrogen bond with urea and acetamide. Our first choice was sugar, and we chose sorbitol, among others. It is the open form of glucose. We envisaged that its inherent flexibility (due to open chain unsaturated nature) would enable sorbitol to form efficient hydrogen bonding compared to closed chain or unsaturated compound. Moreover, such inherent flexibility will allow interaction in all directions. In fact, MD simulation has proved that sorbitol can form more H-bond than its closed-form analog, glucose.[29]

6A.2 Results and Discussion

6A.2.1 Solid-liquid phase diagram

The exact determination of the freezing point of non-ionic DES of acetamide, urea, and sorbitol is quite tricky as they undergo glass transition at lower temperatures. This property might have been imparted from the sorbitol itself as it is known to supercool once it melts.[30] Therefore, a solid-liquid phase diagram was qualitatively determined for two temperatures (253 K and 298 K), as shown in figure 6A.1, and further experiments were carried on with the mixtures in the liquid region.

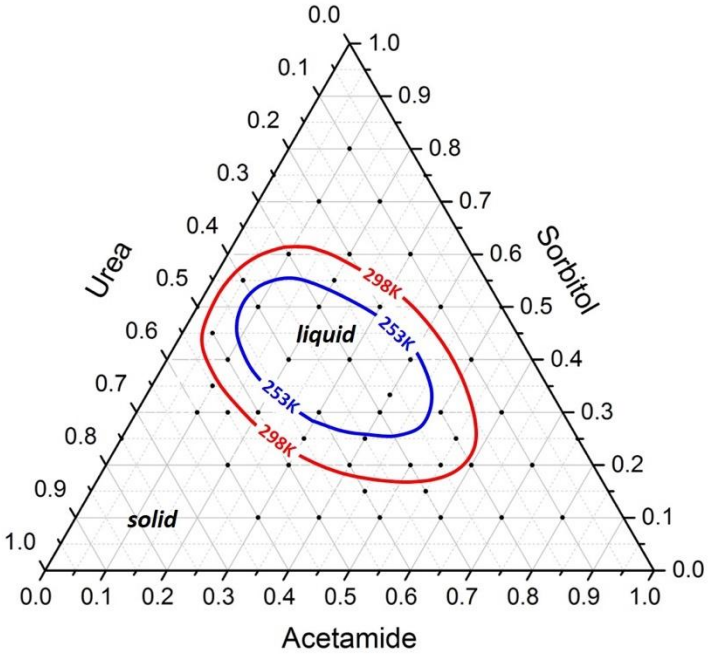

Figure 6A.1 Ternary solid-liquid phase diagram for the mixture of acetamide, urea, and sorbitol. Black dots represent the experimental points.

6A.2.2 Refractive index measurement

The refractive index is an important physical property that gives an idea about the system's electronic polarization. The extent of polarization can be realized from the electronic polarizability (α). It is related to the refractive index by Lorentz-Lorenz equation as[31-34]

$$\alpha = \left[\frac{3}{4\pi N_A}\right]\left[\frac{n^2-1}{n^2+2}\right]V_m \qquad 6.1$$

and,

$$R_m = \left[\frac{n^2-1}{n^2+2}\right]V_m \qquad 6.2$$

Here, N_A, R_m and V_m are Avogadro number, molar polarizability and molar volume, respectively. Measured refractive indices of non-ionic DES [*x*Ac+*y*Ur+*z*Sr] with various mole fractions of acetamide (*x*), urea (*y*), and sorbitol (*z*) are tabulated in table 6A.1. Refractive indices are relatively higher than many common solvents and fall in the range of 1.49–1.52. Here, like in many known solvents,[35-37] ionic liquids[38,39] and deep eutectic solvents,[31,40,41] refractive indices decrease with increasing temperature (see figure 6A.2) and shows nearly linear dependence. In the absence of sorbitol, the refractive index for acetamide/urea DES has been reported to be around 1.38–1.39.[42.] Thus, the presence of sorbitol makes a considerable difference in the refractive index. Using the above equations, molar polarizability and free

volume ($f_m = V_m - R_m$) was calculated for [0.3Ac+0.2Ur+0.5Sr] DES as shown in the appendix of this chapter.

Table 6A.1 Refractive indices (n_D) of non-ionic DES [*x*Ac+*y*Ur+*z*Sr] at different temperatures. The error was estimated for three samples and are shown in the table.

DES	Refractive indices at various temperatures (K)					
	293	**298**	**303**	**313**	**323**	**333**
0.3Ac+0.2Ur+0.5Sr	1.5098	1.5085	1.5072	1.5049	1.5024	1.4998
0.3Ac+0.3Ur+0.4Sr	1.5077	1.5066	1.5049	1.5023	1.4998	1.4975
0.3Ac+0.4Ur+0.3Sr	1.5050	1.5037	1.5024	1.4997	1.4967	1.4942
0.3Ac+0.45Ur+0.25Sr	1.5015 ±0.0003	1.5003 ±0.0003	1.4990 ±0.0003	1.4966 ±0.0003	1.4940 ±0.0003	1.4914 ±0.0003
0.4Ac+0.3Ur+0.3Sr	1.5004	1.4991	1.4975	1.4952	1.4923	1.4899
0.2Ac+0.3Ur+0.5Sr	1.5132 ±0.0004	1.5121 ±0.0004	1.5110 ±0.0004	1.5085 ±0.0004	1.5058 ±0.0004	1.5034 ±0.0004
0.1Ac+0.5Ur+0.4Sr	1.5142	1.5134	1.5118	1.5095	1.5072	1.5044
0.2Ac+0.4Ur+0.4Sr	1.5118 ±0.0004	1.5105 ±0.0004	1.5091 ±0.0004	1.5067 ±0.0004	1.5044 ±0.0004	1.5020 ±0.0004
0.4Ac+0.2Ur+0.4Sr	1.5045	1.5032	1.5017	1.4990	1.4966	1.4939

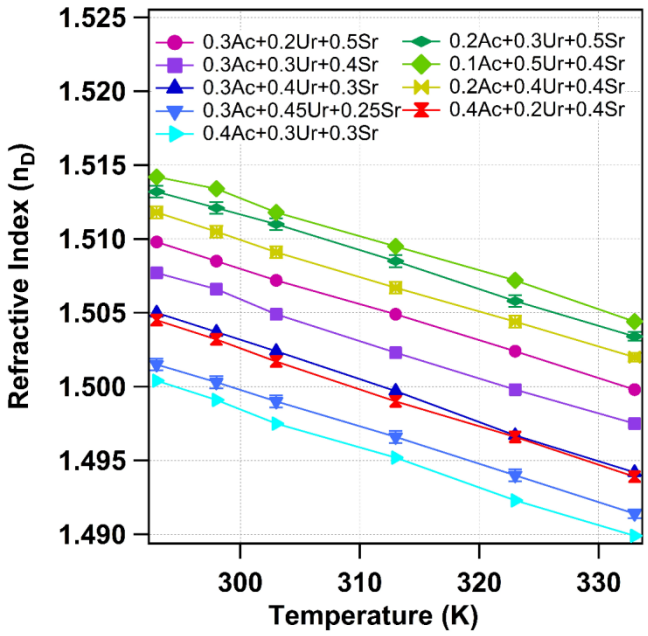

Figure 6A.2. Variation of refractive index of non-ionic DES [*x*Ac+*y*Ur+*z*Sr] as a function of temperature. Lines connecting the data points are for eye guide.

6A.2.3 Density measurement

The experimentally measured densities of non-ionic DES [*x*Ac+*y*Ur+*z*Sr] is given in table 6A.2 at different temperatures. The measured density ranges between 1.2–1.4 g mL^{-1} depending on

the composition. The density of sorbitol is the highest (1.49 g mL^{-1}) among the three components, and apparently, the density of DES is correlated with the proportion of sorbitol present. In general, the experimental densities roughly match the calculated densities $(\rho = x\rho_{Ac} + y\rho_{Ur} + z\rho_{Sr})$ at room temperature. The plot of density as a function of temperature for various DESs under investigation are shown in figure 6A.3. As expected, the densities of all the DESs decrease with increasing temperature due to thermal expansion. Temperature dependence of density can be well fitted linearly (ρ = a + bT) in the measured temperature range. Fitting parameters are listed in table 6A.3. It is important to note that choline chloride and sugar (glucose and fructose) based ionic DES also show such a linear dependence of temperature on density.[41,43] On the other hand, for DESs based on choline chloride and urea/ethylene glycol/glycerol, the density shows a quadratic dependence on the temperature.[44-46]

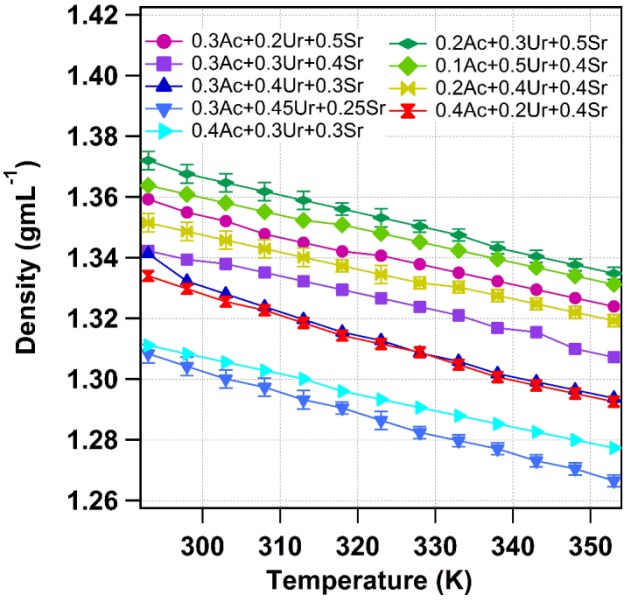

Figure 6A.3 Temperature dependence of density of non-ionic [*x*Ac+*y*Ur+*z*Sr] DES. Lines connecting the data points are for eye guide.

Table 6A.2 Density (ρ) of non-ionic [xAc+yUr+zSr] DES at various temperatures.

DES	**Density (in g mL^{-1}) at different temperatures (K)**												
	293	**298**	**303**	**308**	**313**	**318**	**323**	**328**	**333**	**338**	**343**	**348**	**353**
0.3Ac+0.2Ur+0.5Sr	1.359	1.355	1.352	1.347	1.344	1.342	1.340	1.337	1.335	1.332	1.329	1.326	1.323
0.3Ac+0.3Ur+0.4Sr	1.342	1.339	1.338	1.335	1.332	1.329	1.326	1.323	1.321	1.316	1.315	1.309	1.307
0.3Ac+0.4Ur+0.3Sr	1.341	1.332	1.328	1.323	1.319	1.315	1.312	1.308	1.305	1.301	1.299	1.296	1.293
0.3Ac+0.45Ur+0.25Sr	1.308 ±0.003	1.304 ±0.003	1.300 ±0.003	1.297 ±0.003	1.293 ±0.003	1.290 ±0.003	1.286 ±0.003	1.282 ±0.003	1.279 ±0.003	1.277 ±0.003	1.273 ±0.003	1.270 ±0.003	1.266 ±0.003
0.4Ac+0.3Ur+0.3Sr	1.311	1.308	1.305	1.302	1.300	1.296	1.293	1.290	1.287	1.285	1.282	1.279	1.277
0.2Ac+0.3Ur+0.5Sr	1.372 ±0.003	1.368 ±0.003	1.364 ±0.003	1.361 ±0.003	1.358 ±0.003	1.356 ±0.003	1.353 ±0.003	1.350 ±0.003	1.347 ±0.003	1.343 ±0.003	1.340 ±0.003	1.337 ±0.003	1.334 ±0.003
0.1Ac+0.5Ur+0.4Sr	1.364	1.361	1.358	1.355	1.352	1.350	1.348	1.345	1.342	1.339	1.336	1.333	1.331
0.2Ac+0.4Ur+0.4Sr	1.352 ±0.003	1.349 ±0.003	1.345 ±0.003	1.342 ±0.003	1.340 ±0.003	1.337 ±0.003	1.334 ±0.003	1.331 ±0.003	1.330 ±0.003	1.327 ±0.003	1.324 ±0.003	1.322 ±0.003	1.319 ±0.003
0.4Ac+0.2Ur+0.4Sr	1.334	1.330	1.325	1.322	1.318	1.314	1.311	1.308	1.304	1.300	1.297	1.295	1.292

Table 6A.3 Linear fit parameter of density as function of temperature of [xAc+yUr+zSr] DES.

Fit equation: y=a+bx		
DES	a	b
0.3Ac+0.2Ur+0.5Sr	1.52297	-0.00056
0.3Ac+0.3Ur+0.4Sr	1.51412	-0.00058
0.3Ac+0.4Ur+0.3Sr	1.55541	-0.00075
0.3Ac+0.45Ur+0.25Sr	1.50841	-0.00069
0.4Ac+0.3Ur+0.3Sr	1.47812	-0.00057
0.2Ac+0.3Ur+0.5Sr	1.54988	-0.00061
0.1Ac+0.5Ur+0.4Sr	1.52067	-0.00054
0.2Ac+0.4Ur+0.4Sr	1.50629	-0.00053
0.4Ac+0.2Ur+0.4Sr	1.53579	-0.00069

6A.2.4 Sound velocity measurement

Sound velocity is another important thermophysical property of a material.[47] Such measurement is argued as the only direct way to calculate the isentropic compressibility.[48] However, the acoustic study of DESs is rare in the literature.[49-54] The measured sound velocities in the DESs under consideration at different temperatures are tabulated in table 6A.4, which ranges between 1790–2060 ms^{-1}. The value is comparable to common DESs like reline, ethaline, and glycerine.[49,52] Plot of sound velocity as a function of temperature is shown in figure 6A.4. In general, except water,[52,55] sound velocity decreases with increasing temperature. In the present case also, the sound velocity is found to decrease linearly with increasing temperature. The velocity of the sound (u) is related to the density (ρ) and adiabatic or isentropic compressibility (β_s) by Newton-Laplace equation as[56,57]

$$u = \sqrt{\frac{1}{\rho\beta_s}} \qquad 6.3$$

The isentropic compressibility of the DESs under investigation was calculated to be 0.17–0.24 G Pa^{-1} depending on the temperature and composition (see table 6A.5). The isentropic compressibility of present DESs is more than some of the conventional solvents and ionic liquids (see ref. 48, for example) but comparable or less than that of some of the known DESs.[51,52]

Table 6A.4 Sound velocity (u) in non-ionic DES [xAc+yUr+zSr] at different temperatures.

DES	Sound velocity (in m/s) at various temperatures (K)						
	323	**328**	**333**	**338**	**343**	**348**	**353**
0.3Ac+0.2Ur+0.5Sr	-	-	1982	1970	1961	1950	1942
0.3Ac+0.3Ur+0.4Sr	1939	1927	1913	1896	1881	1869	1859
0.3Ac+0.4Ur+0.3Sr	1898	1888	1877	1867	1854	1845	1837
0.3Ac+0.45Ur+0.25Sr	1899 ±6	1887 ±7	1876 ±5	1860 ±5	1844 ±6	1830 ±5	1817 ±4
0.4Ac+0.3Ur+0.3Sr	1861	1848	1837	1825	1814	1801	1791
0.1Ac+0.5Ur+0.4Sr	-	-	2065	2045	2024	2006	1990
0.2Ac+0.4Ur+0.4Sr	-	-	1952 ±5	1942 ±6	1932 ±6	1920 ±5	1907 ±4
0.4Ac+0.2Ur+0.4Sr	1917	1902	1883	1866	1848	1836	1824

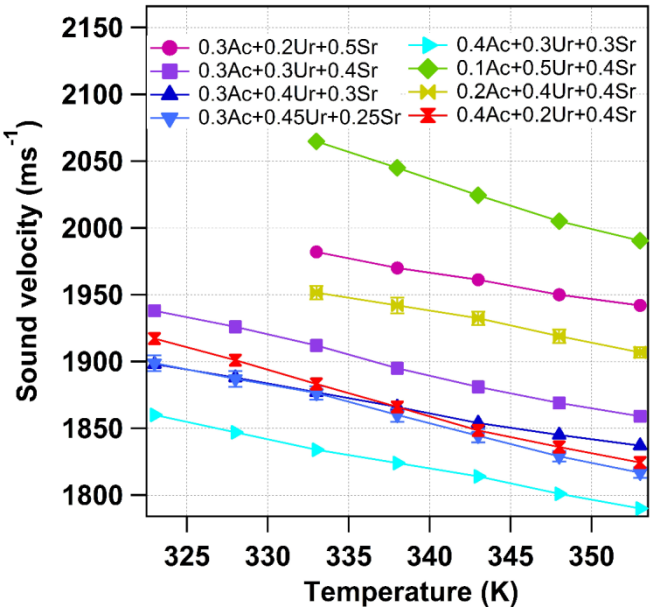

Figure 6A.4 Variation of sound velocity in non-ionic DES [xAc+yUr+zSr] as a function of temperature. Lines connecting the data points are for eye guide.

Table 6A.5 Adiabatic or isentropic compressibility (β_S) in per GPa of [xAc+yUr+zSr] DESs at various temperatures calculated from Newton-Laplace equation.

	Adiabatic compressibility (per GPa) at various temperatures (K)			
DES	323	333	343	353
0.3Ac+0.2Ur+0.5Sr	-	0.191	0.196	0.200
0.3Ac+0.3Ur+0.4Sr	0.201	0.207	0.215	0.221
0.3Ac+0.4Ur+0.3Sr	0.211	0.217	0.224	0.229
0.3Ac+0.45Ur+0.25Sr	0.216	0.222	0.231	0.239
0.4Ac+0.3Ur+0.3Sr	0.223	0.230	0.237	0.244
0.1Ac+0.5Ur+0.4Sr	-	0.175	0.183	0.189
0.2Ac+0.4Ur+0.4Sr	-	0.197	0.202	0.208
0.4Ac+0.2Ur+0.4Sr	0.207	0.216	0.226	0.232

6A.2.5 Dynamic viscosity measurement

Viscosity is another essential physical property of a solvent and controls the transport property. The measured viscosities of present DESs are tabulated in table 6A.6 and depicted in figure 6A.5 for various temperatures. In general, the viscosity is very large at lower temperatures and could not be measured with the available capillary. The value of viscosity in the absence of sorbitol is considerably low (<15 cP)[12] and as mentioned earlier, sorbitol vitrifies after melting and forms glassy or super-cooled liquid having a very high viscosity. Therefore, the high value of viscosity of the DESs under consideration is probably due to the presence of sorbitol. Viscosity of [0.3Ac+0.45Ur+0.25Sr] DES is least among the others while viscosity of [0.2Ac+0.3Ur+0.5Sr] DES is the largest. With increasing temperature, the viscosity of all the DESs decreases. Temperature dependence of viscosity can be adequately described by the Arrhenius equation to estimate the activation energy of viscous flow as[58,59]

$$\ln \eta = \ln \eta_\infty + \frac{E_a}{RT} \qquad 6.4$$

where E_a is the activation energy required for the viscous flow and η_∞ is a constant. All the DESs data fit well with the above equation, as shown in figure 6A.6, and the fitting parameters are tabulated in table 6A.7. The activation energy required for the viscous flow is 61–73 kJ mol^{-1}, which is relatively higher than for many other DESs and ionic liquids reported[60] in the literature. This is probably due to the extensive hydrogen-bonding network in this DES due to the presence of sorbitol with six –OH groups.

Hydrogen bonding interaction is probably the most vital parameter to decipher DES's properties. Recently there are some experimental and computational studies to relate DES's

property to the role of hydrogen bond accepting and donating features of the constituent molecules.[61-63] In the present case, where the DES is non-ionic, the role of hydrogen bonding should become paramount. However, here such a correlation is much difficult compared to the traditional DESs because of the constituents' dual character (both HBA and HBD). All three constituents of the present DES (i.e. acetamide, urea, and sorbitol) might act both as HBA and HBD. Stronger interaction between Ac/Ur/Sor ternary DES components compared to the acetamide/urea binary DES can be predicted from higher viscosity and density.[71-72] Thus, one might expect the possibility of an extended hydrogen-bonding network in the presence of the third component. However, the addition of sorbitol to already known acetamide/urea DES or the addition of acetamide to already known urea/sorbitol DES decreases the freezing point and is against to such a prediction.[25] Perhaps, it is not straightforward to draw a conclusion at this level, and most probably, the properties of the DES is a cumulative result of many factors. The lattice energy of the constituents, modified hydrogen bonding network, geometric constraints, hydrophobic effect, and Van der Waals interactions are to name a few. It is almost impossible to comment further about the role of individual HBA and HBDs as of now. Understanding the role of individual components and bisecting the interactions responsible for DES behavior requires further studies. 2D-IR spectroscopy, neutron scattering, and computational studies will be helpful in deciphering such understanding.

Table 6A.6 Viscosity (η) of non-ionic [*x*Ac+*y*Ur+*z*Sr] DES at various temperatures.

DES	Viscosity (in cP) at different temperatures (K)									
	323	**328**	**333**	**338**	**343**	**348**	**353**	**358**	**363**	**368**
0.3Ac+0.2Ur+0.5Sr	-	-	-	-	-	455	309	215	155	116
0.3Ac+0.3Ur+0.4Sr	-	-	-	416	280	194	138	103	78	60
0.3Ac+0.4Ur+0.3Sr	-	544	347	232	160	116	84	63	49	-
0.3Ac+0.45Ur+0.25Sr	492 ±10	314 ±8	210 ±8	145 ±6	104 ±6	77 ±4	58 ±3	45 ±3	35 ±2	28 ±2
0.4Ac+0.3Ur+0.3Sr	574	373	246	167	120	86	64	-	-	-
0.2Ac+0.3Ur+0.5Sr	-	-	-	-	-	501	340	237	170	126
0.1Ac+0.5Ur+0.4Sr	-	-	-	-	449	303	210	150	112	84
0.2Ac+0.4Ur+0.4Sr	-	-	-	465 ±9	311 ±9	214 ±7	151 ±7	111 ±5	84 ±4	64 ±3
0.4Ac+0.2Ur+0.4Sr	-	-	-	408	274	189	135	101	75	57

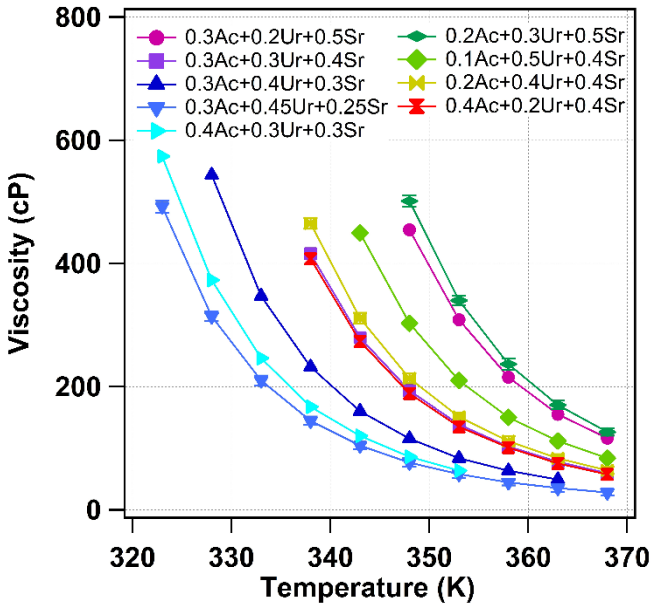

Figure 6A.5 Plot of viscosity of non-ionic [*x*Ac+*y*Ur+*z*Sr] DES as function of temperature.

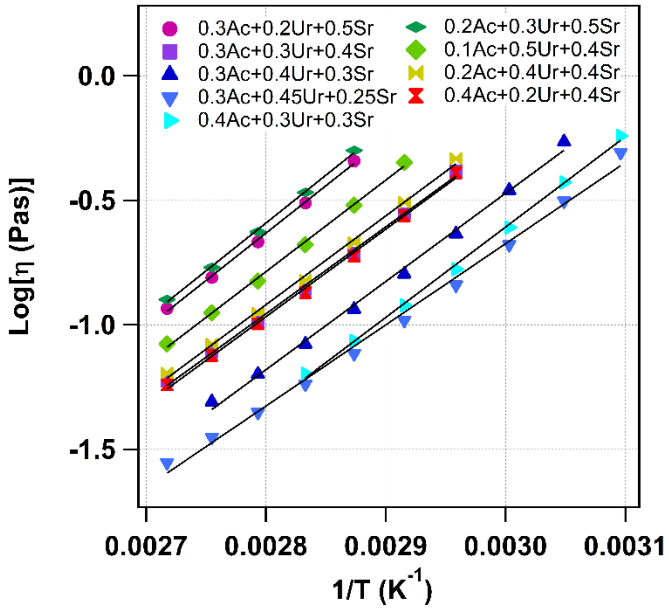

Figure 6A.6 Arrhenius fit of viscosity as function of temperature.

Table 6A.7 Fit parameters for viscosity as a function of temperature of [xAc+yUr+zSr] DES using Arrhenius equation.

DES	Log[η_0]	Ea [J/mol]	Ea [kJ/mol]
0.3Ac+0.2Ur+0.5Sr	-11.2837	72842.3	72.8423
0.3Ac+0.3Ur+0.4Sr	-10.7205	66776.5	66.7765
0.3Ac+0.4Ur+0.3Sr	-11.0994	67830.9	67.8309
0.3Ac+0.45Ur+0.25Sr	-10.4553	62428.7	62.4287
0.4Ac+0.3Ur+0.3Sr	-11.4943	69485.7	69.4857
0.2Ac+0.3Ur+0.5Sr	-11.3414	73514.1	73.5141
0.1Ac+0.5Ur+0.4Sr	-11.0786	70381.2	70.3812
0.2Ac+0.4Ur+0.4Sr	-10.9093	68314.9	68.3149
0.4Ac+0.2Ur+0.4Sr	-10.8003	67240.9	67.2409

6A.3 Conclusion

In conclusion, we prepared a new non-ionic DESs based on acetamide, urea, and sorbitol. Sorbitol, acting as a hydrogen bond donor, is found to facilitate the interspecies hydrogen bond interaction. We measured a few important physical properties like refractive index (n_D), sound velocity (u), density (ρ), and dynamic viscosity (η) at a wide temperature range. We have also calculated molar refraction and free volume from the refractive index for DESs under investigation. In addition to this, adiabatic compressibility was also calculated using sound velocity and density data.

At this point, it is very difficult to predict why a particular composition shows a higher/ lower value of a physical parameter. This is a complex interplay between various forces responsible for the formation of DES. A comparison with its binary analogue (i.e., urea/acetamide or acetamide/sorbitol) or its aqueous mixtures may give more insight into this. Overall, our report expands the knowledge in the hunt for new non-ionic DES and probably offers a rational approach in this search.

References

1. Kerton, F.; Marriott, R. Alternative Solvents for Green Chemistry: Royal Society of Chemistry (RSC), Green Chemistry Series, 2nd Ed., 2013.
2. Clark, J. H.; Tavener, S. J. Alternative Solvents: Shades of Green. *Org. Process Res. Dev*. **2007**, *11*, 149-155.
3. Sheldon, R. A. Green solvents for sustainable organic synthesis: state of the art. *Green Chem*. **2005**, *7*, 267-278.
4. Smith, E. L.; Abbott, A. P.; Ryder, K. S. Deep eutectic solvents (DESs) and their applications. *Chem. Rev*. **2014**, *114*, 11060–11082.
5. Zhang, Q.; Vigier, K. De O.; Royer, S.; Jérôme, F. Deep eutectic solvents: syntheses, properties and applications. *Chem. Soc. Rev*. **2012**, *41*, 7108–7146.
6. Hansen, B. B.; Spittle, S.; Chen, B.; Poe, D.; Zhang, Y.; Klein, J. M.; Horton, A.; Adhikari, L,; Zelovich, T.; Doherty, B. W.; Gurkan, B.; Maginn, E. J.; Ragauskas, A.; Dadmun, M.; Zawodzinski, T. A.; Baker, G. A.; Tuckerman, M. E.; Savinell, R. F.; Sangoro, J. R. Deep Eutectic Solvents: A Review of Fundamentals and Applications. *Chem. Rev*. **2021**, *121*, 1232−1285.
7. Ruß, C.; König, B. Low melting mixtures in organic synthesis – an alternative to ionic liquids? *Green Chem*. **2012**, *14*, 2969-2982.
8. Abbott, A. P. Application of Hole Theory to the Viscosity of Ionic and Molecular Liquids. *ChemPhysChem* **2004**, *5*, 1242-1246.
9. Santana, A. P. R.; Mora-Vargas, J. A.; Guimarães, T. G. S.; Amaral, C. D. B.; Oliveira, A.; Gonzalez, M. H. Sustainable synthesis of natural deep eutectic solvents (NADES) by different methods. *J. Mol. Liq*. **2019**, *293*, 111452.
10. Liu, Y.; Friesen, J. B.; McAlpine, J. B.; Lankin, D. C.; Chen, S.-N.; Pauli, G. F. Natural Deep Eutectic Solvents: Properties, Applications, and Perspectives. *J. Nat. Prod*. **2018**, *81*, 679-690.
11. Cui. Y.; Rushing, J. C.; Seifert, S.; Bedford, N. M.; Kuroda, D. G. Molecularly Heterogeneous Structure of a Nonionic Deep Eutectic Solvent Composed of N-Methylacetamide and Lauric Acid. *J. Phys. Chem. B* **2019**, *123*, 3984-3993.
12. Das, A.; Das, S.; Biswas, R. Density relaxation and particle motion characteristics in a non-ionic deep eutectic solvent (acetamide + urea): Time-resolved fluorescence measurements and all-atom molecular dynamics simulations. *J. Chem. Phys*. **2015**, *142*, 034505.

13. Ribeiro, B. D.; Florindo, C.; Iff, L. C.; Coelho, M. A. Z.; Marrucho, I. M. 2015 Menthol-based Eutectic Mixtures: Hydrophobic Low Viscosity Solvents. *ACS Sustainable Chem. Eng*. **3** 2469−2477.
14. Martins, M. A. R.; Crespo, E. A.; Pontes, P. V. A.; Silva, L. P.; Bülow, M.; Maximo, G. J.; Batista, E. A. C.; Held, C.; Pinho, S. P.; Coutinho, J. A. P. Tunable Hydrophobic Eutectic Solvents Based on Terpenes and Monocarboxylic Acids. *ACS Sustainable Chem. Eng*. **2018**, *6*, 8836−8846.
15. Tarif, E.; Mondal, J.; Biswas, R. Interaction and Dynamics in a Fully Biodegradable Glucose-Containing Naturally Abundant Deep Eutectic Solvent: Temperature-Dependent Time-Resolved Fluorescence Measurements. *J. Phys. Chem. B* **2019**, *123*, 9378-9387.
16. Mukherjee, K.; Tarif, E.; Barman, A.; Biswas, R. Dynamics of a PEG based non-ionic deep eutectic solvent: Temperature dependence. *Fluid Phase Equilib*. **2017**, *448*, 22-29.
17. Olivares, B.;, Martínez, F.;, Rivas, L.; Calderón, C.; Munita, J. M.; Campodonico, P. R. A Natural Deep Eutectic Solvent Formulated to Stabilize β-Lactam Antibiotics. *Sci. Rep*. **2018**, *8*, 14900.
18. Zeng, C.-X.; Qi, S.-J.; Xin, R.-P.; Yang, B.; Wang, Y.-H. Synergistic behavior of betaine–urea mixture: Formation of deep eutectic solvent. *J. Mol. Liq*. **2016**, *219*, 74-78.
19. Ilgen, F.; Ott, D.; Kralisch, D.; Reil, C.; Palmberger, A.; König, B. Conversion of carbohydrates into 5-hydroxymethylfurfural in highly concentrated low melting mixtures. *Green Chem*. **2009**, *11*, 1948-1954.
20. Sanchez-Fernandez, A.; Edler, K. J.; Arnold, T.; Venero, D. A.; Jackson, A. J. Protein conformation in pure and hydrated deep eutectic solvents. *Phys. Chem. Chem. Phys*. **2017**, *19*, 8667-8670.
21. Fu, J.-J.; Sun C.; Xu, X.-B.; Zhou, D.-Y.; Song, L.; Zhu, B.-W. Improving the functional properties of bovine serum albumin-glucose conjugates in natural deep eutectic solvents. *Food Chem*. **2020**, *328*, 127122.
22. Mamashli, F.; Badraghi, J.; Delavari, B.; Lanjanian, H.; Sabbaghian, M.; Hosseini, M.; Saboury, A. A. Improvement of versatile peroxidase activity and stability by a cholinium-based ionic liquid. *J. Mol. Liq*. **2018**, *272*, 597-608.

23. Yadav, N.; Bhakuni, K.; Bisht, M.; Bahadur, I.; Venkatesu, P. Expanding the Potential Role of Deep Eutectic Solvents toward Facilitating the Structural and Thermal Stability of α-Chymotrypsin. *ACS Sustainable Chem. Eng*. **2020**, *8*, 10151–10160.
24. Kist, J. A.; Henzl, M. T ; Bañuelos, J. L.; Baker, G. A. Calorimetric Evaluation of the Operational Thermal Stability of Ribonuclease A in Hydrated Deep Eutectic Solvents. *ACS Sustainable Chem. Eng*. **2019**, *7*, 12682-12687.
25. Milano, F.; Giotta, L.; Guascito, M. R.; Agostiano, A.; Sblendorio, S.; Valli, L.; Perna, F. M.; Cicco, L.; Trotta, M.; Capriati, V. Functional Enzymes in Nonaqueous Environment: The Case of Photosynthetic Reaction Centers in Deep Eutectic Solvents. *ACS Sustainable Chem. Eng*. **2017**, *5*, 7768-7776.
26. Monhemi, H.; Housaindokht, M. R.; Moosavi-Movahedi, A. A.; Bozorgmehr, M. R. How a protein can remain stable in a solvent with high content of urea: insights from molecular dynamics simulation of Candida antarctica lipase B in urea : choline chloride deep eutectic solvent. *Phys. Chem. Chem. Phys*. **2014**, *16*, 14882-14893.
27. Harifi-Mood, A. R.; Ghobadi, R.; Divsalar, A. The effect of deep eutectic solvents on catalytic function and structure of bovine liver catalase. *Int. J. Biol. Macromol*. **2017**, *95*, 115-120.
28. Pal, S.; Roy, R.; Paul, S. Potential of a Natural Deep Eutectic Solvent, Glyceline, in the Thermal Stability of the Trp-Cage Mini-protein. *J. Phys. Chem. B* **2020**, *124*, 7958-7610.
29. Lerbret, A.; Mason, P. E.; Venable, R. M.; Cesaro, A.; Saboungi, M. L.; Pastor, R. W.; Brady, J. W. Molecular dynamics studies of the conformation of sorbitol. *Carbohydr. Res*. **2009**, *344*, 2229-2235.
30. Barkatt, A. Angell, C. A. Optical probe studies of relaxation processes in viscous liquids. *J. Chem. Phys*. **1979**, *70*, 901-911.
31. Florindo, C.; Oliveira, F. S.; Rebelo, L. P. N.; Fernandes, A. M.; Marrucho, I. M. Insights into the Synthesis and Properties of Deep Eutectic Solvents Based on Cholinium Chloride and Carboxylic Acids. *ACS Sustainable Chem. Eng*. **2014**, *2*, 2416-2425.
32. Iwadate, Y.; Kawamura, K.; Igarashi, K.; Mochinaga, J. Effective ionic radii of nitrite and thiocyanate estimated in terms of the Böettcher equation and the Lorentz-Lorenz equation. *J. Phys. Chem*. **1982**, *86*, 5205-5208.
33. Deetlefs, M.; Seddon, K. R.; Shara, M. Predicting physical properties of ionic liquids. *Phys. Chem. Chem. Phys*. **2006**, *8*, 642-649.

34. Iglesias-Otero, M. A.; Troncoso, J.; Carballo, E.; Romaní, L. Density and refractive index in mixtures of ionic liquids and organic solvents: Correlations and predictions. *J. Chem. Thermodyn*. **2008**, *40*, 949-956.
35. Reisler, E.; Eisenberg, H.; Minton, A. P. Temperature and density dependence of the refractive index of pure liquids. *J. Chem. Soc., Faraday Trans. 2* **1972**, *68*, 1001-1015.
36. Valkai, S.; Liszi, J.; Szalai, I; Temperature dependence of the refractive index for three chloromethane liquids at 514.5 nm and 632.8 nm wavelengths. *J. Chem. Thermodyn*. **1998**, *30*, 825-832.
37. Ottani, S.; Vitalini, D.; Comelli, F.; Castellari, C. Densities, Viscosities, and Refractive Indices of Poly(ethylene glycol) 200 and 400 + Cyclic Ethers at 303.15 K. *J. Chem. Eng. Data* **2002**, *47*, 1197-1204.
38. Tariq, M.; Forte, P. A. S.; Gomes, M. F. C.; Lopes, J. N. C.; Rebelo, L. P. N. Densities and refractive indices of imidazolium- and phosphonium-based ionic liquids: Effect of temperature, alkyl chain length, and anion *J. Chem. Thermodynamics* **2009**, *41*, 790-798.
39. Seki, S.; Tsuzuki, S.; Hayamizu, K.; Umebayashi, Y.; Serizawa, N.; Takei, K.; Miyashiro, H. Comprehensive Refractive Index Property for Room-Temperature Ionic Liquids. *J. Chem. Eng. Data* **2012**, *57*, 2211-2216.
40. Siongco, K. R.; Leron, R. B.; Li, M.-H. Densities, refractive indices, and viscosities of N,N-diethylethanol ammonium chloride–glycerol or –ethylene glycol deep eutectic solvents and their aqueous solutions. *J. Chem. Thermodyn.* **2013**, *65*, 65-72.
41. Hayyan, A.; Mjalli, F. S.; AlNashef, I. M.; Al-Wahaibi, T.; Al-Wahaibi, Y. M.; Hashim, M. A. Fruit sugar-based deep eutectic solvents and their physical properties. *Thermochim. Acta* **2012**, *541*, 70-75.
42. Mukherjee, K.; Das, S.; Tarif, E.; Barman, A.; Biswas, R. Dielectric relaxation in acetamide + urea deep eutectics and neat molten urea: Origin of time scales via temperature dependent measurements and computer simulations. *J. Chem. Phys*. **2018**, *149*, 124501.
43. Hayyan, A.; Mjalli, F. S.; AlNashef, I. M.; Al-Wahaibi, Y. M.; Al-Wahaibi, T.; Hashim, M. A. Glucose-based deep eutectic solvents: Physical properties. *J. Mol. Liq*. **2013**, *178*, 137-141.
44. Yadav, A.; Pandey, S. Densities and Viscosities of (Choline Chloride + Urea) Deep Eutectic Solvent and Its Aqueous Mixtures in the Temperature Range 293.15 K to 363.15 K. *J. Chem. Eng. Data* **2014**, *59*, 2221-2229.

45. Yadav, A.; Trivedi, S.; Rai, R.; Pandey, S. Densities and dynamic viscosities of (choline chloride + glycerol) deep eutectic solvent and its aqueous mixtures in the temperature range (283.15–363.15) K. *Fluid Phase Equilib*. **2014**, *367*, 135-142.
46. Harifi-Mood, A. R.; Buchner, R. Density, viscosity, and conductivity of choline chloride + ethylene glycol as a deep eutectic solvent and its binary mixtures with dimethyl sulfoxide. *J. Mol. Liq*. **2017**, *225*, 689-695.
47. Queimada, A. J.; Coutinho, J. A. P.; Marrucho, I. M.; Daridon, J. L. Corresponding-States Modeling of the Speed of Sound of Long-Chain Hydrocarbons. *Int. J. Thermophys*. **2006**, *27*, 1095-1109.
48. Dzida, M.; Zorębski, E.; Zorębski, M.; Żarska, M.; Geppert-Rybczyńska, M.; Chorążewski, M.; Jacquemin, J.; Cibulka, I. Speed of Sound and Ultrasound Absorption in Ionic Liquids. *Chem. Rev*. **2017**, *117*, 3883-3929.
49. Mjalli, F. S.; Jabbar, N. M. A. Acoustic investigation of choline chloride based ionic liquids analogs. *Fluid Phase Equilib*. **2014**, *381*, 71-76.
50. Basaiahgari, A.; Panda, S.; Gardas, R. L. Acoustic, volumetric, transport, optical and rheological properties of Benzyltripropylammonium based Deep Eutectic Solvents. *Fluid Phase Equilib*. **2017**, *448*, 41-49.
51. Ijardar, S. P. Deep eutectic solvents composed of tetrabutylammonium bromide and PEG: Density, speed of sound and viscosity as a function of temperature. *J. Chem. Thermodyn*. **2020**, *140*, 105897.
52. Jabbar, N. M. A.; Mjalli, F. S. Ultrasonic study of binary aqueous mixtures of three common eutectic solvents. *Phy. Chem. Liq*. **2019**, *57*, 1-18.
53. Sas, O. G.; Fidalgo, R.; Domínguez, I.; Macedo, E. A.; González, B. Physical Properties of the Pure Deep Eutectic Solvent, [ChCl]:[Lev] (1:2) DES, and Its Binary Mixtures with Alcohols. *J. Chem. Eng. Data* **2016**, *61*, 4191-4202.
54. Jangir, A. K.; Patel, D.; More, R.; Parmar, A.; Kuperkar, K. New insight into experimental and computational studies of Choline chloride-based 'green' ternary deep eutectic solvent (TDES). *J. Mol. Struct*. **2019**, *1181*, 295-299.
55. Sturtevant, B. T.; Pantea, C.; Sinha, D. N. Measured sound speeds and acoustic nonlinearity parameter in liquid water up to 523 K and 14 MPa. *AIP Advances* **2016**, *6*, 075310.
56. Rowlinson, J. S.; Swinton, F. L. Liquid and Liquid Mixtures, Butterworths, London, 3rd. edn., 1982.

57. Jiu-Xun, S.; Fu-Qian, J.; Qiang, W.; Ling-Cang, C. Modification to the Newton-Laplace formula of sound velocity at high pressure. *Appl. Phys. Lett*. **2006**, *89*, 121922.
58. Tyrrell, H. J. V.; Harris, K. R. Diffusion in Liquids, A theoretical and experimental study, Butterworth-Heinemann, 1984.
59. Geng, Y.; Chen, S.; Wang, T.; Yu, D.; Peng, C.; Liu, H.; Hu, Y. Density, viscosity and electrical conductivity of 1-butyl-3-methylimidazolium hexafluorophosphate + monoethanolamine and + N, N-dimethylethanolamine. *J. Mol. Liq*. **2008**, 143, 100-108.
60. García, G.; Aparicio, S.; Ullah, R.; Atilhan, M. Deep Eutectic Solvents: Physicochemical Properties and Gas Separation Applications. *Energy Fuels* **2015**, *29*, 2616-2644.
61. Kollau, L. J. B. M.; Tuinier, R.; Verhaak, J.; den Doelder, J.; Filot, I. A. W.; Vis, M. Design of Nonideal Eutectic Mixtures Based on Correlations with Molecular Properties. *J. Phys. Chem. B* **2020**, *124*, 5209-5219.
62. Smith, P. J.; Arroyo, C. B.; Hernandez, F. L.; Goeltz, J. C. Ternary Deep Eutectic Solvent Behavior of Water and Urea–Choline Chloride Mixtures. *J. Phys. Chem. B* **2019**, *123*, 5302-5306.
63. Owyeung, R. E.; Sonkusale, S. R.; Panzer, M. J. Influence of Hydrogen Bond Donor Identity and Intentional Water Addition on the Properties of Gelatin-Supported Deep Eutectic Solvent Gels. *J. Phys. Chem. B* **2020**, *124*, 5986-5992.

Appendix: Calculation of formula/molar mass (MW), molar volume (V_m), molar refraction (R_m) and free molar volume (f_m) of DES.

DES constituents	M (Molecular mass) in g/mol
Acetamide (Ac)	59.07
Urea (Ur)	60.06
Sorbitol (Sr)	182.17

$$MW = 10[xM(Ac) + yM(Ur) + zM(Sr)]$$

DES	MW (g/mol
0.3Ac+0.2Ur+0.5Sr	1208.180
0.3Ac+0.3Ur+0.4Sr	1086.070
0.3Ac+0.4Ur+0.3Sr	963.960
0.3Ac+0.45Ur+0.25Sr	902.905
0.4Ac+0.3Ur+0.3Sr	962.970
0.2Ac+0.3Ur+0.5Sr	1209.170
0.1Ac+0.5Ur+0.4Sr	1088.050
0.2Ac+0.4Ur+0.4Sr	1087.060
0.4Ac+0.2Ur+0.4Sr	1085.080

Molar volume (V_m), molar refraction (R_m) and free volume (f_m) calculation for [0.3Ac+0.2Ur+0.5Sr] DES

T (K)	$\boldsymbol{V_m}$ **(mL/mol)**	$\boldsymbol{n_D}$	$\boldsymbol{R_m}$ **(mL/mol)**	$\boldsymbol{f_m = V_m - R_m}$ **(mL/mol)**
293	888.83	1.5098	265.74	623.09
298	891.68	1.5085	266.02	625.65
303	893.58	1.5072	266.01	627.56
308	896.42	-	-	-
313	898.32	1.5049	266.40	631.92
318	900.22	-	-	-
323	901.17	1.5024	266.12	635.04
328	903.06	-	-	-
333	904.96	1.4998	266.07	638.89

Chapter 6B

Correlating Bromelain's Activity with its Structure, Active-site Dynamics and Media's Physical Properties in a Hydrated Deep Eutectic Solvent

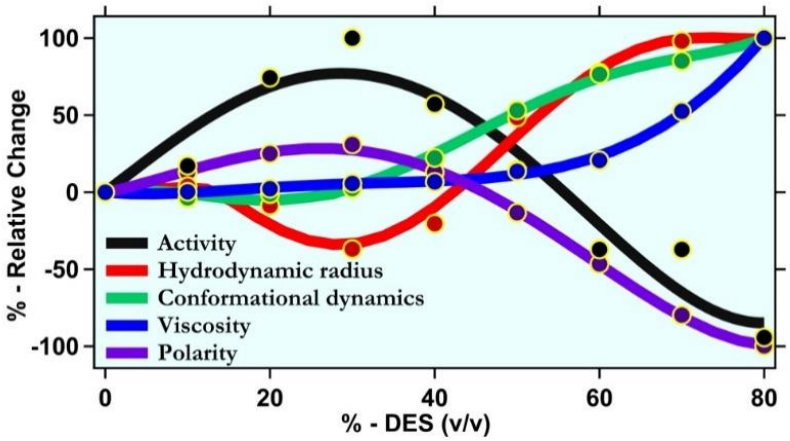

N. Das, T. Khan, **N. Subba** and P. Sen. *Phys. Chem. Chem. Phys.* **2021** (Just accepted)

DESs have been shown to be biocompatible and therefore, emerging as a new media for bio-catalysis. Biomolecules like proteins haven been shown to be stable in DESs while retaining its activity. However, only few studies have been devoted to understand the structure and activity of proteins in DESs. This work represents a systematic study deciphering the behaviour of bromelain in a ternary DES with a composition of acetamide:urea:sorbitol = 0.5:0.3:0.2 (0.5Ac/0.3Ur/0.2Sor) along with various degree of hydration. The purposefully chosen DES here is non-ionic and liquid at room temperature. It provides us a unique opportunity to contemplate protein behaviour in a non-ionic DES for the very first time. I chose bromelain as the model enzyme for this study. The result infers that at low DES concentration (up to 30% V/V DES), bromelain takes up a more compact structural conformation; whereas at higher DES concentration; it becomes somewhat elongated. Microsecond conformational fluctuation time around the active-site of bromelain gradually increases with increasing DES concentration, especially beyond 30% V/V. Interestingly, bromelain retains most of its enzymatic activity inside DES, and at some hydration level it is even higher as compared to that in buffer. Furthermore, we correlate bromelain's activity with its structure, active-site dynamics and media's physical property. Our results demonstrate that compact structural conformation and flexibility of active-site of bromelain favours its proteolytic activity. Similarly, an increased polarity and decreased viscosity of the medium is favourable for its activity.

6B.1 Introduction

Proteins are generally stable only in aqueous solution. Perhaps, if one can stabilize a protein in some alternate media and carry out its function, it will open up a new dimension in bio-catalysis. Therefore, many studies are carried out to investigate the structure and activity of proteins in ILs,[1,2] and in the last few years DES is being explored as a potential media where protein's structure/activity can be retained or even refold/increased.[3-17] Further, DESs also serve as the matrix where proteins remain active in extreme condition.[18-20]

Enzymes are vital entities for cell functioning and moreover there is significant interest in the use of structurally stable and active enzymes in the industrial processes.[21-23] Bromelain is an industrially important plant cysteine protease from pineapple stem.[24] Traditionally it is used in meat tenderizing and protein cleavage.[25] it is also used as medicine to treat inflammation, thrombosis, arthritis, and so forth.[26,27] The structure, stability and activity of bromelain have previously been investigated in the presence of several external perturbation, including osmolytes, denaturants and macromolecular crowders.[28-35] However, like any other enzymes, use of harsh organic solvent might destroy the stability and activity of bromelain to limit its use. On the other hand Kumar *et al.* showed that bromelain's stability and activity can be preserved in presence of choline based IL.[36] Similarly, Venkatesu group showed that bromelain's stability and activity increases at lower content of imidazolium based IL and at higher content the activity decreases.[37,38]

However, there are many gaps in the study of bromelain (and any enzyme in general) in alternate media. First, there is no study on bromelain's structure and activity in DES. Secondly, enzyme is a dynamic entity and the associated dynamics in the μs timescale is very important for its activity.[39,40] Recently, there are some attempts to contemplate the μs dynamics in IL.[41-47] However, to the best of our knowledge, no studies have been conducted to reveal the μs protein dynamics in DES. Thirdly, Most of the DESs are ionic and all the few studies that have been carried out to understand protein's behaviour in DES are done in such ionic DESs.[7-17] Most non-ionic interactions are weaker (than ionic interaction), so non-ionic DESs are challenging to form. However, from the applications point of view of these DES as a solvent, which demands a good solubility, many solutes (like hydrophobic ones) may not dissolve in an ionic DES. Non-ionic DES can overcome this problem. Therefore, understanding protein's behaviour in non-ionic DES is important. However, there is no report till date. Fourthly, the understanding on why proteins are stable and retain their activity in DES is poorly understood. In this direction, we aim to explore the structural, functional, and dynamical response of bromelain in a ternary DES composed of acetamide, urea, and sorbitol with their mole fractions

as 0.5, 0.3, and 0.2, respectively (0.5Ac/0.3Ur/0.2Sor)[48] with various degrees of hydration. The purposefully chosen DES here is non-ionic and liquid at room temperature. We also attempted to decipher the correlations between these responses. Further, the correlation between the activity of bromelain and DES's property (e.g. extent of hydration, viscosity, and polarity) has been explored. The present work might give a physical insight for rational design of a DES.

6B.2 Results and Discussion

6B.2.1 Fluorescent tagging: Bromelain has five cysteine amino acid residues, among which two pairs are connected by disulfide linkage, and the remaining one (Cys-25) is present in the free/reactive form (figure 6B.1). More interestingly, this Cys-25 residue is present at the active site of bromelain.[49]

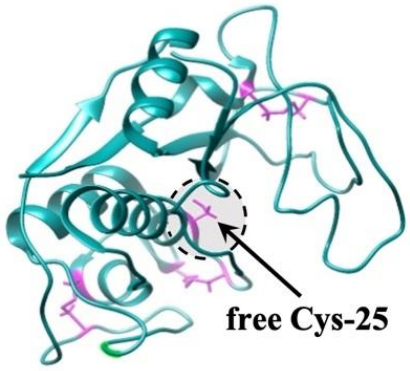

Figure 6B.1 Amino acid sequence and 3D structure of bromelain (PDB ID: 1W0Q). The single free cysteine residue (Cys-25) is highlighted.

This residue was tagged with 7-diethylamino-3-(4-maleimidophenyl)-4-methylcoumarin (CPM) and tetramethylrhodamine-5-maleimide (TMR) (figure 6B.2a and 6B.2c). CPM is weakly fluorescent in water with an emission maximum at 482 nm. Upon tagging, it becomes highly fluorescent, probably because of the restricted rotation of the 7-diethylamino moiety inside the protein matrix, and the emission maximum is blue-shifted to 475 nm (figure 6B.2b). Such a blue shift of the emission maximum might be ascribed to the burial of CPM inside the hydrophobic protein core of bromelain and thus confirms the tagging. TMR is not a solvatochromic dye and there is no change of its emission behaviour upon tagging to Cys-25

of bromelain (figure 6B.2d). The absorption profile of CPM and TMR does not change upon tagging to bromelain (see figure 6B.3) The tagging is confirmed by measuring the diffusion time of the dye through a certain volume using FCS. The diffusion time of free CPM and CPM tagged bromelain are found to be 22 and 67 μs, respectively, through an observation volume of 0.5 fL (figure 6B.2e). For free TMR and TMR tagged bromelain, the diffusion times through 0.7 fL observation volume are respectively measured to be 31 and 94 μs (figure 6B.2f). Such an increase in the diffusion coefficient also proves tagging. Furthermore, taking advantage of CPM's solvatochromism, CPM fluorescence might be used to get information on local conformational alteration around Cys-25. The local conformation around the tagging site has been contemplated by CPM emission for other proteins like human serum albumin and *β*-lactoglobulin.[41,50] However to do this, one needs to confirm that the tagging has not perturbed protein's structure. We compared the CD spectrum of untagged bromelain, CPM tagged bromelain, and TMR tagged bromelain in figure 6B.2g. The almost similar CD spectra (secondary structural parameters are given in table 6B.1) prove that tagging has not significantly perturbed the structural feature of bromelain. The spectroscopic signal of CPM-bromelain and TMR-bromelain remains unaltered even after 3 months.

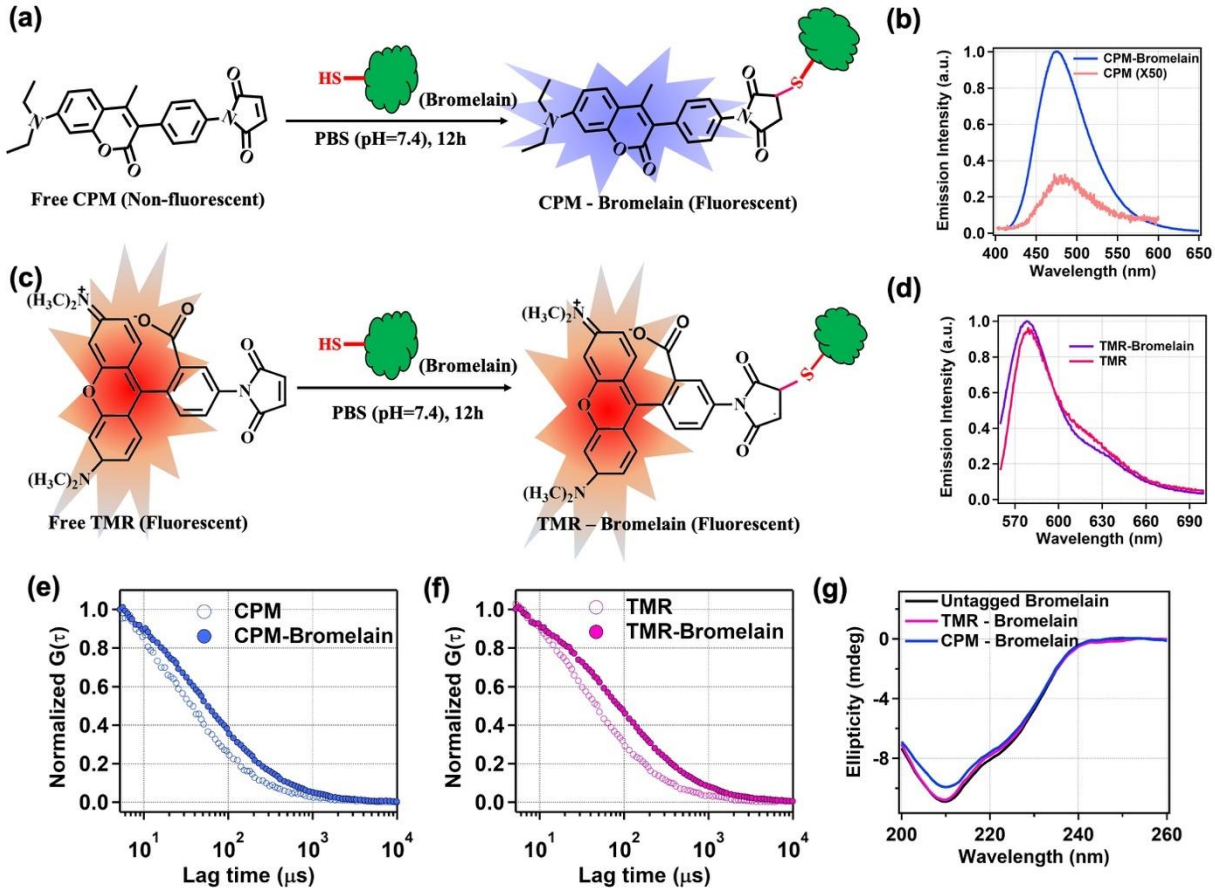

Figure 6B.2 Tagging of bromelain. (a) Site-specific tagging scheme of bromelain with CPM. (b) Emission spectra of CPM (orange) and CPM tagged to Cys-25 of bromelain (blue). The emission spectra of untagged CPM has been multiplied by a factor of 50 to make it visible. (c) Site specific tagging scheme of bromelain with TMR. (d) Emission spectra of TMR (pink) and TMR tagged to Cys-25 of bromelain (purple). (e) Normalised fluorescence intensity autocorrelation traces for CPM (open blue circle) and CPM tagged to bromelain (filled blue circle). (f) Normalised fluorescence intensity autocorrelation traces for TMR (open pink circle) and TMR tagged to bromelain (filled pink circle). (g) CD spectra of untagged bromelain (black), TMR tagged bromelain (pink) and CPM tagged bromelain (blue).

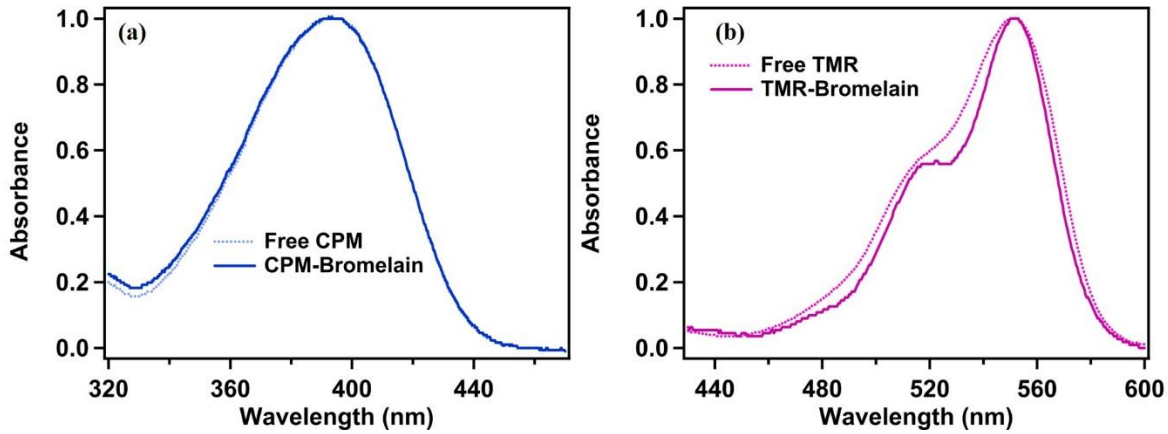

Figure 6B.3 Absorption spectra of (a) free CPM and CPM tagged to bromelain; and (b) free TMR and TMR tagged to bromelain

Table 6B.1 Secondary structural parameters of untagged, CPM tagged and TMR tagged bromelain.

	α-helicity	**β-sheet**	**β-turn**	**Random Coil**
Untagged Bromelain	20.1	22.4	18.0	39.5
CPM-Bromelain	19.6	22.4	17.5	40.5
TMR-Bromelain	20.0	22.3	18.0	39.7

6B.2.2 Steady-state absorption and emission study: As discussed above, the change in the microenvironment around bromelain's active site can be monitored through the steady-state absorption and emission studies of CPM as it is tagged to Cys-25 residue of bromelain. To investigate the effect of 0.5Ac/0.3Ur/0.2Sor DES on this, we recorded the absorption and emission of CPM tagged bromelain in the presence of varying amount of DES (0% to 80% V/V) in phosphate buffer. Absorption spectra of CPM tagged to bromelain does not change in the presence of DES (data not shown). In the presence of 0 – 30 % V/V DES a small redshift in the emission spectrum was observed (λ_{em}^{max} = 478.5 nm in the presence of 30% V/V DES) with a slight decrease of emission intensity (figure 6B.4a and 6B.4b). On further increase in DES content, the emission maximum gradually blue-shifted and reached 471.5 nm at 80 % V/V DES. The result suggests that at lower DES content, CPM in the active site of bromelain experience a hydrophilic environment, and as the DES content increases, the environment near the active site become more hydrophobic. However, only from a steady-state experiment reaching such a conclusion is not right. As the surface accessibility is around 95% of Cys-25

of bromelain,[51] we believe that steady-state emission characteristics of CPM tagged to Cys-25 of bromelain is mainly controlled by external solvent medium rather than protein matrix. Basically, with increasing DES content, the polarity of the solvent might change and it is possible that the trend of emission maxima of CPM at the active site of bromelain follow the bulk solvent polarity. To check this possibility, we estimated the polarity of 0.5Ac/0.3Ur/0.2Sor DES with various degrees of hydration through steady-state emission studies using coumarin 1 (C1) as the solvatochromic dye (see figure 6B.4c and table 6B.2). C1 is analogous with CPM and experiences a large change in dipole moment upon photoexcitation, which makes it an excellent solvatochromic probe.[52] As suspected, the trend is found to be similar as of CPM tagged to the active site of bromelain. We thus conclude that the steady-state measurements are inconclusive.

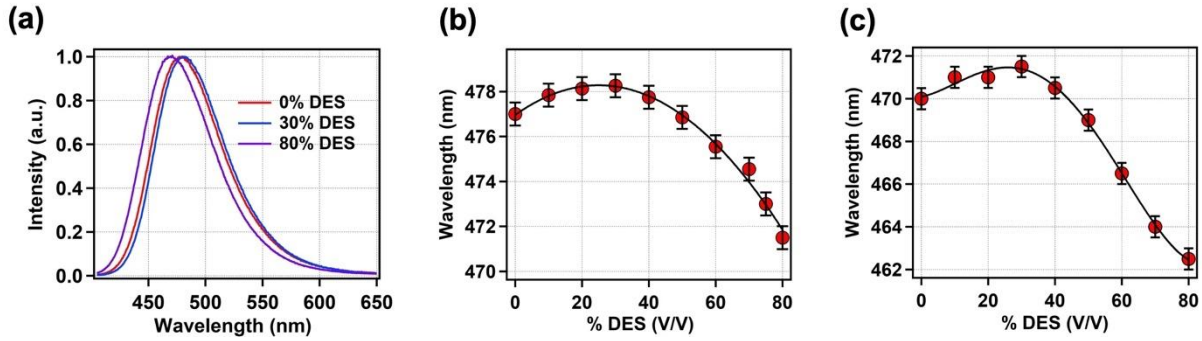

Figure 6B.4 Steady-state emission study. (a) Representative emission spectra of CPM tagged to bromelain at various DES contents. (b) Variation of emission maxima of CPM tagged to bromelain with increasing DES concentration. (c) Variation of emission maxima coumarin-1 with increasing DES concentration. The black lines are eye-guide and every experimental point is the average value of three independent measurements and the error bar represents the standard deviation of the mean.

Table 6B.2 Various properties of bromelain and solvent media as a function of 0.5Ac/0.3Ur/0.2Sor DES content.

DES Content %(V/V)	Emission maxima of coumarin 1 (nm)	Hydrodynamic Radius of bromelain (Å)	Conformational fluctuation time of bromelain (μs)	Activity of bromelain	Viscosity of solvent measured by FCS (cP)
0	470.0	22.0	7.2	0.136	1.0
10	471.0	22.4	6.9	0.142	1.1
20	471.0	21.1	7.1	0.162	1.9
30	471.5	18.2	7.4	0.171	3.3
40	470.5	19.9	9.0	0.156	3.7
50	469.0	27.0	11.5	0.141	6.5
60	466.5	30.0	13.4	0.123	9.4
70	464.0	32.1	14.1	0.123	22.3
80	462.5	32.3	15.3	0.103	41.6

6B.2.3 CD study: CD measurements would be useful in deciphering the modulations of secondary structural parameters of bromelain in the presence of DES. However, we could not perform the CD measurements in the presence of DES as DES has considerable absorption below 240 nm. Therefore, we could not directly comment about the modulation of secondary structure of bromelain in DES. However, we back-extracted bromelain from DES and recorded the CD spectra. If DES modulates the secondary structure of bromelain irreversibly, it will be imprinted in the CD signal. The result is shown in the figure 6B.5 and table 6B.3. It is clear that the back-extracted bromelain from DES retains most of its secondary structure. Therefore, we may conclude that DES does not modify bromelain's secondary structure irreversibly.

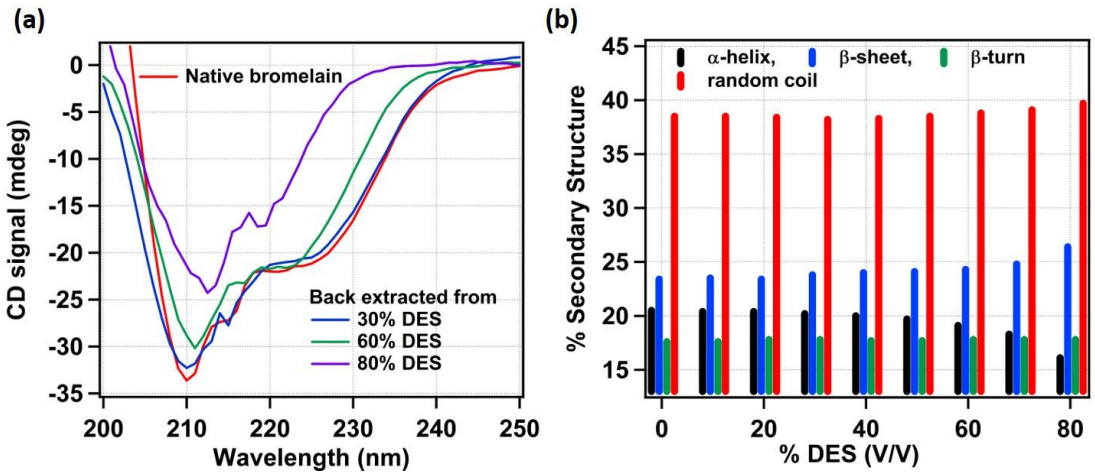

Figure 6B.5 (a) CD spectra of native and back extracted (from various DES composition) bromelain. (b) Secondary structural parameters of native bromelain and back extracted bromelain from various DES composition.

Table 6B.3 Secondary structural parameters of native bromelain and back extracted bromelain from various DES composition.

DES Content %(V/V)	α-helicity	β-sheet	β-turn	Random Coil
0	20.5	23.4	17.6	38.5
10	20.4	23.5	17.6	38.5
20	20.4	23.4	17.8	38.4
30	20.2	23.8	17.8	38.2
40	20	24	17.7	38.3
50	19.7	24.1	17.7	38.5
60	19.1	24.3	17.8	38.8
70	18.3	24.8	17.8	39.1
80	16.1	26.4	17.8	39.7

6B.2.4 FCS study: The fluorescence intensity autocorrelation curve of both CPM and TMR tagged bromelain could be best fitted using equation 2.25 (see figure 6B.6) and returns two time components. The exponential time component of 7 μs is assigned as the conformational fluctuation time of the active site of bromelain. Further, we have performed the following control experiments to confirm it as the timescale of the conformational dynamics. (i) Although CPM is a weakly fluorescent molecule, it is possible to take the FCS data of CPM only. The data can be fitted (from 1 μs) using equation 2.21 quite satisfactorily. TMR is substituted

rhodamine, known to have a triplet state blinking timescale of around 1 µs. The autocorrelation trace of TMR is not correctly fitted by equation 2.21 from 1 µs. However, the fitting quality is quite good when fitted from 5 µs implying that the effect of dye's photophysics dies beyond 5 µs. However, neither the CPM tagged bromelain (from 1 µs) nor the TMR tagged bromelain (from 5 µs) autocorrelation curve can be fitted with equation 2.21 (figure 6B.6). Therefore, the requirement of an additional relaxation term implies that the origin of the term is not the photophysics of dye, but is the protein conformational fluctuation. (ii) Power dependent experiment can also be beneficial in deciding about the origin of the extra relaxation term. Had the term originates from triplet state blinking, the contribution should be affected by the power of the laser. However, that is not the case (see figure 6B.7). (iii) The exponential time component is also similar while employing two different tags (CPM and TMR). These further confirm that the additional time component of 7 µs is the timescale of bromelain's conformational dynamics. The longer time component, τ_D, is converted to hydrodynamic radius as described in chapter 2. The hydrodynamic radius is calculated to be 21 Å for both CPM/TMR tagged bromelain, which is in accordance with previously measured hydrodynamic radius value of 23 Å by dynamic light scattering (DLS).[53] We have taken FCS data of TMR tagged bromelain with increasing DES concentration (see figure 6B.8) instead of CPM.[54]

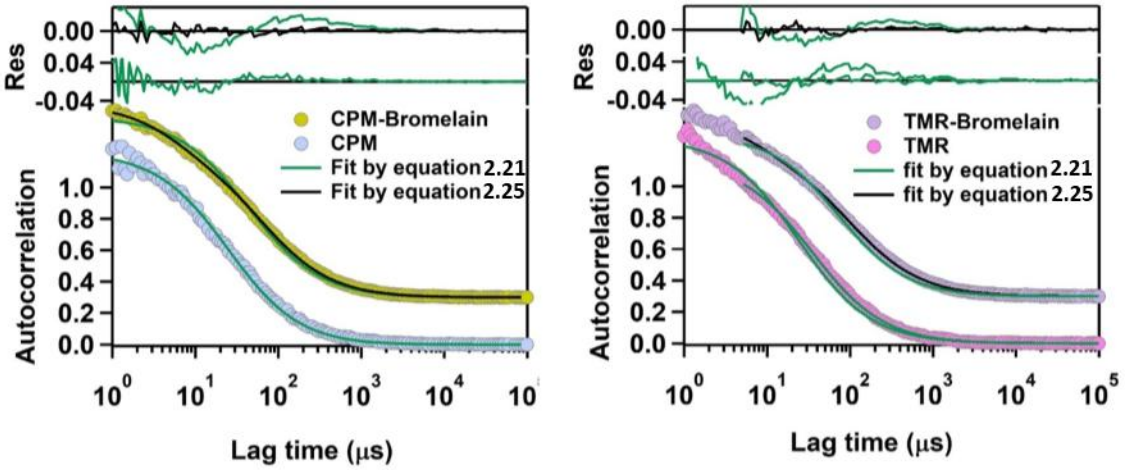

Figure 6B.6 Fitting comparison of fluorescence autocorrelation traces of (a) CPM and CPM tagged to bromelain and (b) TMR and TMR tagged to bromelain. Equation 2.21 can fit the autocorrelation trace of CPM satisfactorily; but extra relaxation term is required to fit the autocorrelation trace of CPM-bromelain. Equation can fit the autocorrelation trace of TMR only when fitted from 5 µs. However, to fit autocorrelation trace of TMR-bromelain from 5 µs, equation 2.25 is required.

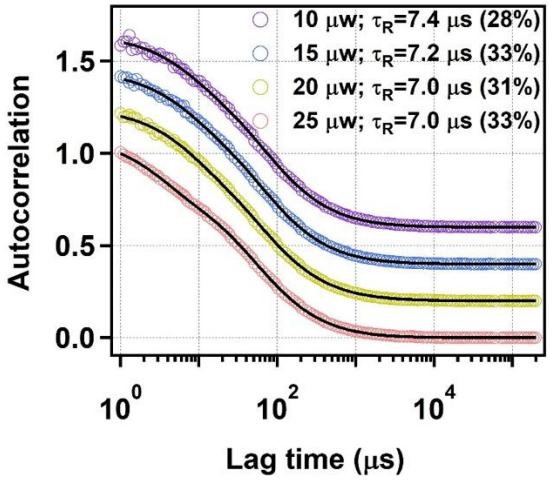

Figure 6B.7 Autocorrelations traces of CPM tagged to bromelain at different laser power. The value of conformational fluctuation time and its contribution remains similar with the variation of power.

With increasing DES content we observe a slight decrease of hydrodynamic radius up to 30% (V/V) of DES, and with a further addition of DES the hydrodynamic radius gradually increases and reaches to 32Å at 80% DES (figure 6B.8b and table 6B.2). The result suggests that bromelain adopts a slightly compact configuration in the presence of a small amount of DES. However, with a further increase of DES, the interactions that held the tertiary structure together gradually break down, and bromelain adopts an elongated/denatured conformation. To note that, emission study apparently contradicts this FCS result. However, emission study gives information about the very local environment of the dye, and FCS furnishes information about global protein structure. Moreover, we have already proved that the change of emission maxima of CPM tagged to bromelain in DES with various degrees of hydration is mainly due to the change of the solvent property, not the protein property.

With increasing DES content the conformational fluctuation time of bromelain gradually increases (more prominently, beyond 30% (V/V) DES) suggesting an increased rigidness of the active site of bromelain (figure 6B.8c and table 6B.2). The rigidity of the protein matrix might be modulated with the structural modulation and with the opening of bromelain such rigidity should decrease. Moreover, the dye tagged to Cys-25 of bromelain is at the protein surface and is mostly solvent-exposed. Therefore, solvent viscosity should also have a crucial role in controlling the timescale of such motion.

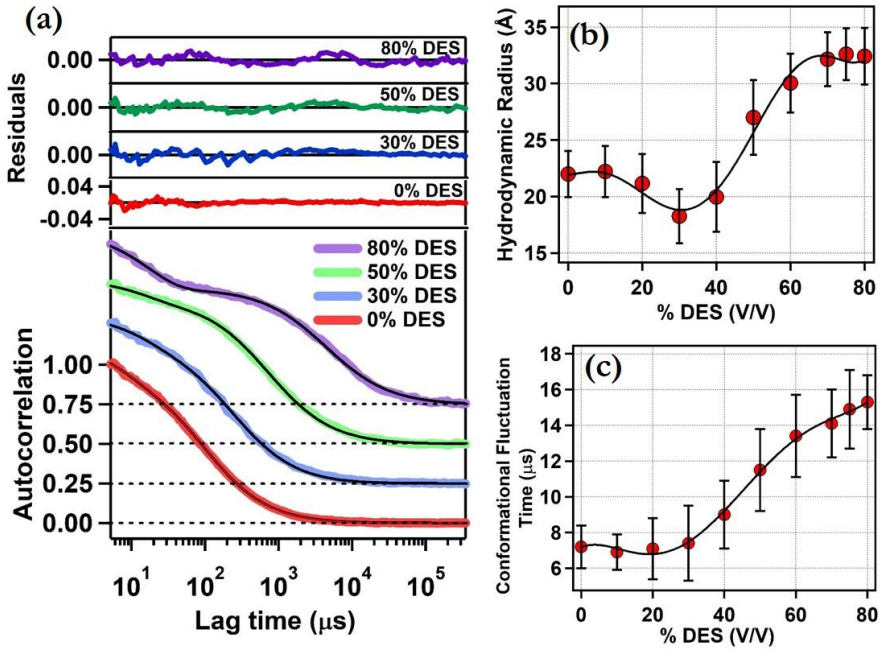

Figure 6B.8 Single molecular level FCS measurement of TMR tagged to bromelain. (a) Normalized fluorescence intensity autocorrelation curve for TMR-tagged bromelain at representative DES concentrations. Fitting lines using equation 2.25 are shown by solid black lines. The residuals of fitting are also shown. (b) Variation of the hydrodynamic radius of TMR-tagged bromelain with increasing DES concentration. (c) Variation of the conformational fluctuation time of TMR-tagged bromelain with increasing DES concentration. The black lines here are guides for the eye. Every experimental data point is the average of three independent measurements, and the error bar indicates the standard deviation of the mean.

6B.2.5 Activity measurement: We studied the protease activity of bromelain taking casein as a substrate in 0.5Ac/0.3Ur/0.2Sor DES with various hydrations. In buffer, the absorbance of digested casein is 0.136. At a low DES content, the activity increases slightly and reaches to 0.171 at 30% (V/V) DES. However, with a further increase in DES content, the activity drops and become 0.103 at 80% (V/V) DES (figure 6B.9 and table 6B.2). It is interesting to note that even in the presence of 80% (V/V) DES, bromelain retains most of its activity. Moreover, at 30% (V/V) DES content bromelain's proteolytic activity found to be higher compared to that in buffer medium. As a control experiment, we performed the activity measurement in a solution of the DES constituents maintaining the same component concentration as in hydrated DES. We cannot perform the experiment beyond 60% for DES components in buffer because of the solubility issue. Here, at 30% (v/v) DES components, the activity is measured to be 0.148.

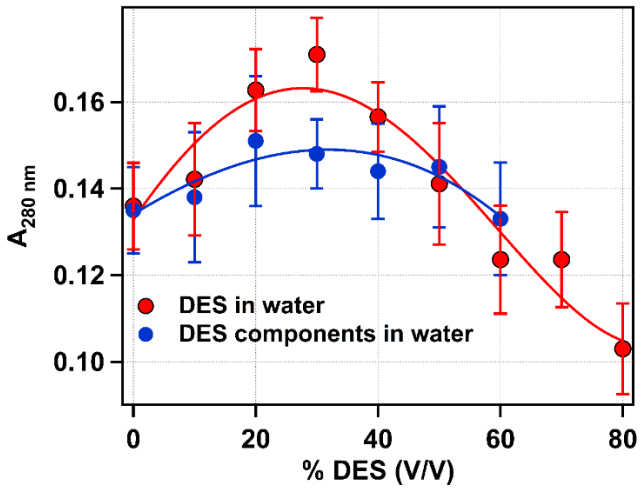

Figure 6B.9 Variation of the activity of untagged bromelain with increasing 0.5Ac/0.3Ur/0.2Sor DES concentration (red), and that in a solution of the DES constituents maintaining the same component concentration as in hydrated DES (blue). We can not perform the experiment beyond 60% for DES components in buffer because of the solubility issue. The solid lines are the eye-guides. Every experimental data point is the average of three independent measurements, and the error bar indicates the standard deviation of the mean.

6B.2.6 Correlating bromelain's activity with its structure/dynamics and DES properties: We attempted to find the correlation of bromelain's activity with its structure and dynamics in 0.5Ac/0.3Ur/0.2Sor DES at various degrees of hydration (figure 6B.10). Upto 30% v/v mixture of DES in buffer enhances the activity of bromelain, followed by a decrease in activity as the fraction of DES increases. The report is in line with several previous experimental reports where enzymes show increased catalytic activity at higher water content and decreases at higher DES content.[14,20,55-57] However, a comprehensive explanation is difficult in this case as it is a mutual interplay of various factors and the enormous complexity in biomolecules put a restriction to draw a general rule. The structure is one of the main factors to determine the function. From FCS measurement we observed that the native structure of bromelain is destroyed at an increased concentration of DES and the activity decreased. However, at low DES content bromelain becomes more compact and shows a greater activity than its native state. Second factor that controls protein's activity is its dynamics. Especially, the µs dynamics of the active site is believed to be the controlling factor of enzymatic activity. We have seen that with an increase in DES concentration, the timescale of conformational fluctuation dynamics of bromelain increases. This suggests that bromelain becomes more and more rigid with an increase in DES content. Probably, the decreased flexibility has a role in reducing bromelain's activity at higher DES content. Overall, we see a beautiful correlation between

structure, active-site dynamics, and bromelain activity, i.e. (i) structural compaction and flexibility favours the activity and (ii) structural elongation and rigidity make it less active (see figure 6B.10).

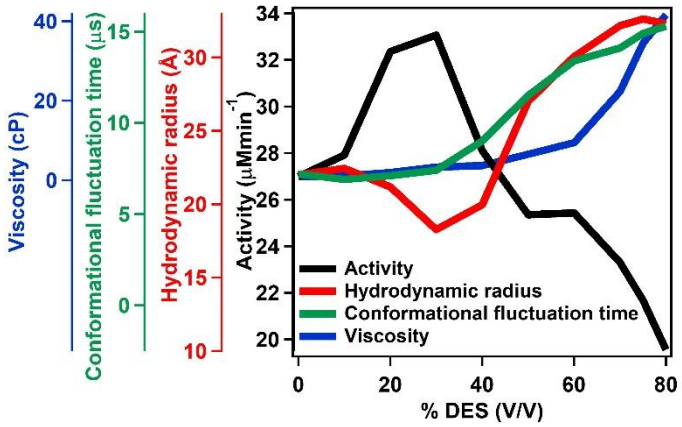

Figure 6B.10 Correlating bromelain's activity with its structure, active-site dynamics, and media's viscosity with increasing DES concentration. Structural compaction, decreased conformational fluctuation time of the active-site and low viscosity favours bromelain's activity. In contrast, an elongated structural conformation, increased conformational fluctuation time and increased viscosity of the medium disfavours bromelain's activity.

Next, we envisaged to understand how the activity of bromelain is modulated with DES's property due to different extent of hydration. The change of emission maxima of coumarin 1 (a positive solvatochrocic dye) in 0.5Ac/0.3Ur/0.2Sor DES with various degrees of hydration can be ascribed to a change in polarity of the DES at different degree of hydration. Here, a redshift in the emission maxima indicates an increased polarity of the solvent. Interestingly, we get a beautiful correlation between polarity and activity (figure 6B.10). At 30% (V/V) DES and 80% (V/V) DES, polarity is maximum and minimum, respectively, and so is bromelain activity. Both the enzyme and the substrate, in this case, are large biomolecules. So, diffusion must have a prominent role to play in controlling the proteolytic activity. Diffusion is dictated by the friction experienced by bromelain or casein while moving in the medium and is greatly governed by the medium viscosity. The viscosity of the medium has been estimated from the diffusion time of R6G (see figure 6B.11 and table 6B.2). With increasing DES content viscosity gradually increases and diffusion becomes progressively slower. As per our prediction, bromelain's activity should decrease gradually with increasing DES content, and in fact at high DES content, we found the activity decreases (figure 6B.10). However, the initial increase of activity cannot be rationalised through viscosity change and we believe it is mostly controlled by its structure. Most probably, the overall result is a combined effect of all possible causes.

Overall, we propose that a solvent that can compact the bromelain structure and increase its flexibility might be a better medium for its activity from such a correlation. Further, probably a solvent with low viscosity and high polarity is a better choice.

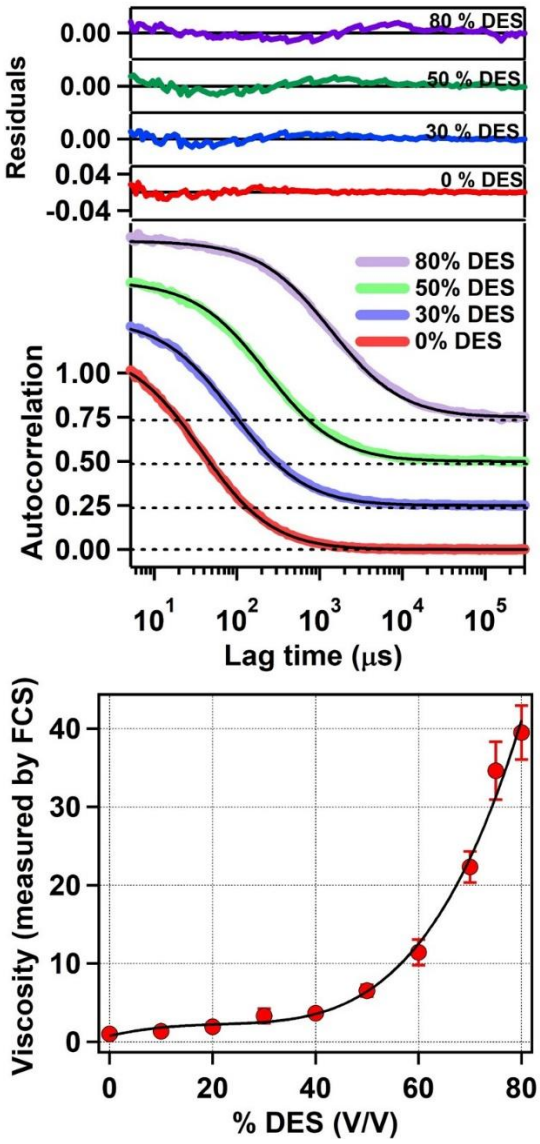

Figure 6B.11 (a) Normalized fluorescence intensity autocorrelation curve for rhodamine-6G at some representative DES concentration. Fitting lines using equation 2.21 are shown by solid black lines. The residuals of fitting are also shown. (b) Variation of viscosity with increasing DES concentration

One may argue that dilution with water might lead to the disruption of DES network. Therefore, it is hard to tell if the noted positive effect of DES at low concentration regime is due to the nature of the DES i.e. a hydrogen bonded solvent network, or due to normal salting in effects. Previous studies have shown that for many DES, the network is maintained up to a certain %

of water.[58-63] For example, in the case of choline chloride/urea DES, the network is found to be maintained until ~83 mol% of water.[58] If that be the case, then at high water content regime the interaction of individual DES components with water and protein will mainly control the protein's behaviour rather than the network-like DES nature. To have more insight on it, we have done a control experiment. We mixed all the three constituents of DES in the water, maintaining the same component concentration as in hydrated DES, and recorded the proteolytic activity of bromelain (see figure 6B.9). Here we observed a definitive but slight increase in the proteolytic activity compared to pure buffer at higher water concentrations, in contrast to the significant effect brought in by the corresponding DES. Therefore, there is a hint that the synergistic action of the individual components might play a role. Nevertheless, the noted positive effect of bromelain activity in hydrated DES is probably controlled by the nature of the DES itself, i.e. a hydrogen bonded solvent network. Earlier, an increase in the peroxidase[14] and lipase[64] activity was proposed not due to the synergistic effect only even at higher degree of dilution. In the present case we also propose that even at high water content, DES still exist as somewhat intact entity. However, the properties of the DES itself would need to be studied to confirm the proposition, where neutron scattering might come handy.

6B.3 Summary and Conclusion:

In conclusion, we examined the behaviour of bromelain, an industrially important proteolytic enzyme, in a hydrated DES composed of acetamide, urea and sorbitol (0.5Ac/0.3Ur/0.2Sor). Moreover, we ventured to correlate the proteolytic behaviour with its structure and dynamics and with various DES's properties. The main findings can be summarised as follows. (i) The structure becomes a little compact at a lower DES concentration (30% V/V), but becomes elongated at higher DES concentrations. (ii) Microsecond protein dynamics becomes progressively slower with increasing DES concentration. (iii) The enzymatic activity of bromelain is retained in DES. More importantly, at some DES concentration, the activity is even higher than that of the native state. (iv) We find a beautiful correlation between bromelain's activity with its structure and dynamics and DES's property. We conclude that a more compact structural conformation, higher flexibility of the active site, the low viscosity of solvent media, and a greater polarity probably facilitates its function. (v) The noted positive effect of DES on bromelain's activity under high diluting condition is probably due to the effect of network-like DES structure.

Overall, our results provide a deeper insight regarding the structure-activity-dynamics correlation of bromelain in 0.5Ac/0.3Ur/0.2Sor DES. We also investigated the correlation

between bromelain's activity with DES's property (i.e. extent of hydration, viscosity, and polarity). We believe such an insight will be beneficial for the rational design of DES as biocatalytic media. However, keeping in mind the enormous complexity of biological system, it is very tough to prescribe how the enzymatic activity can be optimized. A huge effort is necessary in this regard.

References:

1. Janati-Fard, F.; Housaindokht, M. R.; Monhemi, H.; Esmaeili, A. A.; Pour, A. N. The influence of two imidazolium-based ionic liquids on the structure and activity of glucose oxidase: Experimental and theoretical studies. *Int. J. Biol. Macromol.* **2018**, *114*, 656-665.
2. van Rantwijk, F.; Secundo, F.; Sheldon, R. A. Structure and activity of Candida antarctica lipase B in ionic liquids. *Green Chem.* **2006**, *8*, 282-286.
3. Yadav, N.; Bhakuni, K.; Bisht, M.; Bahadur, I.; Venkatesu, P. Expanding the Potential Role of Deep Eutectic Solvents toward Facilitating the Structural and Thermal Stability of α-Chymotrypsin. *ACS Sustainable Chem. Eng.* **2020**, *8*, 10151–10160.
4. Sanchez-Fernandez, A.; Edler, K. J.; Arnold, T.; Venero, D. A.; Jackson, A. J. Protein conformation in pure and hydrated deep eutectic solvents. *Phys. Chem. Chem. Phys.* **2017**, *19*, 8667-8670.
5. Andler, S. M.; Wang, L.-S.; Rotello, V. M.; Goddard, J. M. Influence of Hierarchical Interfacial Assembly on Lipase Stability and Performance in Deep Eutectic Solvent. *J. Agric. Food. Chem*. **2017**, *65*, 1907-1914.
6. Kist, J. A.; Henzl, M. T.; Bañuelos, J. L.; Baker, G. A. Calorimetric Evaluation of the Operational Thermal Stability of Ribonuclease A in Hydrated Deep Eutectic Solvents. *ACS Sustainable Chem. Eng.* **2019**, *7*, 12682-12687.
7. Pradeepkumar, P.; Rajendran, N. K.; Alarfaj, A. A.; Munusamy, M. A.; Rajan, M. Deep Eutectic Solvent-Mediated FA-*g*-β-Alanine-*co*-PCL Drug Carrier for Sustainable and Site-Specific Drug Delivery. *ACS Appl. Bio Mater*. **2018**, *1*, 2094-2109.
8. Cao,S.-L.; Xu, H.; Li, X.-H.; Lou, W.-Y.; Zong, M.-H. Papain@Magnetic Nanocrystalline Cellulose Nanobiocatalyst: A Highly Efficient Biocatalyst for Dipeptide Biosynthesis in Deep Eutectic Solvents. *ACS Sustainable Chem. Eng.* **2015**, *3*, 1589-1599.
9. Esquembre, R.; Sanz, J. M.; Wall, J. G.; del Monte, F.; Mateo, C. R.; Ferrer, M. L. Thermal unfolding and refolding of lysozyme in deep eutectic solvents and their aqueous dilutions. *Phys. Chem. Chem. Phys.* **2013**, *15*, 11248-11256.
10. Sindhu, A.; Kumar, S.; Mondal, D.; Bahadur, I.; Venkatesu, P.; Protein packaging in ionic liquid mixtures: an ecofriendly approach towards the improved stability of β-

lactoglobulin in cholinium-based mixed ionic liquids. *Phys. Chem. Chem. Phys.* **2020**, *22*, 14811-14821.

11. Monhemi, H.; Housaindokht, M. R.; Moosavi-Movahedi, A. A.; Bozorgmehr, M. R. How a protein can remain stable in a solvent with high content of urea: insights from molecular dynamics simulation of *Candida antarctica* lipase B in urea: choline chloride deep eutectic solvent. *Phys. Chem. Chem. Phys.* **2014**, *16*, 14882-14893.
12. Zhao, C.; Ren, J.; Qu, X. G-Quadruplexes Form Ultrastable Parallel Structures in Deep Eutectic Solvent. *Langmuir* **2013**, *29*, 1183-1191.
13. Toledo, M. L.; Pereira, M. M.; Freire, M. G.; Silva, J. P. A.; Coutinho, J. A. P.; Tavares, A. P. M. Laccase Activation in Deep Eutectic Solvents. *ACS Sustainable Chem. Eng.* **2019**, *7*, 11806-11814.
14. Papadopoulou, A. A.; Efstathiadou, E.; Patila, M.; Polydera, A. C.; Stamatis, H. Deep Eutectic Solvents as Media for Peroxidation Reactions Catalyzed by Heme-Dependent Biocatalysts. *Ind. Eng. Chem. Res.* **2016**, *55*, 5145-5151.
15. Qu, W.; Häkkinen, R.; Allen, J.; D'Agostino, C.; Abbott, A. P. Globular and Fibrous Proteins Modified with Deep Eutectic Solvents: Materials for Drug Delivery. *Molecules* **2019**, *24*, 3583.
16. B. Olivares, F. Martínez, L. Rivas, C. Calderón, J. M. Munita, P. R. Campodonico, A Natural Deep Eutectic Solvent Formulated to Stabilize β-Lactam Antibiotics. *Sci. Rep.* **2018**, *8*, 14900.
17. Elgharbawy, A. A.; Hayyan, A.; Hayyan, M.; Rashid, S. N.; Nor, M. R. M.; Zulkifli, M. Y.; Alias, Y.; Mirghani, M. E. S. Shedding Light on Lipase Stability in Natural Deep Eutectic Solvents. *Chem. Biochem. Eng. Q.* **2018**, *32*, 359-370.
18. Dai, Y.; van Spronsen, J.; Witkamp, G.-J.; Verpoorte, R.; Choi, Y. H. Natural deep eutectic solvents as new potential media for green technology. *Anal. Chim. Acta*. **2013**, *766*, 61-68.
19. Gertrudes, A.; Craveiro, R.; Eltayari, Z.; Reis, R. L.; Paiva, A.; Duarte, A. R. C. How Do Animals Survive Extreme Temperature Amplitudes? The Role of Natural Deep Eutectic Solvents. *ACS Sustainable Chem. Eng.* **2017**, ***5***, 9542-9553.
20. Choi, Y. H.; van Spronsen, J.; Dai, Y.; Verberne, M.; Hollmann, F.; I. Arends, W. C. E.; Witkamp, G.-J.; Verpoorte, R. Are Natural Deep Eutectic Solvents the Missing Link in Understanding Cellular Metabolism and Physiology? *Plant Physiol.* **2011**, *156*, 1701-1705.

21. Cavicchioli, R.; Charlton, T.; Ertan, H.; Omar, S. M.; Siddiqui, K. S.; Williams, T. J. Biotechnological uses of enzymes from psychrophiles. *Microb. Biotechnol.* **2011**, *4*, 449-460.
22. Kirk, O.; Borchert, T. V.; Fuglsang, C. C. Industrial enzyme applications. *Curr. Opin. Biotechnol*. **2002**, *13*, 345-351.
23. Alkorta, I.; Garbisu, C.; Llama, M. J.; Serra, J. L. Industrial applications of pectic enzymes: a review. *Process Biochem.* **1998**, *33*, 21-28.
24. López-García, B.; Hernández, M.; Segundo, B. S. Bromelain, a cysteine protease from pineapple (*Ananas comosus*) stem, is an inhibitor of fungal plant pathogens. *Lett. Appl. Microbiol*. **2012**, *55*, 62-67.
25. Pavan, R.; Jain, S.; Shraddha; Kumar, A. Properties and Therapeutic Application of Bromelain: A Review. *Biotechnol. Res. Int*. **2012**, *2012*, 976203.
26. Seligman, B. Bromelain: an Anti-Inflammatory Agent. *Angiology* **1962**, *13*, 508-510.
27. Metzig, C.; Grabowska, E.; Eckert, K.; Rehse, K.; Maurer, H. R. Bromelain proteases reduce human platelet aggregation in vitro, adhesion to bovine endothelial cells and thrombus formation in rat vessels in vivo. *In vivo* **1999**, *13*, 7-12.
28. Rani, A.; Venkatesu, P. Insights into the interactions between enzyme and co-solvents: Stability and activity of stem bromelain. *Int. J. Biol. Macromol.* **2015**, *73*, 189–201.
29. Jha, I.; Bisht, M.; Venkatesu, P. Does 1-Allyl-3-methylimidazolium chloride Act as a Biocompatible Solvent for Stem Bromelain? *J. Phys. Chem. B* **2016**, *120*, 5625– 5633.
30. Jha, I.; Bisht, M.; Mogha, N. K.; Venkatesu, P. Effect of Imidazolium-Based Ionic Liquids on the Structure and Stability of Stem Bromelain: Concentration and Alkyl Chain Length Effect. *J. Phys. Chem. B* **2018**, *122*, 7522– 7529.
31. Habib, S.; Khan, M. A.; Younus, H. Thermal destabilization of stem bromelain by trehalose. *Protein J.* **2007**, *26*, 117-124.
32. Rani, A.; Venkatesu, P. A Distinct Proof on Interplay between Trehalose and Guanidinium Chloride for the Stability of Stem Bromelain. *J. Phys. Chem. B* **2016**, *120*, 8863– 8872.
33. Rani, A.; Taha, M.; Venkatesu, P.; Lee, M.-J. Coherent Experimental and Simulation Approach To Explore the Underlying Mechanism of Denaturation of Stem Bromelain in Osmolytes. *J. Phys. Chem. B* **2017**, *121*, 6456–6470.
34. Bhakuni, K.; Venkatesu, P. Does macromolecular crowding compatible with enzyme stem bromelain structure and stability? *Int. J. Biol. Macromol.* **2019**, *131*, 527–535.

35. Kiran, P. K.; Jha, I.; Sindhu, A.; Venkatesu, P.; Bahadur, I.; Ebenso, E. E. Experimental and molecular docking studies in understanding the biomolecular interactions between stem bromelain and imidazolium-based ionic liquids. *J. Mol. Liq.* **2020**, *297*, 111785.
36. Kumar, P. K.; Bisht, M.; Venkatesu, P.; Bahadur, I.; Ebenso, E. E. Exploring the Effect of Choline-Based Ionic Liquids on the Stability and Activity of Stem Bromelain. *J. Phys. Chem. B* **2018**, *122*, 10435-10444.
37. Kumar, P. K.; Jha, I.; Venkatesu, P.; Bahadur, I.; Ebenso, E. E. A comparative study of the stability of stem bromelain based on the variation of anions of imidazolium-based ionic liquids. *J. Mol. Liq.* **2017**, *246*, 178– 186.
38. Mogha, N. K.; Sindhu, A.; Venkatesu, P. A biophysical strategy to examine the impact of newly synthesized polymerizable ammonium-based ionic liquids on the structural stability and proteolytic activity of stem bromelain. *Int. J. Biol. Macromol*. **2020**, *151*, 957-966.
39. J. Guo, H.-X. Zhou, Protein Allostery and Conformational Dynamics. *Chem. Rev.* **2016**, *116*, 6503-6515.
40. Yon, J. M.; Perahia, D.; Ghélis, C.; Conformational dynamics and enzyme activity. *Biochimie* **1998**, *80*, 33-42.
41. Sasmal, D. K.; Mondal, T.; Mojumdar, S. S.; Choudhury, A.; Banerjee, R.; Bhattacharyya, K. An FCS Study of Unfolding and Refolding of CPM-Labeled Human Serum Albumin: Role of Ionic Liquid. *J. Phys. Chem. B* **2011**, *115*, 13075–13083.
42. Mojumdar,S. S.; Chowdhury, R.; Chattoraj, S.; Bhattacharyya, K. Role of Ionic Liquid on the Conformational Dynamics in the Native, Molten Globule, and Unfolded States of Cytochrome C: A Fluorescence Correlation Spectroscopy Study. *J. Phys. Chem. B* **2012**, *116*, 12189-12198.
43. Ghosh, S.; Parui, S.; Jana, B.; Bhattacharyya, K. Ionic liquid induced dehydration and domain closure in lysozyme: FCS and MD simulation. *J. Chem. Phys.* **2015**, *143*, 125103.
44. Pabbathi, A.; Samanta, A. On the Stability and Conformational Dynamics of Cytochrome c in Ammonium Ionic Liquids. *J. Phys. Chem. B* **2020**, *124*, 8132–8140.
45. Pabbathi, A.; Ghosh, S.; Samanta, A. FCS Study of the Structural Stability of Lysozyme in the Presence of Morpholinium Salts. *J. Phys. Chem. B* **2013**, *117*, 16587−16593.

46. Islam, M. M.; Barik, S.; Preeyanka, N.; Sarkar, M. Interaction of Lysozyme with Monocationic and Dicationic Ionic Liquids: Toward Finding a Suitable Medium for Biomacromolecules. *J. Phys. Chem. B* **2020**, *124*, 961–973.
47. Islam, M. M.; Barik, S.; Sarkar, M. Probing the Interactions of 1-Alkyl-3-methylimidazolium Tetrafluoroborate (Alkyl = Octyl, Hexyl, Butyl, and Ethyl) Ionic Liquids with Bovine Serum Albumin: An Alkyl Chain Length-Dependent Study. *J. Phys. Chem. B* **2019**, *123*, 1512–1526.
48. Subba, N.; Sahu, P.; Das, N.; Sen, P. Rational design, preparation and characterization of a ternary non-ionic room-temperature deep eutectic solvent derived from urea, acetamide, and sorbitol. *J. Chem. Sci.* **2021**, *133*, 25.
49. Husain, S. S.; Lowe, G. The amino acid sequence around the active-site cysteine and histidine residues of stem bromelain. *Biochem. J.* **1970**, *117*, 341–346.
50. J. R. Lakowicz, *Principles of Fluorescence Spectroscopy*, 3rd ed.; Springer, New York, 2006.
51. http://www.cbs.dtu.dk/services/NetSurfP-1.1/ (July 2020).
52. N. Nemkovich,; Reis, H.; Baumann, W. Ground and excited state dipole moments of coumarin laser dyes: Investigation by electro-optical absorption and emission methods. *J. Lumin*. **1997**, *71*, 255-263.
53. Zaman, M.; Zakariya, S. M.; Nusrat, S.; Khan, M. V.; Qadeer, A.; Ajmal, M. R.; Khan, R. H. Surfactant-mediated amyloidogenesis behavior of stem bromelain; a biophysical insight. *J. Biomol. Struct. Dyn*. 2017, **35**, 1407-1419.
54. Note: Steady-state fluorescence has been taken with CPM tagged bromelain because TMR is not a solvatochromic dye. In the case of FCS measurement, solvatochromism is not a necessary criterion. Moreover, Ac/Ur/Sor DES shows tiny emission around 450 nm when excited at 400 nm. This much emission is negligible compared to the emission from CPM molecule tagged to bromelain in the steady-state experiment when the concentration is around 5 µM. However, in the case of FCS, the sample concentration is in the nM range and therefore DES emission interfere with the fluorescence signal from the CPM tagged bromelain.
55. Durand, E.; Lecomte, J.; Baréa, B.; Villeneuve, P. Towards a better understanding of how to improve lipase-catalyzed reactions using deep eutectic solvents based on choline chloride. *Eur. J. Lipid Sci. Technol.* **2014**, *116*, 16-23.

56. Lindberg, D.; de la Fuente Revenga, M.; Widersten, M. Deep eutectic solvents (DESs) are viable cosolvents for enzyme-catalyzed epoxide hydrolysis. *J. Biotechnol.* **2010**, *147*, 169-171.
57. Durand,E.; Lecomte, J.; Baréa, B.; Dubreucq, E.; Lortie, R.; Villeneuve, P. Evaluation of deep eutectic solvent–water binary mixtures for lipase-catalyzed lipophilization of phenolic acids. *Green Chem.* **2013**, *15*, 2275-2282.
58. Hammond, O. S.; Bowron, D. T.; Edler, K. J. The Effect of Water upon Deep Eutectic Solvent Nanostructure: An Unusual Transition from Ionic Mixture to Aqueous Solution. *Angew. Chem. Int. Ed*. **2017**, 56, 9782-9785.
59. Kaur, S.; Gupta, A.; Kashyap, H. K. How Hydration Affects the Microscopic Structural Morphology in a Deep Eutectic Solvent. *J. Phys. Chem. B* **2020**, *124*, 2230-2237.
60. Panda, S.; Kundu, K.; Kiefer, J.; Umapathy, S.; Gardas, R. L. Molecular-Level Insights into the Microstructure of a Hydrated and Nanoconfined Deep Eutectic Solvent. *J. Phys. Chem. B* **2019**, *123*, 3359-3371.
61. Weng, L.; Toner, M. Janus-faced role of water in definingnanostructure of choline chloride/glyceroldeep eutectic solvent. *Phys. Chem. Chem. Phys.* **2018**, *20***,** 22455-22462.
62. Posada, E.; López-Salas, N.; Riobóo, R. J. J.; Ferrer, M. L.; Gutiérrez, M. C.; del Monte, F. Reline aqueous solutions behaving as liquid mixtures of H-bonded co-solvents: microphase segregation and formation of co-continuous structures as indicated by Brillouin and ^{1}H NMR spectroscopies. *Phys. Chem. Chem. Phys.* **2017**, *19*, 17103-17110.
63. Contreras, R.; Lodeiro, L.; Rozas-Castro, N.; Ormazábal-Toledo, R. On the role of water in the hydrogen bond network in DESs: an ab initio molecular dynamics and quantum mechanical study on the urea–betaine system. *Phys. Chem. Chem. Phys.* **2021**, *23*, 1994-2004.
64. Huang, Z.-L.; Wu, B.-P.; Wen, Q.; Yang, T.-X.; Yang, Z. Deep eutectic solvents can be viable enzyme activators and stabilizers. *J. Chem. Technol. Biotechnol.* **2014**, *89*, 1975-1981.

Chapter 7

Concluding Remarks and Future Prospects

In my quest to study DESs, I mainly focused on the physical chemistry aspect of various types of DESs. Using time-resolved spectroscopic techniques, I explored various dynamics (solvation, rotation and translation dynamic) in DESs and their extent of decoupling with bulk viscosity, which was explained in terms of dynamic heterogeneity.

We for the first time studied ultrafast solvent dynamics in a DES using femtosecond transient absorption spectroscopy and femtosecond optical Kerr-effect (OKE) spectroscopy. In the acetamide/urea DES, we found that the longest time constant of the solvation dynamics is associated with rotation of the solvent molecules. Major portion of the solvation is ultrafast (100 fs). Solvation was found to have small degree of decoupling from bulk viscosity indicating mild dynamic heterogeneity of the system. Translational diffusion of fluorescent probe studied by FCS nearly adheres to SE relation indicating mild heterogeneity.

Next we studied spectroscopically less explored hydrophobic DES made up of lauric acid and menthol. From the combined result of solvation, probe rotation and translation diffusion, we proposed this DES to have micelle like structure. We observed that the decoupling of various dynamics from the bulk viscosity is length dependent. Rotational dynamics of a solute is confined to the first solvation shell and nearly adheres to SED whereas translational dynamics of a solute takes places beyond the first solvation shell and therefore, encounter different environments showing stronger decoupling from the medium viscosity. Thus we showed that the heterogeneity is modulated by the length scale.

We also explored ultrafast solvation dynamics and solute translational diffusion in an ionic DES based on acetamide and lithium salts (NO_3^-, Br^- and ClO_4^-). Surprisingly, in this study, we missed almost half of the Stokes-shift dynamics despite having good temporal resolution of the technique used. We believe that the missed Stokes-shift dynamics is because of the breaking of hydrogen bond network of acetamide by the ionic species. We also found that the sub-picosecond time component increases as the concentration of Br^- increases. Translational diffusion of solute showed strong decoupling from the bulk viscosity indicating dynamic heterogeneity as reported before.

In an attempt to contribute to non-ionic DESs, we synthesized a new DES based on acetamide, urea and sorbitol. Temperature and concentration dependent thermo-physical properties of this new DES have been reported. Since DESs are proving to be a biocompatible medium, we studied the activity of a protein, bromelain, in newly prepared DES at varying degree of

hydration. Interestingly, it was found that the activity of bromelain in hydrated DES up to certain concentration is more than that in water.

Despite having studied various dynamics of different DESs and arriving at some conclusions in previous chapters, complete understanding is DESs yet to be achieved. Many open questions remain unanswered. For example, how structure and dynamics of DESs is different from its pure counterparts or its constituents? This is as important as determining the complete phase diagram of DESs. However, it is difficult to address this as at least one of the constituent is usually solid at working temperatures and may have higher melting point. Most of the instruments have access to only a certain range of temperatures.

One of the main reasons DESs captured the attention of the researchers is because of the transformation of solid to liquid. Therefore it is simply a mixture with some unusual and interesting physical and chemical properties. There are numerous studies on binary solvent mixtures where the depression of freezing points is not reported as there is no change of state upon mixing. These two types of mixtures could be studied and compared. The way I see it, DESs generally consist of "*heavy molecules*" in comparison to binary solvent mixtures i.e. size/mass of the constituent molecules in DESs are relatively higher than that of the constituents of binary mixtures. For example, choline chloride, menthol, sorbitol, etc. are fairly large molecules. According to hole theory (chapter 1), solvent containing species larger than the hole size will have higher viscosity. Therefore, all the dynamics coupled with viscosity will be slowed down. This creates an opportunity to study two dynamics (slow and fast) of different time domains separately.

Apart from this, the molecular level understanding of the interaction present in DES, which essentially answer how DESs are different from the normal mixtures where the sole reason is the colligative property, needs to be explored.

Because of several advantages of DESs over conventional solvents, it has a huge potential to go beyond academic confinement. However, from the applications point of view, DESs need to be extensively explored for its implementation at the industrial level in the forthcoming years. Both academia and industries still heavily rely on conventional solvent. For now, we can only hope that DESs is opted for more and more applications.

This Page Intentionally Left Blank

List of Publications

1. Temperature-Dependent Ultrafast Solvation Response and Solute Diffusion in Acetamide−Urea Deep Eutectic Solvent. *Journal of Physical Chemistry B* **2019**, 123, 9212-9221.

   Authors: **Navin Subba**, Kamil Polok, Piotr Piatkowski, Bozena Ratajska-Gadomska, Ranjit Biswas, Wojciech Gadomski, and Pratik Sen.

2. Partial Viscosity Decoupling of Solute Solvation, Rotation, and Translation Dynamics in Lauric Acid/Menthol Deep Eutectic Solvent: Modulation of Dynamic Heterogeneity with Length Scale. *Journal of Physical Chemistry B* **2020**, 124, 6875–6884.

   Authors: **Navin Subba**, Nilimesh Das and Pratik Sen.

3. Subpicosecond Solvation Response and Partial Viscosity Decoupling of Solute Diffusion in Ionic Acetamide Deep Eutectic Solvents: Fluorescence Up-Conversion and Fluorescence Correlation Spectroscopic Measurements. *Journal of Physical Chemistry B* **2020**, 124, 1995–2005.

   Authors: **Navin Subba**, Ejaj Tarif, Pratik Sen and Ranjit Biswas.

4. Rational Design, Preparation and Characterization of a Ternary Non-ionic Room-temperature Deep Eutectic Solvent Derived from Urea, Acetamide and Sorbitol. *Journal of Chemical Sciences* **2021**, 133, 25.

   Authors: **Navin Subba**, Pushpkant Sahu, Nilimesh Das and Pratik Sen.

5. Correlating Bromelain's Activity with its Structure, Active-site Dynamics and Media's Physical Properties in a Hydrated Deep Eutectic Solvent. *Phys. Chem. Chem. Phys*. **2021** (Accepted)

   Authors: Nilimesh Das, Tanmoy Khan, **Navin Subba** and Pratik Sen.

6. Search for the origin of synergistic solvation in methanol/chloroform mixture using optical Kerr effect spectroscopy (Manuscript submitted).

   Authors: Kamil Polok, **Navin Subba**, Wojciech Gadomski and Pratik Sen.

7. Investigation of solvation, rotation and translational dynamics in molten menthol, molten salol and their eutectic mixture. A comparison of pure components and mixture. (Manuscript under preparation).

   Authors: **Navin Subba** and Pratik Sen.

8. Tracking Worm-like Micelle Formation in Solution: A Fluorescence Correlation Spectroscopic Study (Manuscript under preparation).

   Authors: **Navin Subba** and Pratik Sen.